NASA CONTRACTOR REPORT

N73-21413
NASA CR-2206

NASA CR-2206

CASE FILE COPY

RHEOLOGICAL EFFECTS ON FRICTION IN ELASTOHYDRODYNAMIC LUBRICATION

by Edward G. Trachman and H. S. Cheng

Prepared by
NORTHWESTERN UNIVERSITY
Evanston, Ill.
for Lewis Research Center

NATIONAL AERONAUTICS AND SPACE ADMINISTRATION • WASHINGTON, D. C. • MARCH 1973

1. Report No.	2. Government Accession No.	3. Recipient's Catalog No.
NASA CR-2206		

4. Title and Subtitle
RHEOLOGICAL EFFECTS ON FRICTION IN ELASTOHYDRODYNAMIC LUBRICATION

5. Report Date
March 1973

6. Performing Organization Code

7. Author(s)
Edward G. Trachman and H. S. Cheng

8. Performing Organization Report No.
None

9. Performing Organization Name and Address
Northwestern University
Evanston, Illinois

10. Work Unit No.

11. Contract or Grant No.
NGL 14-007-084

12. Sponsoring Agency Name and Address
National Aeronautics and Space Administration
Washington, D.C. 20546

13. Type of Report and Period Covered
Contractor Report

14. Sponsoring Agency Code

15. Supplementary Notes
Project Manager, Erwin V. Zaretsky, Fluid System Components Division, NASA Lewis Research Center, Cleveland, Ohio

16. Abstract
This report presents an analytical and experimental investigation of the friction in a rolling and sliding elastohydrodynamic lubricated contact. The rheological behavior of the lubricant is described in terms of two viscoelastic models. These models represent the separate effects of non-Newtonian behavior and the transient response of the fluid. A unified description of the non-Newtonian shear rate dependence of the viscosity is presented as a new hyperbolic liquid model. The transient response of viscosity, following the rapid pressure rise encountered in the contact, is described by a compressional viscoelastic model of the volume response of a liquid to an applied pressure step. The resulting momentum and energy equations are solved by an iterative numerical technique, and a friction coefficient is calculated. The experimental study was performed, with two synthetic paraffinic lubricants, to verify the friction predictions of the analysis. The values of friction coefficient from theory and experiment are in close agreement. The variation of the friction coefficient with rolling speed in a rolling contact system is closely investigated. Good agreement with existing experimental results is obtained at rolling speeds above 50 in/sec. At lower rolling speeds, a very rapid change in the effective viscosity of the lubricant is predicted. This behavior, in conjunction with shear rate effects, leads to large errors when experimental data is extrapolated to zero rolling speed.

17. Key Words (Suggested by Author(s))	18. Distribution Statement
Rheology Friction Elastohydrodynamics Lubrication Traction	Unclassified - unlimited

19. Security Classif. (of this report)	20. Security Classif. (of this page)	21. No. of Pages	22. Price*
Unclassified	Unclassified	213	$3.00

* For sale by the National Technical Information Service, Springfield, Virginia 22151

Page Intentionally Left Blank

TABLE OF CONTENTS

and Kelley [3] . However, these papers were not concerned with promoting the basic understanding of the traction between elastohydrodynamic contacts.

Crook [4] used two kinds of rolling disk machines in measuring the friction in a line contact as a function of sliding speed. In the region of small sliding speeds, he used the four-disk machine, a center disk surrounded by three equally spaced outer disks, shown in Figure 1.1. The center disk is free-floating and the measured torque does not contain any extraneous torque from the supporting bearings. For this reason, the four-disk machine gives very accurate frictional torque measurements at small sliding speeds. The four-disk machine is not suitable in the region of high slips, however, since it cannot maintain a stable sliding speed. For high sliding speeds, Crook used the two-disk machine shown in Figure 1.2, where the rotations of both disks are controlled by variable speed motors. Thus, Crook was able to measure the friction characteristics throughout the entire range of sliding speeds, using the four-disk machine in the low slip region and the two-disk machine in the high sliding speed region.

Crook found a profound influence of rolling speed upon the frictional torque in the low slip region. In this region, the slope of the traction versus slip curve is equal to the "effective viscosity" divided by the oil film thickness. Therefore, the effective viscosity may be evaluated by measuring the slope of the traction curve and calculating the oil film thickness from existing elastohydrodynamic theory. If the thermal effects and the non-Newtonian effects of the lubricant were both absent in this region, the effective viscosity would not be a function of rolling speed. However, this condition was

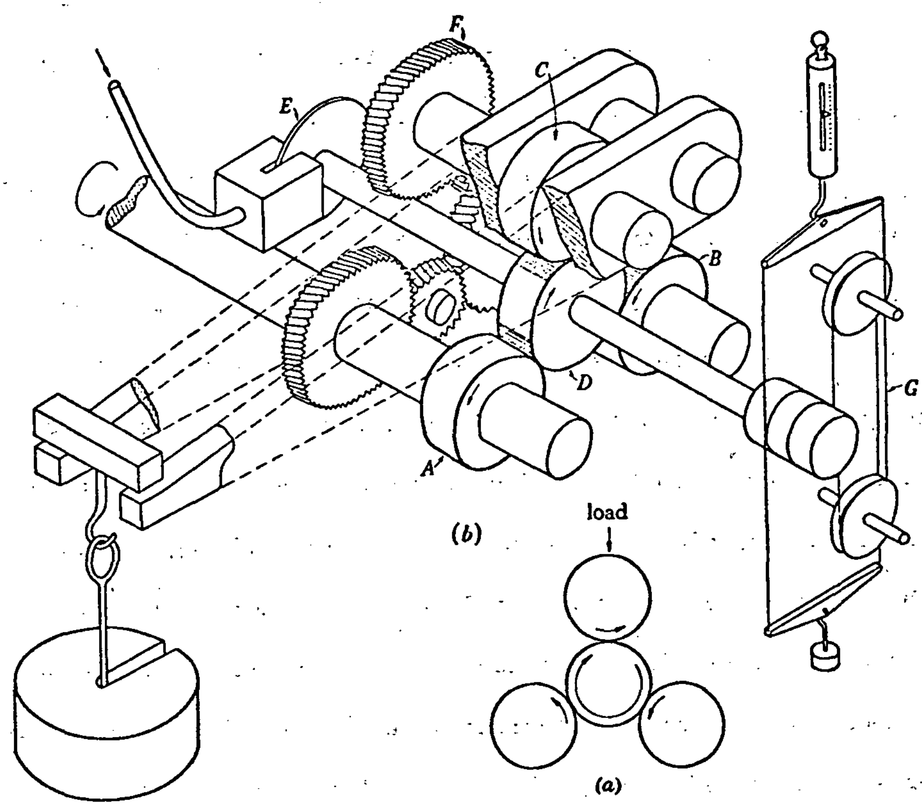

Figure 1.1. Crook's four-disk machine. (a) Principle, (b) construction (diagrammatic). A to D, disks; E, aerostatic thrust; F, gear train; G, band brake. Figure from Crook [4] .

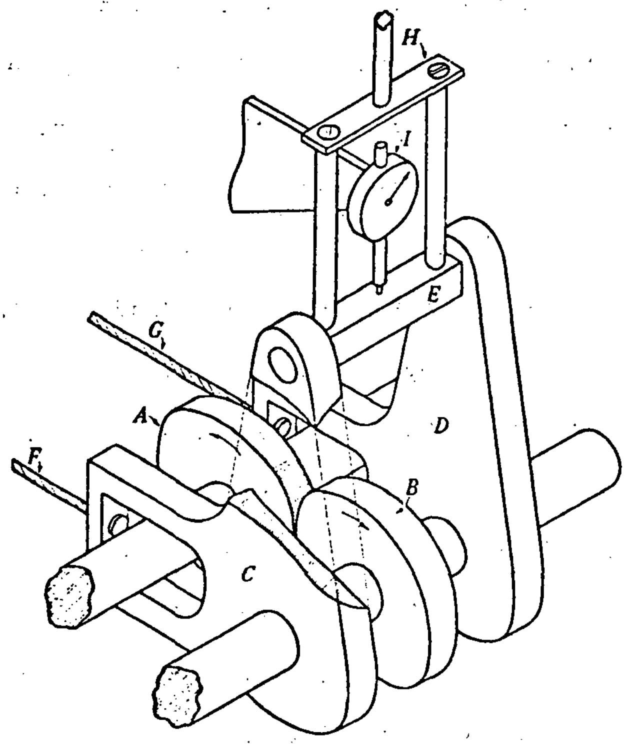

Figure 1.2. Crook's two-disk machine. A and B disks; C and D swinging arms; E axle; F and G loading cables; H spring beam; I dial gauge. Figure from Crook [4] .

not found in Crook's experimental results. On the contrary, he found a marked influence of the rolling speed on the effective viscosity of the lubricant that does not appear to be due to thermal effects only. Crook speculated that it was the viscoelastic effect of the lubricant which prevented it from reaching the static viscosity in the short time interval as it passes through the contact zone.

Crook was able to extend the friction data in the high slip region, with his two-disk machine, for loads ranging from 7.5 to 20 x 10^7 dynes/cm^2 and rolling speeds from 400 cm/sec to 1200 cm/sec. All the friction curves show the same basic trend which is characterized by an ascending portion at small sliding speeds and a descending friction at high sliding speeds. An increase in load does not change the basic characteristics of the friction curve, but does increase the level of the friction force. Similarly, Crook found that an increase in the rolling speed decreases the friction level.

Crook also attempted to predict the friction analytically by a simplified thermal friction theory based on the following four assumptions: the film thickness within the contact zone is uniform; the pressure distribution in the contact region is Hertzian; the heat carried away by the lubricant due to convection may be neglected; and the temperature rise on the surface of the disk may also be neglected. Using this simplified theory for a Newtonian lubricant, Crook was able to calculate the coefficient of friction or the effective viscosity as a function of sliding speed. However, he could not predict the sharp reduction of the effective viscosity at small sliding speeds. He concluded that the friction force at small sliding speeds cannot be accurately predicted by considering the thermal effects only.

Cheng [5] employed his full elastohydrodynamic theory in calculating the friction for the conditions corresponding to those used in Crook's experiments. The temperature calculations are based on the finite difference solution of the energy equation and are free from all the assumptions made earlier by Crook. It is seen in Figure 1.3 that even with this refined thermal analysis there still exists a large discrepancy in the low slip region. This strengthens Crook's argument that the thermal effects alone cannot account for the sharp reduction of effective viscosity in the low slip region.

Bell, Kannel and Allen [6] developed an approximate analysis to predict the temperature rise in the lubricant film at low sliding speeds. Their analysis included the heat due to convection and the heat generation due to the compression of the lubricant. They also concluded that the temperature effects are too small to account for the loss of effective viscosity at low sliding speeds. In addition to the thermal theory, they developed a non-Newtonian friction theory using a rheological model proposed by Ree and Eyring [7] . The results of this analysis indicate that drastic reductions of friction can exist if the lubricant viscosity is shear rate-dependent according to Ree-Eyring. However, in all their calculated data, the friction force was found to be dependent upon $1/h$ as the rolling speed is varied, whereas all the experimental data gathered thus far has shown the proportionality to be far greater than $1/h$ and in most cases more nearly proportional to $1/h^2$. Thus, the inclusion of the Ree-Eyring model alone in the friction analysis would not be able to predict a sufficient reduction of friction at low rolling speeds.

Smith [8] employed the rolling contact machine shown in Figure 1.4

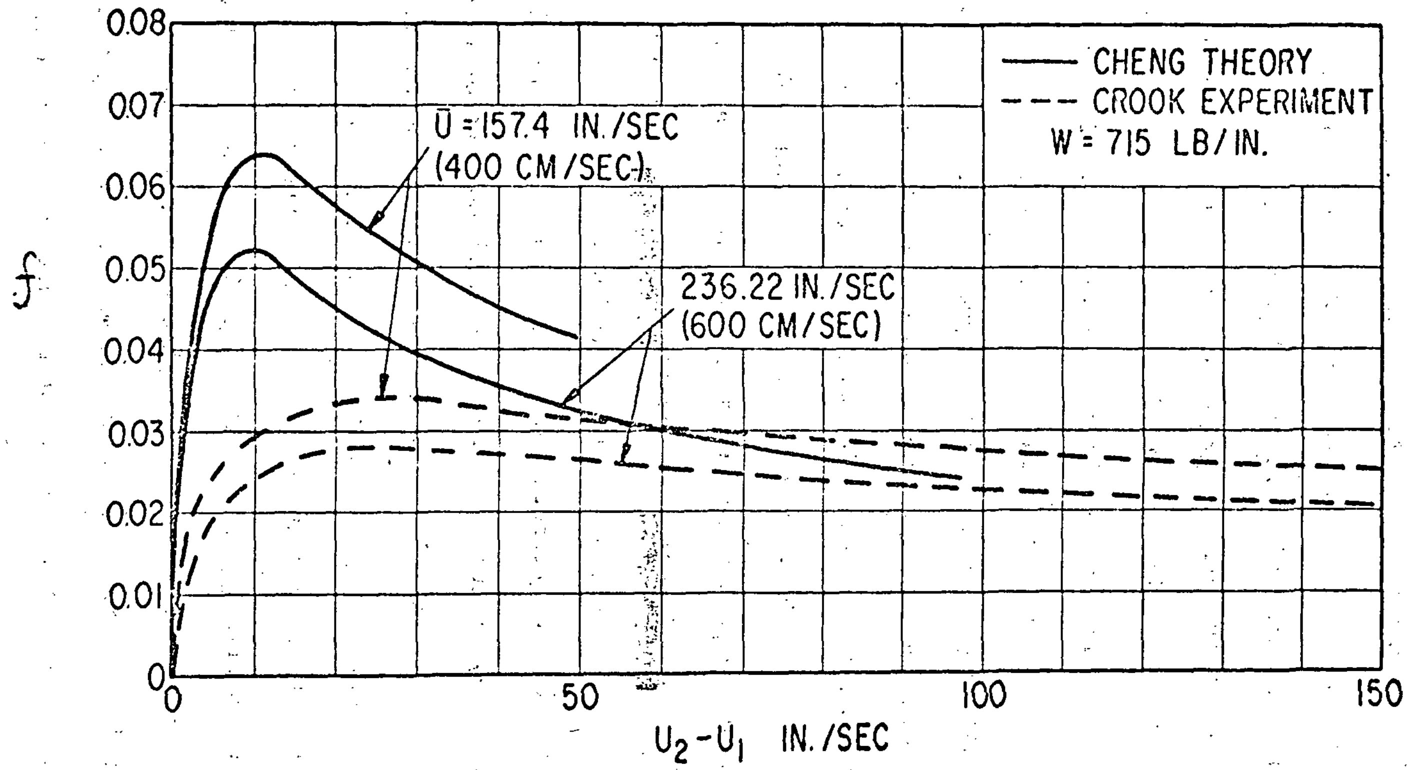

Figure 1.3. Comparison of Cheng's thermal theory with Crook's experiments. Curve from McGrew, Gu, Cheng and Murray [9] .

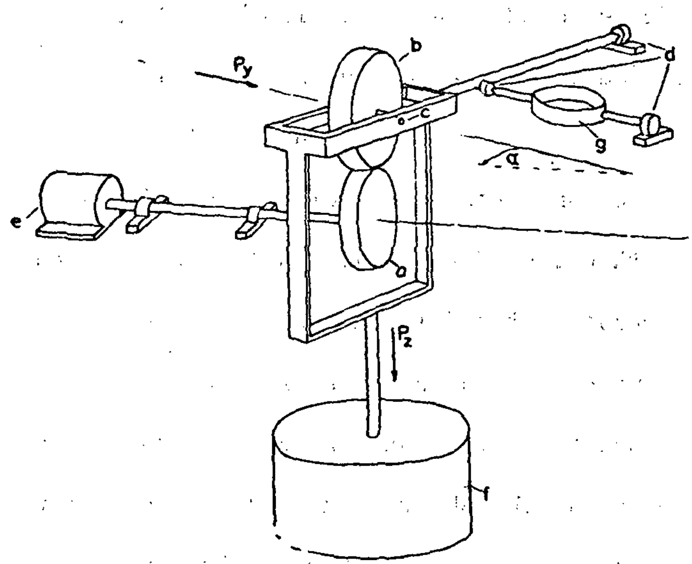

Figure 1.4. Smith's disk machine.

a Cylindrical roller
b Spherical roller
c Bearings
d Pivots
e Motor
f Normal load
g Strain gauge dynamometer

Figure from Smith [10] .

to measure the friction between two rollers whose axes are skewed at an arbitrary angle. With this skewed arrangement, he was able to measure the friction force due to the sliding velocity component. The resulting friction versus sliding speed curves show trends similar to those observed by Crook. Smith divided these curves into several regions. He believed a Newtonian isothermal friction theory is applicable in the region where the friction varies proportionally with the sliding speed. In the ascending portion of the friction curves, where the friction force increases with sliding speed in a non-linear fashion, Smith believed that the non-linearity is due to the non-Newtonian behavior of the lubricant. He postulated that there is also a region in which a shear plane exists at the center of the lubricant film, such that the lubricant behaves like two solid layers sliding over each other at the shear plane. He further stated that the resistance to sliding at the shear plane is dependent upon the shear plane temperature and the hydrostatic stress in the lubricant. Finally, he defined a region where seizure would take place.

A more comprehensive study of friction covering a wide range of loads, rolling speeds and sliding speeds was carried out more recently by Johnson and Cameron [11] with a two-disk machine. The maximum Hertzian pressure was varied from 62,000 psi to 243,000 psi; the rolling speed was varied from 8 in/sec to 260 in/sec; and the oil inlet temperature was varied from 30 ^{o}C to 90 ^{o}C. The most striking feature of Johnson and Cameron's data is that there exists a ceiling to all the experimental traction coefficients which cannot be exceeded no matter how the load and the rolling speed are varied. They also took extensive data in the low slip region, and from the slope of the traction versus slip curve were able to calculate the effective viscosity as a function of rolling speed. Johnson and Cameron furnished more convincing evidence that the thermal effects alone cannot account for the experimentally measured friction, and that a Smith-type limiting shear stress is dependent only on the shear plane temperature and pressure.

Jeffris and Johnson [12] investigated the effect of surface roughness upon friction between two lubricated rollers. They concluded that the measured coefficient of friction showed remarkably little variation throughout the whole range of experimental conditions for Hertzian pressures in excess of 175 kpsi. At lower Hertzian pressures, the surface roughness effect can be substantial.

A rather interesting qualitative explanation of the velocity, rate of shear, viscosity and temperature variations across the film thickness of an elastohydrodynamic contact was offered by Plint [13] He postulated that at the entrance of the contact zone, the rate of shear, viscosity and temperature are constant across the film thickness and the velocity profile is linear. As the thermal effects take over, the temperature at the mid-film increases and the viscosity is at a minimum at this position. This thermal effect causes the velocity profile to distort into a cusp such that the rate of shear becomes a maximum at the mid-film. A ceiling curve similar to that of Johnson and Cameron's was also found in Plint's experimental friction data.

Dowson and Holmes [14] modified Crook's four-disk machine and investigated the effect of surface quality upon the traction characteristics of rolling and sliding contacts. They showed that the friction initially decreases with surface roughness, reaches a minimum, and then increases steadily with surface roughness. Unlike Jefferis and Johnson's conclusion on the effect of surface roughness on friction, Dowson and Holmes found that the influence of surface quality is quite pronounced. However, these two results may not be in direct contradiction since the loads used by Dowson and Holmes were much smaller than those used in Jefferis and Johnson's experiments.

Recently, Dyson [15] has made a pioneering study analyzing the frictional force in an elastohydrodynamic contact by considering the lubricant as a viscoelastic liquid. He simplified his analysis by dividing the friction versus sliding speed curve into three regions, as shown in Figure 1.5: the linear region, where the frictional force varies linearly with the sliding speed; the non-linear ascending region, where the slope of the friction curve reduces rapidly as the sliding speed increases; and the thermal region, where the frictional force decreases with the sliding speed. The results of this study are most encouraging and have inspired the author's investigation of the rheological effects in an elastohydrodynamic lubricated contact.

The friction analysis presented in this thesis describes the rheological behavior of the lubricant in an elastohydrodynamic concentrated contact in terms of two viscoelastic models. These models represent the separate effects of non-Newtonian behavior and the transient response of the fluid.

A unified description of the non-Newtonian shear rate dependence of the viscosity is presented in Chapter II as a new hyperbolic liquid model. The hyperbolic model is based upon a shear viscoelastic liquid model with the addition of a limiting value of shear stress. The limiting shear stress is related to the high frequency limiting shear modulus

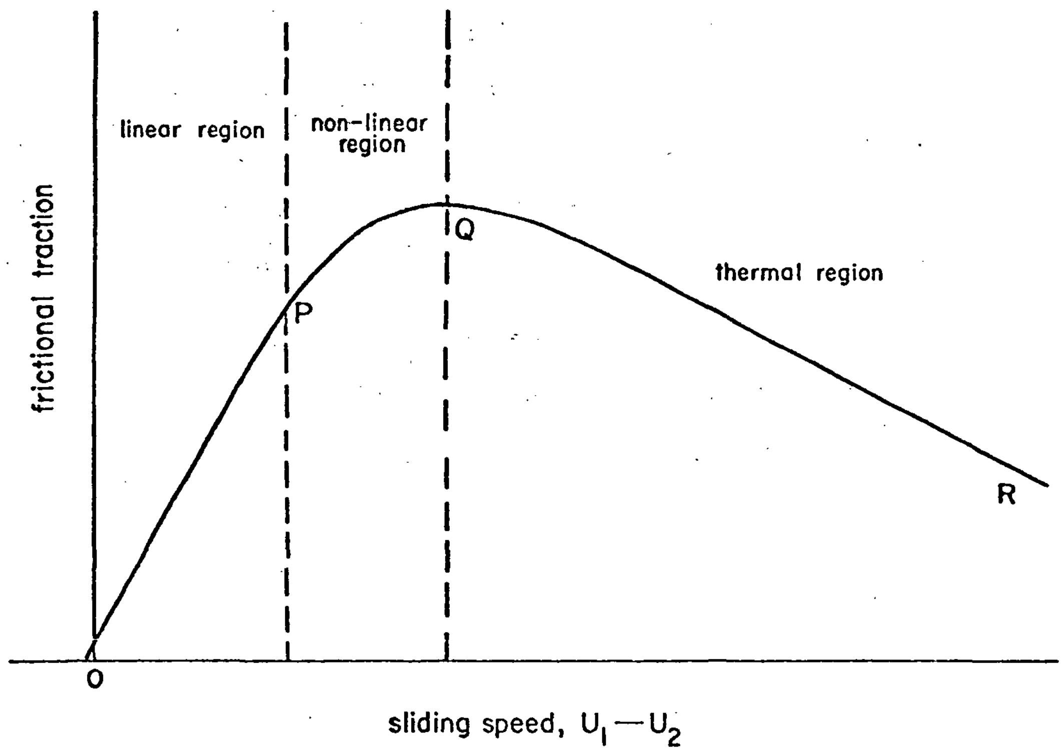

Figure 1.5. Friction versus sliding speed curve. Curve from Dyson [15] .

of the lubricant G_∞ , as proposed by Dyson [15] .

The transient response of the viscosity, following the rapid pressure rise encountered in the contact, is described in Chapter III by a compressional viscoelastic model of the volume response of a liquid to an applied pressure step. Kovacs [16] first investigated this non-linear model for the volume creep of polymer melts.

The governing equations, the fluid property functions and the technique used to calculate the tractive force transmitted during sliding between the two surfaces of a rolling disk machine are developed in Chapter IV. The experimental investigation is detailed in Chapter V and the analytical and experimental results are discussed and correlated in Chapter VI.

CHAPTER II

NON-LINEAR SHEAR STRESS-STRAIN RELATION

A friction analysis based upon a Newtonian lubricant having a viscosity varying with the statically measured pressure and temperature can yield a frictional coefficient far greater than those measured. There is little doubt that the fluid ceases to be Newtonian. Thus, a realistic friction analysis must consider a non-linear relationship between shear stress and shear rate.

A major difficulty in predicting the friction for elastohydrodynamic lubrication is the lack of data available for the physical properties of the lubricant at the extreme values of pressure, temperature and shear rate encountered in the concentrated contact. It is very difficult to make direct measurements of shear stress versus shear rate in continuous shear under EHD conditions. Therefore, the physical property data must come from other fields. One source is the study of supercooled liquids under oscillatory shear. A correlation between this data and the behavior under conditions of continuous shear, as well as the restrictions of such a correlation, are discussed in this chapter. A hyperbolic shear stress-strain function is then proposed as a useful non-linear model for use under elastohydrodynamic conditions.

2.1 Shear Viscoelasticity

The phenomenological theory of viscoelasticity attempts to describe the mechanical behavior of a material in terms of time-dependent, or frequency-dependent, functions which relate the stress in the material to the deformation. Classical elasticity theory for solids is based on Hooke's Law which requires the stress to be directly proportional to the instantaneous strain but independent of the rate of strain. Classical hydrodynamic theory is based on Newton's Law. Newton's Law states that the steady-state shear stress in a liquid is directly proportional to the instantaneous rate of strain but independent of the strain itself. Many materials closely follow the behavior specified by these laws. It is often impossible, however, to characterize a material by either of the two classical types of behavior. Substances which exhibit both solid-like and liquid-like properties show viscoelastic behavior.

The term viscoelastic is used to describe the properties of any material which is able to store energy in elastic deformation and dissipate energy as heat. If the strain and strain rate are kept sufficient small, so that in a given experiment the ratio of stress to strain is a function of time only and independent of the stress level, the material shows linear viscoelastic behavior. Most of the physical properties of viscoelastic materials have been determined by oscillatory shear experiments. Linear viscoelastic behavior is easily obtained in these experiments since the amplitude of deformation is extremely small.

The work of Gross [17] and Alfrey [18] are examples of the large literature concerning the mathematical aspects of the phenomenological theory of linear viscoelasticity. It is more appropriate here to develop the subject in terms of simple mechanical models. The model approach is easier to understand and more closely related to the physical behavior of the materials.

2.2 Viscoelastic Functions

In most of the high frequency techniques used for measuring the viscoelastic properties of liquids, a plane shear wave is propagated through the liquid. The shear stress τ and the shear strain γ are related by a complex quantity, the shear modulus

$$G^* = \frac{\tau}{\gamma} \tag{2.1}$$

In a Hookean solid,the shear modulus is a real quantity since the stress varies in phase with the strain. In a Newtonian liquid, the stress is 90° out of phase with the strain. In the latter case, the shear modulus is an imaginary quantity and is determined from Newton's Law. The strain rate is represented by

$$\dot{\gamma} = \frac{d}{dt}(\gamma_o e^{i\omega t}) = i\omega\gamma \tag{2.2}$$

and therefore the stress is calculated as

$$\tau = \eta\dot{\gamma} = i\omega\gamma\eta \tag{2.3}$$

The shear modulus is now calculated by its definition, equation (2.1).

$$G^* = i\omega\eta \tag{2.4}$$

For a viscoelastic material, the stress and strain differ by a phase angle between 0° and 90°. Therefore, the frequency-dependent shear modulus is a complex quantity with both real and imaginary components, as represented by

$$G^*(i\omega) = G'(\omega) + i\,G''(\omega) \tag{2.5}$$

The shear modulus will not have the simple form given in equation (2.4) for a Newtonian liquid except at low frequencies where sufficient time is available during each stress cycle for viscous flow to occur. At higher frequencies, the time required for molecular translation becomes comparable with the period of the stress cycle and the liquid exhibits a shear rigidity. At sufficiently high frequencies, the behavior will be purely elastic. There is no molecular transition during each cycle and, consequently, the energy loss due to viscous flow is negligible. Under these conditions, the liquid behaves like a glass.

The real component of the complex modulus G', the ratio of the stress in phase with the strain to the strain, is called the storage modulus because of its association with the storage and release of elastic energy. The imaginary component G", the ratio of the stress 90° out of phase with the strain to the strain, is called the loss modulus because of its association with the dissipation of energy as heat by viscous flow.

The modulus components for a liquid have the following limits. At low frequencies where the behavior is purely viscous, or Newtonian:

$$\lim_{\omega \to 0} G'(\omega) = 0 \tag{2.6}$$

$$\lim_{\omega \to 0} G''(\omega) = \omega\eta \tag{2.7}$$

At high frequencies where the behavior is purely elastic:

$$\lim_{\omega \to \infty} G'(\omega) = G_{\infty} \tag{2.8}$$

$$\lim_{\omega \to \infty} G''(\omega) = 0 \tag{2.9}$$

where G_{∞} is the limiting elastic modulus.

The shear mechanical impedance Z^*, defined as the ratio of shear stress to particle velocity, is the quantity most easily measured in the oscillatory experiments. It is mathematically related to the shear modulus by the equations governing shear wave propagation through a liquid medium. Barlow and Lamb [19] show this relationship to be

$$(Z^*)^2 = \rho G^*(i\omega) \tag{2.10}$$

where ρ is the density of the liquid.

For a Newtonian liquid, where G^* is given by equation (2.4), the real and imaginary components of the shear mechanical impedance are given by

$$Z^* = Z' + i\, Z'' = (1 + i) \sqrt{\frac{\omega\eta\rho}{2}} \tag{2.11}$$

Equation (2.10) allows the components of the shear modulus to be calculated from the experimentally measured components of the shear mechanical impedance as follows:

$$G'(\omega) = \frac{(Z')^2 - (Z'')^2}{\rho} \tag{2.12}$$

$$G''(\omega) = \frac{2\, Z'\, Z''}{\rho} \tag{2.13}$$

The liquid properties may be alternatively represented by a complex viscosity defined by

$$\eta^*(i\omega) = \eta'(\omega) - i\eta''(\omega) = \frac{G^*(i\omega)}{i\omega} \tag{2.14}$$

The definition requires

$$\eta'(\omega) = \frac{G''(\omega)}{\omega} \tag{2.15}$$

and

$$\eta''(\omega) = \frac{G'(\omega)}{\omega} \tag{2.16}$$

The low frequency limit of the dynamic viscosity η' is η , the steady flow Newtonian viscosity.

The complex compliance of J^* is the inverse of the complex modulus.

$$J^*(i\omega) = J'(\omega) - i\, J''(\omega) = \frac{1}{G^*(i\omega)} \tag{2.17}$$

It follows that

$$J' = \frac{G'}{\left[(G')^2 + (G'')^2\right]} \tag{2.18}$$

and

$$J'' = \frac{G''}{\left[(G')^2 + (G'')^2\right]} \tag{2.19}$$

The real component J' is the storage compliance and J'' is the loss compliance.

The inverse of the complex viscosity is the complex fluidity μ^*.

$$\mu^*(i\omega) = \mu'(\omega) + i\mu''(\omega) = \frac{1}{\eta^*(i\omega)} \tag{2.20}$$

The definitions and interrelations of the viscoelastic functions are summarized in Table 2.1.

2.3 The Maxwell Model

It is often convenient to visualize the behavior of a complex material in terms of models. The basic mechanical model elements are a coiled spring to represent Hookean elastic deformation and a dashpot to represent Newtonian viscous flow. Extension of the elements is analogous to shear strain and the associated force is analogous to the shear stress.

The combination of a spring in series with a dashpot was studied by Maxwell [20] . This simple model, shown in Figure 2.1, exhibits both viscous and elastic behavior. Viscous flow in the dashpot with negligible extension of the spring takes place if the extension rate is small. If the model is rapidly extended and immediately released, the deformation is purely elastic since sufficient time is not available for flow to occur in the dashpot. Between these extremes, the

Table 2.1

VISCOELASTIC FUNCTIONS IN OSCILLATORY SHEAR

τ = shear stress acting in x-direction on x-z plane

ξ = particle displacement in x-direction

$\gamma = \partial\xi/\partial y$ = shear strain

$\dot{\xi} = \partial\xi/\partial t$ = particle velocity in x-direction

$\dot{\gamma} = \partial\gamma/\partial t = \partial\dot{\xi}/\partial y$ = shear rate, rate of strain

ω = angular frequency

<u>DEFINITIONS:</u>

Complex shear modulus:	$G^*(i\omega) = \tau/\gamma = G'(\omega) + i\,G''(\omega)$
Complex mechanical impedance:	$Z^*(i\omega) = -\tau/\dot{\xi} = Z'(\omega) + i\,Z''(\omega)$
Complex viscosity:	$\eta^*(i\omega) = \tau/\dot{\gamma} = \eta'(\omega) - i\,\eta''(\omega)$
Complex shear compliance:	$J^*(i\omega) = \gamma/\tau = J'(\omega) - i\,J''(\omega)$
Complex fluidity:	$\mu^*(i\omega) = \dot{\gamma}/\tau = \mu'(\omega) + i\,\mu''(\omega)$

<u>INTERRELATIONS:</u>

$$G^*(i\omega) = \frac{(Z^*)^2}{\rho} = i\omega\eta(i\omega) = \frac{1}{J^*(i\omega)} = \frac{i\omega}{\mu(i\omega)}$$

behavior will be a combination of both the elastic and the viscous modes.

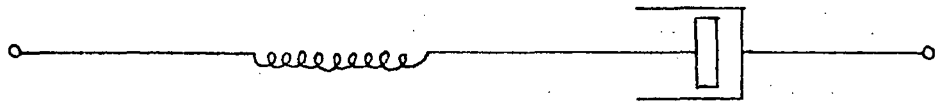

Figure 2.1. The Maxwell element. The spring corresponds to a shear modulus G and the dashpot corresponds to a viscosity η .

The basic equations of motion for the components of the model are:

$$\tau = \eta\dot{\gamma}_N \tag{2.21}$$

for the dashpot; and

$$\tau = G\gamma_H \tag{2.22}$$

for the spring, where

τ = the applied stress

$\dot{\gamma}_N$ = the rate of extension of the dashpot

γ_H = the extension of the spring

The rate of extension of the spring is $\dot{\gamma}_H = \dot{\tau}/G$ and the total rate of extension is then

$$\dot{\gamma} = \dot{\gamma}_N + \dot{\gamma}_H = \frac{\tau}{\eta} + \frac{\dot{\tau}}{G} \tag{2.23}$$

or

$$\tau + \frac{\eta}{G}\dot{\tau} = \eta\dot{\gamma} \tag{2.24}$$

Equation (2.24) is the constitutive equation of the Maxwell element. The ratio η/G has the dimensions of time and is called the Maxwell relation time λ .

$$\lambda = \frac{\eta}{G} \tag{2.25}$$

For sinusoidal variations of stress and strain of frequency ω, equation (2.24) becomes

$$\tau + i\omega\lambda\tau = i\omega\eta\gamma \tag{2.26}$$

The complex shear modulus is evaluated from equation (2.1) as

$$G^*(i\omega) = \frac{i\omega\eta}{1 + i\omega\lambda} \tag{2.27}$$

Rationalizing this expression yields

$$G^*(i\omega) = \frac{\omega^2\eta\lambda + i\omega\eta}{1 + \omega^2\lambda^2} \tag{2.28}$$

and substituting for η from equation (2.25) gives the final form of the complex shear modulus

$$G^*(i\omega) = G \cdot \frac{\omega^2\lambda^2 + i\omega\lambda}{1 + \omega^2\lambda^2} \tag{2.29}$$

The storage modulus is

$$G'(\omega) = G \cdot \frac{\omega^2\lambda^2}{1 + \omega^2\lambda^2} \tag{2.30}$$

which reduces to $G'(\omega) = G$ in the limit as $\omega \to \infty$; but this limiting value has been defined as G_∞. Thus, the spring in the Maxwell element corresponds to the instantaneous or limiting high frequency shear modulus of a liquid. The loss modulus is given by

$$G''(\omega) = G_\infty \cdot \frac{\omega\lambda}{1 + \omega^2\lambda^2} \tag{2.31}$$

which in the limit as $\omega \to 0$ becomes $G''(\omega) = G_\infty \cdot \omega\lambda = \omega\eta$. The dashpot of the Maxwell element therefore corresponds to the steady flow viscosity of a liquid. In normalized form, the variation with frequency of the modulus components and the dynamic viscosity is given by equations (2.32), (2.33) and (2.34).

$$\frac{G'(\omega)}{G_\infty} = \frac{\omega^2\lambda^2}{1 + \omega^2\lambda^2} \tag{2.32}$$

$$\frac{G''(\omega)}{G_\infty} = \frac{\omega\lambda}{1 + \omega^2\lambda^2} \tag{2.33}$$

$$\frac{\eta'}{\eta} = \frac{G''(\omega)}{\omega\eta} = \frac{1}{1 + \omega^2\lambda^2} \tag{2.34}$$

The complex compliance of J^* for the Maxwell element is given by the simple expression

$$J^*(i\omega) = \frac{\gamma}{\tau} = \frac{1 + i\omega\lambda}{i\omega\eta} = \frac{1}{G_\infty} - i\,\frac{1}{\omega\eta} \tag{2.35}$$

The frequency variation of the modulus components and the dynamic viscosity for the Maxwell element are shown in Figure 2.2.

Gruber and Litovitz [21] have postulated that a Maxwell element can predict the behavior of certain liquids. The viscosity of these liquids is governed primarily by the energy required for a molecule to surmount the potential barrier due to interaction with its nearest neighbors, and jump from one site in the liquid to another. The steady flow viscosity of such a liquid is given by the Arrhenius equation:

$$\ln \eta = A + B/T \tag{2.36}$$

where T is the absolute temperature.

For liquids which have viscosities above about 0.1 poise, however, the viscosity is primarily a function of the relative availability of free volume as described by Barlow, Lamb and Matheson [22] . Therefore, the Arrhenius viscosity-temperature relation and the Maxwell description of viscoelastic relaxation are not adequate governing equations. The lubricant in an EHD concentrated contact is in a state where the viscosity is limited by available free volume and, therefore, another viscoelastic liquid model proposed for such liquids by Barlow, Erginsav and Lamb [23] must be investigated.

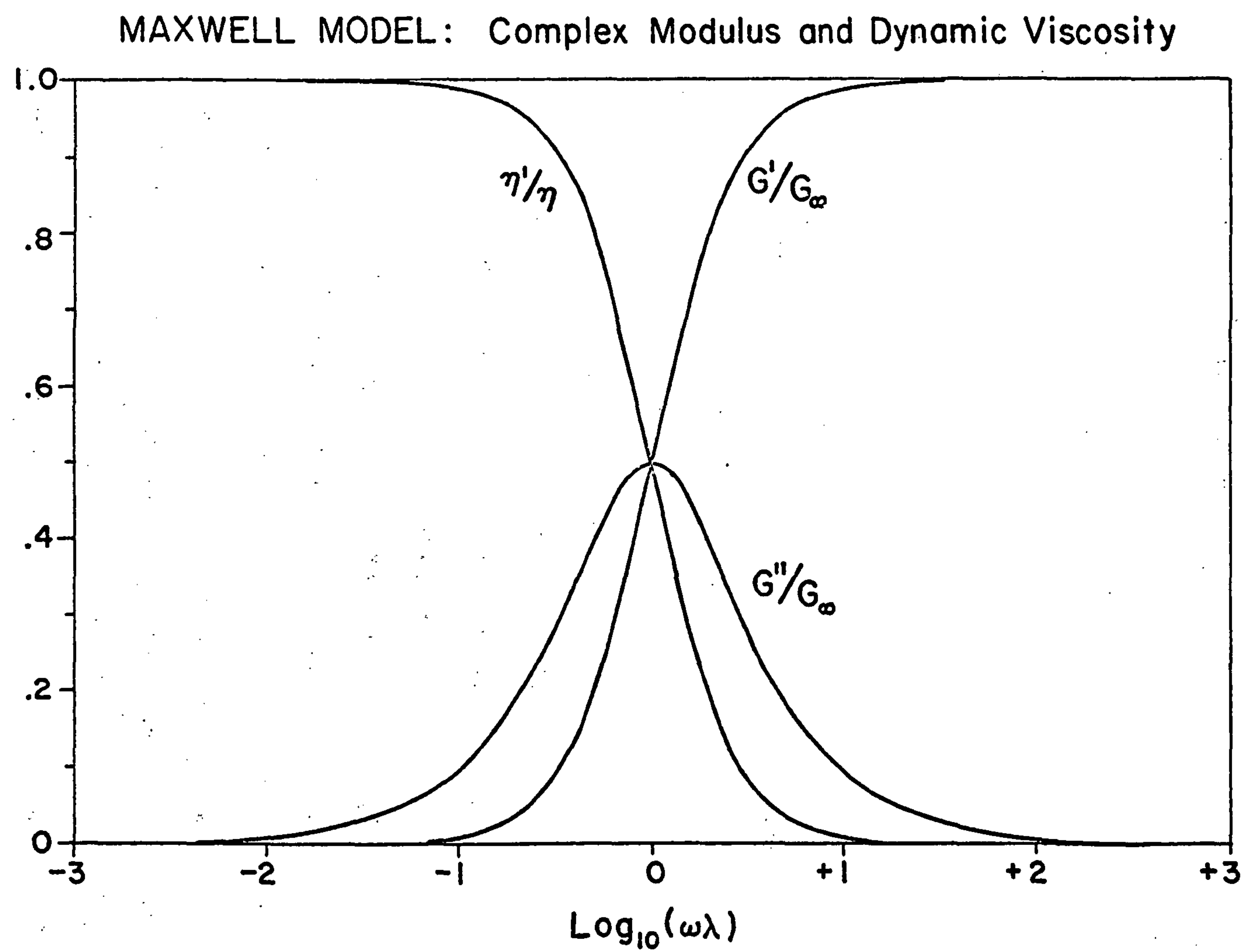

Figure 2.2. The frequency variation of the modulus components and the dynamic viscosity for the Maxwell element.

2.4 The B. E. L. Liquid Model

Barlow, Lamb and Matheson [22] have shown that liquids having viscosities above about 0.1 poise obey the Doolittle free-volume [24] equation:

$$\ln \eta = A + B \frac{v_o}{v_f} \tag{2.37}$$

where η = viscosity

v_o = occupied volume

v_f = free volume

A,B = constants of a given liquid

The specific volume $v = v_o + v_f$ and the density is a linear function of temperature. Therefore, equation (2.37) becomes

$$\ln \eta = A' + B'/(T-T_o) \tag{2.38}$$

where η = viscosity at temperature T

T = absolute temperature

T_o = reference temperature, at which there would be no free volume

A',B' = constants for a given liquid

Barlow, Lamb, Matheson, Padmini and Richter [25] and Barlow, Erginsav and Lamb [23] have demonstrated that the viscoelastic properties for a large number and wide variety of liquids, which obey the Doolittle viscosity-temperature relation, can be represented by two standard curves: $Z'/(\rho G_\infty)^{\frac{1}{2}}$ and $Z''/(\rho G_\infty)^{\frac{1}{2}}$ versus $\log_{10}(\omega\eta/G_\infty)$. Figure 2.3 shows that the experimental results for many liquids are indistinguishable when plotted in this manner. This suggests a simple underlying phenomenological explanation. Barlow, Erginsav and Lamb propose a new liquid model consisting of the parallel combination of

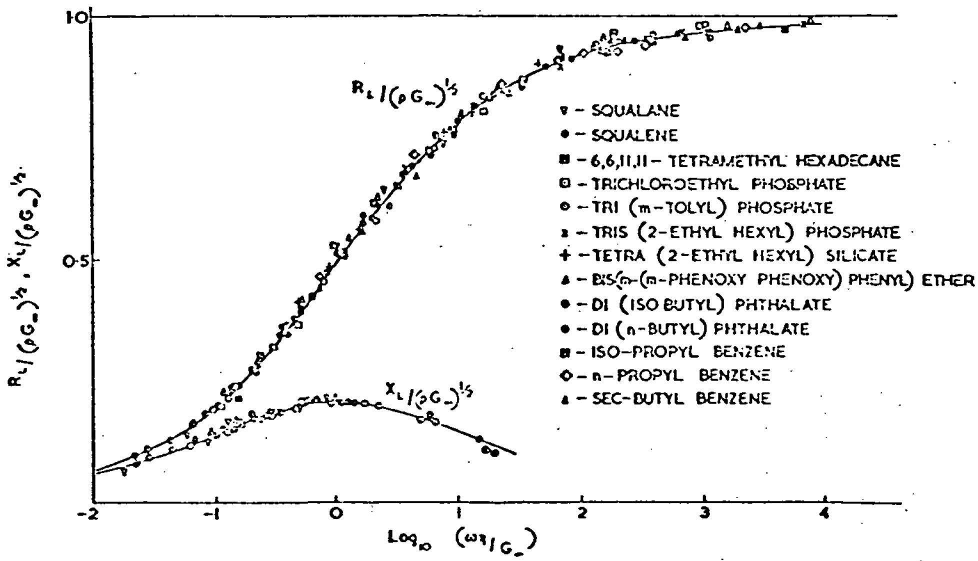

Figure 2.3. Normalized plots of $\frac{Z'}{(\rho G_\infty)^{\frac{1}{2}}}$ and $\frac{Z''}{(\rho G_\infty)^{\frac{1}{2}}}$ versus $\log_{10}\left(\frac{\omega\eta}{G_\infty}\right)$

Curve from Lamb [26].

the shear mechanical impedances for a Newtonian liquid and a Hookean solid. The shear mechanical impedances result from equations (2.8), (2.10) and (2.11). Thus,

$$Z_N = (1 + i) \left(\frac{\omega\eta\rho}{2}\right)^{\frac{1}{2}} \tag{2.39}$$

for a Newtonian liquid and

$$Z_H = (\rho G_\infty)^{\frac{1}{2}} \tag{2.40}$$

for a Hookean solid.

Accordingly, the components of the shear mechanical impedance are given by:

$$Z' = \frac{(\rho G_\infty)^{\frac{1}{2}}(\omega\eta/2G_\infty)^{\frac{1}{2}}\left[1 + (2\omega\eta/G_\infty)^{\frac{1}{2}}\right]}{\left[1 + (\omega\eta/2G_\infty)^{\frac{1}{2}}\right]^2 + (\omega\eta/2G_\infty)} \tag{2.41}$$

$$Z'' = \frac{(\rho G_\infty)^{\frac{1}{2}}(\omega\eta/2G_\infty)^{\frac{1}{2}}}{\left[1 + (\omega\eta/2G_\infty)^{\frac{1}{2}}\right]^2 + (\omega\eta/2G_\infty)} \tag{2.42}$$

The components of the shear modulus G^* and the compliance J^* for the B. E. L. model are given by:

$$G' = \frac{4G_\infty(\omega\eta/2G_\infty)^{3/2}\left[1 + (\omega\eta/2G_\infty)^{\frac{1}{2}}\right]}{\left\{\left[1 + (\omega\eta/2G_\infty)^{\frac{1}{2}}\right]^2 + (\omega\eta/2G_\infty)\right\}^2} \tag{2.43}$$

$$G'' = \frac{2G_\infty(\omega\eta/2G_\infty)\left[1 + (\omega\eta/2G_\infty)^{\frac{1}{2}}\right]}{\left\{\left[1 + (\omega\eta/2G_\infty)^{\frac{1}{2}}\right]^2 + (\omega\eta/2G_\infty)\right\}^2} \tag{2.44}$$

$$J' = \frac{1}{G_\infty} + \frac{1}{(\omega\eta G_\infty/2)^{\frac{1}{2}}} \tag{2.45}$$

$$J'' = \frac{1}{\omega\eta} + \frac{1}{(\omega\eta G_\infty/2)^{\frac{1}{2}}} \tag{2.46}$$

Finally, the dynamic viscosity is given by

$$\eta' = \frac{G''}{\omega} = \frac{\eta\left[1 + (\omega\eta/2G_\infty)^{\frac{1}{2}}\right]}{\left\{\left[1 + (\omega\eta/2G_\infty)^{\frac{1}{2}}\right]^2 + (\omega\eta/2G_\infty)\right\}^2} \qquad (2.47)$$

The variations of the storage modulus, the loss modulus and the dynamic viscosity with frequency, calculated according to equations (2.43), (2.44) and (2.47), are graphically displayed in Figure 2.4. As compared with the results for a Maxwell element, displayed in Figure 2.2, the B. E. L. liquid model has a longer relaxation time. This is consistent with the results of previous correlations based upon distributions of Maxwell elements.

The curves plotted through the data points of Figure 2.3 are calculated according to the B. E. L. liquid model from equations (2.41) and (2.42). There is excellent agreement with the experimental results.

2.5 Relationship of Continuous and Oscillatory Shear

Dyson [15] has had considerable success in correlating the results of elastohydrodynamic lubrication experiments with the properties of fluids experimentally determined in oscillatory shear. Dyson bases his comparison on a simplification of Oldroyd's [39] theory of the steady motion of an idealized liquid.

The analysis postulates that a simple continuous shear deformation includes a rotation of the liquid elements. It is therefore necessary to refer all equations that describe its viscoelastic behavior in continuous shear to reference axes which rotate with the element of fluid. The rotating axes yield additional time derivative terms in the equation of motion of the fluid and thus additional deformations. These equations are solved subject to the velocity boundary conditions,

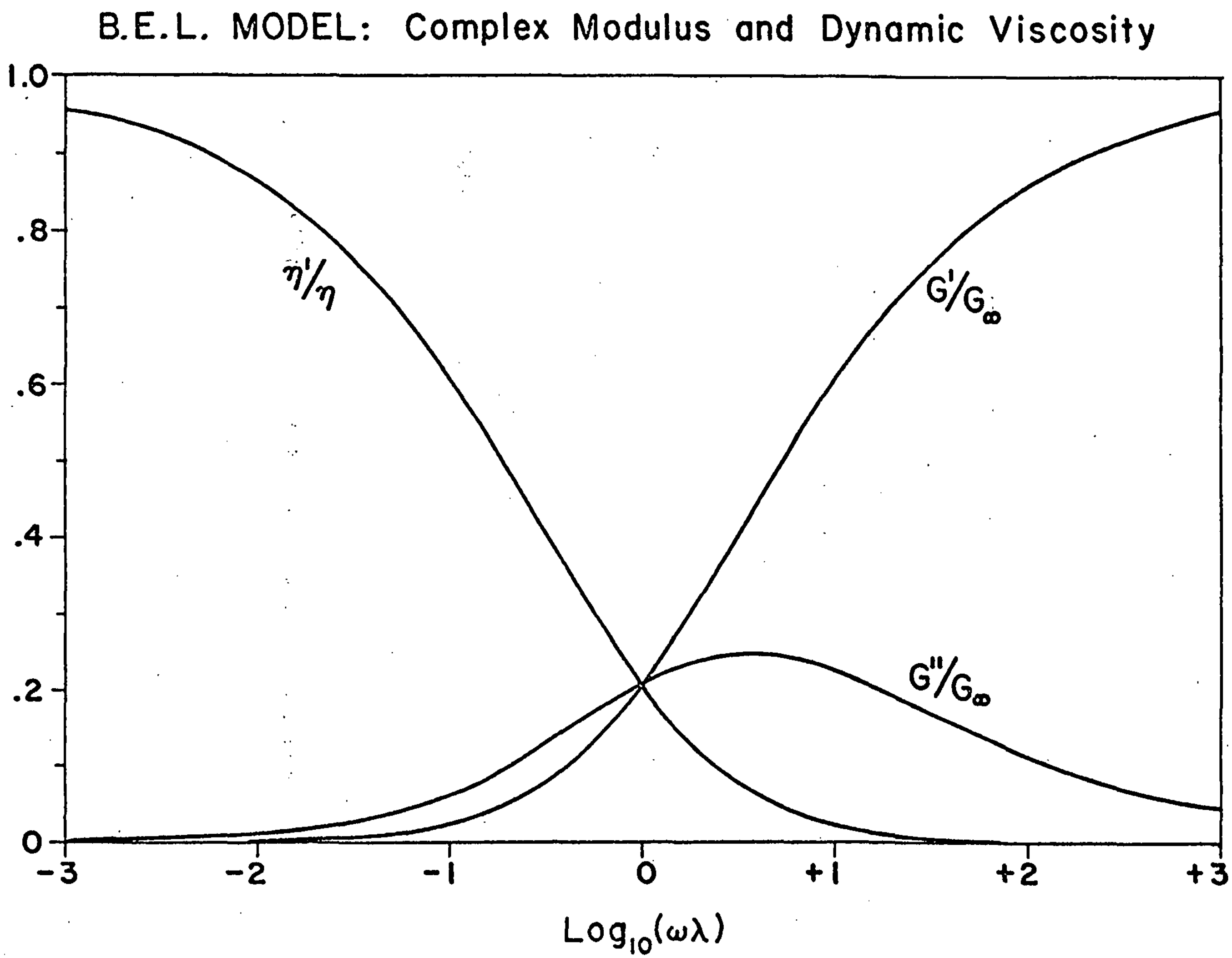

Figure 2.4. The frequency variation of the modulus components and the dynamic viscosity for the B. E. L. liquid model.

to determine the stresses in the fluid. Finally, the normal stresses are described with reference to the fixed axes.

Dyson's [27] simplification of the Oldroyd parameters permits the normal stresses for a fluid with relaxation time $\lambda = \eta/G_\infty$, in simple laminar shear, to be expressed in terms of one parameter K:

$$\frac{P_{xx}}{G_\infty} = \frac{2}{K^2} \cdot \frac{K^2D^2\lambda^2}{1 + K^2D^2\lambda^2} \tag{2.48}$$

$$\frac{P_{xy}}{G_\infty} = \frac{1}{K} \cdot \frac{KD\lambda}{1 + K^2D^2\lambda^2} \tag{2.49}$$

$$P_{yy} = P_{zz} = 0 \tag{2.50}$$

where P_{--} = normal stresses

G_∞ = limiting shear modulus

K = parameter of the analysis

λ = Maxwell relaxation time

D = shear rate

x = direction of flow

y = direction of velocity gradient

z = direction normal to both x and y

Equations (2.32) and (2.33), repeated below, have been derived for a Maxwell fluid subject to oscillatory shear.

$$\frac{G'}{G_\infty} = \frac{w^2\lambda^2}{1 + \omega^2\lambda^2} \tag{2.51}$$

$$\frac{G''}{G_\infty} = \frac{\omega\lambda}{1 + \omega^2\lambda^2} \ . \tag{2.52}$$

Dyson observed, as a result of the comparison of equations (2.48) and (2.49) with (2.51) and (2.52), that the shear stress P_{xy} is equal to 1/K of the value of G" at an angular frequency $\omega = KD$. Furthermore, one half of the normal stress difference, $\frac{1}{2}(P_{xx}-P_{yy})$, should be $1/K^2$ of the value of G' at an angular frequency $\omega = KD$. A comparison of the dynamic viscosity for continuous shear

$$\eta' = \frac{P_{xy}}{D} = \frac{\eta}{1 + K^2D^2\lambda^2} \tag{2.53}$$

with equation (2.34), the dynamic viscosity in oscillatory shear,

$$\eta' = \frac{G''}{\omega} = \frac{\eta}{1 + \omega^2\lambda^2} \tag{2.54}$$

shows the variation with shear rate D is the same as with angular frequency ω, with ω replaced by KD.

The hypothesis above is checked against the results of Russel [28] in Figure 2.5. The variation of apparent viscosity is shown for the same three fluids in both oscillatory and continuous shear. Note that the two curves begin to diverge at an abscissa value between 1 and 10. This corresponds to the conditions where G" reaches its maximum.

Whatever model is employed to represent the viscoelastic properties of the liquid, its application to continuous shear must be made in the rotating coordinate system. Therefore, the generalization of this analysis is stated as

$$\tau(D) = \frac{G''(\omega)}{K} \tag{2.55}$$

Dyson's application of equation (2.55) to the B. E. L. liquid model is compared with the experimental results of Smith [29] at low shear rates in Figure 2.6. Dyson [15] reports that a constant value of K = 7.5 shows good correlation over all Smith's experimental conditions.

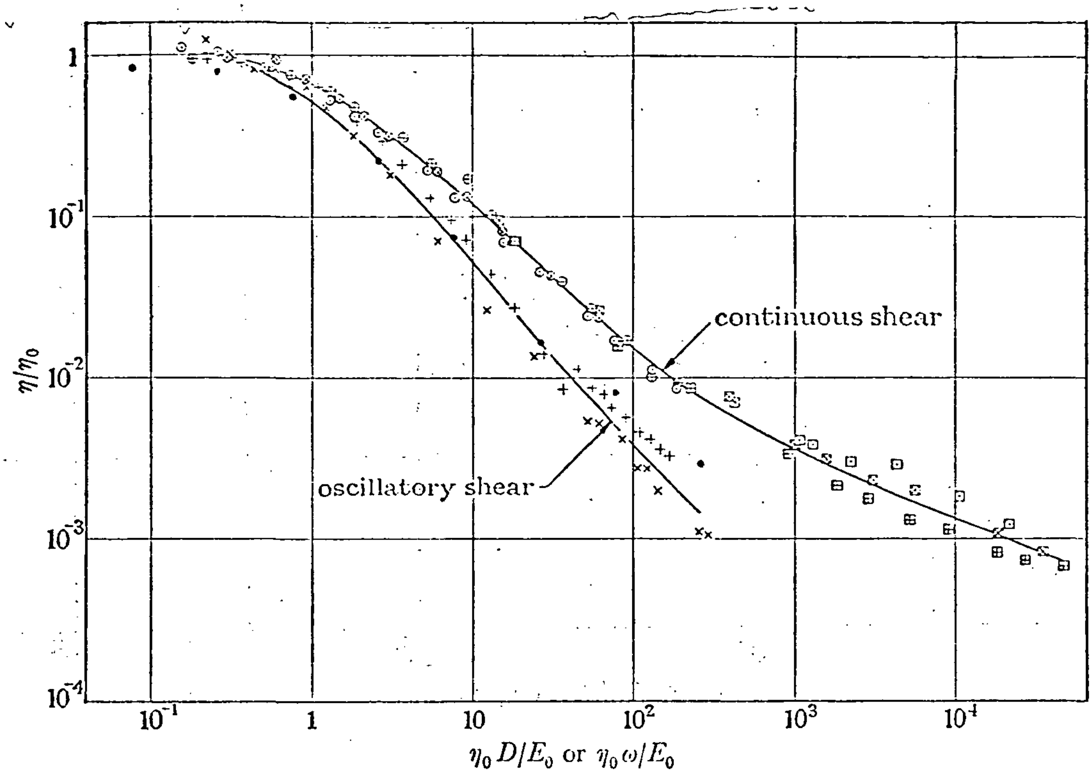

Figure 2.5. Comparison of variation of apparent viscosity in oscillatory and in continuous shear.

		AFGO/H	AFGO/L	SLW.10
oscillatory shear, η/η_0 against $\eta_0\omega/E_0$		×	•	+
continuous shear, η/η_0 against $\eta_0 D/E_0$	disks	⊗	⊙	⊕
	capillaries	⊠	⊡	⊞

E_o is a parameter of the order of G_∞. Curve from Dyson [27] .

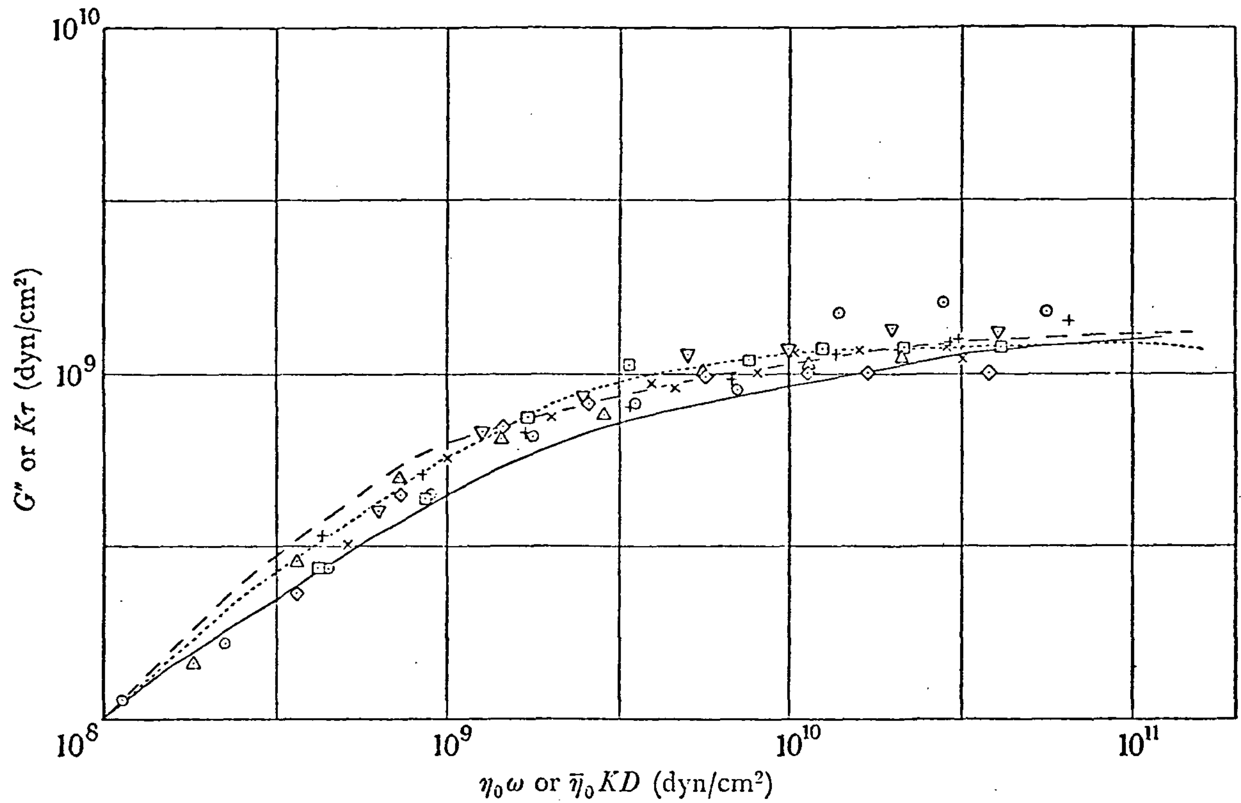

Figure 2.6

Comparison of results of Barlow & Lamb in oscillatory shear with those of Smith in continuous shear—mineral oils, steel surfaces.

Oscillatory shear G'' against $\eta_0\omega$ results of Barlow & Lamb [19] : ······, LVI mineral oil; – – –, MVI mineral oil; ——, HVI mineral oil.

Continuous shear $K\tau$ against $\eta_0 KD$ results of Smith [29] : (figure number in original reference):

	fig. 8		fig. 9		fig. 10
×	23 °C	▽	23 °C	□	25 °C
⊙	100 °C	+	100 °C	◇	100 °C
				△	190 °C

Curve from Dyson [27] .

As a result of equation (2.55), (G_∞/K), and not G_∞, will appear in the equations of motion. A new limiting shear modulus for continuous shear is now defined to include the Oldroyd-Dyson parameter K:

$$\bar{G}_\infty = (G_\infty/K) \tag{2.56}$$

2.6 Limiting Shear Stress

The Maxwell or B. E. L. liquid model, when applied to continuous shear, predicts a shear stress that rises to a maximum and then falls with increasing shear rate independent of thermal effects. This behavior is intuitively doubtful and Dyson [27] reviews the mathematical objections. It is suggested that this behavior would give rise to an unstable flow pattern. The correlation shown in Figure 2.5 suggests a transition to another mechanism of flow as the shear rate approaches the value which corresponds to a maximum shear stress. At this shear rate, the correlation between experimental and predicted values weakens.

As an alternative to the falling portion of the shear stress-deformation relation, the possibility of a limiting shear stress is suggested. The limiting shear stress is the maximum stress a fluid can transmit; an increase in the rate of shear can no longer cause an increase in the shearing stress. Smith [29] first suggested this behavior of a fluid analagous to plastic deformation of a solid. Plint's [13] results further suggest the existence of a limiting shear stress in an EHD fluid film. He interpreted the limiting shear stress to be the result of a discontinuous shear failure. Dyson [15] suggested the limiting shear stress be a function of the limiting shear modulus $\bar{G}_\infty$. Figure 2.7 shows this results in a good correlation with the experimental data of Johnson and Cameron [11] .

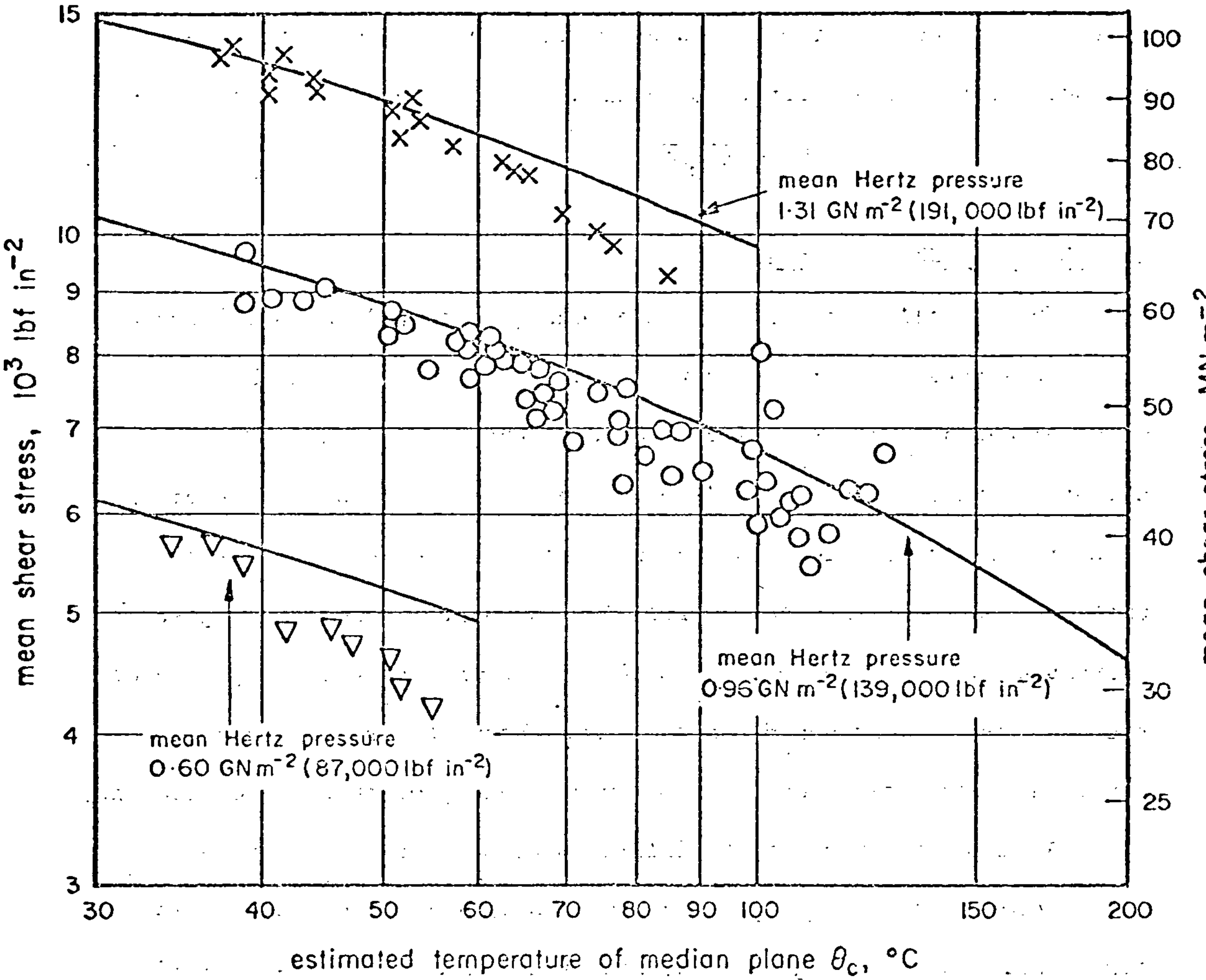

Figure 2.7. Dyson's correlation with the experimental data of Johnson and Cameron [11] at high shear rates. Curve from Dyson [15] .

Consequently, it is surmised that there are two mechanisms of flow for a liquid under the conditions of continuous shear. The material properties of the liquid, as well as the transition between these two mechanisms of flow, are continuous. The liquid model for continuous shear is, therefore, a composite non-linear shear stress-strain relation. It is comprised of a viscoelastic relation for shear rates up to the value predicting the maximum shear stress, and a limiting shear stress equal to this maximum at higher shear rates.

2.7 Hyperbolic Liquid Model

Barlow and Lamb [19] investigated the viscoelastic relaxation in three mineral oils of different viscosity index and composition. The experimental results, shown in Figure 2.8, show slight deviations from the B. E. L. liquid model. The experimental results are displaced to higher values of frequency and lower values of the loss modulus.

To add flexibility in the analysis, a "hyperbolic" shear stress-strain relation is used which allows easy changes in the limiting shear stress or the rate of rise to this limit. The relation has the additional feature of providing a smooth transition to the flow dominated by a limiting shear stress. The model is mathematically represented by

$$\Omega = \frac{-c^2}{\left(\frac{\tau}{\bar{G}_\infty} - c\right)} \left[1 + a\left(1 + \frac{c}{\left(\frac{\tau}{\bar{G}_\infty} - c\right)}\right)^2\right] - c \qquad (2.57)$$

where τ = shear stress

$\bar{G}_\infty$ = limiting shear modulus

$$\Omega = \frac{\eta}{\bar{G}_\infty}\frac{\partial u}{\partial y}, \text{ dimensionless shear rate} \qquad (2.58)$$

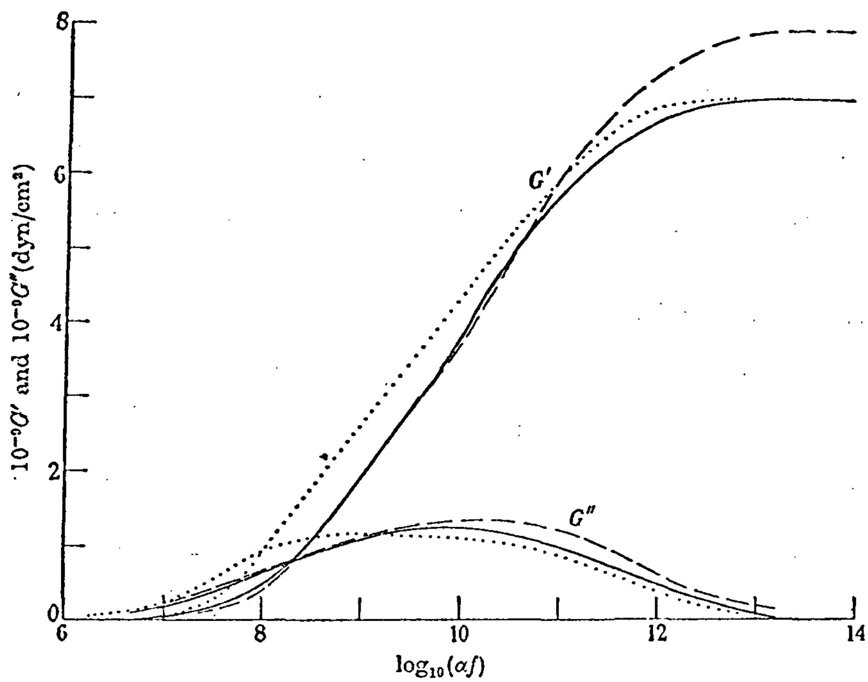

Figure 2.8. Components of the shear modulus calculated from measured values of Z' and Z": ——, h.v.i.; - - - -, m.v.i.; ····, l.v.i. Curve from Barlow and Lamb [19] .

c = limiting shear stress/limiting shear modulus ratio

a = rise parameter, rate of rise to limiting shear stress decreases as a increases

Four models of interest, the hyperbolic model for c = .25 and c = .20, and the Maxwell and B. E. L. - limiting shear models are illustrated in Figure 2.9.

The hyperbolic liquid model has the following limiting values:

$$\lim_{\Omega \to 0} \frac{\tau}{\bar{G}_\infty} = 0 \tag{2.59}$$

$$\lim_{\Omega \to 0} \left[\frac{d}{dD} \frac{\tau}{\bar{G}_\infty}\right] \cdot \bar{G}_\infty = \eta \tag{2.60}$$

$$\lim_{\Omega \to \infty} \frac{\tau}{\bar{G}_\infty} = c \tag{2.61}$$

$$\lim_{\Omega \to \infty} \left[\frac{d}{dD} \frac{\tau}{\bar{G}_\infty}\right] \tag{2.62}$$

For the case of a = 0, equation (2.57) reduces to the true hyperbola:

$$\Omega = \frac{c \dfrac{\tau}{\bar{G}_\infty}}{c - \dfrac{\tau}{\bar{G}_\infty}} \tag{2.63}$$

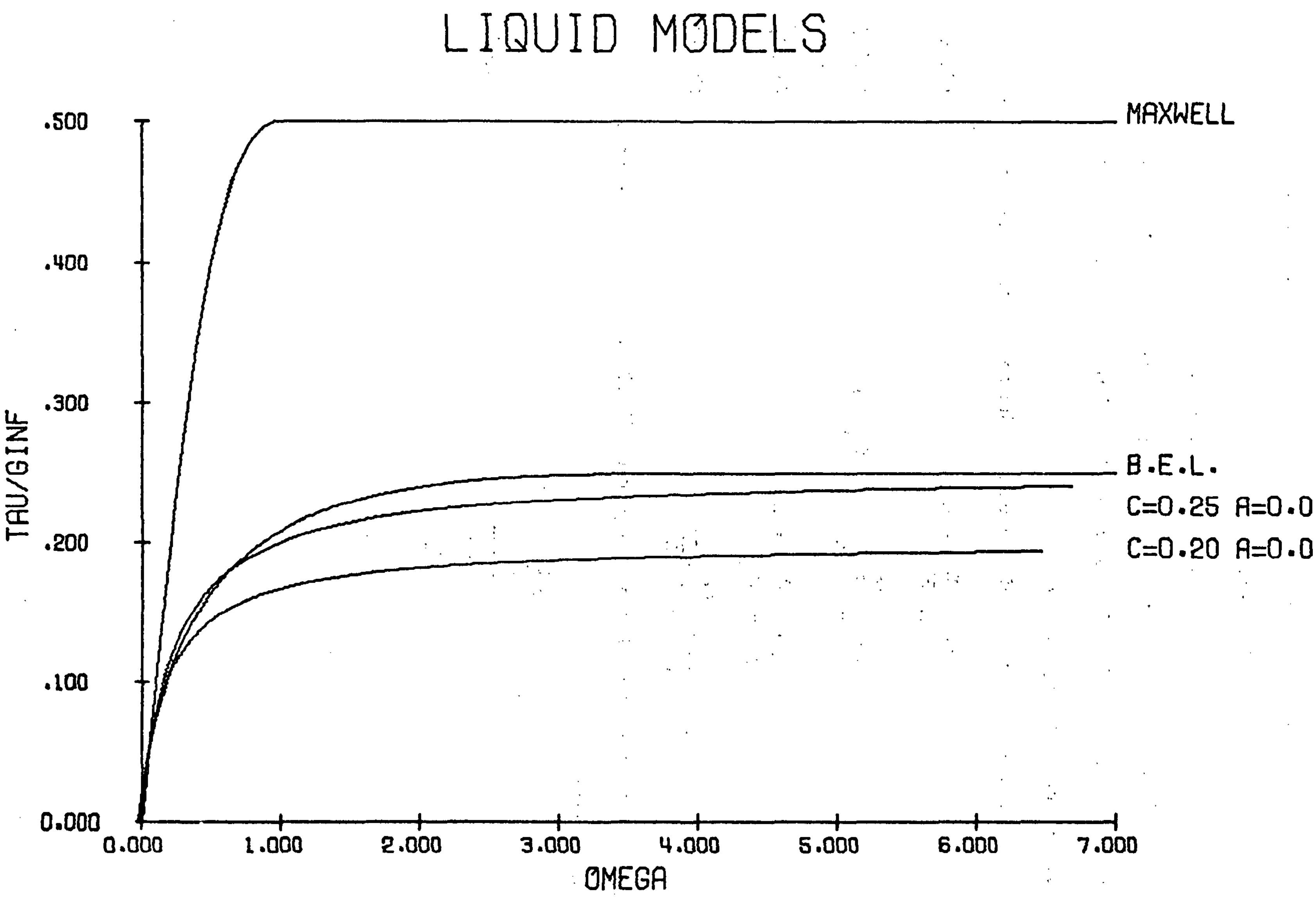

Figure 2.9. Comparison of liquid models.

CHAPTER III

TRANSIENT VISCOSITY

The maximum pressure in the lubricant film between highly loaded contacts may be as high as 250,000 psi. The lubricant film is therefore subjected to a large pressure transient as it passes through the contact, and the equilibrium viscosity at the maximum pressure is several orders of magnitude greater than the atmospheric pressure value.

Measurement of the tractional force between the two contact surfaces at low values of slip enables an "effective viscosity" of the lubricant to be calculated. At high rolling speeds, this effective viscosity is found to be lower than the value calculated from the equilibrium value of the viscosity as a function of pressure. The effective viscosity also decreases with increasing rolling speed, in a manner which is not adequately explained by either viscous heating of the lubricant film or by variation of the viscosity as a function of shear rate.

Fein [30] has suggested the failure of the lubricant viscosity to respond to the rapid pressure changes encountered in the contact area could be an explanation for the low values of effective viscosity which are observed. His analysis shows that under certain conditions the time of transit of the lubricant through the contact zone could be small compared with the time required for the lubricant to reach a state of equilibrium following an applied pressure step. Consequently, the compression of the lubricant never reaches the equilibrium state corresponding to the peak pressure, and the viscosity has a lower value than that measured under equilibrium conditions. An increase in the rolling speed reduces the residence time of the lubricant in the contact zone. This results in an even lower value for the viscosity attained by the lubricant, and a consequent decrease in the effective viscosity.

Chapter III is an analysis of the effect of compressional viscoelasticity on the pressure-induced viscosity changes that occur in concentrated contact lubrication. The variation of viscosity with time, following an applied step in pressure, is described by a nonlinear model proposed by Kovacs [16] for the volume creep of polymer melts.

3.1 Compressional Viscoelasticity

The response of a liquid to a rapid change in pressure consists of an instantaneous volume change, followed by a time-dependent volume change. The instantaneous change is attributed to the elastic compression of the liquid "lattice", while the time-dependent response is attributed to molecular rearrangements. The instantaneous response of the liquid, when the experimental time scale is small compared with the time required for molecular rearrangements, is characterized by a bulk modulus K_∞. When the experimental time scale is large compared with the molecular rearrangement time, the bulk modulus has a lower value, the equilibrium value K_o. This behavior may be represented by the simple models shown in Figure 3.1.

Model A is widely used when volume relaxation is investigated as a function of frequency. The overall modulus then rises from a low frequency value K_o to a high frequency limiting value $K_\infty = K_o + K_2$. K_2 is the high frequency value of the real part of the complex relaxational modulus, $K_r(j\omega) = K_r'(\omega) + i\,K_r''(\omega)$. For model A, the total bulk modulus is given by the expression

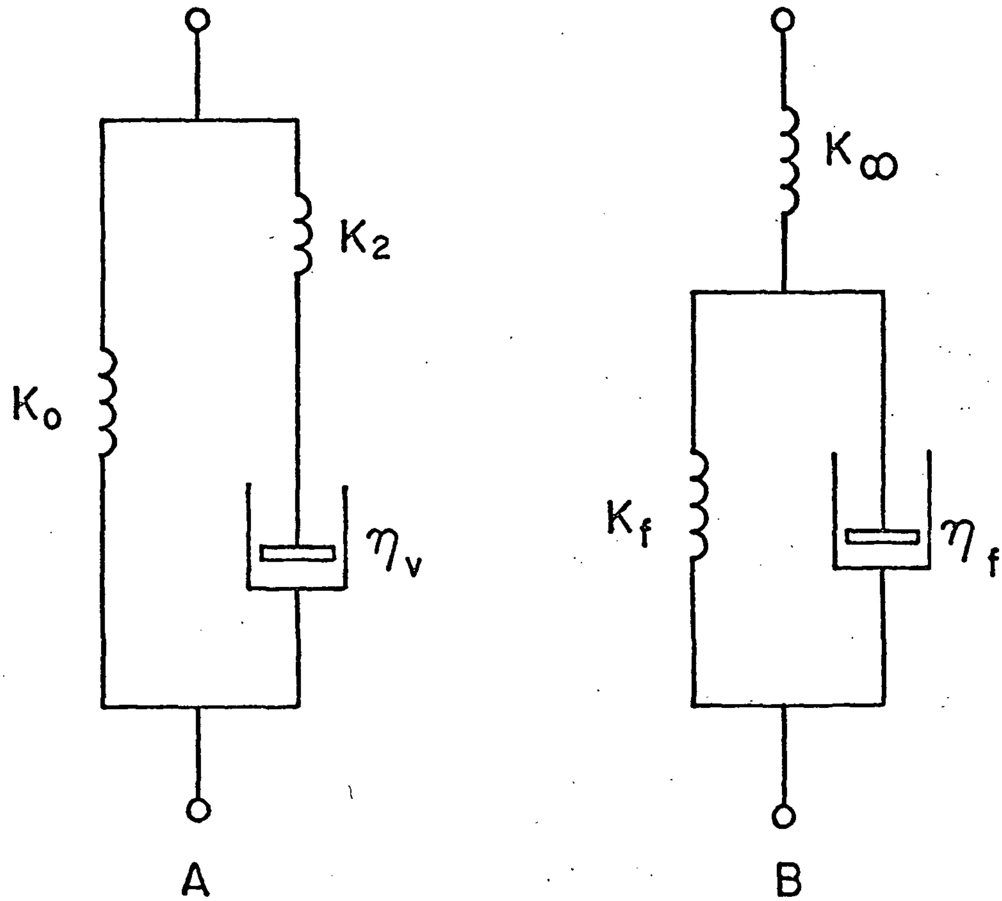

Figure 3.1. Models for compressional viscoelasticity.

$$K = K_o + K_r(i\omega) = K_o + K_2 \frac{i\omega\lambda_v}{1 + i\omega\lambda_v} \tag{3.1}$$

and the relaxation time

$$\lambda_v = \frac{\eta_v}{K_2} \tag{3.2}$$

where η_v = volume viscosity

ω = angular frequency

Model B is more suited to a description of the change in volume following a sudden increase in pressure, volume creep, since the instantaneous and time-dependent parts of the response are easily separated. The response is more simply expressed in terms of the over-all compressibility, the reciprocal of the bulk modulus, given by equation (3.3) as a function of frequency.

$$\frac{1}{K} = \frac{1}{K_\infty} + \frac{1}{K_f(1 + i\omega\lambda_f)} \tag{3.3}$$

K_f is a modulus associated with molecular rearrangements corresponding to changes in the free volume and λ_f is the retardation time given by

$$\lambda_f = \frac{\eta_f}{K_f} \tag{3.4}$$

The viscosity η_f is associated with the changes in the free volume. The low frequency or equilibrium modulus K_o is obtained from equation (3.3) for $\omega = 0$.

$$\frac{1}{K_o} = \frac{1}{K_\infty} + \frac{1}{K_f} \tag{3.5}$$

or

$$K_o = \frac{K_\infty K_f}{K_\infty + K_f} \tag{3.6}$$

Models A and B describe the same behavior and a comparison of equations (3.1) and (3.3) yields the following additional relations between the parameters of the two models:

$$K_\infty = K_o + K_2 \tag{3.7}$$

$$\eta_f = \eta_v\left(\frac{K_\infty}{K_2}\right)^2 \tag{3.8}$$

It follows from equations (3.5) and (3.7) that

$$\frac{K_f}{K_o} = \frac{K_\infty}{K_2} \tag{3.9}$$

The behavior of liquids is generally found to be more complex than that described by these simple models and a combination of several models, each with different time constant and moduli, is necessary. Alternatively, a continuous distribution of relaxation, or retardation, times may be used to characterize the liquid behavior. The introduction of a distributed spectrum causes considerable complication in the analysis and is not warranted in the present study. Model B of Figure 3.1 will be used to characterize the behavior of the lubricant.

3.2 Viscosity Response to a Pressure Step

The overall change in volume from an initial volume v_1 to a final volume v_2, caused by a pressure change P, is given by the definition of the secant bulk modulus K_o:

$$v_1 - v_2 = \frac{v_1 P}{K_o} \tag{3.10}$$

The volume change corresponding to the purely elastic deformation $(v_1 - v_i)$ is given by

$$v_1 - v_i = \frac{v_1 P}{K_\infty} \tag{3.11}$$

Equation (3.10), with the aid of equations (3.5), (3.10) and (3.11), may be written as

$$(v_1 - v_i) + (v_i - v_2) = \frac{v_1 P}{K_\infty} + \frac{v_1 P}{K_f} \tag{3.12}$$

Therefore,

$$\frac{v_i - v_2}{v_1} = \frac{P}{K_f} \tag{3.13}$$

Equation (3.13) may be taken as a definition of K_f.

The time dependence of this volume change is given by the parallel spring and dashpot combination of model B. The response is governed by

$$P = \frac{\eta_f}{v_1}\frac{dv}{dt} + K_f \frac{v_i - v}{v_1} \tag{3.14}$$

Combining equations (3.13) and (3.14) yields

$$\frac{\eta_f}{K_f}\frac{dv}{dt} = v_2 - v \tag{3.15}$$

where v varies between v_i and v_2. For small changes in pressure, when η_f and K_f can be regarded as constants, equation (3.15) has the solution

$$v - v_2 = (v_i - v_2)\exp(-t/\lambda_f) \tag{3.16}$$

and the total response to the pressure step is

$$\frac{v_1 - v}{v_1} = P\left\{\frac{1}{K_\infty} + \frac{1}{K_f}\left[1 - \exp(-t/\lambda_f)\right]\right\} \tag{3.17}$$

where the retardation time $\lambda_f = \eta_f/K_f$.

However, for large pressure changes the parameters η_f, K_∞ and K_f can no longer be regarded as constants. In particular, the viscosity η_f may be expected to change by many orders of magnitude under the pressures occuring in the contact zone. There is considerable evidence from ultrasonic studies of liquids that the volume viscosity η_v, and hence η_f, is closely related to the shear viscosity η and has the same temperature dependence. Litovitz and Davis [31] and Tasköprülü, Barlow and Lamb [45] offer such evidence for liquids including lubricating oils. It is assumed here that η_f has the same dependence on the free volume as the shear viscosity. Then η_f is related to the free volume v_f by the Doolittle [24] equation:

$$\ln \eta_f = A + B/f \tag{3.18}$$

where $$f = \frac{v-v_o}{v_o}\text{, fractional free volume} \tag{3.19}$$

v_o = specific occupied volume

A,B = constants

The value of A is characteristic of the liquid; the value of B is usually close to unity. The occupied volume, a function of pressure, is assumed to be independent of time and thus is associated with the instantaneous bulk modulus K_∞. The variation of η_f with pressure is described by the parameter s, defined by

$$s = \ln\left(\frac{\eta_{f_2}}{\eta_f}\right) = B\left[\frac{1}{f_2} - \frac{1}{f}\right] \tag{3.20}$$

where f_2 is the final volume of the fractional free volume, and η_{f_2} is the final value of η_f, at pressure P. If no change in the fractional free volume occurs during the instantaneous compression, the initial value of s is

$$s_1 = \ln\left(\frac{\eta_{f_2}}{\eta_{f_1}}\right) = B\left[\frac{1}{f_2} - \frac{1}{f_1}\right] \tag{3.21}$$

where η_{f_1} and f_1 are the values of η_f and f at the initial equilibrium state when P = 0. The shear viscosity is also described by equations (3.18) and (3.20), so that

$$s_1 = \ln\left(\frac{\eta_2}{\eta_1}\right) \tag{3.22}$$

where η_1 and η_2 are the initial and final equilibrium values, respectively, of the shear viscosity η .

Following Kovacs [16] , if it is assumed that the occupied volume v_o remains constant after the initial compression, the parameter s is evaluated from its definition:

$$s = B\left[\frac{(v-v_2)v_o}{(v-v_o)(v_2-v_o)}\right] \tag{3.23}$$

Therefore, the differential dv is

$$dv = \frac{(v-v_o)^2}{Bv_o}\, ds \tag{3.24}$$

Equation (3.15) is written in terms of the parameter s with substitutions from equations (3.20) and (3.24):

$$-\frac{\exp(-s)}{s}\,\frac{(v-v_o)}{(v_2-v_o)}\, ds = \frac{dt}{\lambda_2} \tag{3.25}$$

Noting that

$$1 - \frac{sf_2}{B} = \frac{(v_2-v_o)}{(v-v_o)} \tag{3.26}$$

equation (3.25) becomes

$$\frac{\exp(-s)}{s}\,\frac{1}{1-\left(\frac{sf_2}{B}\right)}\, ds = -\frac{dt}{\lambda_2} \tag{3.27}$$

where λ_2 is a retardation time characteristic of the final equilibrium state, given by

$$\lambda_2 K_f = \eta_{f_2} = \eta_{f_1} \exp(s_1) \tag{3.28}$$

The term (sf_2/B) in equation (3.27) is typically much less than unity, so that the expression $(1-sf_2/B)^{-1}$ may be expanded to give

$$\frac{\exp(-s)}{s} ds + \exp(-s) \frac{f_2}{B} ds = - \frac{dt}{\lambda_2} \tag{3.29}$$

as the differential equation describing the time-dependent compression of the liquid. This may then be integrated from the initial value s_1 at $t = 0$ to an intermediate value s at time t:

$$Ei(-s_1) - Ei(-s) + \frac{f_2}{B}\left[\exp(-s)-\exp(-s_1)\right] = \frac{t}{\lambda_2} \tag{3.30}$$

where Ei is the exponential integral. The viscosity at time t is given by

$$\eta = \eta_2 \exp(-s) \tag{3.31}$$

Figure 3.2 shows the variation of viscosity with time predicted by equation (3.30) for the following parameters: $P = 200{,}000$ psi; $\eta_1 = 10^{-5}$ lbf-sec/in^2; $\eta_2 = 10^3$ lbf-sec/in^2; $f_2 = 0.05$; $B = 1$. These values are typical of those experienced by a lubricant in the contact zone of a heavily loaded rolling contact. For values of t of the order of λ_2 or less, the viscosity is seen to be significantly less than the equilibrium value.

3.3 Viscosity Response of a Lubricant to a Pressure Step

To determine whether the behavior described by equation (3.30) has a significant effect on the properties of the lubricant, values of the residence time of the lubricant in the contact and the retardation

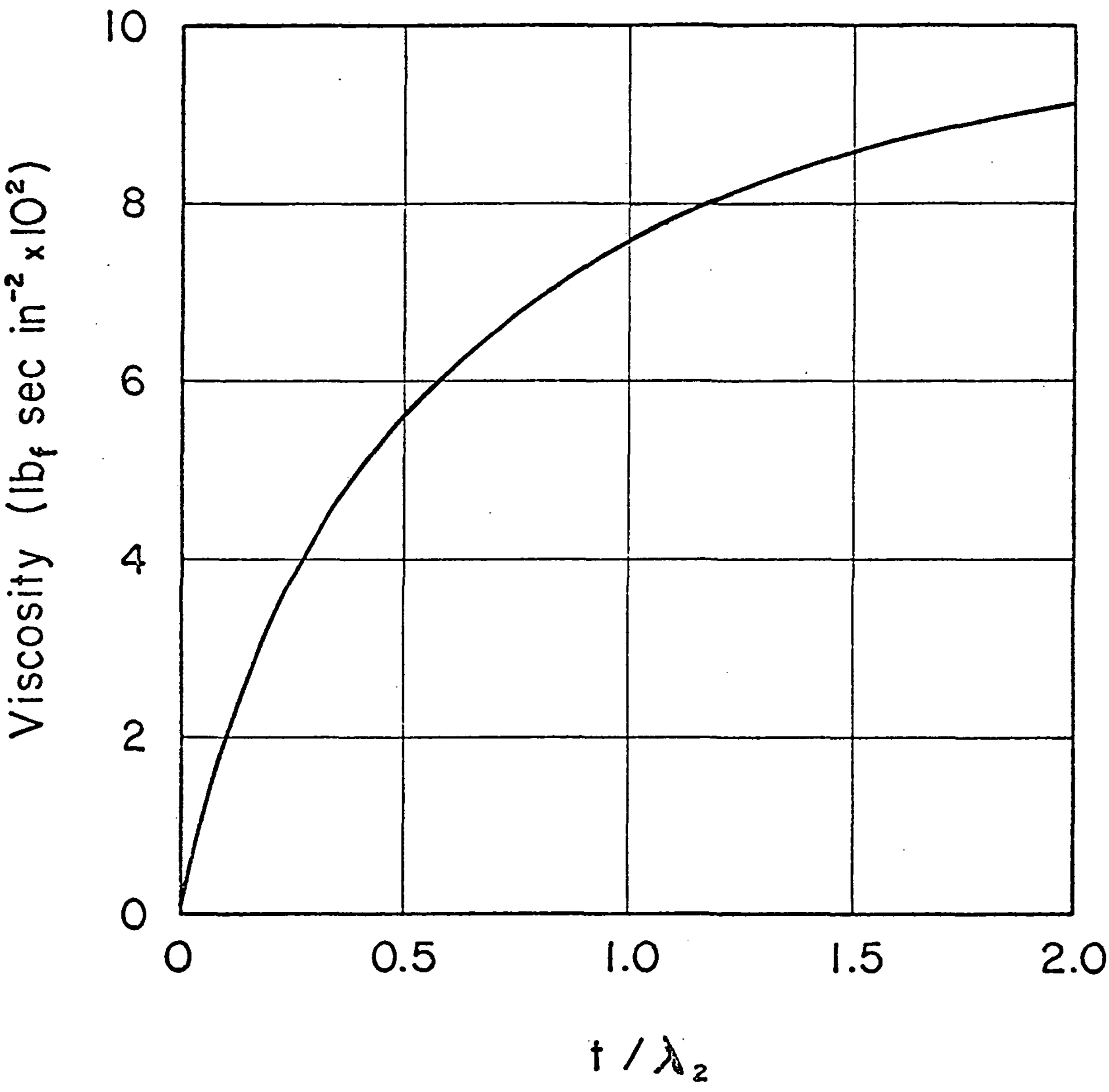

Figure 3.2. Variation of viscosity with time, following an applied pressure step. Initial viscosity = 10^{-5} lbf-sec-in^{-2}; final viscosity = 10^{3} lbf-sec-in^{-2}.

time λ_2 must be determined. The lubricant in a rolling contact is subjected to high pressure for a time equal to 2b/U where b is the half-width of the contact zone and U is the rolling speed. For typical values of $b = 10^{-2}$ in and $U = 100$ in/sec, the residence time is of the order of 10^{-4} sec.

The time constant λ_2 is characteristic of the final equilibrium state of the liquid. Values of η_f and K_f for lubricants are not available, but reasonable estimates may be made from ultrasonic data on other liquids. The viscosity η_f is related to the volume viscosity η_v by equation (3.8), $\eta_f = \eta_v(K_\infty/K_2)^2$. Litovitz and Davis [31] report that the ratio K_∞/K_2 is of the order of 3 for many liquids. Therefore, a value for $(K_\infty/K_2)^2$ of 10 may be used. Ultrasonic studies also indicate that η_v is closely related to the shear viscosity; a ratio of $\eta_v/\eta = 5$ has recently been reported by Barlow, Lamb and Taskoprulu [32] . The value of η_f is then given by $50\eta_1$, where η_1 is the atmospheric pressure shear viscosity. The time constant λ_2 is given by $\exp(s_1)\eta_f/K_f = 50\eta_2/K_f$. The bulk modulus K_f is related to the relaxational modulus K_2 by equations (3.7) and (3.9); for a ratio $K_f/K_o = K_\infty/K_2 = 3$, then $K_f = 6K_2$. But K_2 is experimentally found to be approximately equal to $4/3G_\infty$, where G_∞ is the high frequency limiting shear modulus of the liquid. A value for G_∞ of 4.35×10^4 psi (3×10^9 dyn. cm^{-2}) has been reported by Hutton [33] for a H.V.I. lubricating oil at 30 ^{o}C giving a value of K_f of 3.5×10^5 psi. This modulus will change significantly with pressure. Dyson [15] reports measurements of G_∞ as a function of pressure give a typical value for $\partial G_\infty/\partial P$ of 3, and K_o for lubricants varies in a similar manner in the Pressure-Viscosity Report [34] . If it is assumed that the ratio

K_f/K_o remains independent of pressure, then $K_f = (3.5 \times 10^5 + 9P)$ psi, and the retardation time λ_2 is given by

$$\lambda_2 = \frac{50\eta_2}{(3.5 \times 10^5 + 9P)} \tag{3.32}$$

For the values given above, λ_2 has a value of the order of 2×10^{-2} sec, which is much greater than the residence time of the lubricant in the contact zone. The "instantaneous viscosity" of the lubricant will therefore be much less than the equilibrium value, resulting in greatly reduced values of effective viscosity in accordance with experimental observations.

CHAPTER IV

MATHEMATICAL FORMULATION

The present analysis of traction in elastohydrodynamic contacts includes the iterative solution of the momentum and energy equations with the fluid properties functions of pressure and temperature. The shear rate and transient time effects have been isolated as discussed in Chapters II and III.

In this chapter the momentum and energy equations are developed and the pressure profile, the film thickness and the material property functions are discussed. The set of equations developed are then solved numerically.

4.1 Geometry and Coordinates

The geometry of a typical disk machine is shown in Figure 4.1. Two cylinders of radii R_1 and R_2, rolling with velocities U_1 and U_2, respectively, are separated by a lubricant film of thickness 2h. A closer view of the contact zone as shown in Figure 4.2 is more useful for the purposes of this analysis. The disks have deformed elastically to form a contact zone of width 2b and the film thickness is approximately constant with the surfaces of the disks remaining nearly parallel.

The coordinate system is defined to have the origin on the center lines of both the fluid film and the flat contact zone. The x-axis is the center line of the lubricant film with the positive direction in the direction of flow; while the y-axis, the perpendicular bisector of the flat contact zone, is arbitrarily taken positive toward the disk rolling with velocity U_2. The z-axis, not shown in Figure 4.2,

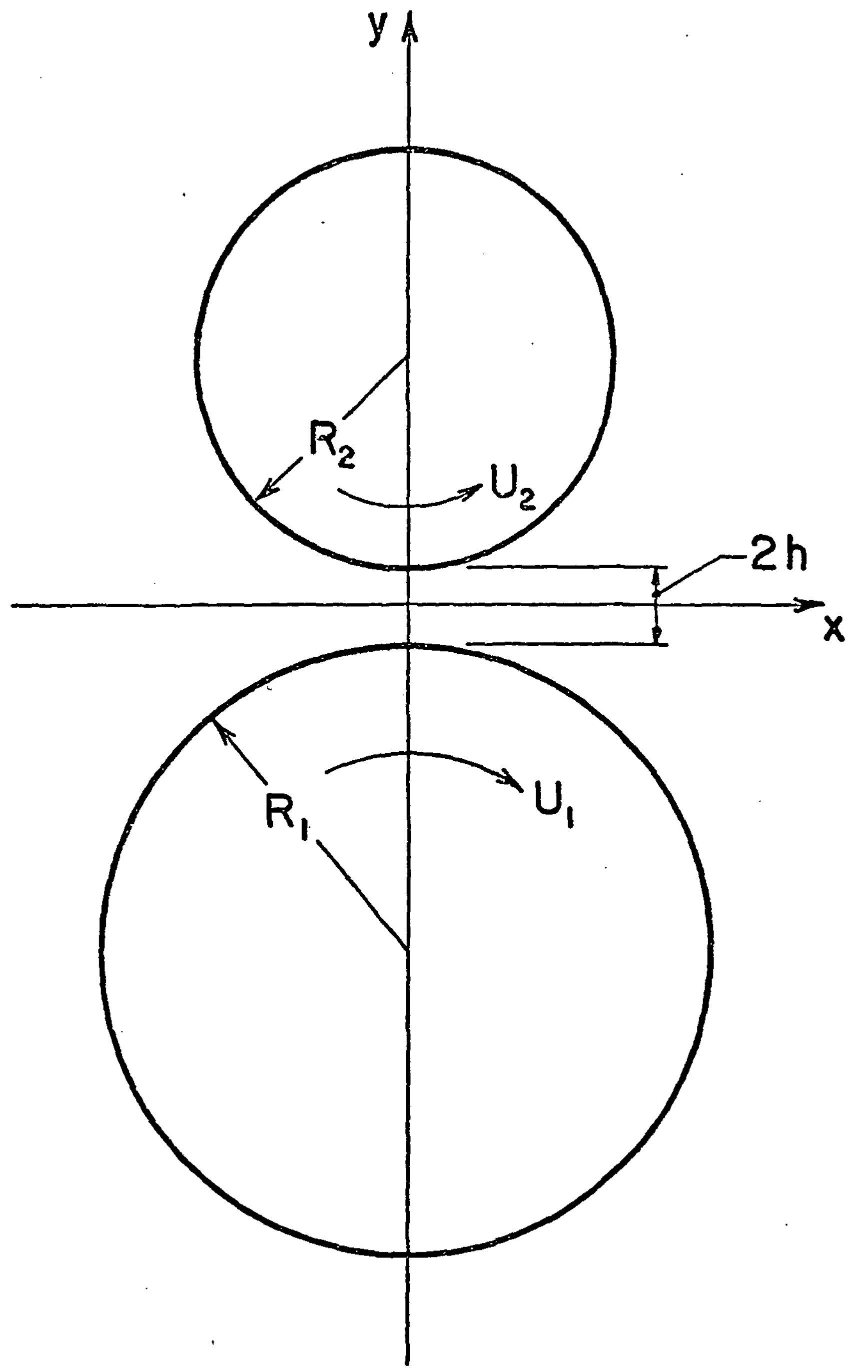

Figure 4.1. Typical disk machine geometry.

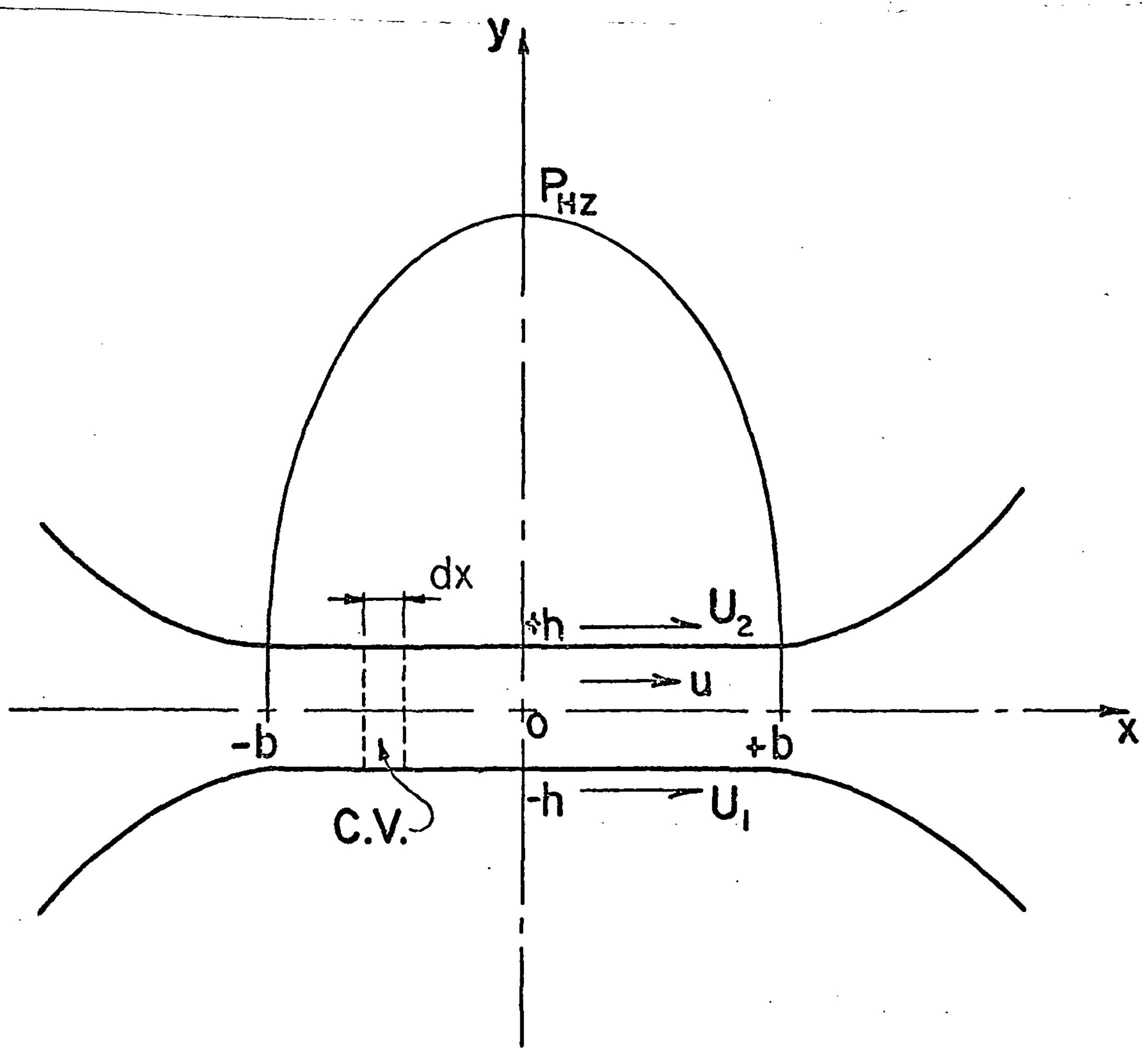

Figure 4.2. Contact zone geometry and Hertzian pressure profile.

is perpendicular to both the x and y-axes with the positive direction consistent with a right-handed Cartesian coordinate system.

The control volume of interest is defined as an element of fluid of length dx in the direction of flow, bounded by the disk surfaces in the y-direction and of unit thickness in the third direction.

4.2 Pressure Distribution

The pressure distribution in the contact zone is assumed to have the elliptical Hertzian dry contact profile given by

$$p(x) = p_{Hz}\sqrt{1 - \left(\frac{x}{b}\right)^2} \tag{4.1}$$

where p_{Hz} = maximum Hertzian pressure

x = distance from the center of the contact

$$b = \frac{4R\ p_{Hz}}{E} \tag{4.2}$$

= half Hertzian width

R = effective radius of the disks

E = effective modulus of elasticity

The deviations from this assumed distribution are mainly in the entrance zone at low pressure levels. Their effect on the sliding friction is very small and is neglected.

4.3 Film Thickness

The minimum film thickness in elastohydrodynamic contacts at moderate rolling speeds can be accurately predicted by the Dowson and Higginson [35] formula:

$$h_o = \frac{1.6\ \alpha^{0.6}\ (\eta_{ent}U)^{0.7}\ (E)^{0.03}\ R^{0.43}}{w^{0.13}} \tag{4.3}$$

where h_o = minimum film thickness

α = viscosity-pressure exponent

η_{ent} = viscosity of the lubricant at the conditions of entry to the contact

U = mean rolling speed

E = effective modulus of elasticity

R = effective radius of the disk pair

w = load per unit length of cylinder

Note that the minimum film thickness is only slightly dependent on the load w and virtually independent of the elastic modulus E.

Dowson and Higginson [36] suggest the parallel film thickness 2h is 20% greater than the minimum film thickness h_o.

The Dowson and Higginson prediction of film thickness is based on an isothermal analysis which is no longer adequate for heavily loaded contacts operating at high rolling speeds. Cheng [37] has calculated the lubricant film thickness in the Hertzian flat for high speed and heavily loaded rolling and sliding contacts. He used a Grubin-type inlet analysis including full thermal-hydrodynamic effects. The results obtained for a wide range of load, speeds and lubricant properties showed that the loss of film due to thermal effects is strongly influenced by the rolling velocity and the inlet viscosity of the lubricant, while it is somewhat insensitive to the change of load. The presence of sliding does not have a significant influence on the calculated film thickness, whereas the rolling speed has a far more predominant effect at the inlet.

The loss of film thickness due to thermal effects can be most conveniently represented by a thermal reduction factor Φ_T, which is defined as the ratio of the actual film thickness to that predicted by isothermal theory. Run #29 of Cheng's work is most applicable to the lubricant properties of this study and has been reproduced in Figure 4.3. Cheng's parameter Q_m is defined by

$$Q_m = \frac{2\eta_{ent} U^2}{k T_{ent}} \tag{4.4}$$

where η_{ent} = viscosity at entry conditions (lbf-sec/in^2)

U = average rolling speed (in/sec)

k = thermal conductivity of lubricant (Btu/$^{\circ}$F-hr-ft)

T_{ent} = temperature of lubricant at entry ($^{\circ}$R)

The film thickness including the thermal effects is calculated by multiplying the isothermal film thickness, based on the Dowson-Higginson formula, by the parameter Φ_T determined in Figure 4.3. For example, at a rolling speed of 500 in/sec at 175 $^{\circ}$F, equation (4.4) requires

$$Q_m = \frac{2(.87 \times 10^{-5})(500)^2}{(.0216)(635)} = .32$$

and Figure 4.3 determines the thermal reduction factor

$$\Phi_T = .81$$

Values for other conditions are similarly calculated. The results are shown in Table 4.1.

4.4 Momentum Equation

In applying the principle of conservation of momentum to the lubricant in the contact zone, we make the following assumptions:

1. For the case of a line contact, all the variables are independent of z, the direction of the axes of the disks.

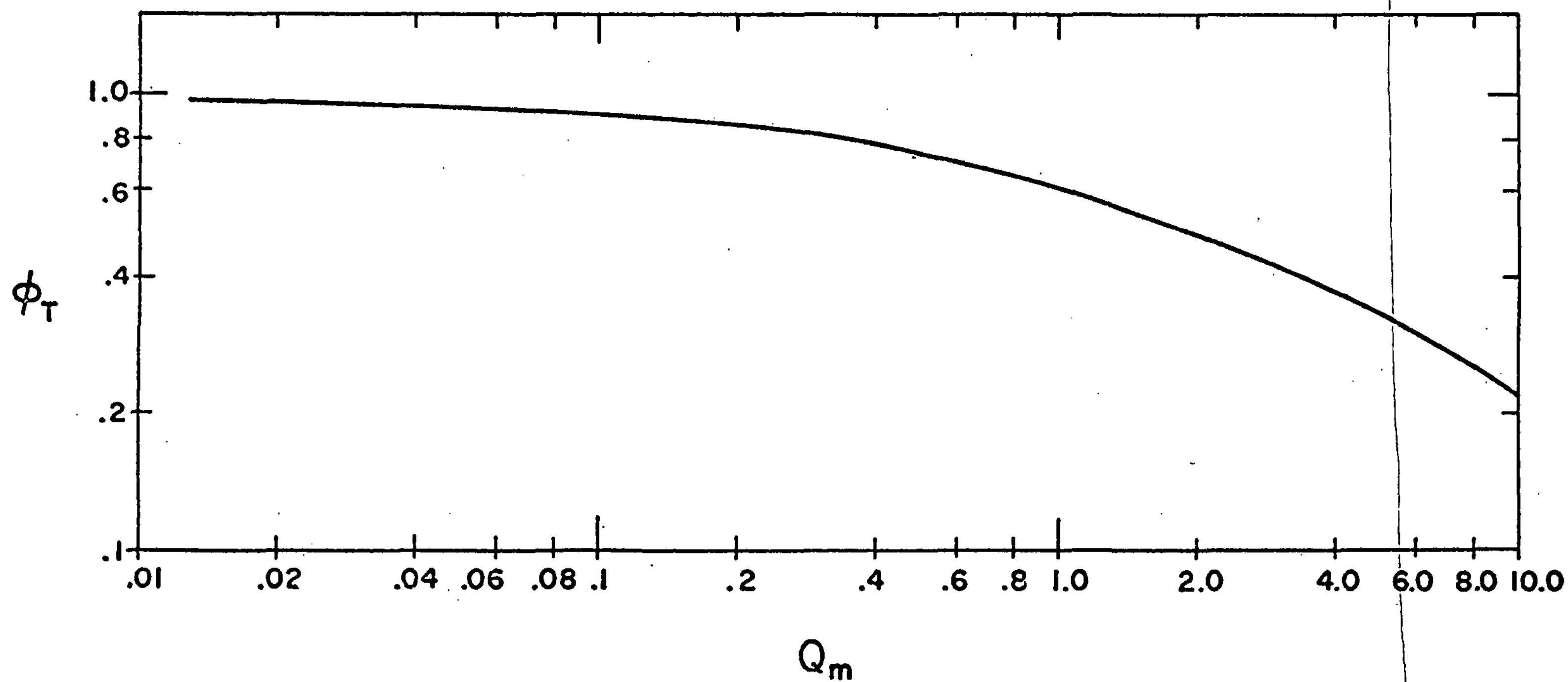

Figure 4.3. Curve for the determination of the thermal reduction factor Φ_T, taken from Cheng [37].

Table 4.1

VALUES OF THERMAL REDUCTION FACTOR AT

TYPICAL EXPERIMENTAL CONDITIONS

	175 °F	220 °F
500 in/sec	$Q_m = .32$ $\Phi_T = .81$	$Q_m = .15$ $\Phi_T = .89$
1000 in/sec	$Q_m = 1.27$ $\Phi_T = .58$	$Q_m = .60$ $\Phi_T = .72$

2. As compared with the lubricant film thickness, the radii of curvature of bearing components are generally very large. In the specific case of the disk machine, the radii of the disks R_1 and $R_2 \gg 2h$. Accordingly, all effects due to curvature of the fluid film are neglected.

3. As compared with the much larger pressure and viscous forces, the inertia and body forces of the lubricant are negligible. This imples that the pressure and viscous forces acting on the fluid are in equilibrium.

4. As compared with the other dimensions of a lubricated concentrated contact, the film thickness is very small. Therefore, the derivative of u with respect to y is large in comparison with all other velocity gradients.

5. The pressure gradient across the lubricant film is also insignificant due to the relative smallness of the film thickness. Accordingly, $p = p(x) \neq p(x,y)$.

The assumptions outlined above reduce the surface forces acting on a fluid element in the contact zone to those shown in Figure 4.4. The momentum equation can be derived directly from the balance of these surface forces. Equilibrium in the x-direction requires

$$\frac{dp}{dx} = \frac{\partial \tau_{xy}}{\partial y} \qquad (4.5)$$

The shear stress τ_{xy} must have two components. The rolling of the two cylinders produces the first component, while the second component results from the difference in rolling velocities, or slip. Consider a control volume bounded in the y-direction by the surfaces of the disks as shown below.

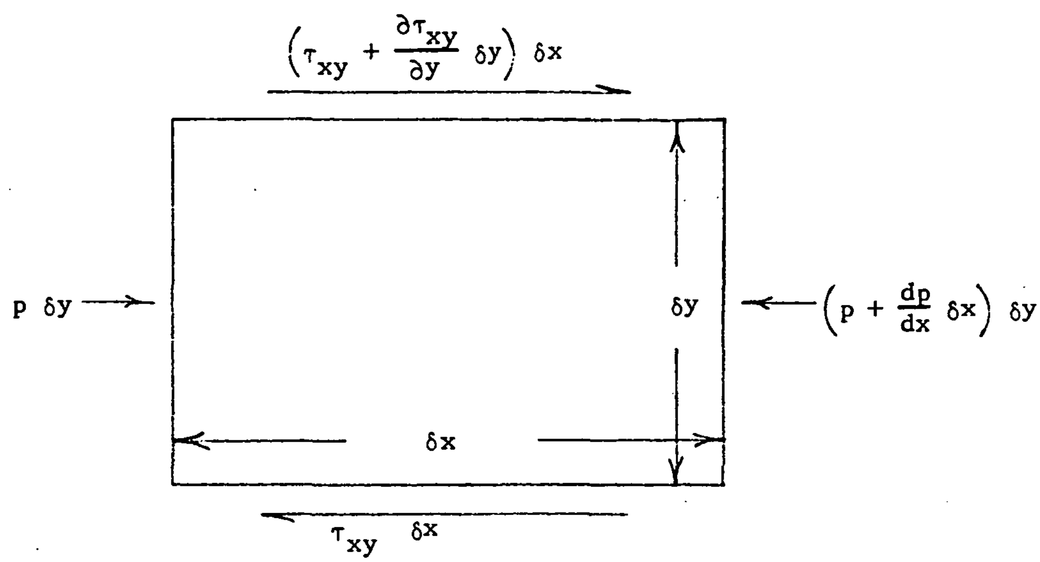

Figure 4.4. Surface forces acting on a fluid element.

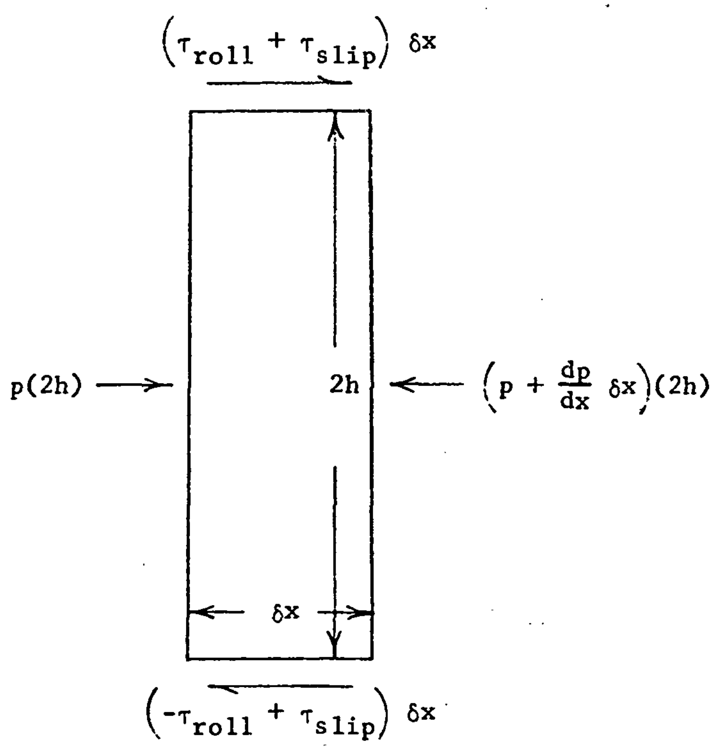

Figure 4.5. Forces acting on the control volume.

The size of the fluid element considered in Figure 4.4 can be increased to that of the control volume used in Figure 4.5 by integrating equation (4.5) with respect to y over the film thickness.

$$\int_{-h}^{+h} \frac{dp(x)}{dx}\, dy = \int_{-h}^{+h} \frac{\partial \tau_{xy}}{\partial y}\, dy$$

or

$$2h \frac{dp}{dx} = (\tau_{xy})_{y=h} - (\tau_{xy})_{y=-h}$$

$$h \frac{dp}{dx} = \tau_{roll} \tag{4.6}$$

Thus, the rolling component is independent of the slip and is a function of the pressure gradient through the contact zone. Only the component of stress that arises due to the relative sliding of the two disks is of interest in this study. This component is easily separated by neglecting the pressure gradient term of equation (4.5). For convenience, we redefine $(\tau_{xy})_{slip} = \tau$ and the final form of the momentum equation becomes

$$\frac{\partial \tau}{\partial y} = 0 \tag{4.7}$$

The shear stress τ is supplied by one of the rheological models considered for the lubricant. The form of the model is

$$\tau = f\left(\frac{\partial u}{\partial y}\right) \tag{4.8}$$

Therefore at any position x

$$\frac{\partial f\left(\frac{\partial u}{\partial y}\right)}{\partial y} = 0 \tag{4.9}$$

and

$$f\left(\frac{\partial u}{\partial y}\right) = C_1 \tag{4.10}$$

where C_1 is a constant of integration. When a specific model is used, one can isolate $\frac{\partial u}{\partial y}$ and integrate with respect to y from y = -h to y = h. Moreover, it is assumed that the profile for $\frac{\partial u}{\partial y}$ is symmetric with respect to the x-axis. The symmetry of $\frac{\partial u}{\partial y}$ allows the use of twice the integral from $y = 0$ to $y = h$ for evaluation of $U_1 - U_2$.

At the surface $y = h$, the fluid must have the same velocity as the disk. Therefore,

$$u = U_2 \quad \text{at} \quad y = h \tag{4.11}$$

Similarly, at the surface $y = -h$, the fluid will have a velocity $u = U_1$. Due to the symmetry of $\frac{\partial u}{\partial y}$, one can specify the velocity at the center line of the film as the boundary condition. Therefore,

$$u = \tfrac{1}{2}(U_1 + U_2) \quad \text{at} \quad y = 0 \tag{4.12}$$

4.5 Energy Equation

Figure 4.6 illustrates the energy transfer from the fluid element in the concentrated contact.

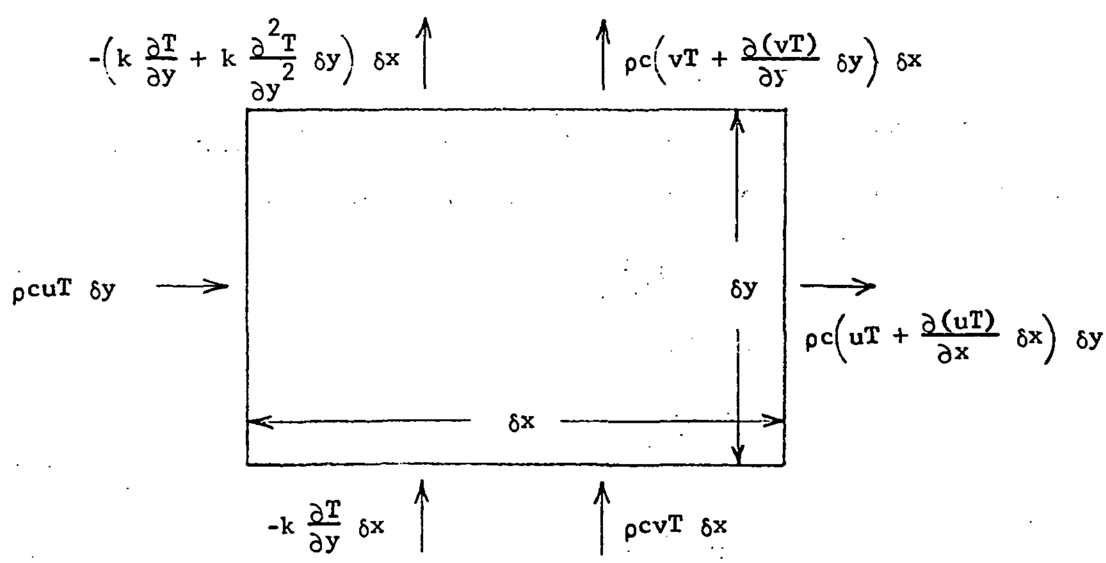

Figure 4.6. Energy balance for a fluid element.

It is assumed that the heat generated in the fluid element will be dissipated in two modes. Convection, the first mode of heat transfer, is the process by which energy is carried out of the contact zone with the lubricant. In the second mode, heat will be conducted across the film to the disks. Since the lubricant film thickness is small in comparison with the Hertzian contact width (x-direction) and even smaller in comparison with the cylinder width (z-direction), the temperature gradients in the x and z-directions must be small in comparison with those across the film. Therefore, only conduction in the y-direction is considered. These modes of energy transfer are shown for the fluid element in Figure 4.6.

The rate of heat generation per unit volume q is given by the product of stress with the rate of strain.

$$q = \tau \frac{\partial u}{\partial y} \tag{4.13}$$

An energy balance on this fluid element requires that the net energy into the control volume be zero.

$$\underbrace{-\rho c \frac{\partial(uT)}{\partial x} - \rho c \frac{\partial(vT)}{\partial y}}_{\text{Heat Transported to Control Volume}} + \underbrace{k \frac{\partial^2 T}{\partial y^2}}_{\text{Heat Conducted to Control Volume}} - \underbrace{\tau \frac{\partial u}{\partial y}}_{\text{Heat Generated in Control Volume}} = 0 \tag{4.14}$$

where T = temperature of the lubricant

ρ = density of the lubricant

c = specific heat of the lubricant

k = thermal conductivity of the lubricant

Continuity requires that

$$\frac{\partial u}{\partial x} + \frac{\partial v}{\partial y} = 0 \tag{4.15}$$

Therefore,

$$- \rho c\left(u \frac{\partial T}{\partial x} + v \frac{\partial T}{\partial y}\right) + k \frac{\partial^2 T}{\partial y^2} = -\tau \frac{\partial u}{\partial y} \qquad (4.16)$$

Convection   Cross-Convection   Conduction   Viscous Heat Generation

The ratio of convection to conduction is estimated, by assuming a triangular temperature profile, to be

$$\frac{\rho c U h^2}{2bk} \qquad (4.17)$$

Equation (4.17) demonstrates that convection will have its largest effect for a maximum value of (Uh^2/b). This corresponds to the condition of maximum rolling speed and minimum load.

For the thin lubricant films in EHD contacts, where $h \ll b$, the convective heat transfer can usually be neglected. Therefore, the governing energy equation may be written as a balance of viscous heat generation and heat transported by conduction.

$$k \frac{\partial^2 T}{\partial y^2} = -\tau \frac{\partial u}{\partial y} \qquad (4.18)$$

The consequences of this assumption are discussed in section 6.3.

The lubricant in contact with the disks assumes the surface temperature of the disks. Blok [38] has analyzed the problem of a moving heat source. His results demonstrate that the disk surfaces in the concentrated contact will have a mean "flash temperature" higher than the bulk temperature of the disk. Equation (4.19) is the expression Blok derived for the flash temperature.

$$T_s - T_b = \frac{0.48\ \mu w |U_1 - U_2|}{(k_m \rho_m c_m U\ b)^{\frac{1}{2}}} \qquad (4.19)$$

where T_s = mean surface temperature in the contact zone, "flash temperature"

T_b = surface temperature entering the junction, bulk temperature of the disk

k_m = thermal conductivity of the disks

c_m = specific heat of the disks

ρ_m = density of the disks

4.6 Equilibrium Viscosity Function

The equilibrium viscosity is the viscosity measured after the lubricant has reached a state of static equilibrium under a given temperature and pressure. Viscosity deserves special attention in the study of friction in concentrated contacts. Unlike other physical properties, which change only slightly with temperature and pressure, the viscosity of a lubricant can change by several orders of magnitude.

Viscosity is most simply defined by Newton's Law:

$$\tau = \eta\dot{\gamma} \tag{4.20}$$

where τ = shear stress (dynes/cm^2)

$\dot{\gamma}$ = shear rate (sec^{-1})

η = viscosity (Poise)

This can be generalized to equation (4.21) for a viscoelastic fluid.

$$\eta = \lim_{\dot{\gamma} \to 0} \left(\frac{\tau}{\dot{\gamma}}\right) \tag{4.21}$$

The viscosity of a liquid is basically the resistance of molecules to move past the force fields of neighboring molecules. It is a complicated pressure and temperature-dependent function.

The viscosity of a liquid and the rate of change of the viscosity due to a temperature change decrease with increasing temperature. An increase in temperature of the fluid increases the thermal agitation of the molecules which, in turn, lessens the forces of attraction between molecules. Thus the viscosity decreases.

The has been considerable effort to find an accurate relationship for predicting the variation of viscosity with temperature. Some of these relationships have theoretical foundations but the empirical formulas provide the most satisfactory predictions. The viscosity-temperature relationship found by Herschel [46] is

$$\log_{10}\left(\frac{\eta}{\eta_{ref}}\right) = \beta \cdot \log_{10} T \tag{4.22}$$

where η is the viscosity (centipoise) at the temperature T (^{o}F) and η_{ref} and β are constants. Thus the "Herschel Chart", a plot of equation (4.22) on log-log graph paper, is a straight line for a given lubricant. The equation is simple but Appeldoorn [40] has found it surprisingly accurate for oils of very different viscosities.

The viscosity-temperature data for Mobil XRM 109 F4 and Shell Turbo 33 is given in Table 4.2. This data determines the Herschel equations:

$$\log_{10} \eta = 8.974 - 3.2 \log_{10} T \tag{4.23}$$

for Mobil XRM 109 F4 and

$$\log_{10} \eta = 7.3409 - 2.8 \log_{10} T \tag{4.24}$$

for Shell Turbo 33. Both of the equations above may be plotted on log-log graph paper as shown in Figures 4.7 and 4.8 and used as convenient Herschel Charts.

The effect of pressure on viscosity is influenced by both the

TABLE 4.2

VISCOSITY-TEMPERATURE DATA

Mobil XRM 109 F4		Shell Turbo 33	
Viscosity (cP)	Temperature (^{o}F)	Viscosity (cP)	Temperature (^{o}F)
32,150.	0		
375.0	100	84	86
32.5	210	21	140
4.46	400	8.5	194

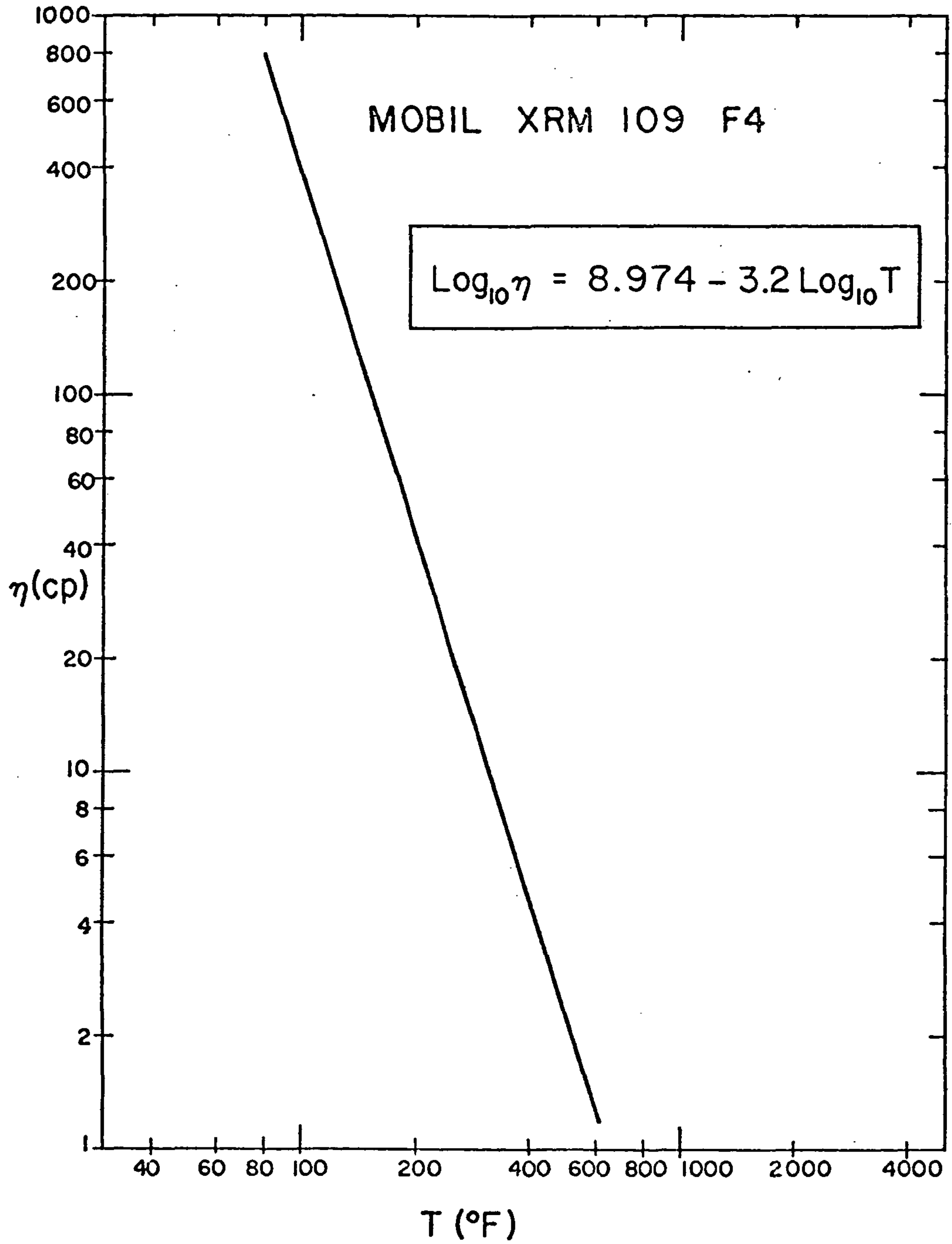

Figure 4.7. Herschel Chart for Mobil XRM 109 F4 calculated from equation (4.24).

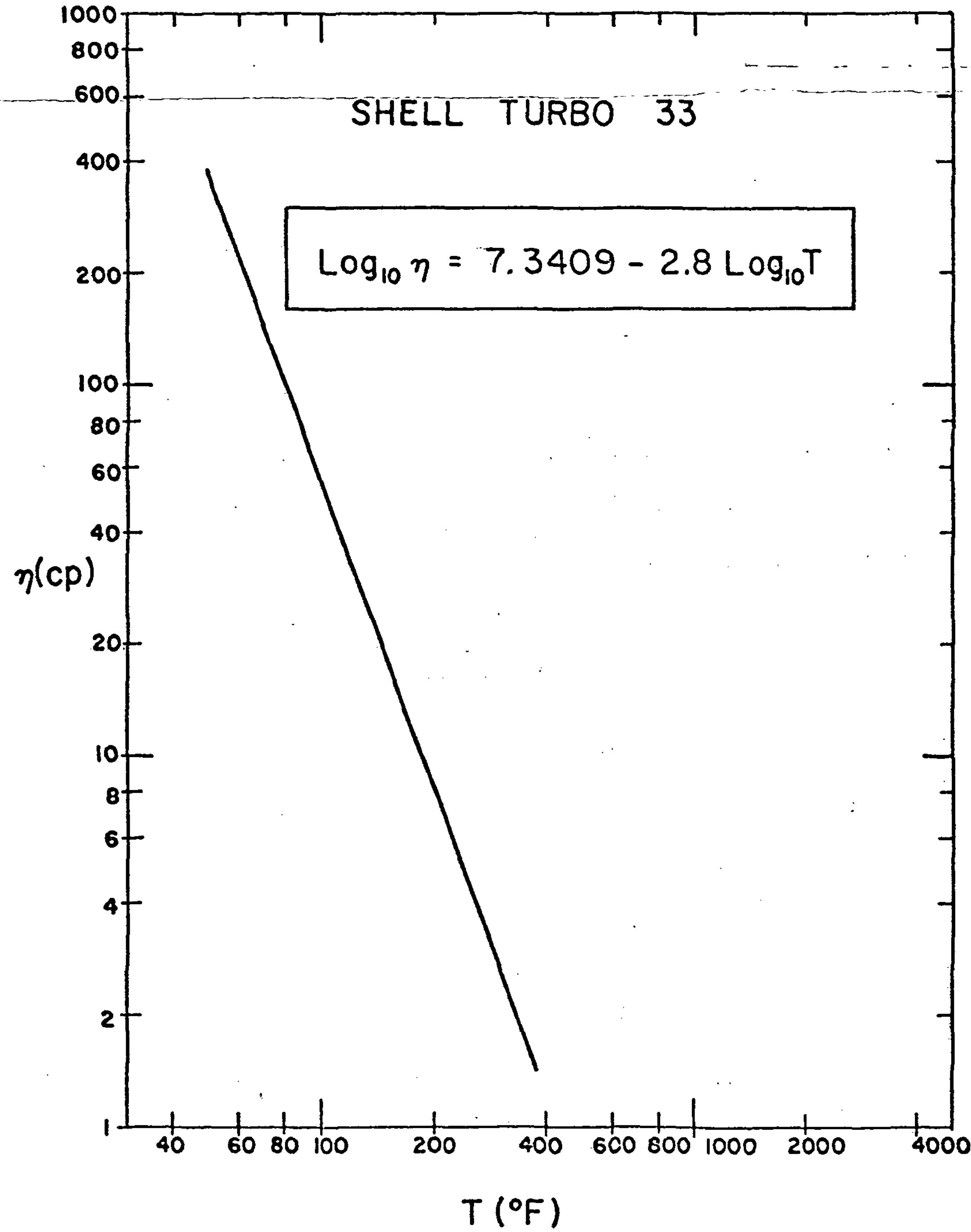

Figure 4.8. Herschel Chart for Shell Turbo 33 calculated from equation (4.25).

pressure level and the bulk viscosity of the fluid. The same increase in pressure will have a greater effect on the viscosity at a high pressure level than at a lower level. This results from the fact that more of the free space between molecules is already taken up at the higher pressure level. The same effect is responsible for a fluid of high viscosity undergoing a greater viscosity change than a fluid of lower viscosity for the same increase in pressure.

The Pressure-Viscosity Report [34] , which includes data on several paraffinic and napthenic mineral oils, pure hydrocarbons and synthetics, is an excellent source of pressure-viscosity data.

Chu and Cameron [41] have analyzed the results of this report in an attempt to find a sufficiently accurate pressure law and correlation. The usual simple exponential law was found inadequate for paraffinic oils. Paraffinics were found to obey the law

$$(\log_{10} \eta)^{3/2} = m(p + a) \qquad (4.25)$$

and there was a simple correlation between m and η_{base} the base viscosity. Including this correlation, equation (4.25) becomes

$$\log_{10} \eta = 0.18(\log_{10} \eta_{base})^{2/3} \left(p + 13.2 \sqrt{\log_{10} \eta_{base}}\right)^{2/3} \qquad (4.26)$$

where η = viscosity in centipoise at pressure p

η_{base} = base viscosity at p = 0

p = pressure in kpsi

Note that this convenient form of the Chu and Cameron viscosity-pressure law automatically correlates to each lubricant through η_{base}.

Cheng [37] has analyzed the data of the same Pressure-Viscosity Report. He used the following alternative viscosity-pressure relationship:

$$\frac{\eta}{\eta_o} = \exp\left[\alpha p + (\beta + \gamma p)\left(\frac{1}{T} - \frac{1}{T_o}\right)\right] \tag{4.27}$$

where η = viscosity at pressure p

η_o = reference to viscosity at p = 0 and T = T_o

p = pressure (psi)

T = absolute temperature (^{o}R)

α = viscosity-pressure coefficient

$\beta = 5.1 \times 10^7\ \alpha$

$\gamma = 930\ \alpha$

Figure 4.9 exemplifies the pressure dependence of the equilibrium viscosity function according to Cheng, and Chu and Cameron. It has been calculated for the Mobil XRM 109 F4 lubricant at 175 ^{o}F.

4.7 Limiting Shear Modulus

The pressure and temperature function for the high frequency limiting shear modulus has been developed by Dyson [15] in a correlation with Smith's [29] experimental data. The development is outlined below.

Hutton [33] experimentally determined that a high viscosity index mineral oil at atmospheric pressure varies with temperature according to

$$\frac{1}{G_\infty} = 2.52 + 0.024\ T \tag{4.28}$$

and referenced to conditions at 20 ^{o}C,

$$\frac{G_\infty(T)}{G_\infty(20^oC)} = \frac{3}{2.52 + 0.024\ T} \tag{4.29}$$

where G_∞ is in GNm^{-2} (10^{10} dynes/cm^2) and T is in ^{o}C.

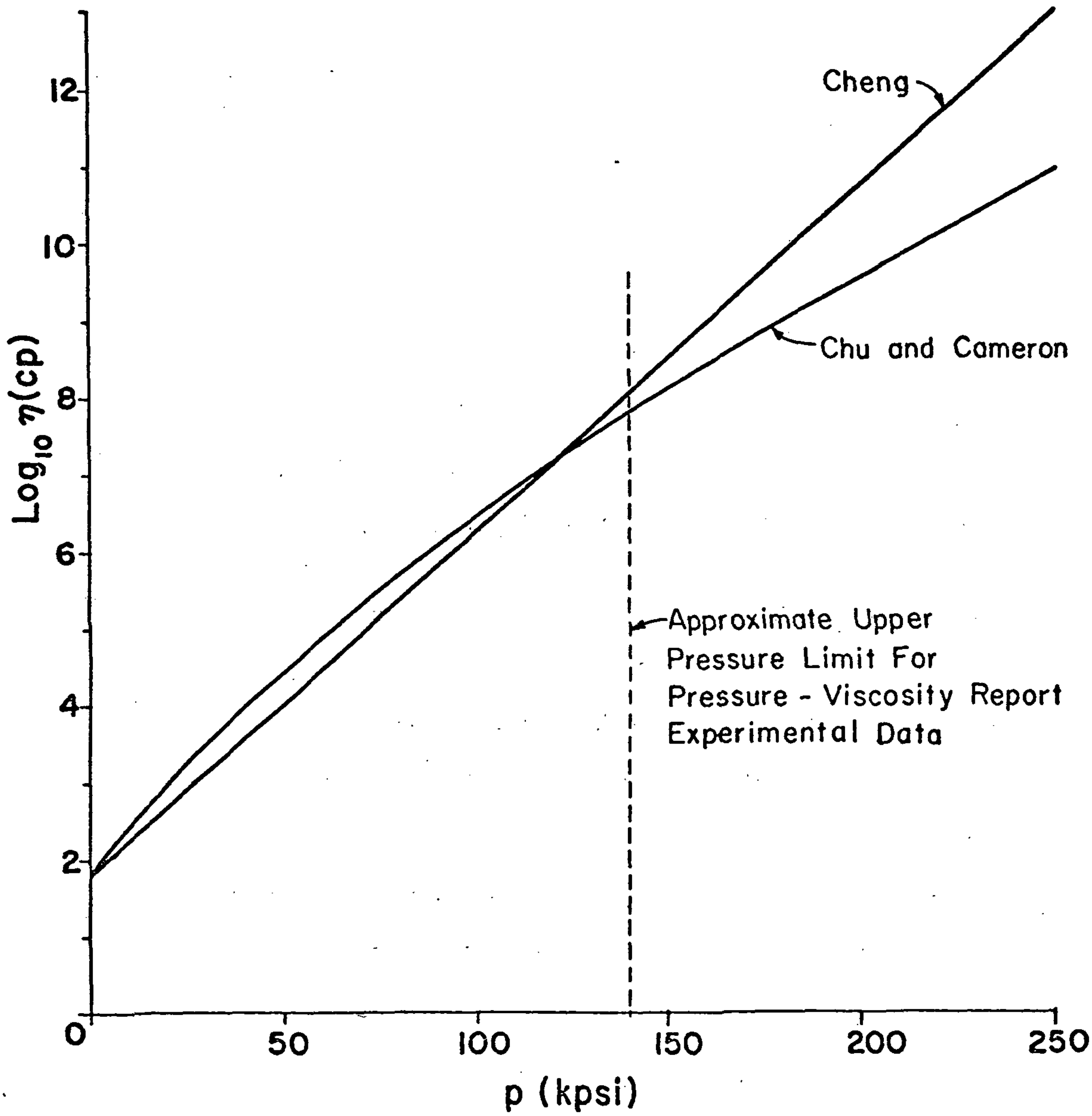

Figure 4.9. Example of $\eta(p)$ for XRM 109 F4 at 175 ^{o}F calculated from equations (4.26) and (4.27).

Variation with pressure of the high frequency limiting shear modulus is more difficult to estimate, since there is insufficient lubricant data at high pressures. Guided by equation (4.29), Dyson looked for a correlation of the shear modulus with the quantity

$$\frac{3p}{2.52 + 0.024\ T}$$

Figure 4.10 is the correlation found with Smith's experimental results. Although this correlation predicts an impossible negative value for $\bar{G}_\infty$ at p = 0, the predicted values at higher pressures are the best available. The limiting shear modulus function, as determined from Figure 4.10, is

$$\bar{G}_\infty(p,T) = 0.4 \left[\frac{3p}{2.52 + 0.024\ T}\right] - 10^8 \tag{4.30}$$

Converting equation (4.30) into English units, one obtains

$$\bar{G}_\infty(p,T) = \frac{1.2p}{2.52 + .0133(T-492)} - 1.45 \times 10^4 \tag{4.31}$$

where $\bar{G}_\infty$ is now in psi, p is in psi and T is in $^{\circ}$R. Equation (4.31) has been used in determining the limiting shear stress in the liquid models.

4.8 Numerical Solution

The numerical solution of the equations governing the friction in elastohydrodynamic lubrication is a Fortran IV coding for use on a CDC 6400 digital computer. The program is outlined in Figure 4.11 and a complete listing is given in Appendix B.

Program CONTROL is the backbone of the traction calculation calling on several subroutines as they are needed. The load is a Hertzian elliptical pressure profile, as developed in section 4.2, and the lubricant film of uniform thickness is calculated according to

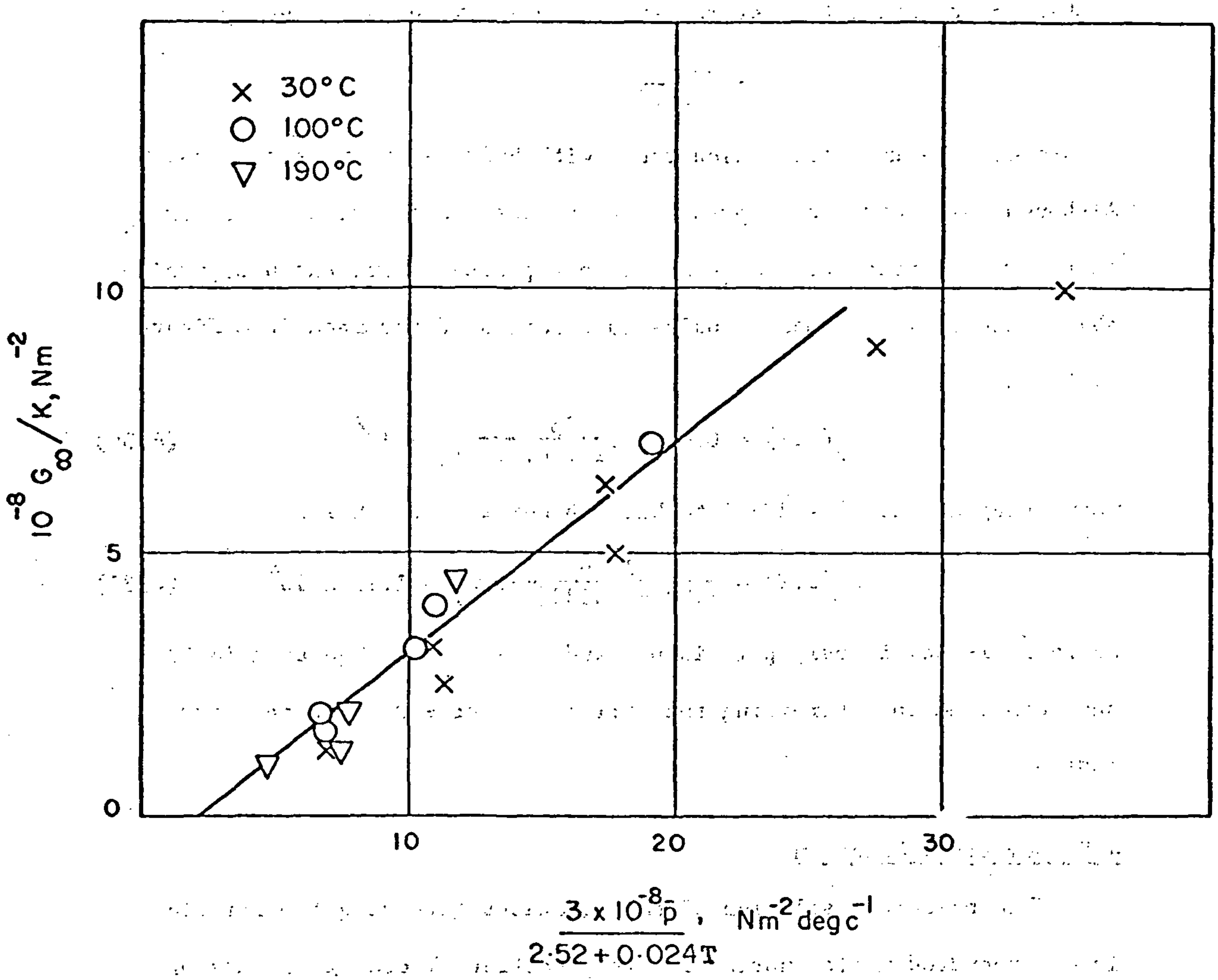

Figure 4.10. Correlation of limiting shear modulus with the experimental values of Smith [29]. Curve from Dyson [15].

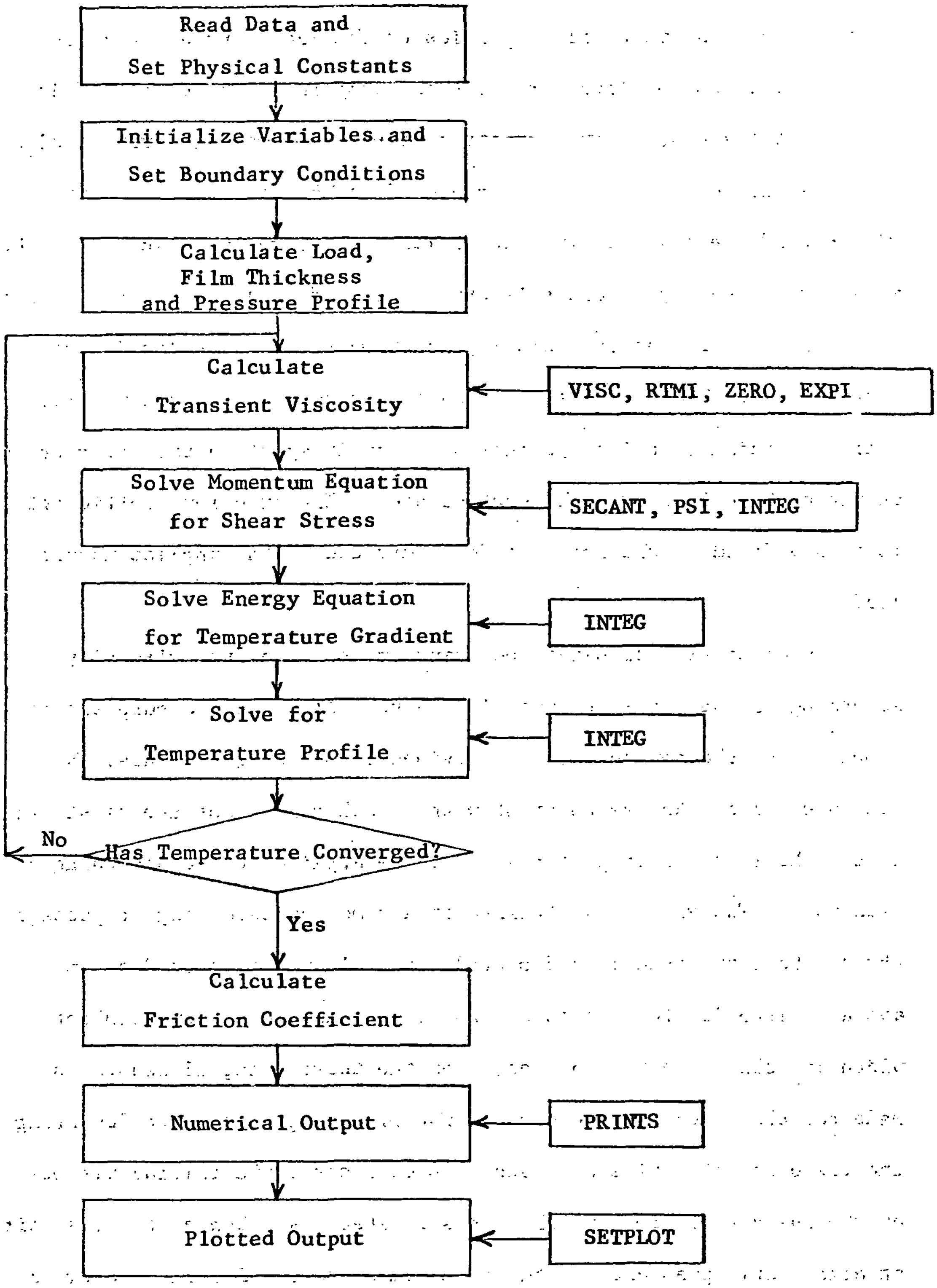

Figure 4.11. Simplified diagram of Program CONTROL and its subroutines.

section 4.3. The material properties of the lubricant are allowed to vary as functions of local pressure and temperature as discussed in sections 4.4 and 4.5. The variation of the lubricant properties also includes the shear rate effects proposed in Chapter II and the transient time dependence analyzed in Chapter III. An iterative solution of the momentum and energy balances (sections 4.6 and 4.7) is used to determine the shear stress, and the velocity and temperature profiles in the contact zone. The tractive force on a disk surface, resulting from a given sliding velocity, is determined by integrating the shear stress at the disk surface over the contact area. The traction coefficient is then defined as the tractive force divided by the applied normal load.

Function VISC supplies the transient value of the viscosity according to the model analyzed in Chapter III. For the purposes of computation, the contact area is divided into six equal zones, the pressure being taken as constant within each zone. For the first two zones, the pressure step is assumed to be applied at the beginning of each zone. The viscosity attained at a time corresponding to passage through half the zone is calculated, and this value is used as an average viscosity for the zone. For a rolling speed U and contact width 2b, this time is b/6U sec. For the third zone, allowance is made for the viscosity increase in the preceding zones by calculating the viscosity at a time b/2U sec. In each case, the initial viscosity, at the instant of applying the pressure step, is taken as the viscosity at atmospheric pressure and the disk temperature. For simplicity, a viscosity distribution which is symmetrical about the center of the contact is assumed, although the actual distribution is asymmetrical, with the maximum viscosity occurring on the exit side of the center. This approximate method provides a rapid and simple method of computing the effect of the rolling speed on the viscosity of the lubricant.

If the transient effect is to be neglected for any reason, the following trivial subprogram may be substituted for Subroutines VISC, RTMI, ZERO and EXPI.

```
FUNCTION VISC (P,ETA2,CODE)
VISC = ETA2
RETURN
END
```

Subroutine RTMI supplies the solution s_i of equation (3.30)

$$Ei(-s_1) - Ei(-s) + \frac{f_2}{B}\left[\exp(-s) - \exp(-s_1)\right] = \frac{t}{\lambda_2}$$

to Function VISC. Muller's iteration scheme of successive bisections and inverse parabolic interpolations is used. RTMI is available in the Vogelback Computing Center at Northwestern University. Its listing is included in Appendix B for completeness. It is a requirement of RTMI that equation (3.30) be represented as a separate function subprogram. Function ZERO meets this need.

The evaluation of the exponential integral in equation (3.30) is performed in Function EXPI. This routine computes the exponential integral for negative arguments in the range -20 to zero. For negative values of argument x the exponential integral is defined by

$$Ei(x) = \int_{-x}^{\infty} \frac{e^{-t}}{t}\, dt \qquad (4.32)$$

In equation (4.32), a polynomial approximation is obtained, for values of the argument between zero and -5, by means of the Taylor series expansion by Luke and Wimp [42] :

$$\mathrm{EXPI}(x) = \ln|x| - \sum_{v=0}^{14} b_v(-x)^v \qquad (4.33)$$

where

$b_0 = -.57721566$

$b_1 = 1.0$

$b_2 = -.25$

$b_3 = .055555520$

$b_4 = -.010216662$

$b_5 = .0016666906$

$b_6 = -.23148392 \times 10^{-3}$

$b_7 = .28337590 \times 10^{-4}$

$b_8 = -.30996040 \times 10^{-5}$

$b_9 = .30726221 \times 10^{-6}$

$b_{10} = -.27635830 \times 10^{-7}$

$b_{11} = .21915699 \times 10^{-8}$

$b_{12} = -.16826592 \times 10^{-9}$

$b_{13} = .15798675 \times 10^{-10}$

$b_{14} = -.10317602 \times 10^{-11}$

Equation (4.34) is the exponential approximation used for arguments in the range -5 to -20.

$$\mathrm{EXPI}(x) = -2.658760 \cdot 3^x \qquad (4.34)$$

Function PSI specifies the shear stress-strain relationship to be used in the momentum equation. The liquid model may be changed simply by replacing the deck of this function. Routines for the following three liquid models are included in the listing of the program:

1. Maxwell - Limiting Shear Stress Model

2. B. E. L. - Limiting Shear Stress Model

3. Hyperbolic Shear Stress-Strain Model.

The routine defines the function Ψ as

$$\Psi = \log_{10} \frac{2\int_0^h \frac{\partial u}{\partial y} dy}{(U_2 - U_1)} \tag{4.35}$$

where the velocity gradient $\partial u/\partial y$ is a function of the shear stress, and therefore, dependent upon the liquid model.

$$\frac{\partial u}{\partial y} = \frac{\bar{G}_\infty}{\eta} \cdot \frac{1 - \sqrt{1-4\left(\frac{\tau}{\bar{G}_\infty}\right)^2}}{2\frac{\tau}{\bar{G}_\infty}} \tag{4.36}$$

for the Maxwell model;

$$\frac{\partial u}{\partial y} \approx \frac{\bar{G}_\infty}{\eta} \left[55.2\left(\frac{\tau}{\bar{G}_\infty}\right)^2 + \frac{\tau}{\bar{G}_\infty}\right] \tag{4.37}$$

for the B. E. L. model; and

$$\frac{\partial u}{\partial y} = \frac{\bar{G}_\infty}{\eta} \cdot \frac{c\frac{\tau}{\bar{G}_\infty}}{c - \frac{\tau}{\bar{G}_\infty}} \tag{4.38}$$

for the hyperbolic model. The boundary conditions specified by equations (4.11) and (4.12) require

$$\int_0^h \frac{\partial u}{\partial y} dy = \frac{(U_2 - U_1)}{2} \tag{4.39}$$

Equations (4.35) and (4.39) combine to require

$$\Psi = 0 \tag{4.40}$$

Subroutine SECANT determines the shear stress solution of the momentum equation by solving equation (4.40). This routine is a modification of Newton's method. For any function f(x), two initial guesses of the root x_1 and x_2 are required. A straight line is "drawn" through $f(x_1)$ and $f(x_2)$ and extended to cross the x-axis. This new point x_3 determines $f(x_3)$ which is then connected with $f(x_2)$ to determine x_4, as depicted in Figure 4.12. This process continues until the root of the function is determined. A number of checks are also included in Subroutine SECANT to both guarantee and expedite convergence.

Subroutine INTEG integrates any non-equidistantly tabulated function $f(x_i)$ between the limits a and b, where a or b must equal $f(x_1)$. The integrated function may be defined as

$$\text{INTEG}\left[f(x_i)\right] = \int_a^b f(x_i)dx_i$$

A method of overlapping parabolas is employed with suitable modifications to yield the fastest possible integration with second order accuracy. The development of the quadrature for this subroutine is shown in Appendix A. Subroutine INTEG is called upon to integrate the velocity gradient in the solution of the momentum equation and again, to integrate both the Laplacian and temperature gradient in the solution of the energy equation.

Subroutine PRINTS provides the numerical output of the program, and Subroutine SETPLOT issues rapid line printer plotting of the temperature profiles and traction coefficient versus slip curves. SETPLOT is a library routine of Vogelback Computing Center and will probably require considerable changes in the coding for use at another facility. Since it is not required for the traction analysis, the listing for SETPLOT is not included with that of the program.

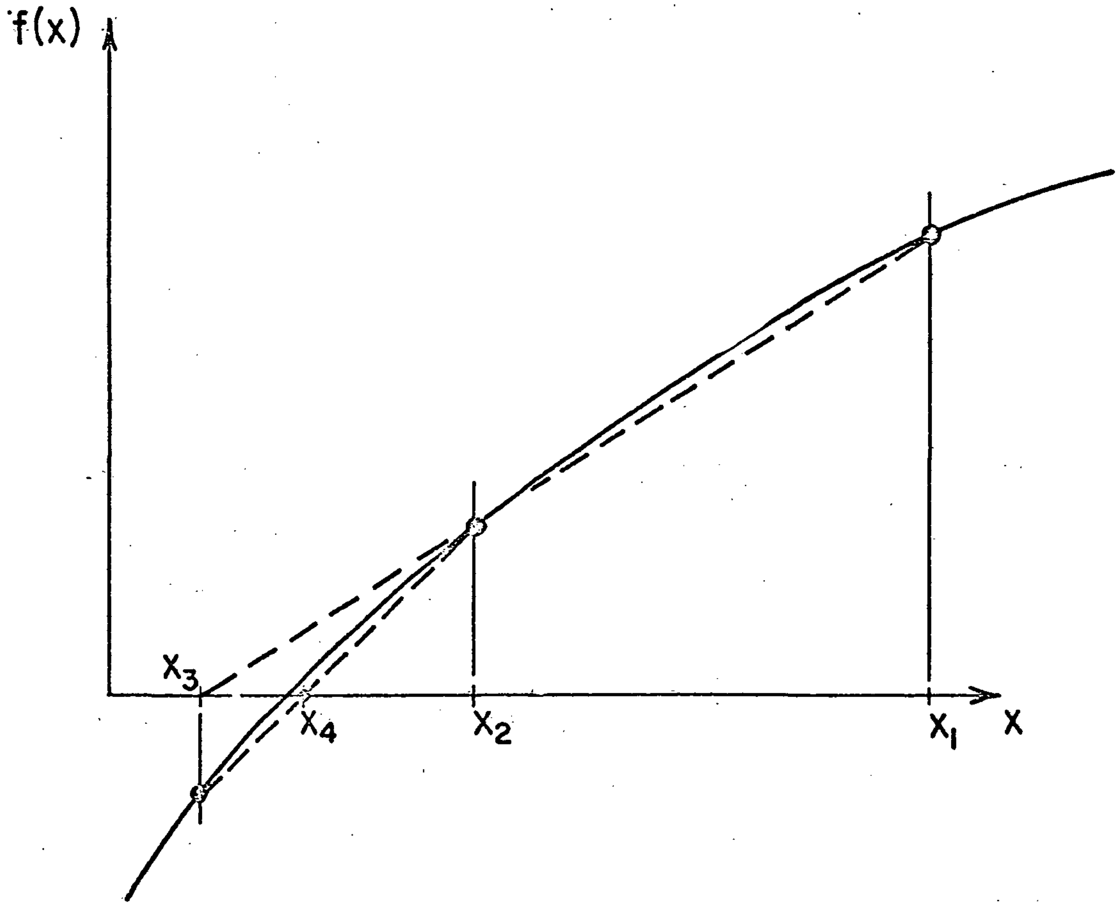

Figure 4.12. Secant method of solving f(x) = 0.

CHAPTER V

EXPERIMENTAL INVESTIGATION

The design and manufacture of a disk machine was completed as part of this study. The purpose of the experimental investigation was to gather extensive data for two new synthetic lubricants, Mobil XRM 109 F4 and Mobil XRM 177 F4. The conditions under study were those of high loads and high rolling speeds where there was a paucity of experimental data. Special emphasis was given to the effect of additives upon the frictional torque. This chapter describes the disk machine, the lubricant properties and the test procedure.

5.1 The Disk Machine

The design of the disk machine for this experimental investigation was guided by the following requirements. The disk machine must be capable of accurately measuring the tractive force transmitted across the line contact of the two disks for a wide range of loads, rolling speeds and slips. A sufficient normal load is required between the disks to insure operation in the elastohydrodynamic regime. The drive to the disks must allow easy adjustments of the mean rolling speed and the amount of sliding at the contact. The lubricant must be delivered to the contact at a controlled rate and temperature. Instrumentation is required to measure the normal and tangential forces on the disks. The angular velocities of the disks, as well as the slip or difference in the disk velocities, must also be accurately measured. Finally, the surface temperature of the disks as they enter the contact zone is required for an accurate knowledge of the friction. A detailed description of the machine designed to meet these requirements follows.

The disk machine, pictured in Figures 5.1 through 5.3, was designed with two 6-inch diameter disks. These large disks were selected to allow a direct drive system at high speeds, thus minimizing any possible vibrations. The lower disk is supported on two high-speed roller bearings which are mounted in the main frame and the upper disk is contained in a loading arm which is hinged on the frame with a spherical roller bearing.

The load is applied by an air cylinder at the far end of the loading arm. With a 30 psi air supply, a maximum Hertzian stress of 300,000 psi can be obtained for a $\frac{1}{4}$-inch contacting width. The applied normal load is monitored by a four-strain gauge bridge mounted on the air cylinder shaft. This is necessary for accurate measurement of the normal load, as the friction in the air cylinder is inconsistent. The loading arm was designed to permit the necessary alignment to insure a uniform load across the line contact in the axial direction.

Each of the disks is attached through flexible couplings to separate 40 hp D.C. field controlled electrical machines. The shunt-field current method of speed control is simple and efficient and the speed regulation, for a given speed adjustment, is excellent. The complete electrical circuit, schematically shown in Figure 5.4, is the Hopkinson mechanical-loss-supply feedback circuit described, for example, by Kloeffler, Kerchner and Brenneman [43] . This circuit was inspired by a related feedback system successfully used in the experiments of Jefferis and Johnson [12] . One of the D. C. machines behaves as a motor driving one of the disks. The second disk is driven by the friction force transmitted at the contact and drives

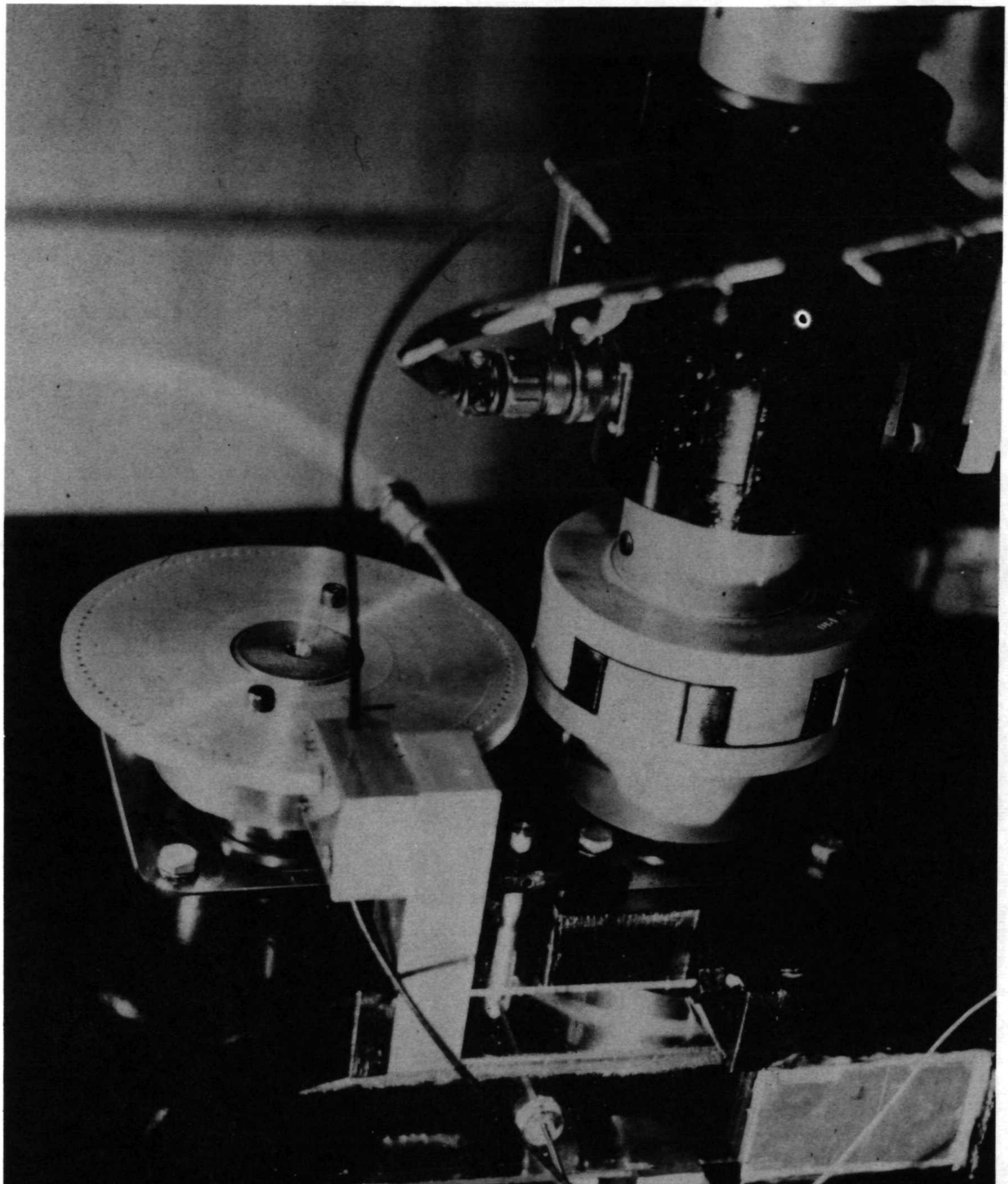

Figure 5.3. The disk machine.

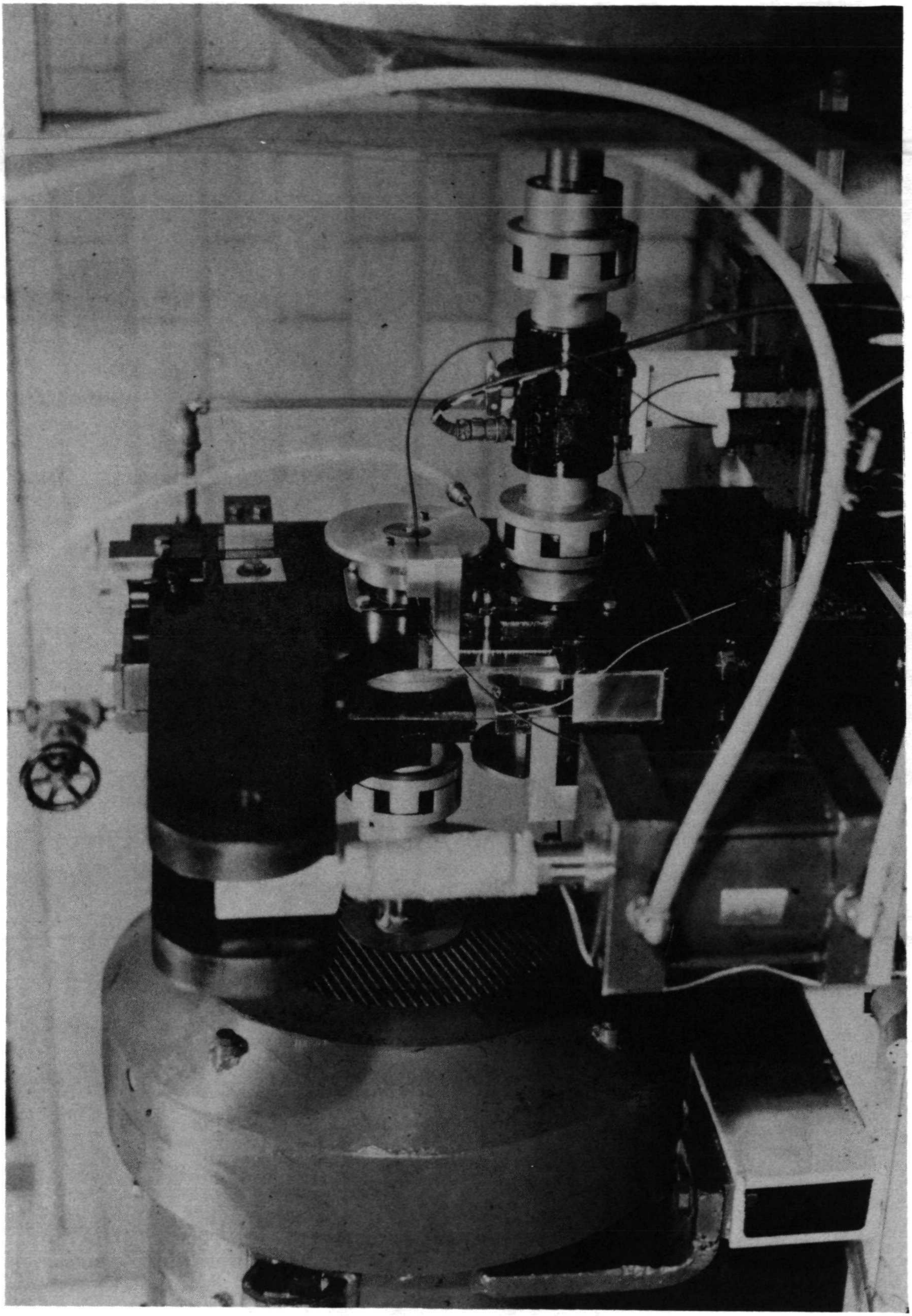

Figure 5.2. The disk machine.

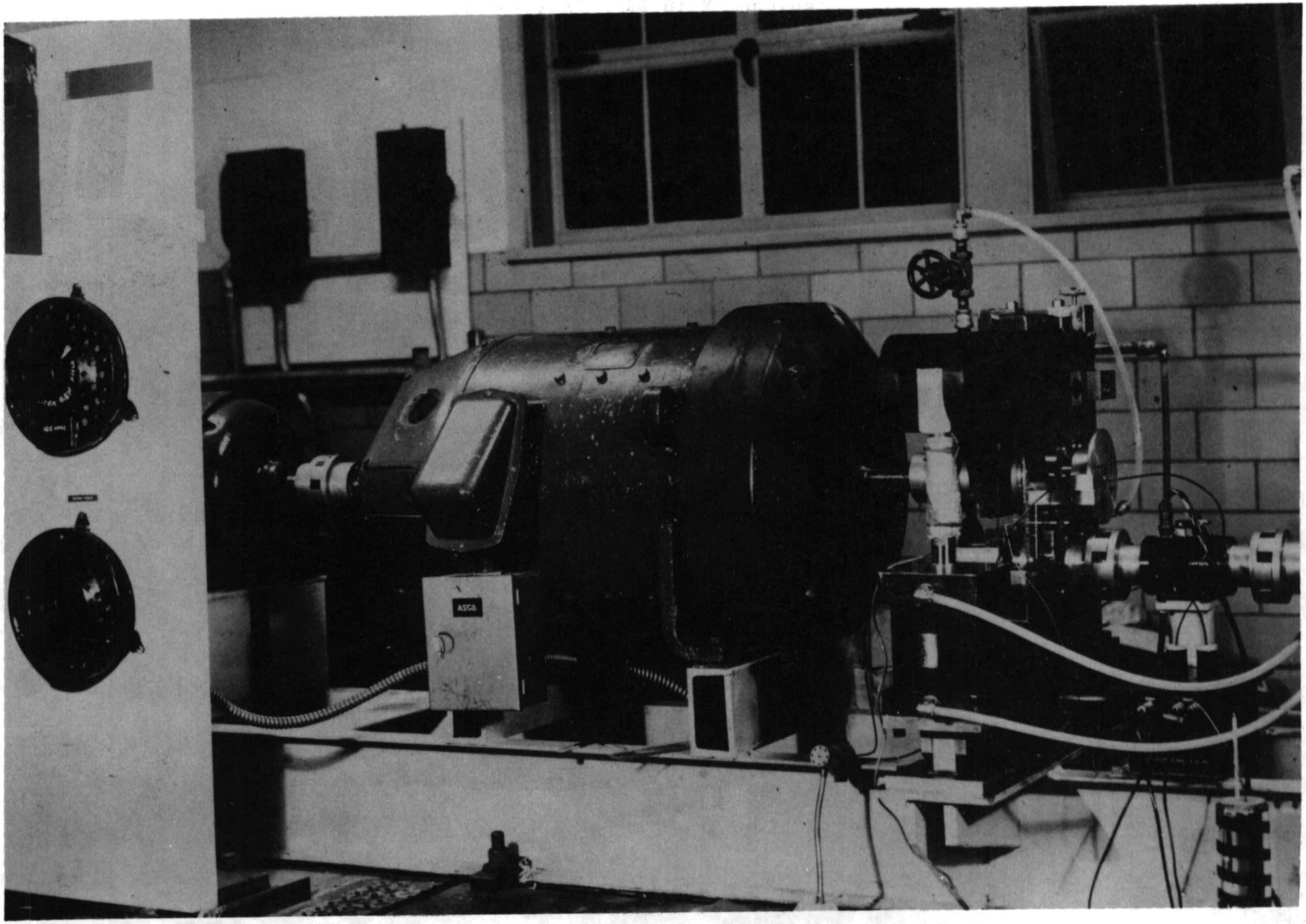

Figure 5.1. The disk machine.

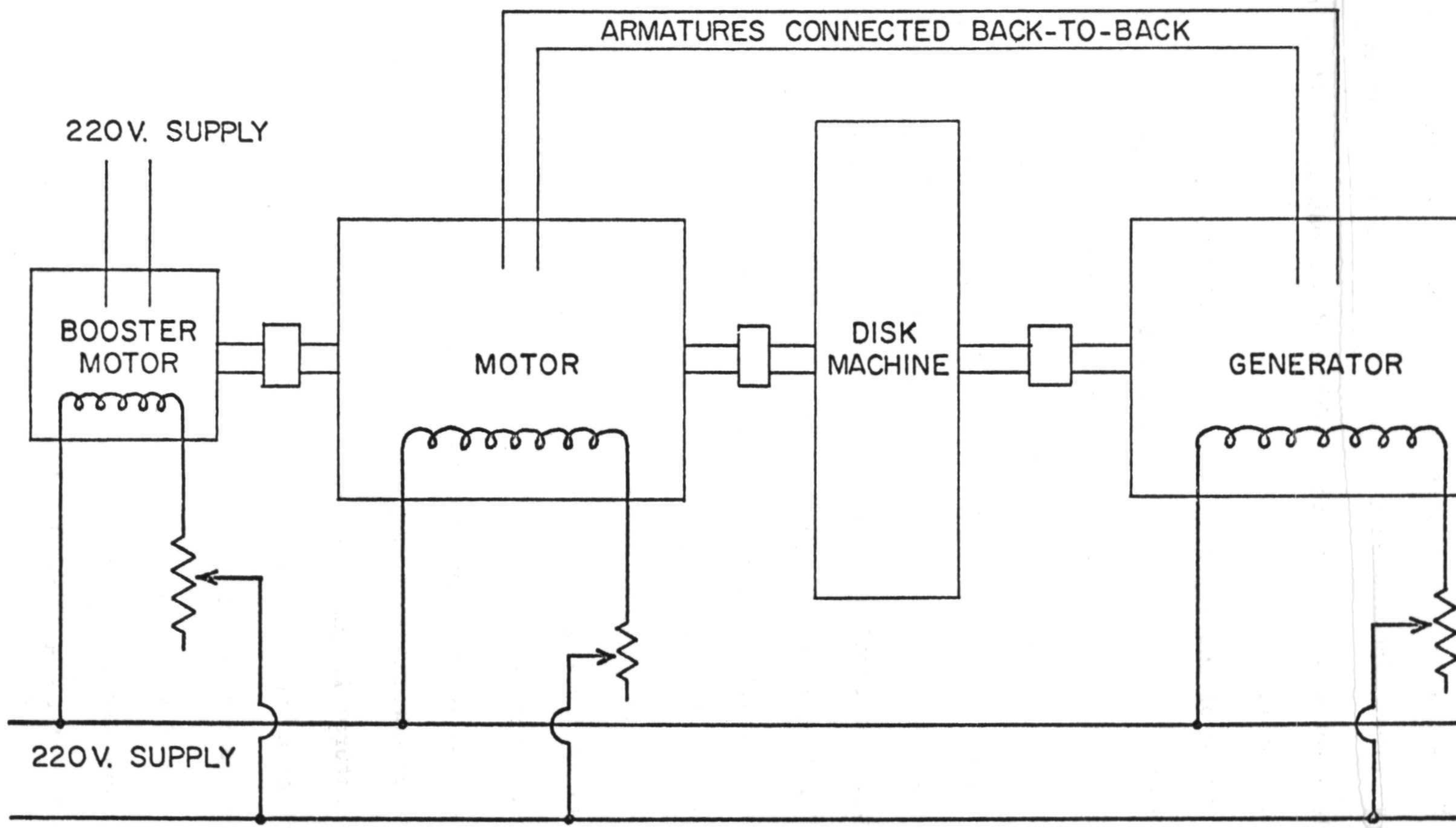

Figure 5.4. Electrical connections for the disk machine.

the second D. C. machine as a generator. The energy is electrically recycled by supplying the generated voltage to the armature of the motoring machine. The losses in this cycle are mechanically supplied by a 20 hp motor connected to the double-ended armature shaft of the 40 hp D. C. motor.

The speed of the upper shaft is controlled by the small 20 hp booster motor. A wide range of rolling speeds can be obtained by varying the supply voltage and the field resistance of the booster motor. The speed differential between the two shafts is controlled by adjusting the field resistors of the 40 hp D.C. motors which are connected together across the armature terminals. This arrangement allows a wide and continuous range of sliding speeds to be easily obtained. This differs greatly from the typical two-disk machine arrangement in which the slide-to-roll ratio is fixed by a gear ratio, or the ratio of the diameters to the disks.

Jefferis and Johnson reported torsional vibration difficulties with the original design of their disk machine. Every effort was made to eliminate vibration problems in this design. The lower shaft of the disk machine can be approximated as indicated in Figure 5.5, for the purpose of determining the natural torsional frequency of the shaft. The lowest natural frequency of this system is calculated to be 55 cycles per second which is slightly above the condition existing at the maximum experimental rolling speed of 1000 in/sec. The flexible couplings used in the system were chosen, in part, for their high damping characteristics to further insure smooth operation. Vibration problems were not encountered in the course of the experiments.

The frictional torque transmitted through the line contact is

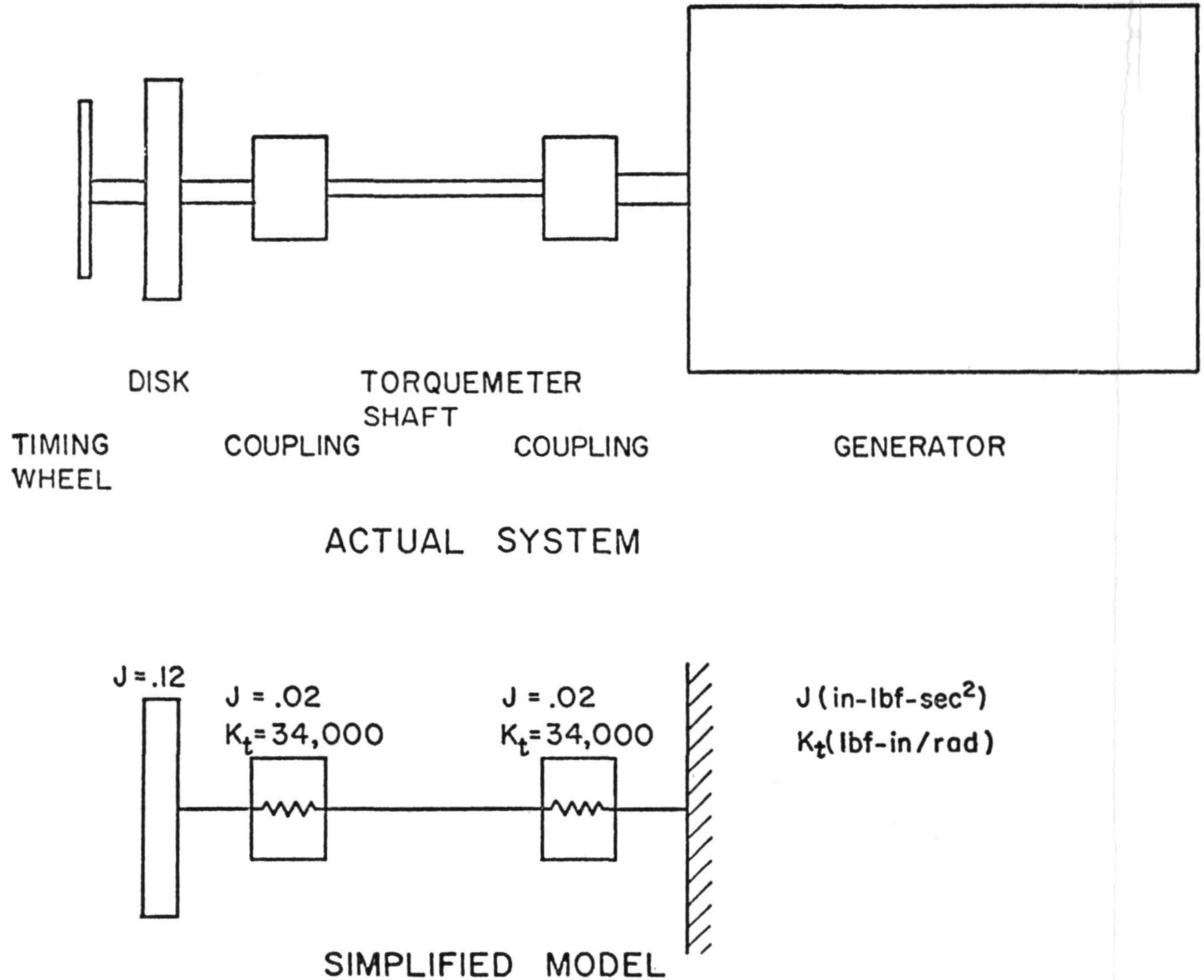

Figure 5.5. Model of the disk machine lower shaft used for vibration analysis.

measured by a torquemeter mounted in the lower shaft of the disk machine. The measured torque and the known radius of the disk are used to calculate the tangential tractive force of the contact. The torquemeter consists of a four-strain gauge bridge mounted on a calibrated torsion shaft. The electrical output signal of the torquemeter, passed from the rotating shaft through a set of slip rings, is a measure of the instantaneous torque in the lower shaft. This signal is displayed on an oscilloscope or measured by a digital voltmeter if an integrated average value is desired. The torque measured in this manner includes the frictional torque of the two lower support bearings which is accounted for as follows. The Hopkinson electrical circuit allows rotation of the disks in both directions and, therefore, pure rolling is possible. The bearing friction and any minute rolling friction are calculated from the measurements at pure rolling. The combined value is small and averages to a frictional torque corresponding to a friction coefficient of 0.002.

The angular velocity of each disk is measured by a timing wheel, seen in Figure 5.3. Each timing wheel has 100 equally spaced holes along the circumference. Light supplied from a high intensity source to the timing wheels is chopped into a stream of pulses as the timing wheel rotates. A pair of photomultiplier tubes converts these light pulses to electrical pulses which are then counted electronically. Thus the speed of the disk is measured. Fiber optic light guides are used for the transport of the light beams throughout this system. The sliding velocities are calculated as the difference of the measured velocities of the disks.

Filtered oil is supplied to the exit side of the contact allowing the lubricant one revolution with the disk before entering the conjunction. The lubricant is pumped from a 5 gallon supply tank, with a thermostatically controlled electric immersion heater and circulator, at rates up to 1 gallon per minute. The filter has a paper filter element which removes particles down to 1 micron.

The surface temperature of the disk as it enters the contact zone is monitored by an iron-constantan thermocouple trailing on the moving surface. An ice bath reference junction is used with the thermocouple. Crook [44] has demonstrated that this method gives accurate results; and Johnson and Cameron [11] have found this method agrees closely with the temperatures measured by a thermocouple embedded in the surface of the disk.

The electrical output signals of the strain gauges, photomultiplier tubes and the thermocouple are continually monitored by a scanning digital voltmeter.

A surface trace of a disk, shown in Figure 5.6, indicates that the disks were manufactured with a maximum peak-to-valley roughness of 4 micro-inches.

5.2 The Lubricants

The experimental program consisted of the gathering of extensive friction data for the two experimental fluids, Mobil XRM 109 F4 and Mobil XRM 177 F4. Mobil XRM 109 F4 is a synthesized paraffinic hydrocarbon base fluid. Mobil XRM 177 F4 is comprised of Mobil XRM 109 F4 formulated to improve its anti-fatigue properties. Table 5.1 is the physical property data, kindly supplied by the Mobil Research and Development Corporation, determined on Mobil XRM 109 F4. The properties of Mobil XRM 177 F4 are expected to be the same within experimental error.

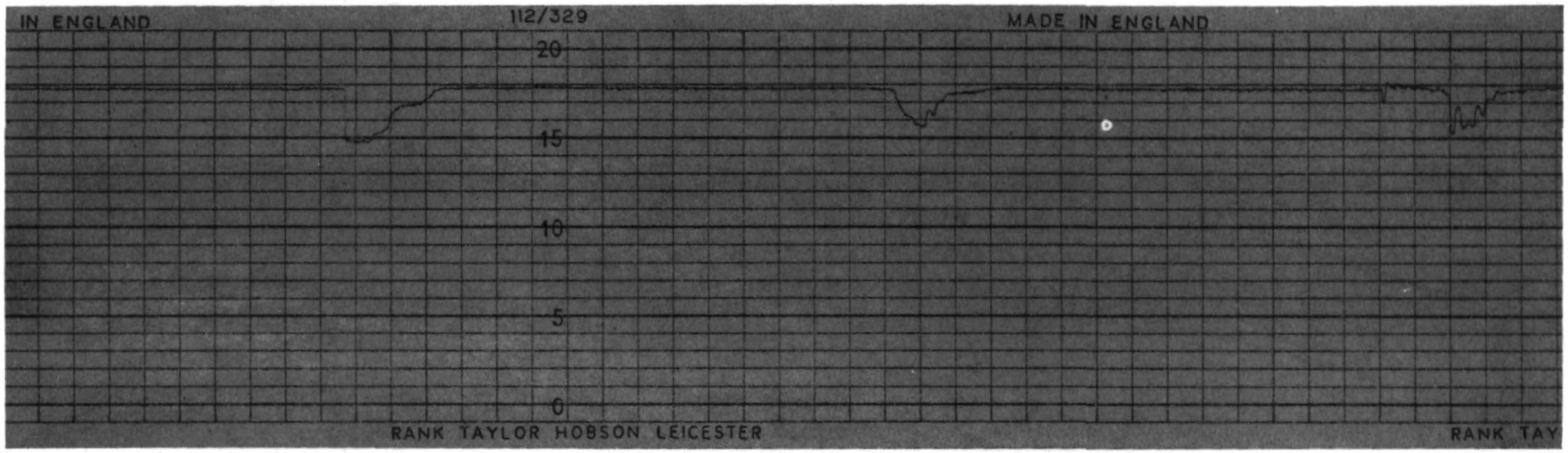

Figure 5.6 Trace of the disk surface.

Table 5.1

PHYSICAL PROPERTIES OF MOBIL XRM 109 F4

Kinematic Viscosity, cs	@ 400°F	6.0
	@ 210°F	40.4
	@ 100°F	447
	@ 0°F	37,000
Total Acid No.		0.0
Flash Point, °F		520
Fire Point, °F		595
Pour Point, °F		-60
Density	@ 100°F	0.8389
	@ 200°F	0.8082
	@ 300°F	0.7777
	@ 400°F	0.7428
Specific Heat	@ 300°F	0.635
	@ 400°F	0.692
Autogeneous Ignition Temp., °F		760
Surface Tension		30.9

5.3 Test Procedure

The strain gauges, photomultiplier tubes, voltage supplies, and digital voltmeter must warm up and reach a stable temperature before any calibrations are performed. The lubricant supply is also heated to the desired temperature during this time. After the warm-up, the strain gauge bridges measuring the normal load and frictional torque are calibrated. The air cylinder gauges are calibrated to zero load, while the torquemeter gauges are calibrated against a shunt resistance simulating a known torque.

The oil supply is then turned on and the disk machine may be started at minimum load with the field resistances of the two 40 hp machines at equal settings. The load and rolling speed are then increased to the desired values and the bearing torque is measured at pure rolling conditions.

The sliding speed is now varied, while maintaining a constant mean rolling speed, to obtain the data for a friction versus sliding speed curve. It is easiest to keep the surface temperature within a 5 degree C range by making some high slip torque measurements first and then returning to the low and middle slip values.

5.4 Results

A typical set of experimental results is shown in Figure 5.7. The friction coefficient, defined as the tractive force divided by the applied normal load, is plotted against the sliding speed. The maximum Hertzian pressure, rolling speed and lubricant inlet temperature remain constant. The friction coefficient rises from zero at pure rolling to a maximum value and then decreases with any further increase in sliding speed.

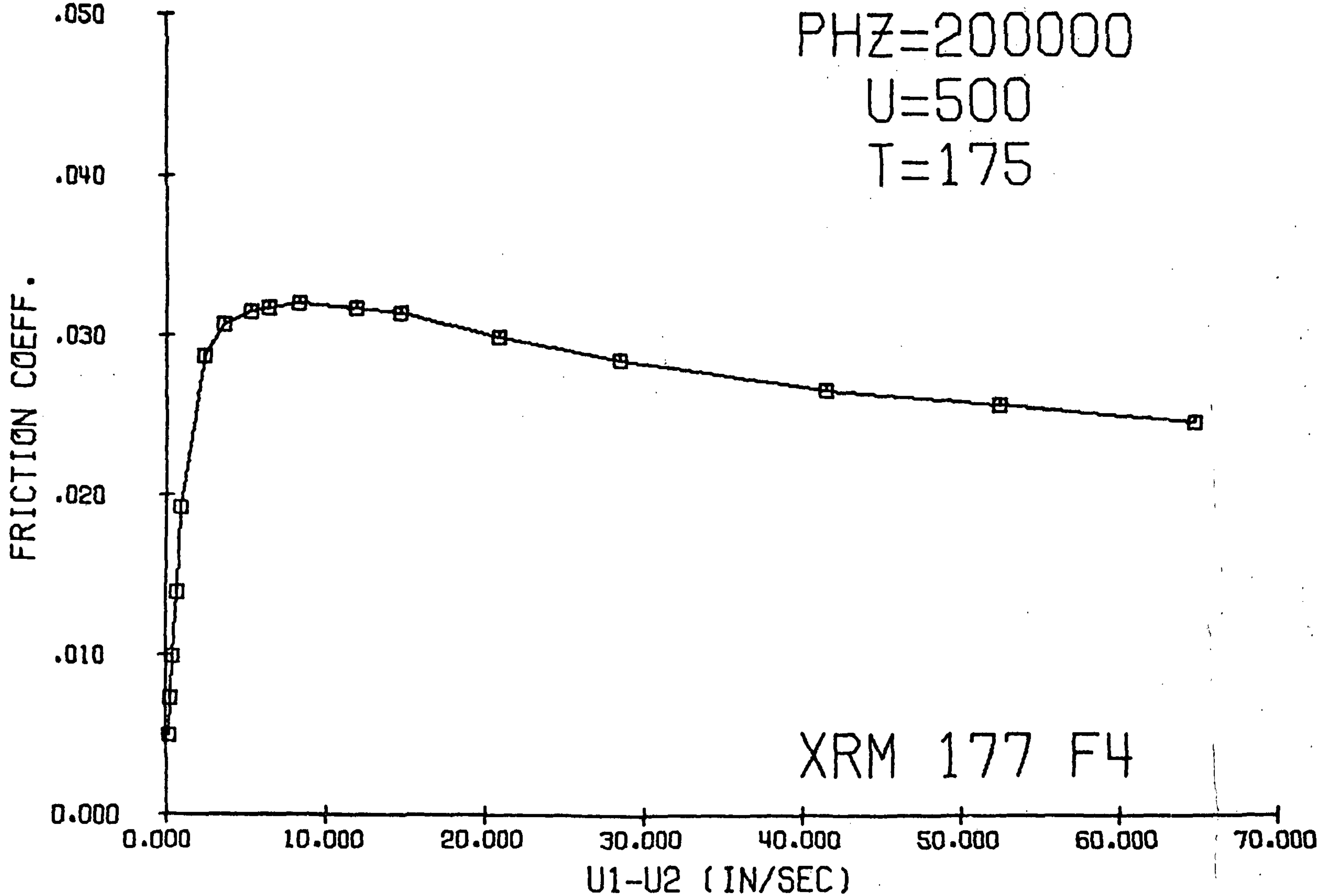

Figure 5.7. Typical experimental results.

Complete results of the experimental study are presented with discussion in the next chapter.

CHAPTER VI

DISCUSSION OF RESULTS

A new elastohydrodynamic friction analysis has been developed in Chapters II, III and IV. The separate effects of both shear rate and time have been included. Shear viscoelasticity results in a non-Newtonian relation between the shear stress and shear rate, while compressional viscoelasticity results in a time-dependent viscosity function. A numerical solution of the momentum and energy equations, with pressure, temperature and time-dependent parameters, is achieved.

Traction measurements have been made on two synthesized hydrocarbon fluids under elastohydrodynamic conditions. The experimental apparatus and procedure have been described in Chapter V.

This chapter discusses the results of these analytical and experimental programs. A good correlation of the friction coefficients determined by analysis and experiment is shown.

6.1 Values of the Friction Coefficient Determined by Experiment

The tractive force transmitted by a thin lubricant film under elastohydrodynamic conditions has been measured for a wide range of loads and sliding speeds at high rolling speeds. Specifically, the loads ranged from 115,000 psi maximum Hertzian stress to 250,000 psi; the sliding speeds varied from zero to over 60 in/sec; the high rolling speeds were 500 and 1000 in/sec; and the oil entrance temperatures were 175 ^{o}F and 220 ^{o}F. The friction coefficient, or traction coefficient, calculated from this data for two synthetic paraffinic fluids, show variations similar to those found for other lubricating oils by

Johnson and Cameron [11] , Crook [4] and Bell, and Kannel and Allen [6] .

The friction coefficient rises to a maximum value with increasing sliding speed and then decreases with any further increase in the sliding speed. The coefficient is also found to increase with increasing pressure and to decrease with increasing rolling speed and temperature. Any parameter variation that results in an increase in the friction coefficient also results in the maximum friction occurring at a lower sliding speed. Examples of this behavior for both experimental fluids are shown in Figures 6.1 through 6.14 where the friction coefficient is plotted as a function of sliding speed for fixed values of maximum Hertzian pressure, rolling speed and oil inlet temperature.

This behavior may be explained in terms of the liquid model that has been developed. At low values of sliding and therefore, low shear rate, there is no appreciable temperature gradient across the lubricant film. The shear stress increases with shear rate according to the effective viscosity predicted by the compressional viscoelastic model developed in Chapter III. At slightly higher sliding speeds, the temperature rise in the fluid film is significant and cannot be neglected. For the range of conditions under study, the analysis predicts a rise of film temperature of 15 $^{\circ}$F to 20 $^{\circ}$F at the sliding speed corresponding to the maximum friction coefficient. For even higher sliding speeds, it is hypothesized that the mechanism of flow changes and is dominated by a pressure and temperature-dependent limiting shear modulus. The temperature at the center of the lubricant film at the highest sliding speeds is calculated to be 100 $^{\circ}$F to 150 $^{\circ}$F higher than the surface temperature of the disks.

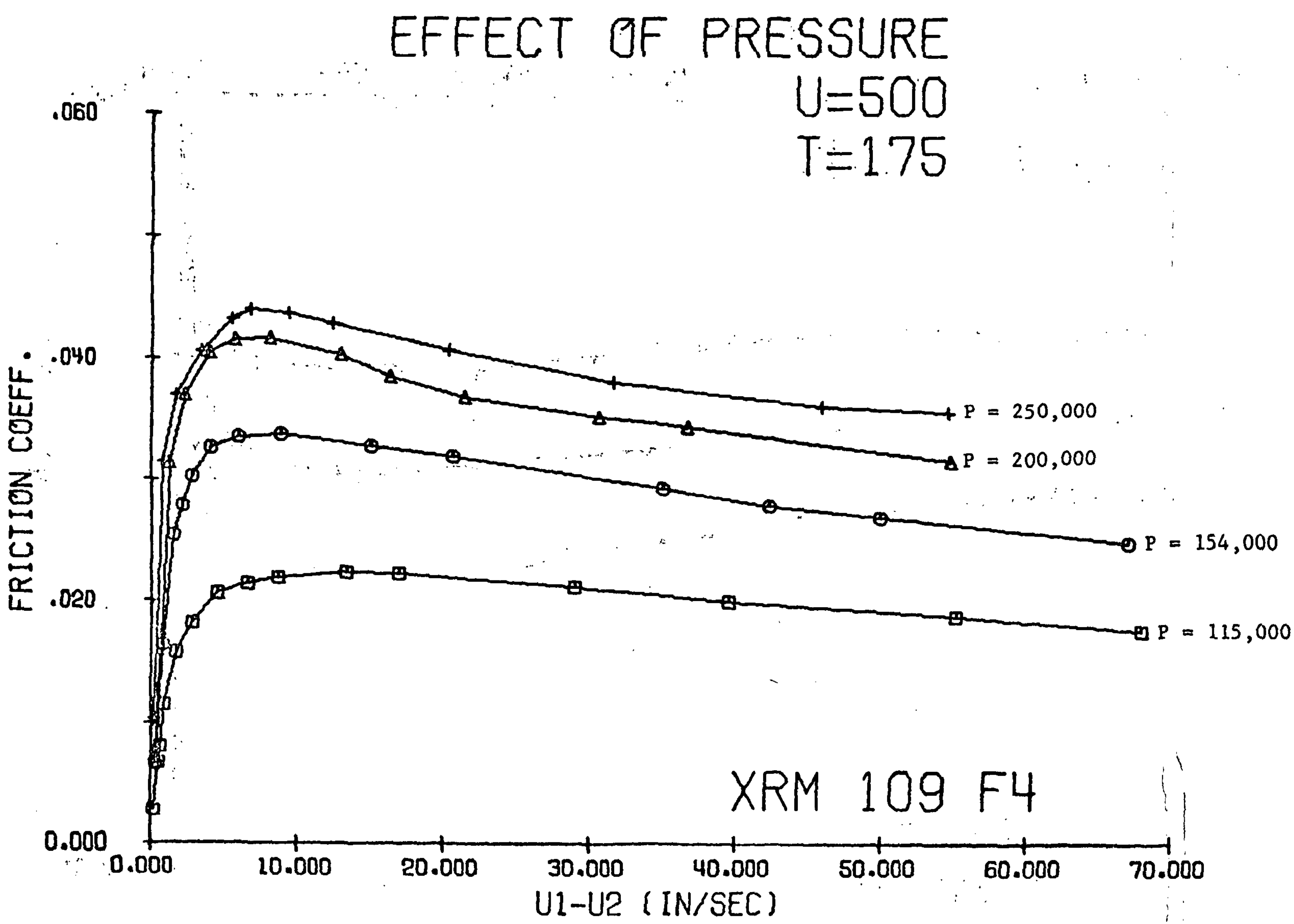

Figure 6.1. The effect of load on the friction coefficient.

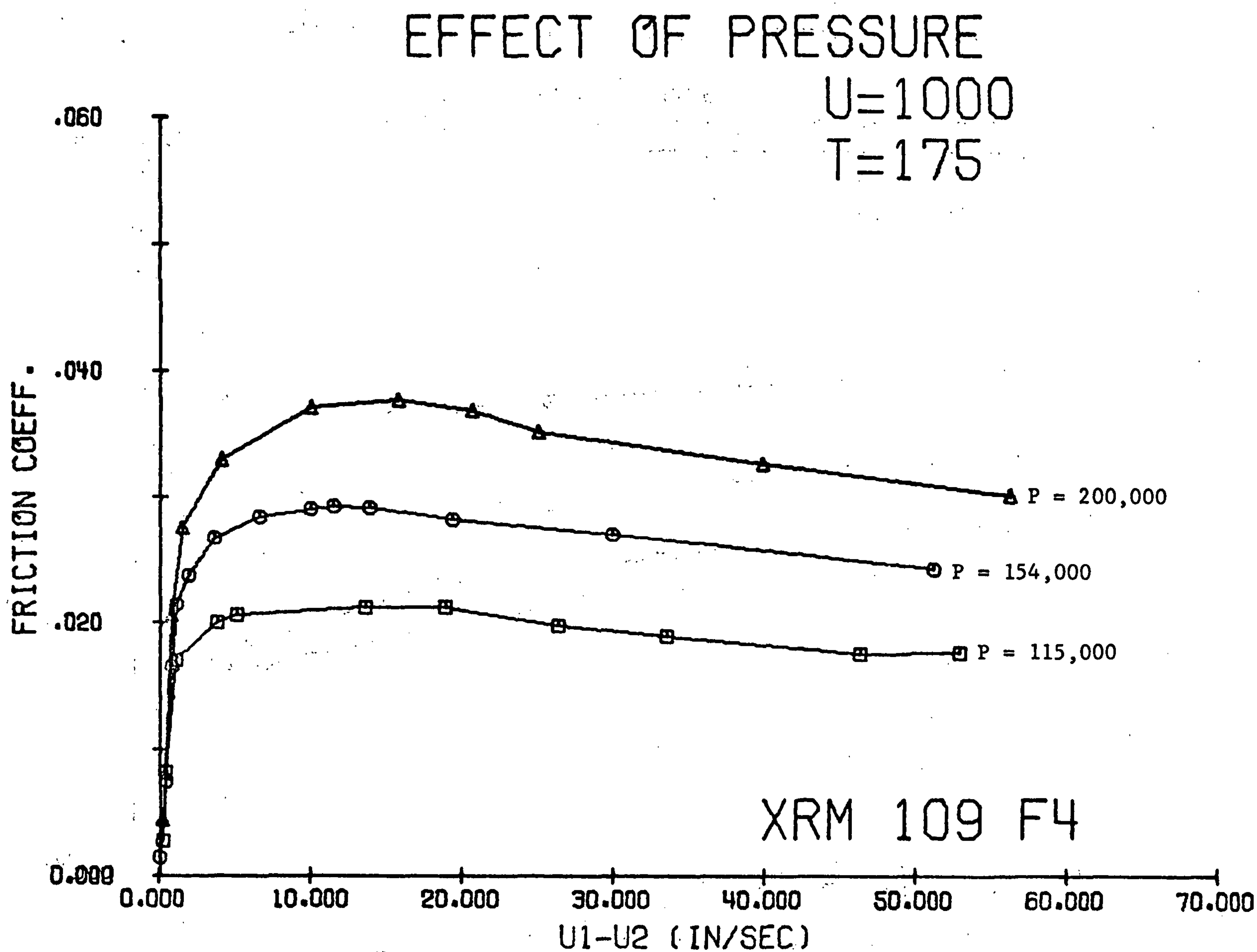

Figure 6.2. The effect of load on the friction coefficient.

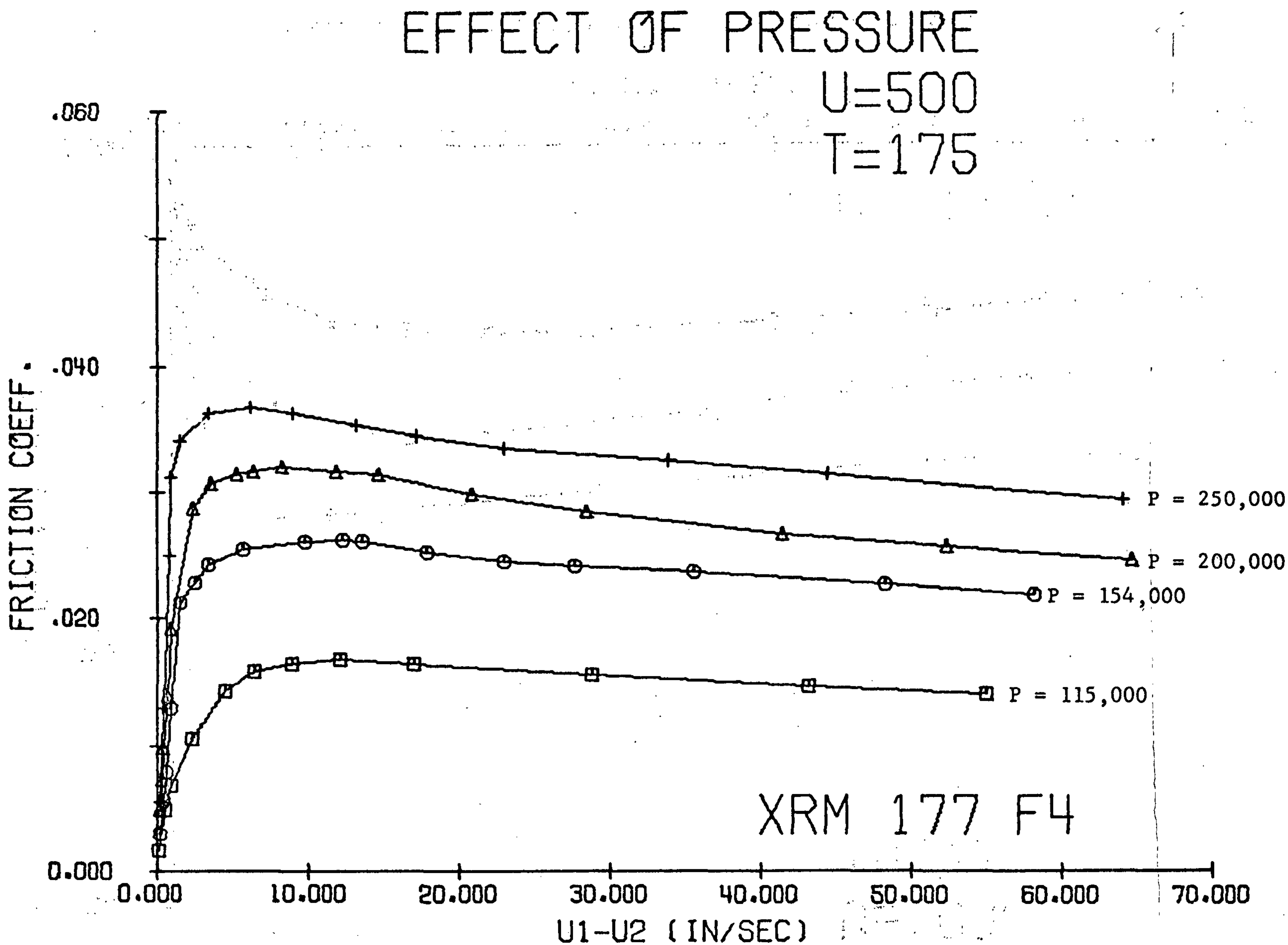

Figure 6.3. The effect of load on the friction coefficient.

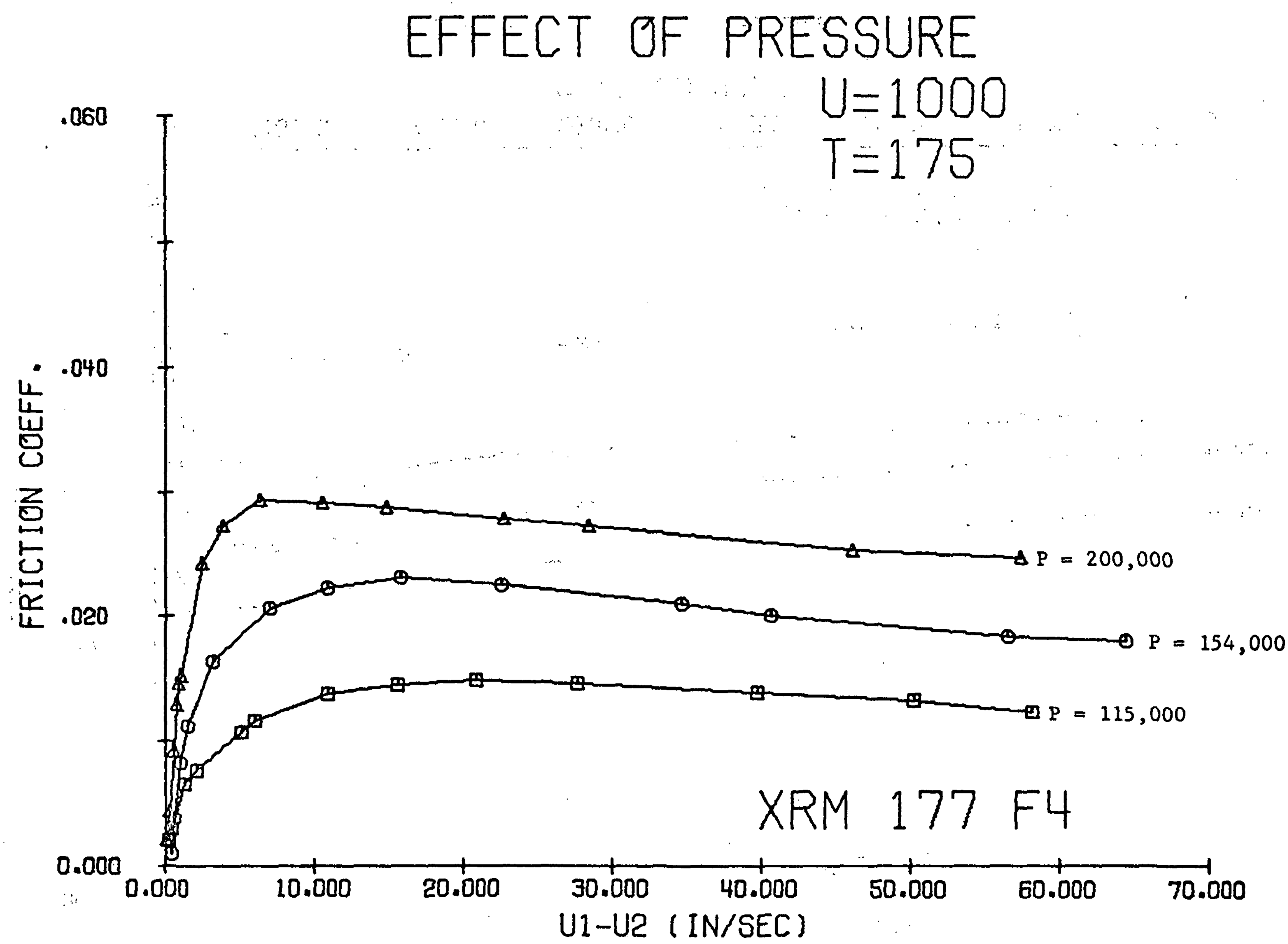

Figure 6.4. The effect of load on the friction coefficient.

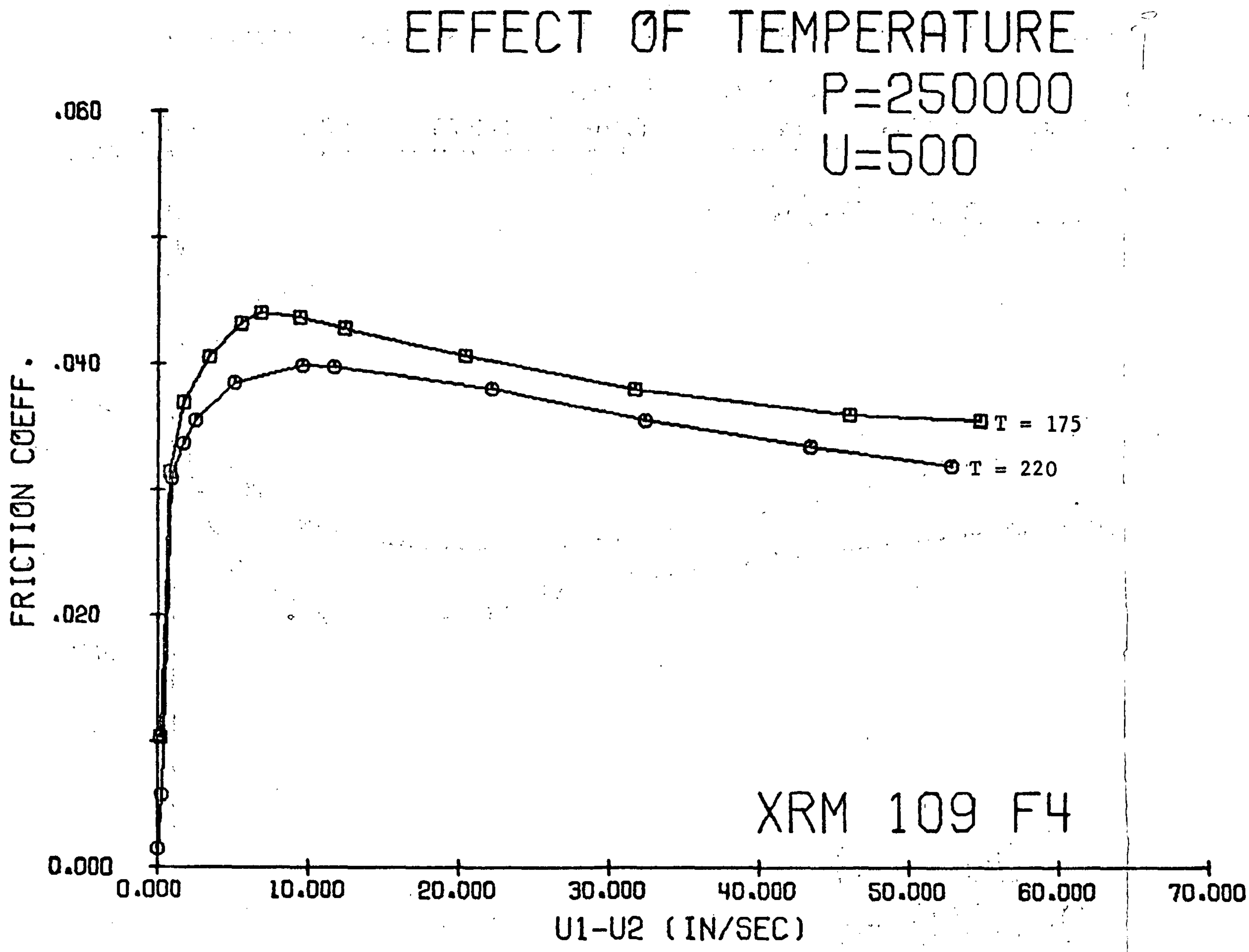

Figure 6.5. The effect of lubricant inlet temperature on the friction coefficient.

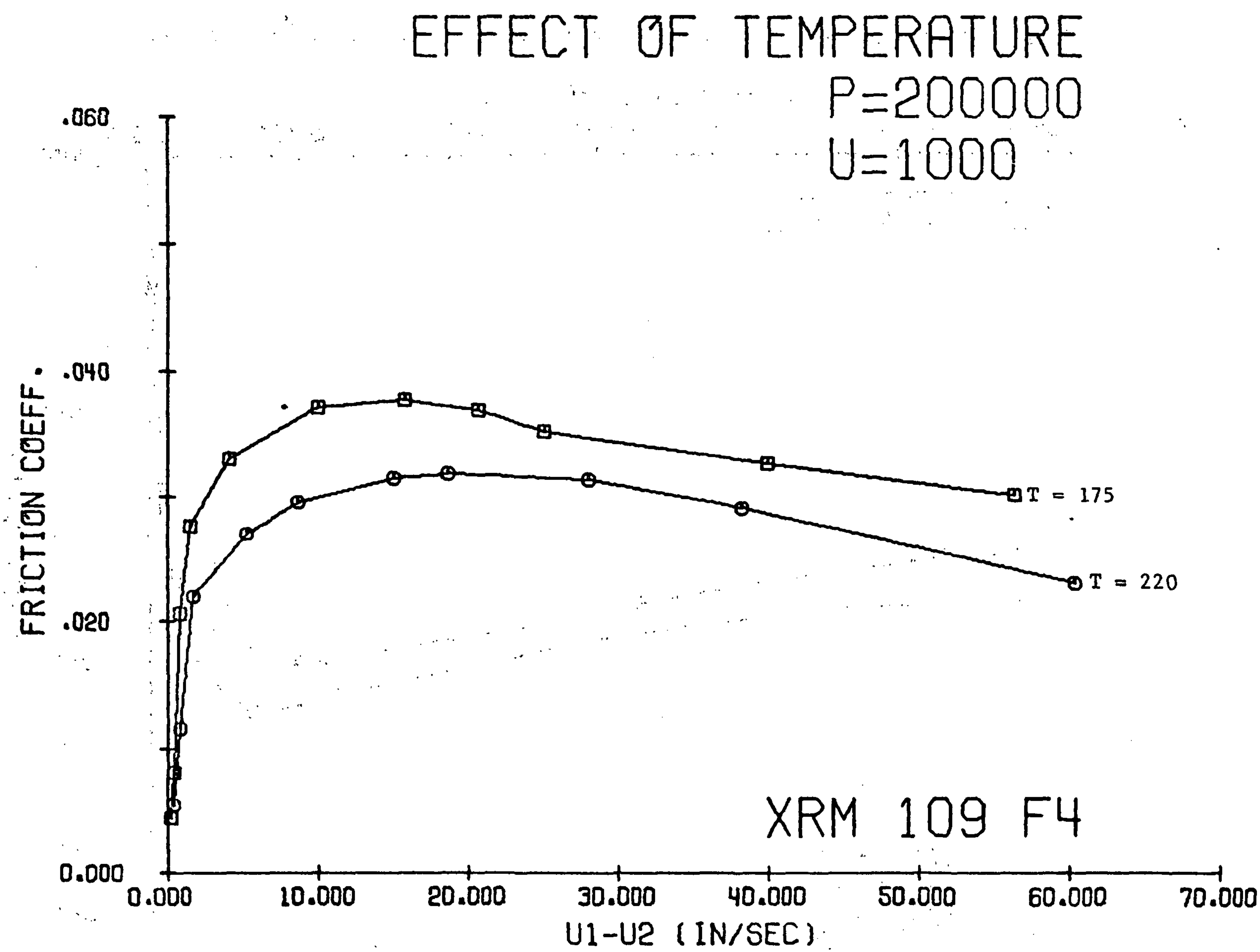

Figure 6.6. The effect of lubricant inlet temperature on the friction coefficient.

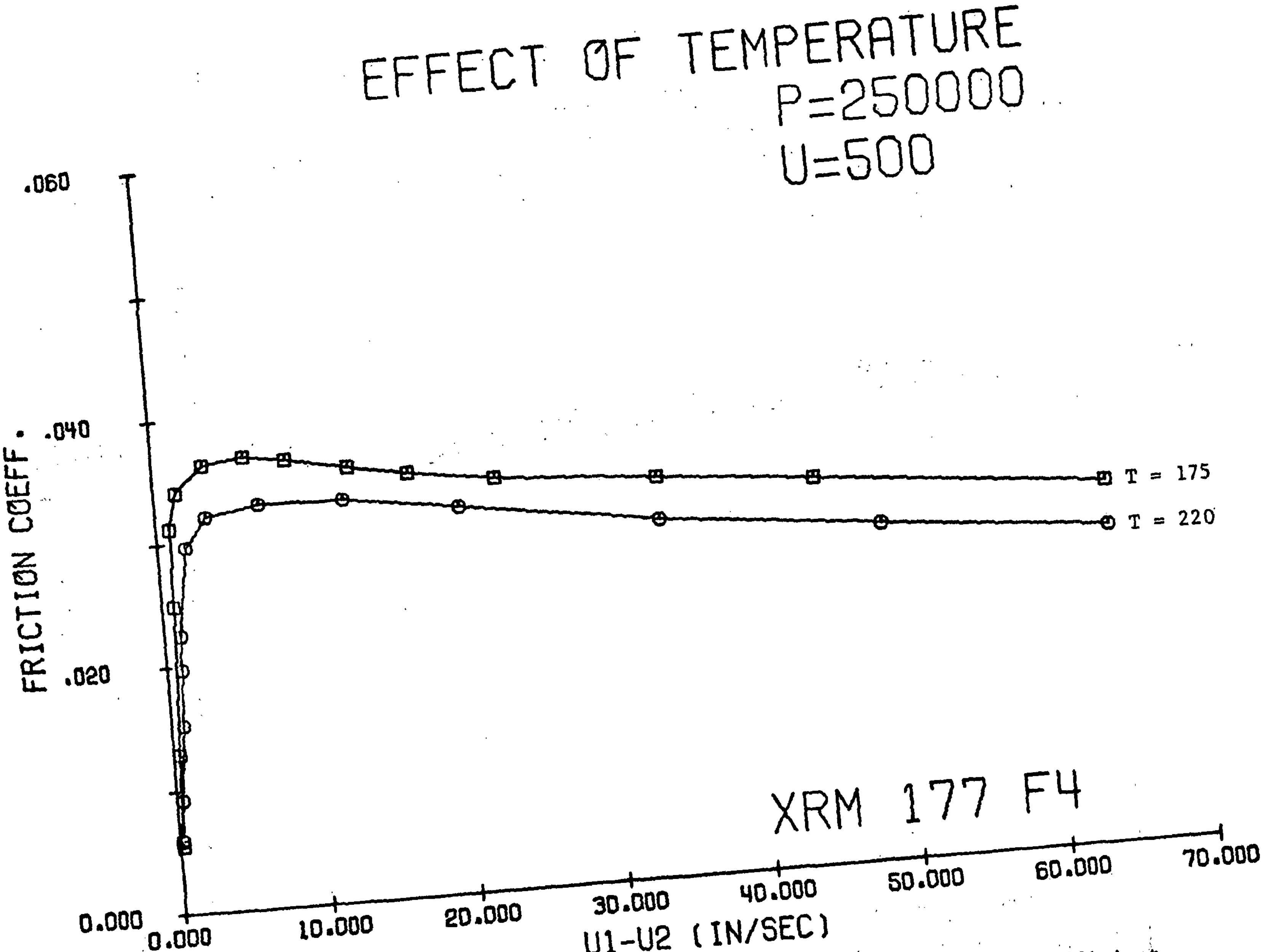

Figure 6.7. The effect of lubricant inlet temperature on the friction coefficient.

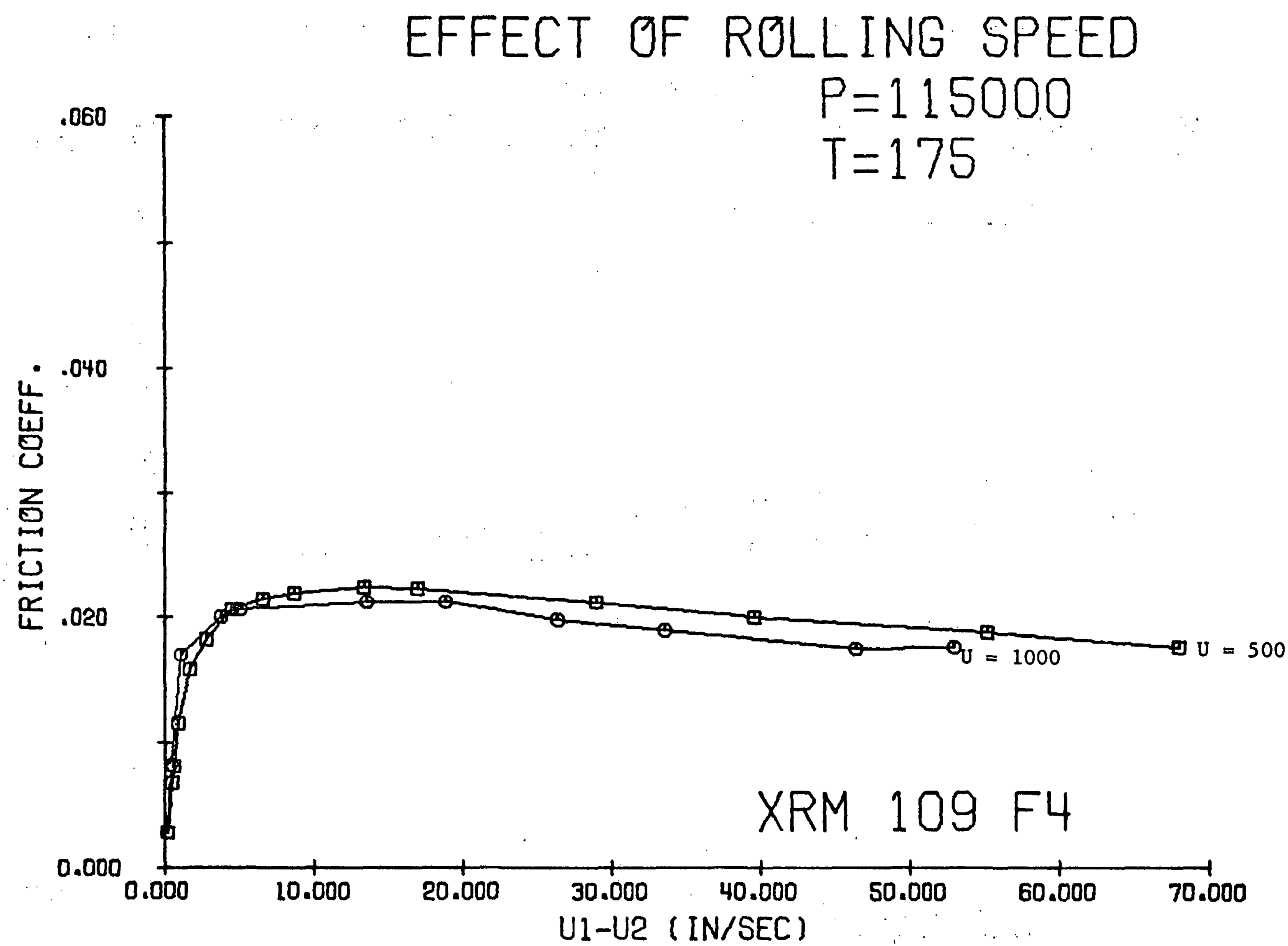

Figure 6.8. The effect of rolling speed on the friction coefficient.

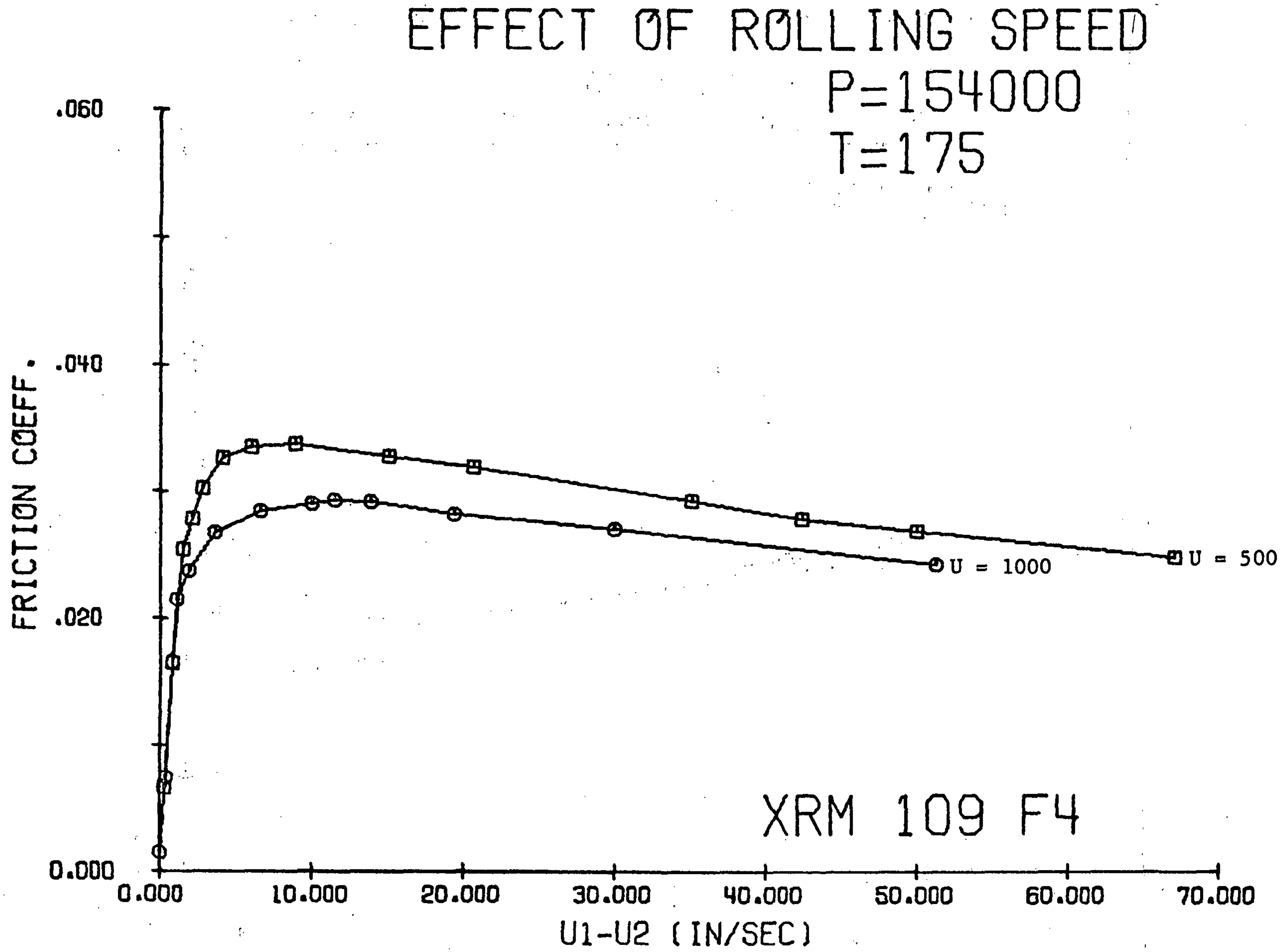

Figure 6.9. The effect of rolling speed on the friction coefficient.

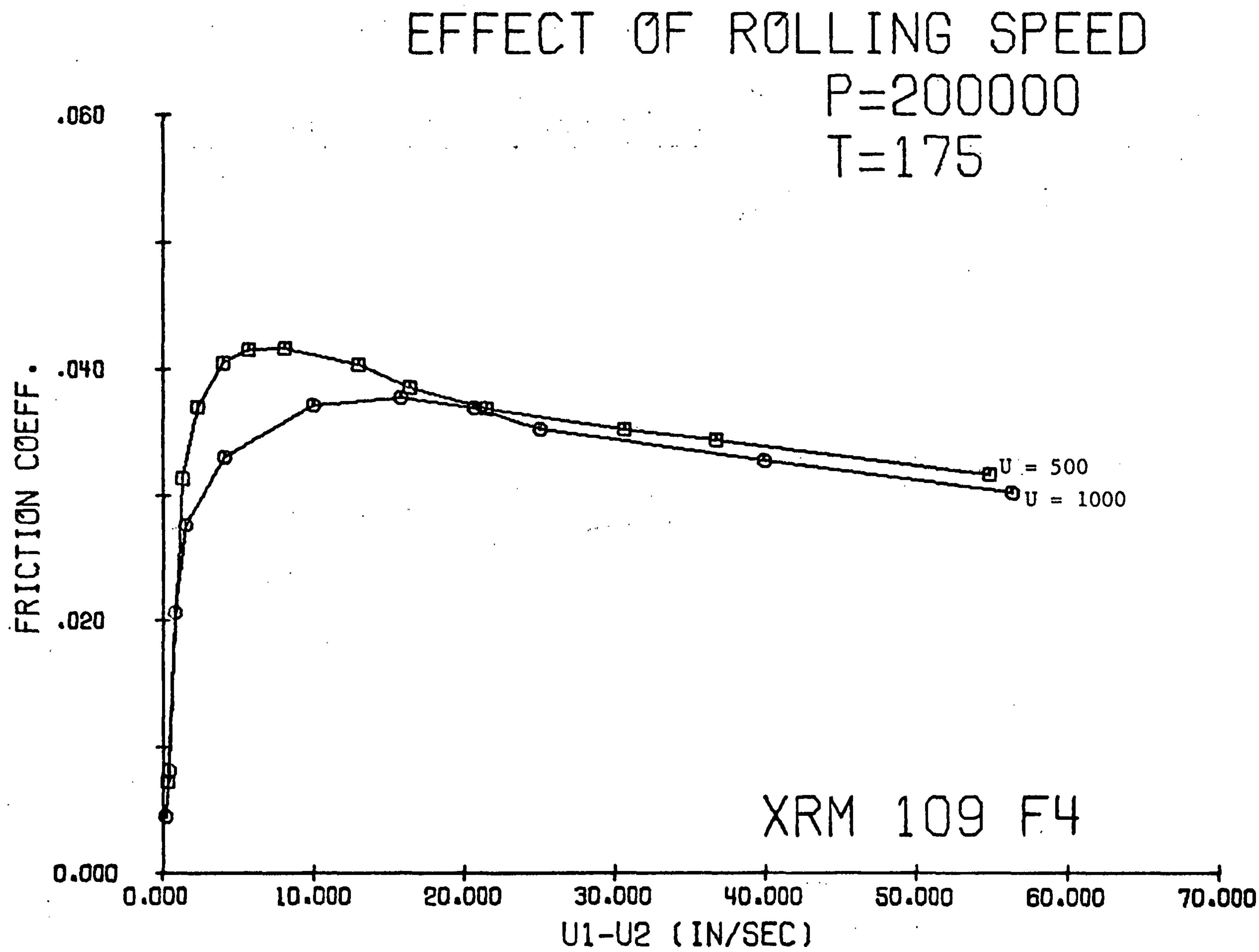

Figure 6.10. The effect of rolling speed on the friction coefficient.

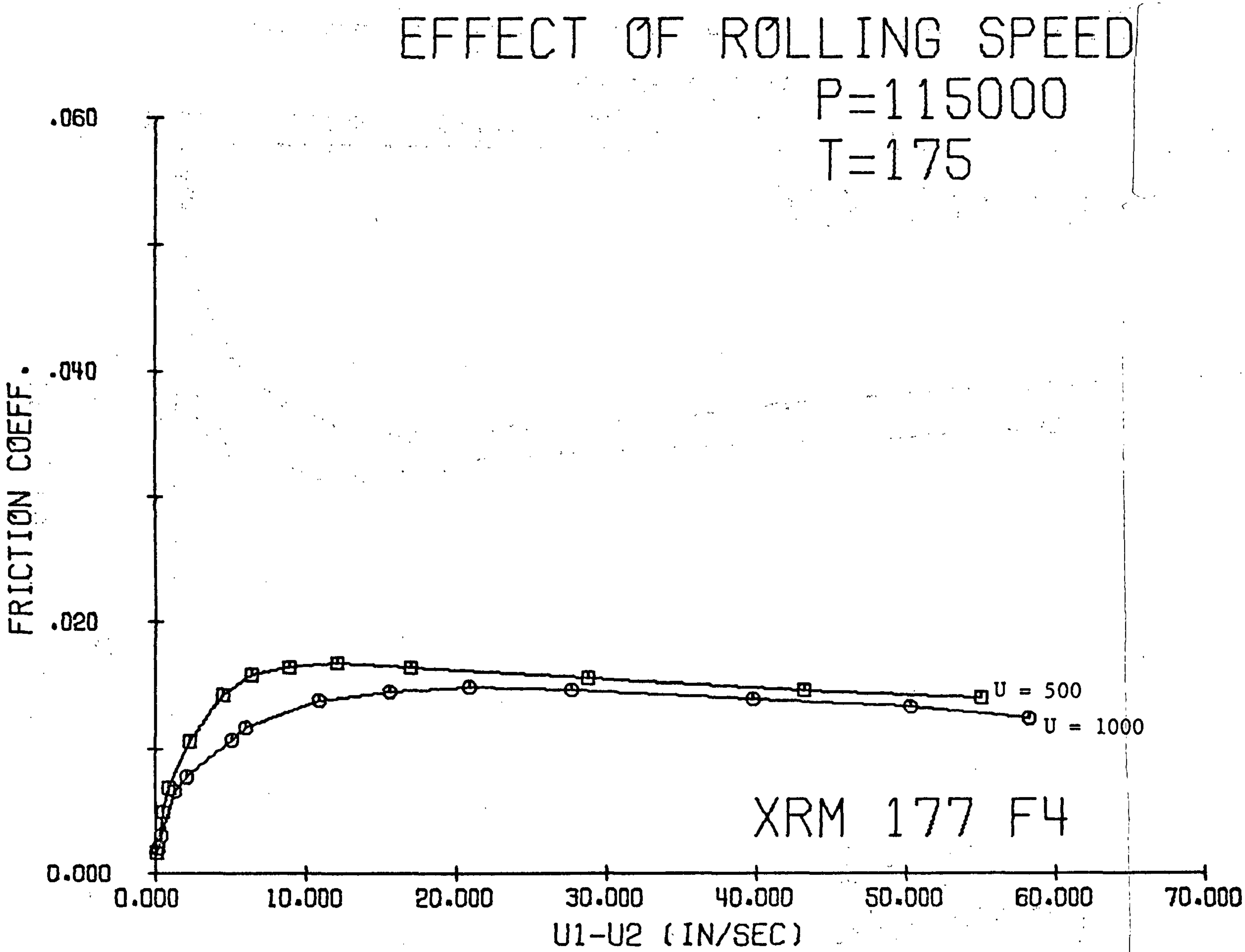

Figure 6.11. The effect of rolling speed on the friction coefficient.

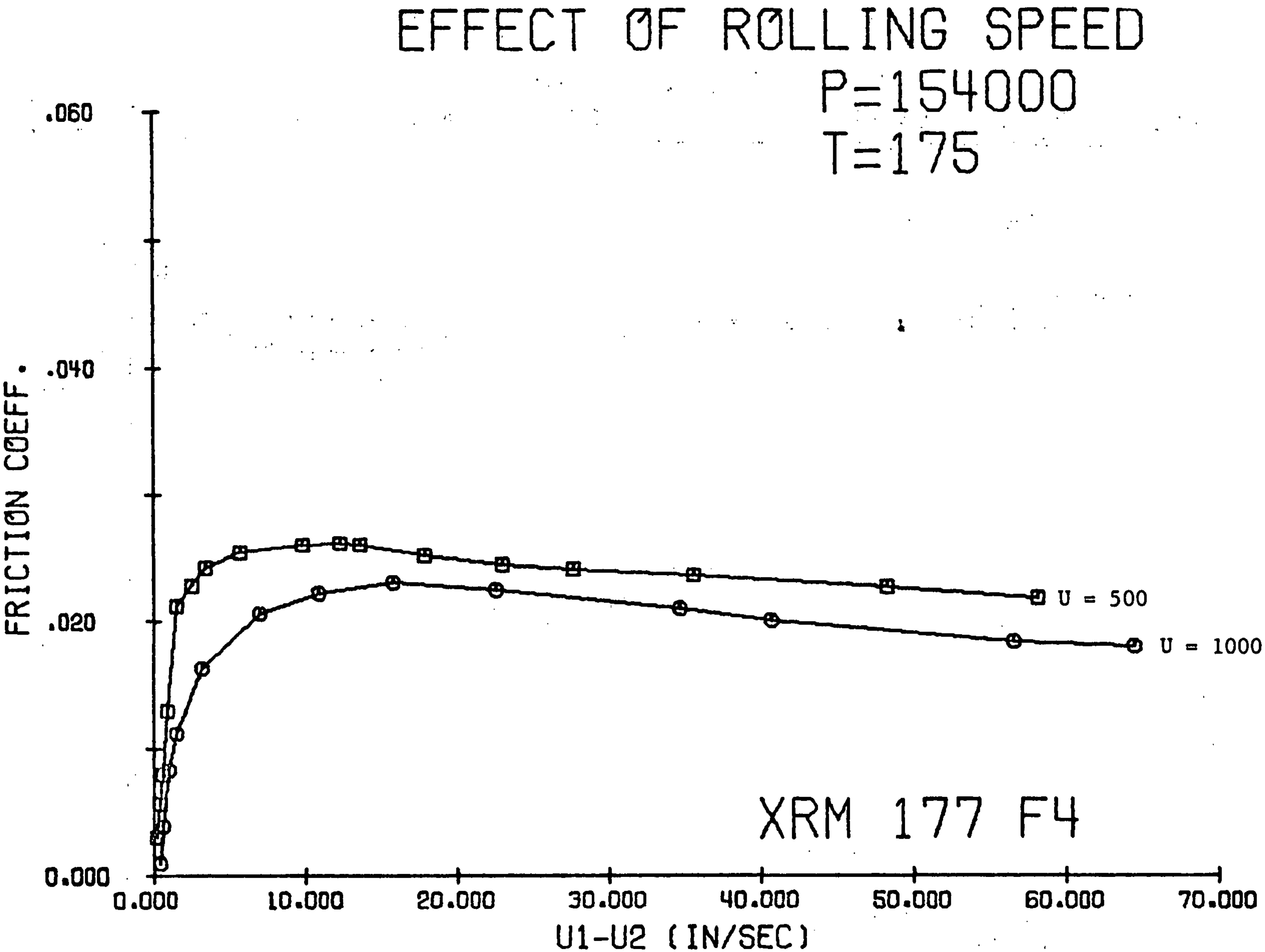

Figure 6.12. The effect of rolling speed on the friction coefficient.

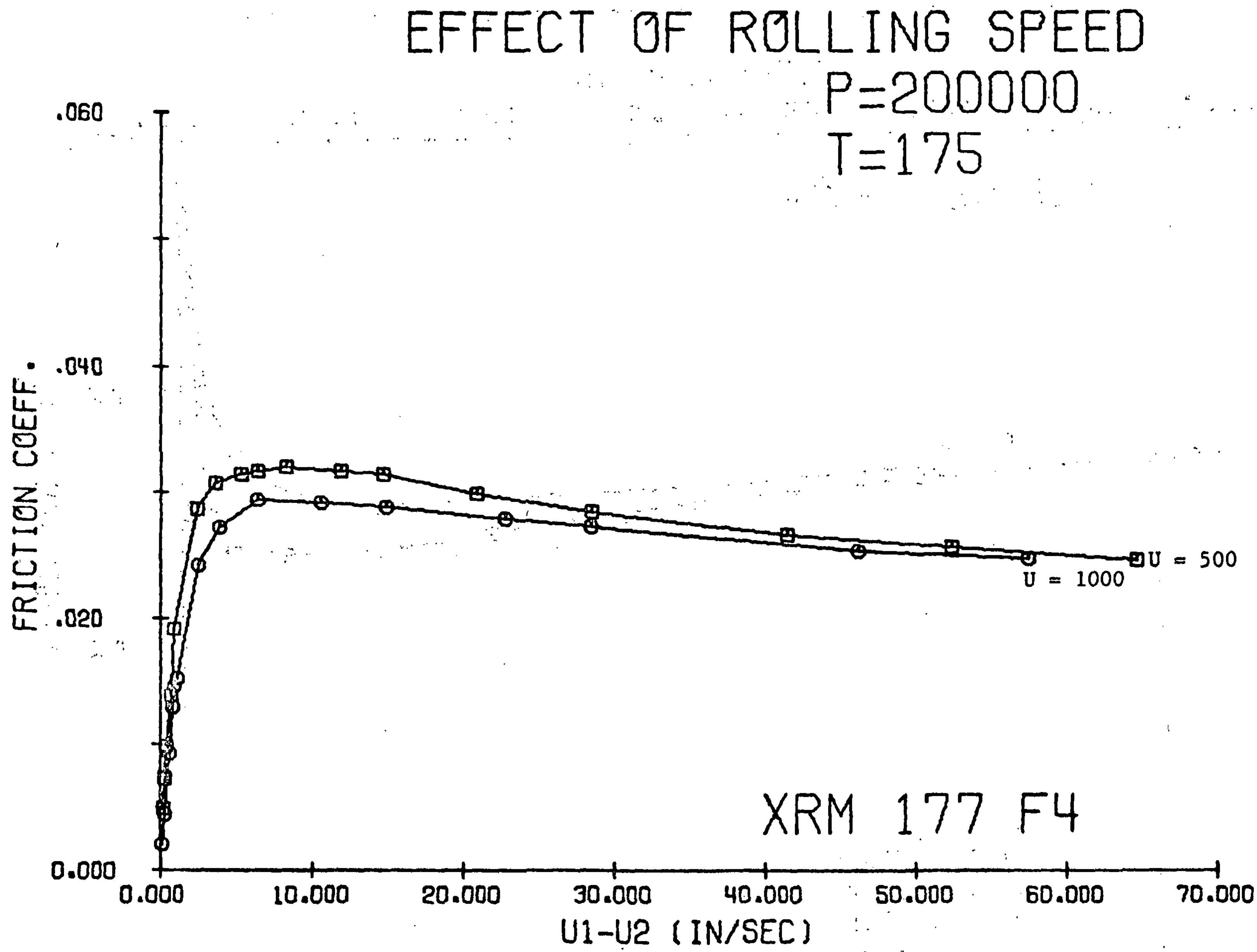

Figure 6.13. The effect of rolling speed on the friction coefficient.

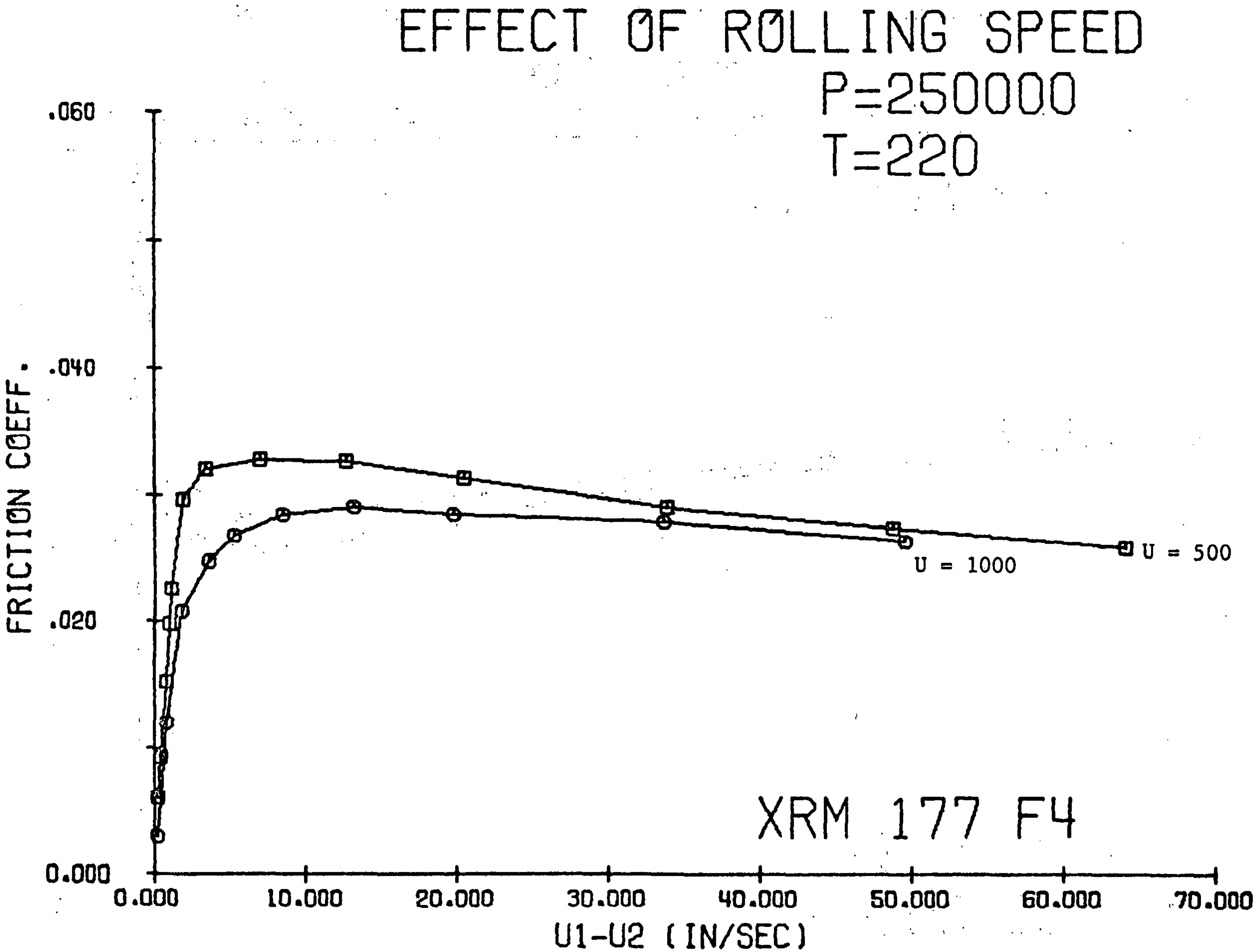

Figure 6.14. The effect of rolling speed on the friction coefficient.

Therefore, the friction coefficient μ, which is defined as the ratio of the tractive force transmitted to the normal load, is proportional to the following:

$$\mu \propto \eta f\left(\frac{\partial u}{\partial y}\right) \tag{6.1}$$

for sliding speeds smaller than that corresponding to the maximum value of the friction coefficient; and

$$\mu \propto \frac{\overline{G}_\infty}{p} \tag{6.2}$$

for higher sliding speeds.

An increase in the pressure level results in an increased viscosity η, which accounts for the higher friction coefficient at low sliding speeds seen in Figures 6.1 through 6.4. For higher sliding speeds, the limiting shear modulus as a function of pressure must be reviewed. Figure 6.15 simplifies the relationship of Figure 4.10 and equation (4.31).

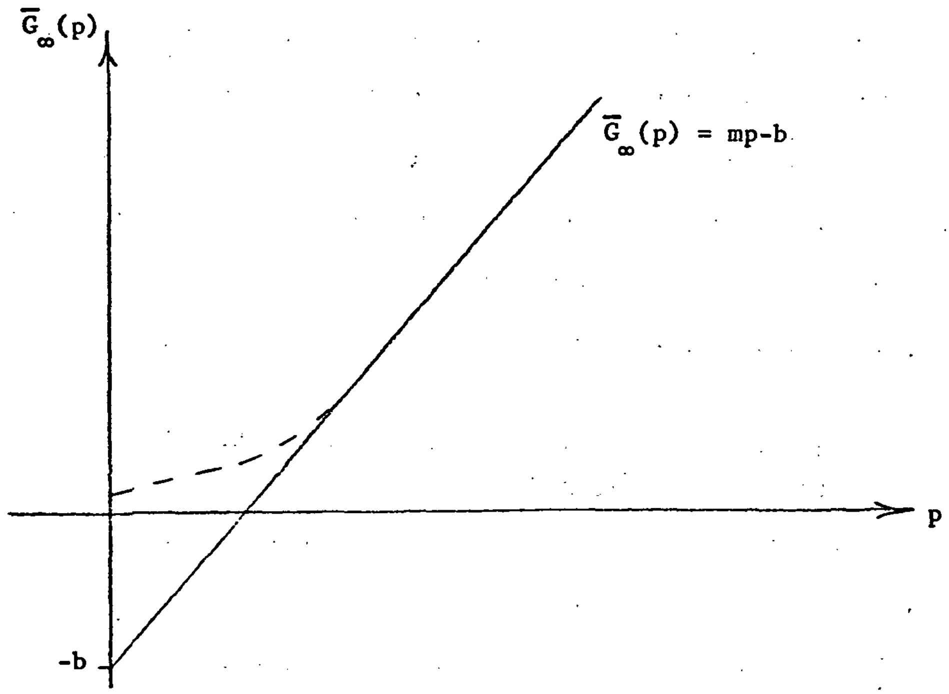

Figure 6.15. Simplified limiting shear modulus-pressure relationship.

Although the actual limiting shear modulus probably follows the dashed line, the linear portion at higher pressure levels may be given by the relationship shown. Equation (6.2) therefore yields

$$\mu \alpha m - \frac{b}{p} \tag{6.3}$$

and the friction coefficient also increases with pressure at high sliding speeds.

An increase in the inlet temperature of the lubricant results in lower values of both the viscosity and limiting shear modulus. The entire friction coefficient versus sliding speed curve is thus lowered according to equations (6.1) and (6.2). This is seen in Figures 6.5 through 6.7.

As the rolling speed increases, the film thickness increases according to equation (4.3). At low sliding speeds, this higher film thickness will reduce the shear rate, which in turn reduces the shear stress according to the viscoelastic fluid model. At higher values of sliding speed, an increased film thickness results in a higher film temperature as indicated by equation (4.18). This will then lower the limiting shear modulus. Either of these results, the lower shear stress or the lower limiting shear modulus, causes lower friction coefficients as seen in Figures 6.8 through 6.14 for the two experimental lubricants.

6.2 Correlation of Values of the Friction Coefficient Determined by Experiment and Analysis

The values of the friction coefficient determined by experiment for the Mobil XRM 109 F4 synthetic paraffinic base fluid are compared with those predicted by the new analysis in Figures 6.16 through 6.23.

Figures 6.24 through 6.31 show a similar comparison for the Mobil XRM 177 F4 paraffinic fluid with anti-fatigue additives. A further correlation is shown in Figures 6.32 through 6.37 for some of the experimental data of Johnson and Cameron [11] .

As in the previous section, the values of the friction coefficient are plotted as a function of the sliding speed U_1-U_2, for fixed values of maximum Hertzian pressure P, rolling speed U and oil entrance temperature T. The units of P, U and T are psi, in/sec and degrees F, respectively, except for the Shell Turbo 33 correlations where the oil entrance temperature is given in degrees C. Values determined by experiment are shown as data points on the curves, while values predicted by the analysis are shown by smooth curves.

The analysis predicts friction coefficients that show the same variations as observed experimentally. The friction coefficients rise to a maximum value and then decrease with increasing sliding speed; they increase with increasing pressure and decrease with increasing rolling speed and oil temperature.

Good correlation is found between the experimental data for Mobil XRM 109 F4 and Shell Turbo 33 and the values predicted by the analysis using the straight exponential viscosity function adopted by Cheng [5] and the hyperbolic liquid model with c = .25. This corresponds to the Barlow, Erginsav and Lamb [23] liquid model with a limiting shear stress. In most cases, the friction coefficients agree within 10%, with a few extreme cases differing by less than 25%.

It is necessary to use the hyperbolic model with c = .20 to obtain the same correlation for the Mobil XRM 177 F4 lubricant. This

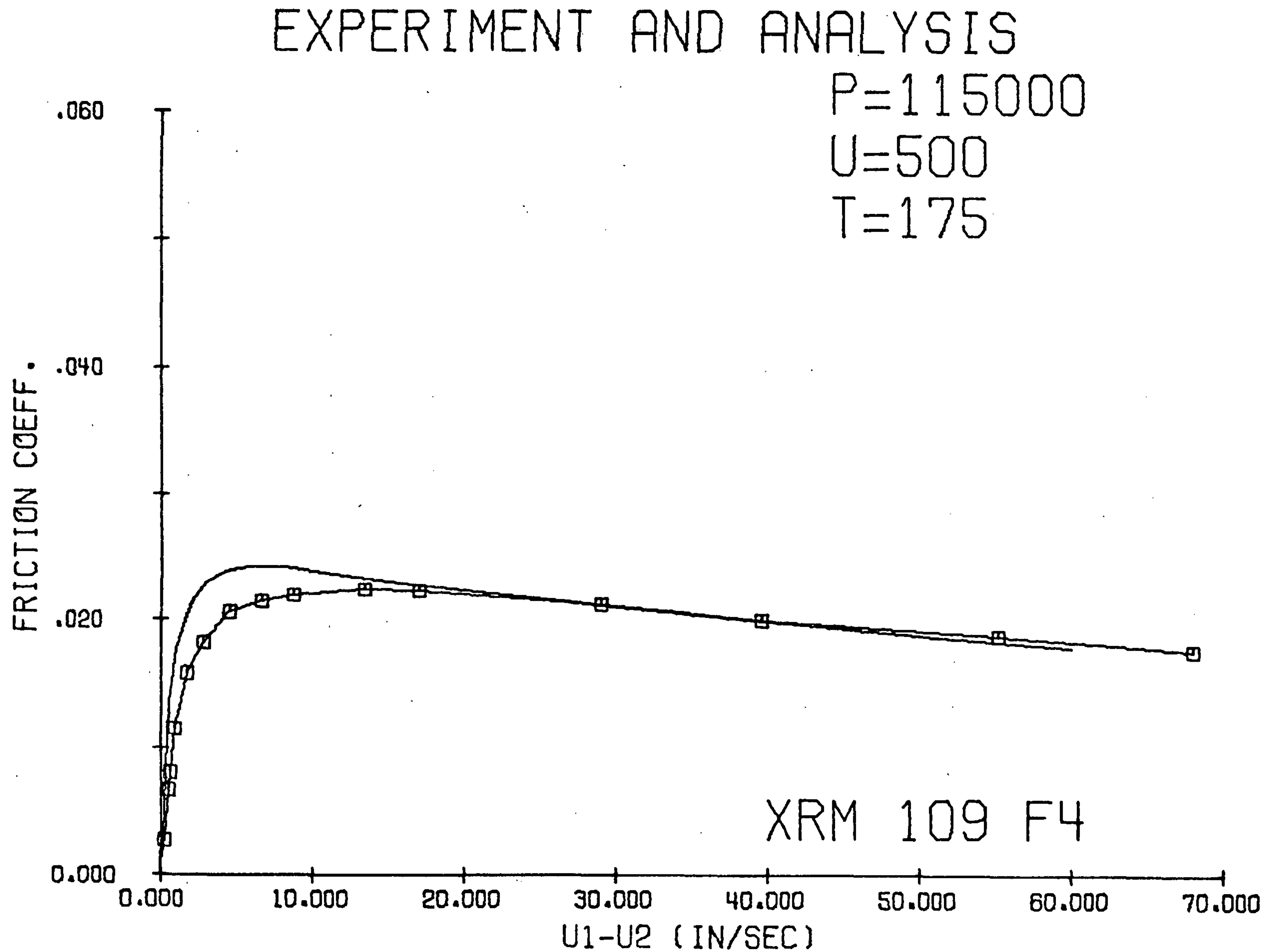

Figure 6.16. Correlation of theoretical friction with experimental data.

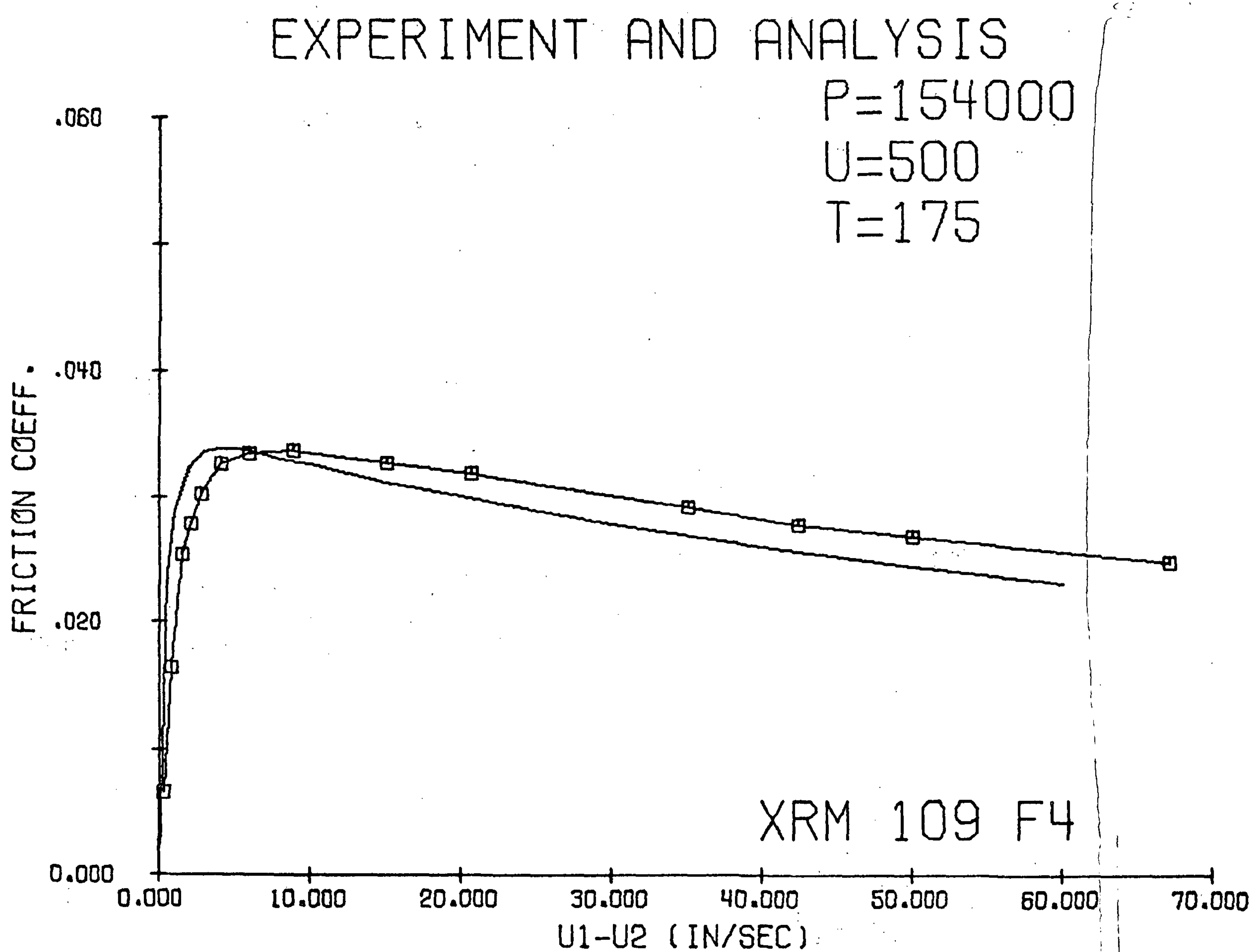

Figure 6.17. Correlation of theoretical friction with experimental data.

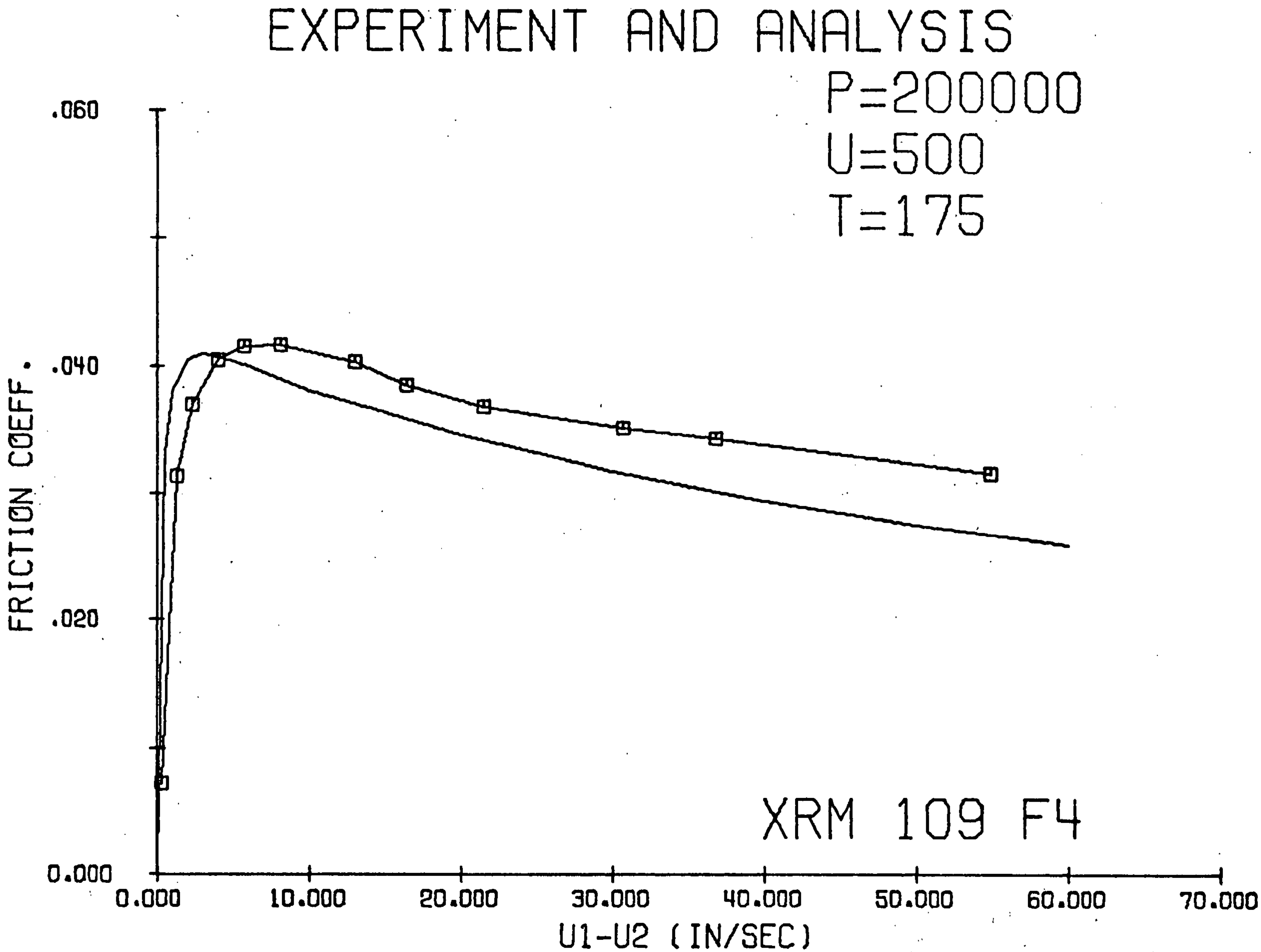

Figure 6.18. Correlation of theoretical friction with experimental data.

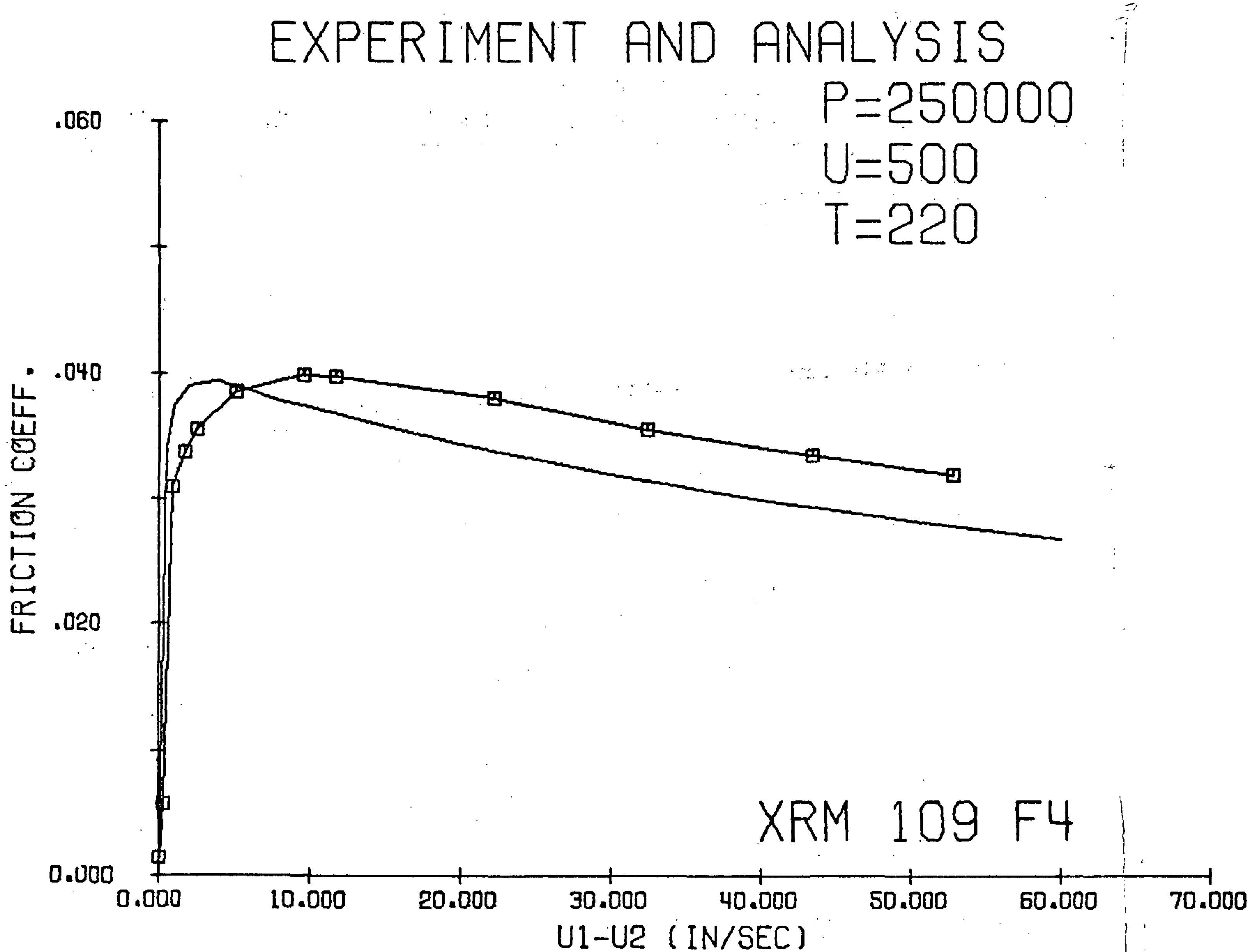

Figure 6.19. Correlation of theoretical friction with experimental data.

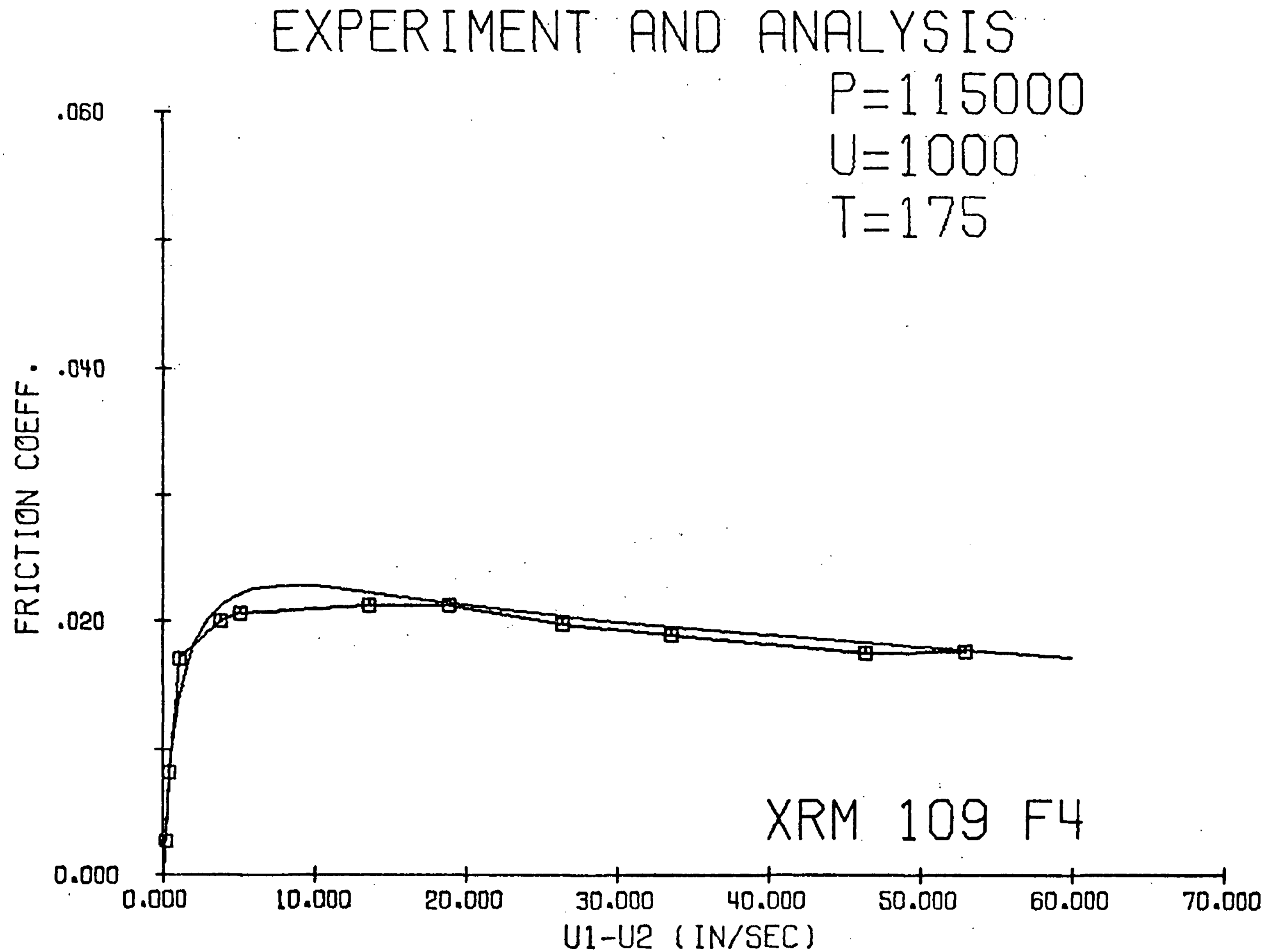

Figure 6.20. Correlation of theoretical friction with experimental data.

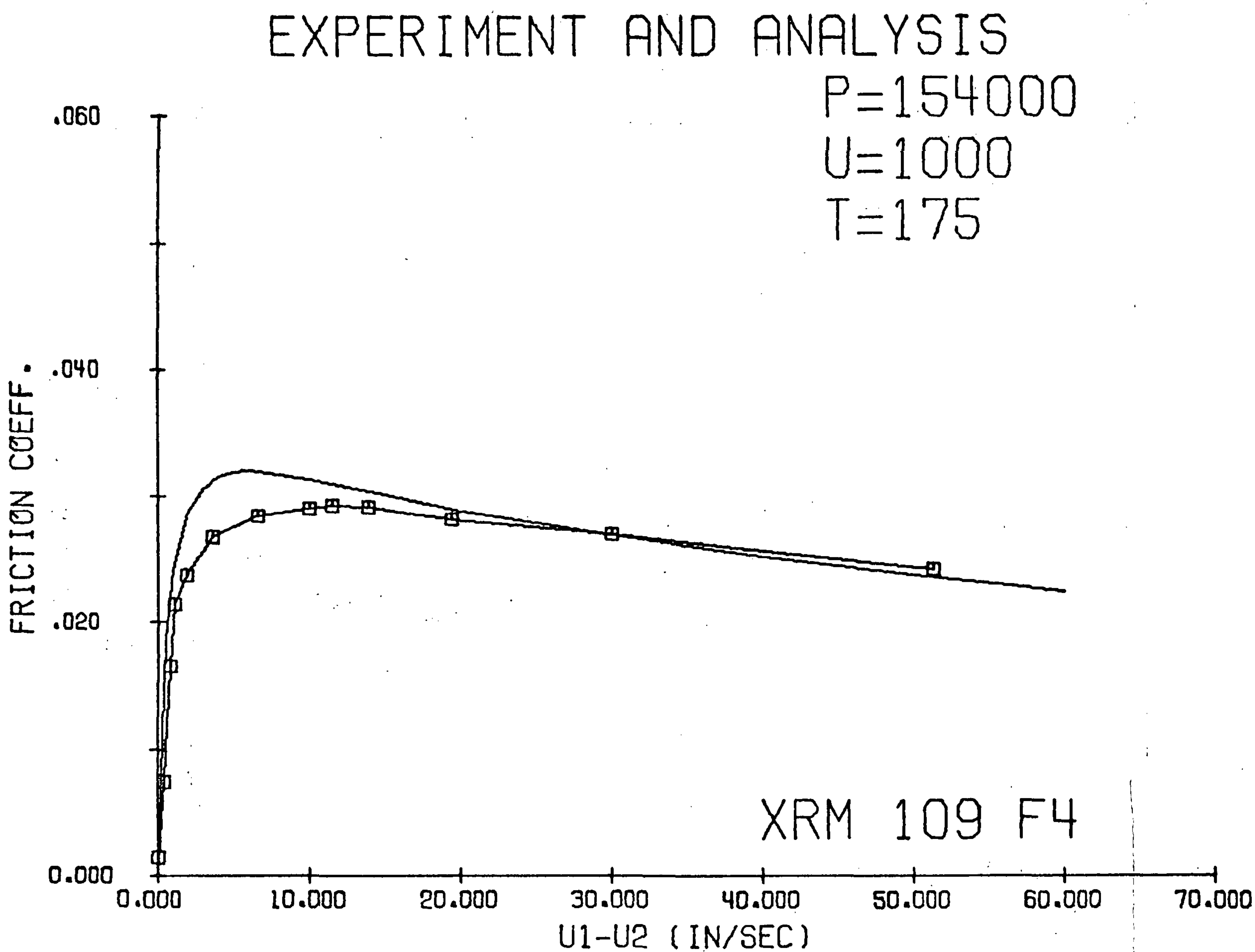

Figure 6.21. Correlation of theoretical friction with experimental data.

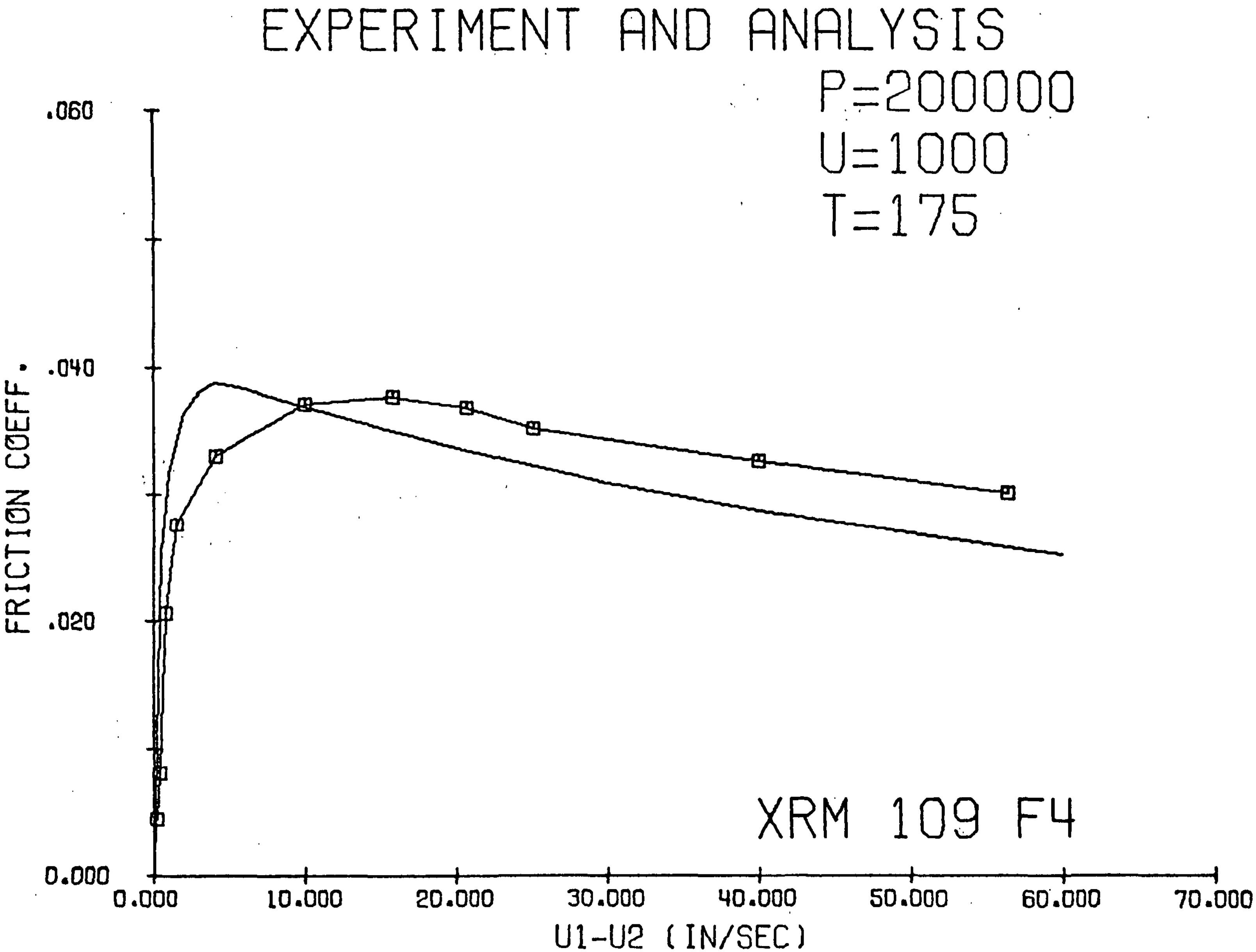

Figure 6.22. Correlation of theoretical friction with experimental data.

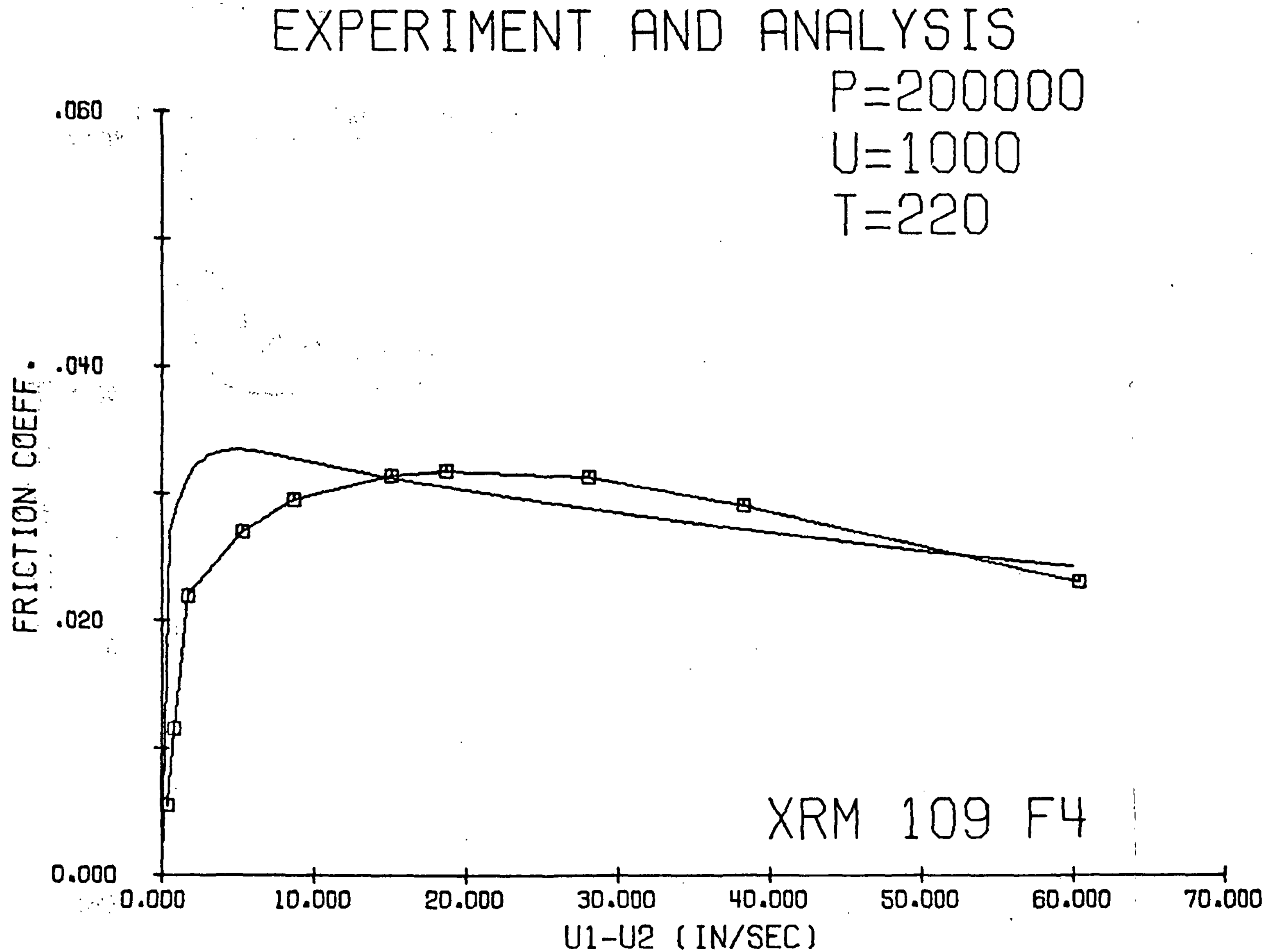

Figure 6.23. Correlation of theoretical friction with experimental data.

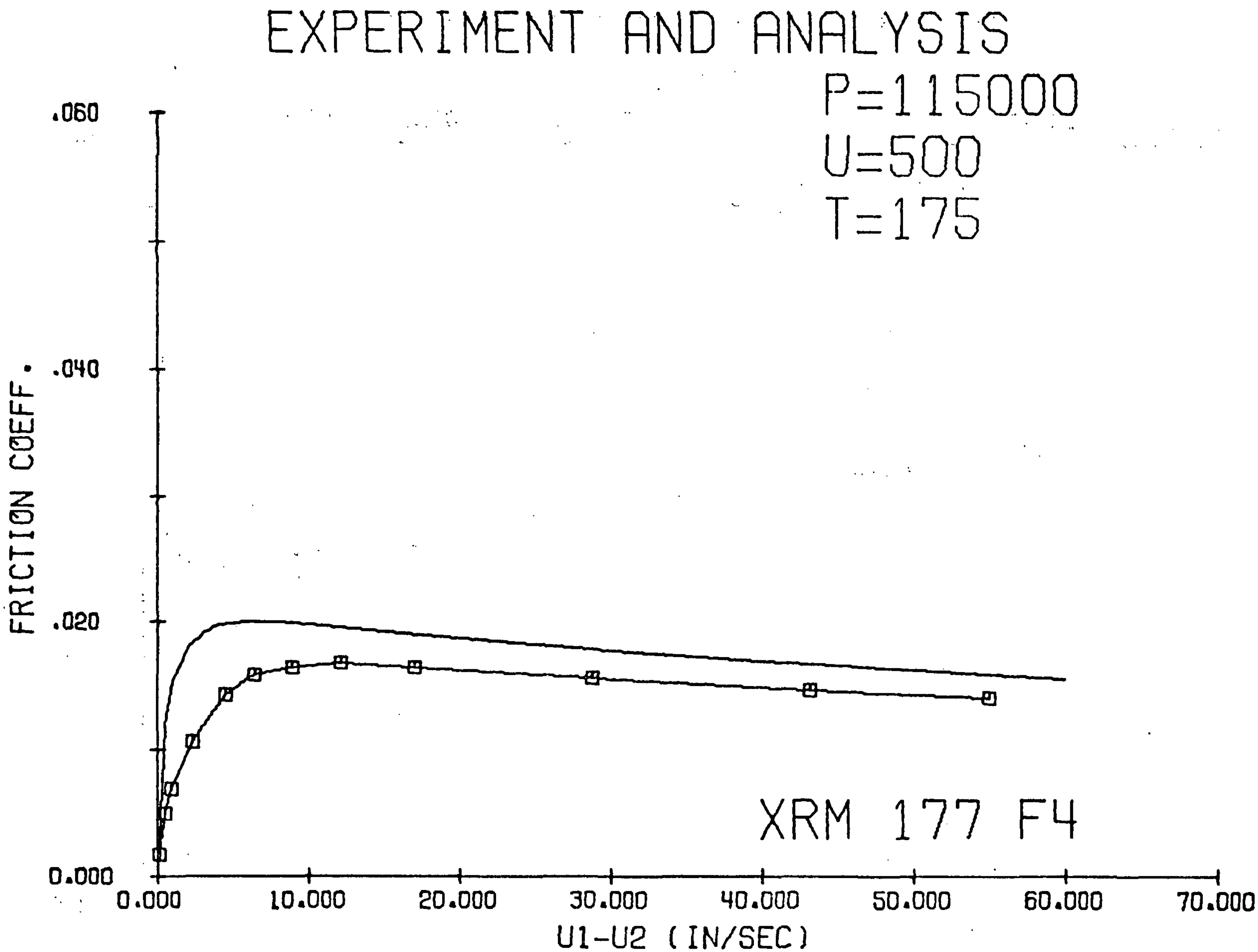

Figure 6.24. Correlation of theoretical friction with experimental data.

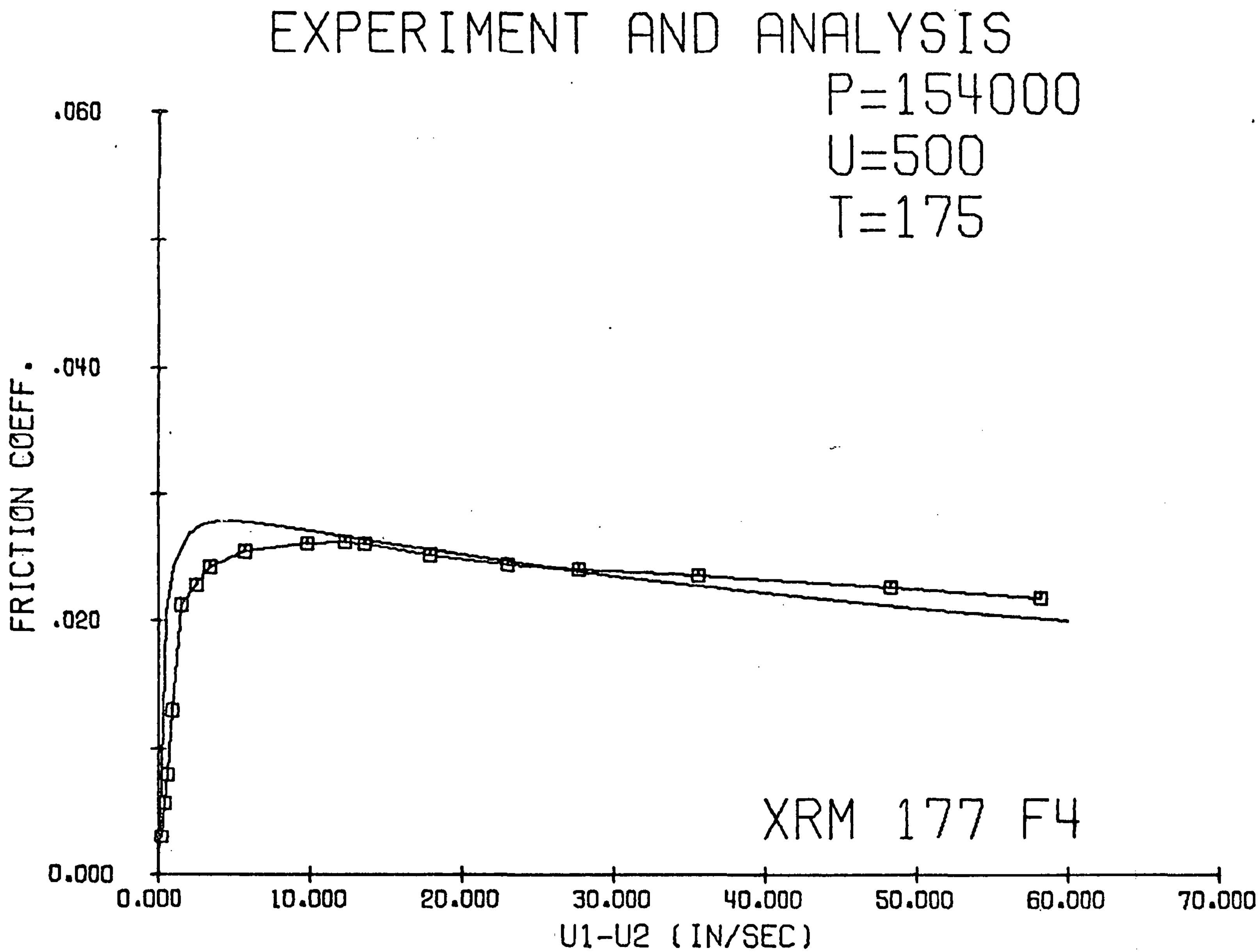

Figure 6.25. Correlation of theoretical friction with experimental data.

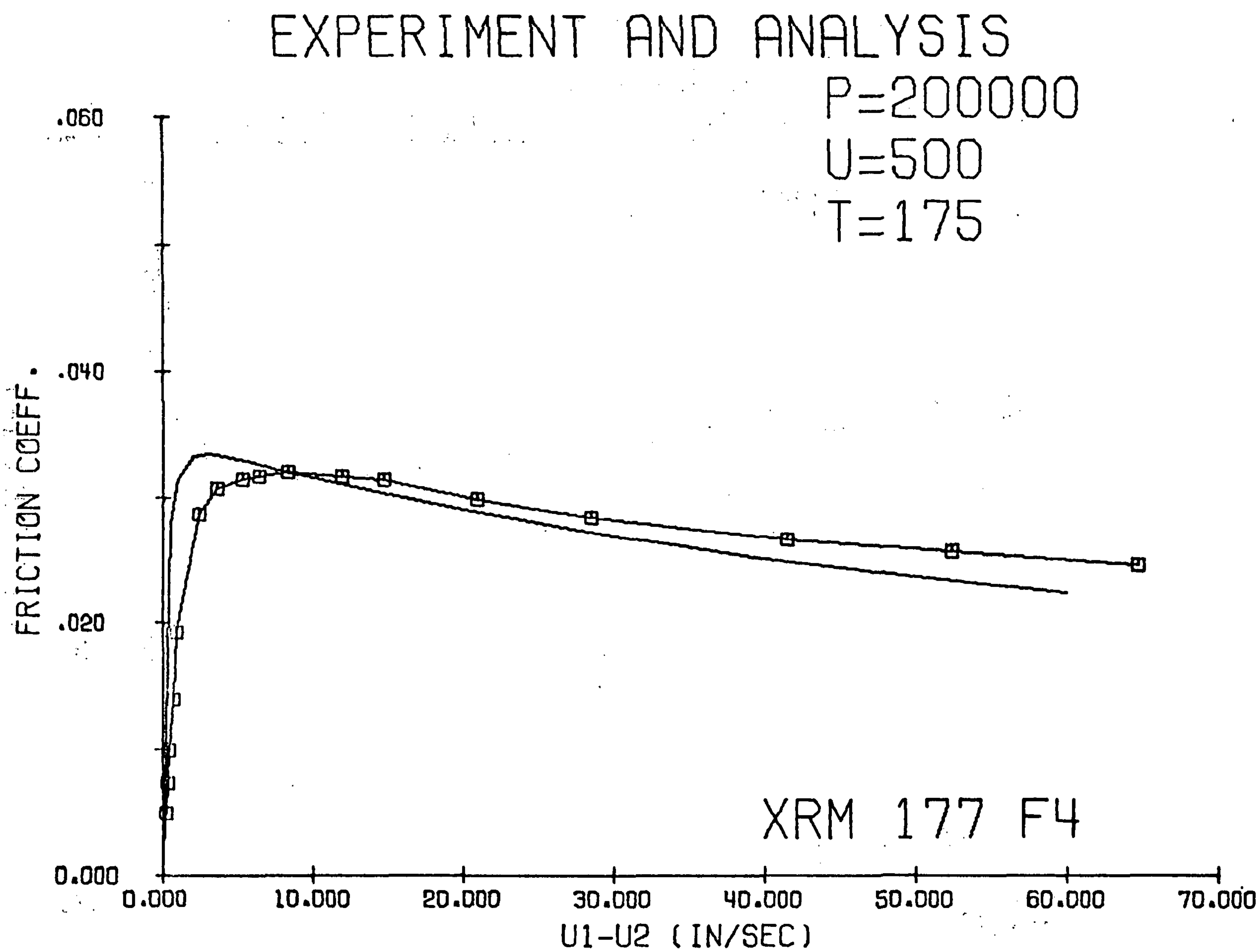

Figure 6.26. Correlation of theoretical friction with experimental data.

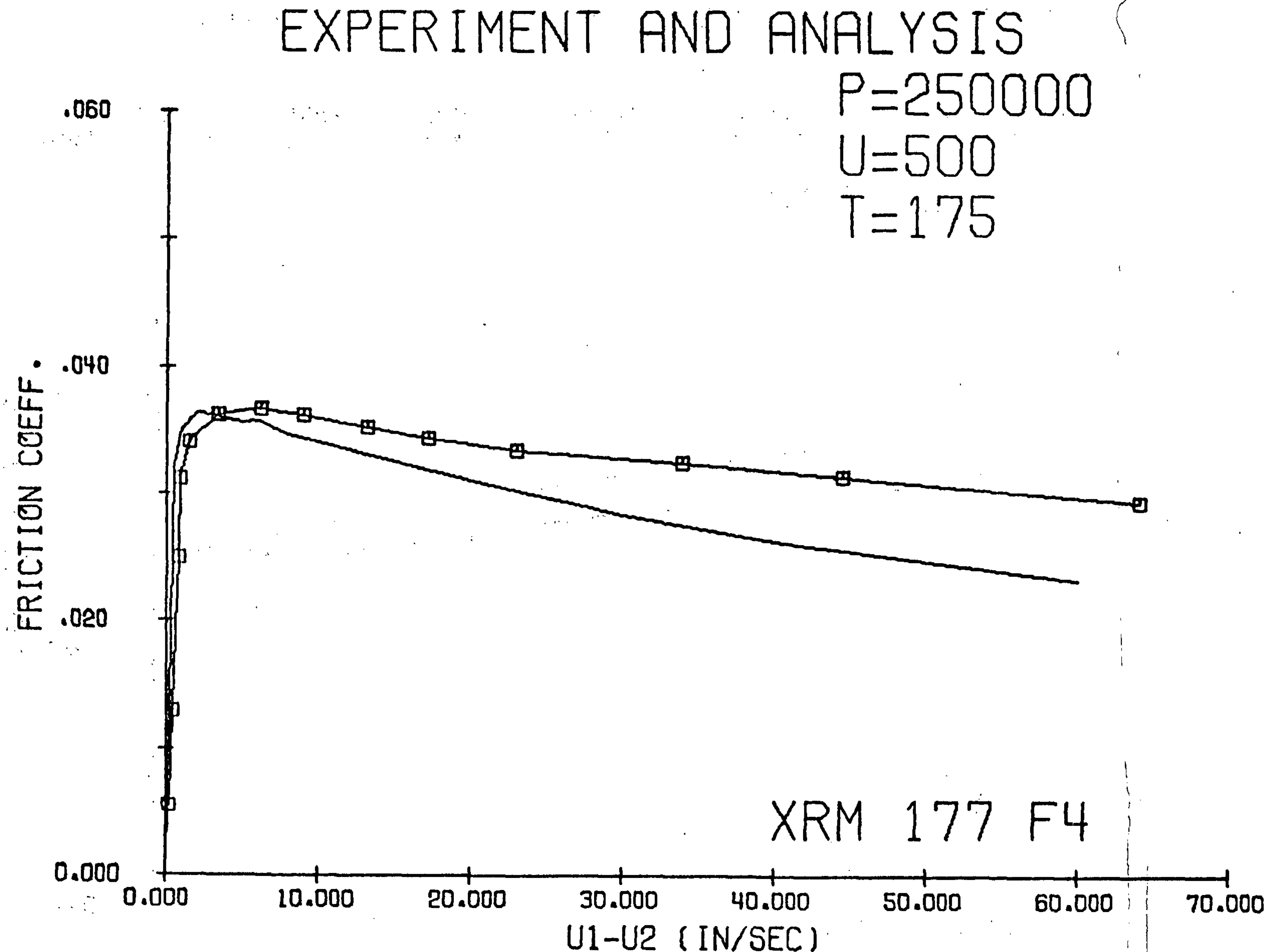

Figure 6.27. Correlation of theoretical friction with experimental data.

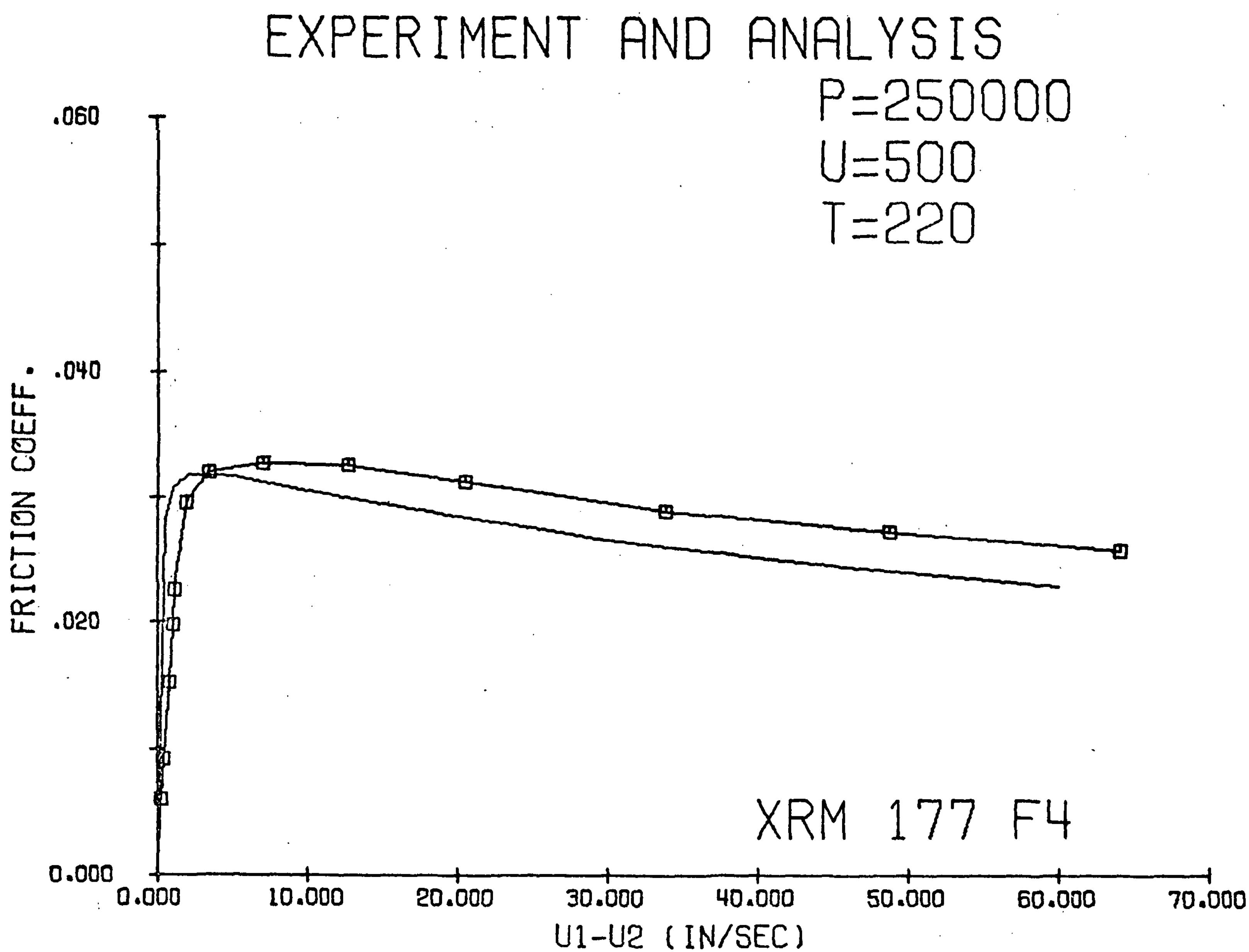

Figure 6.28. Correlation of theoretical friction with experimental data.

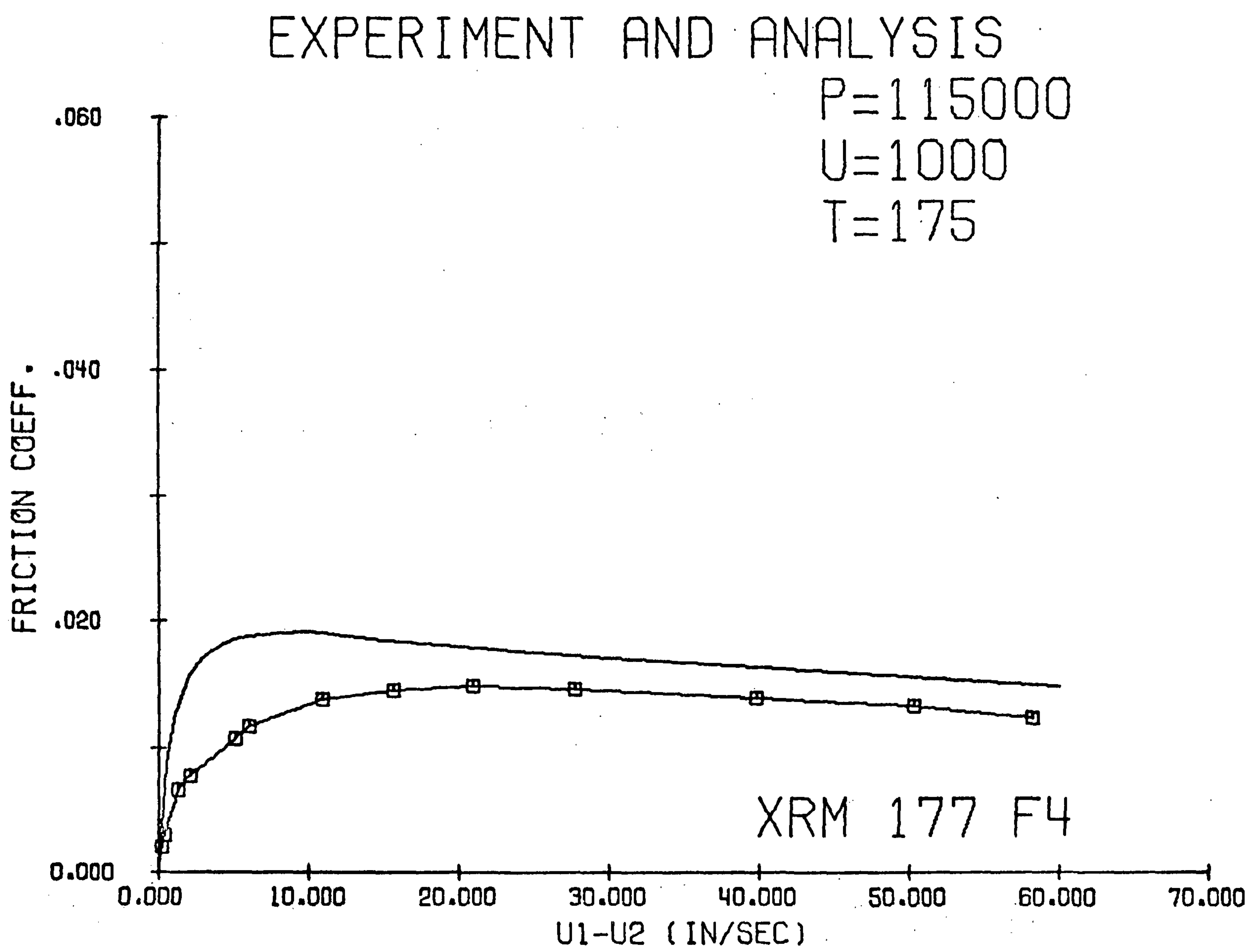

Figure 6.29. Correlation of theoretical friction with experimental data.

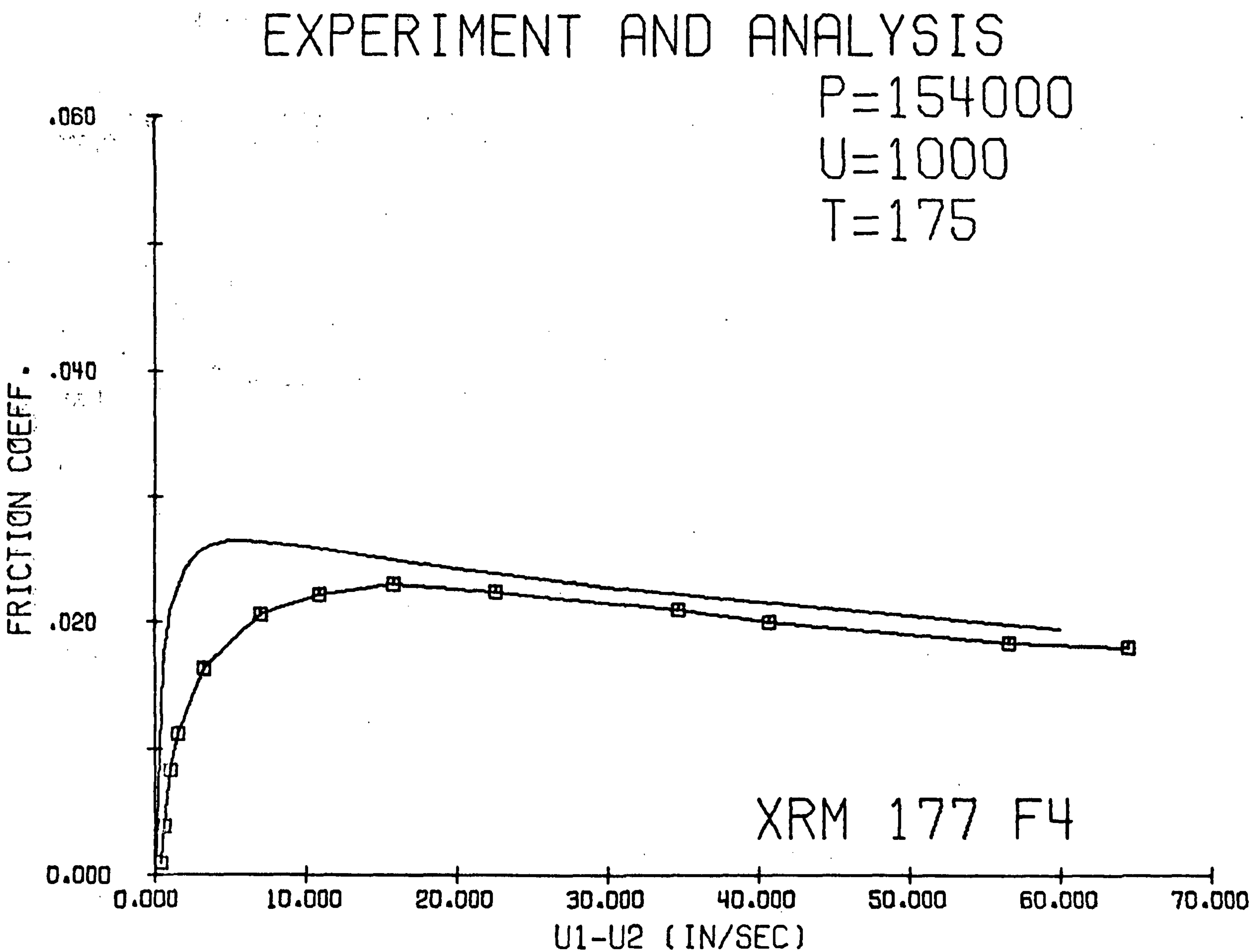

Figure 6.30. Correlation of theoretical friction with experimental data.

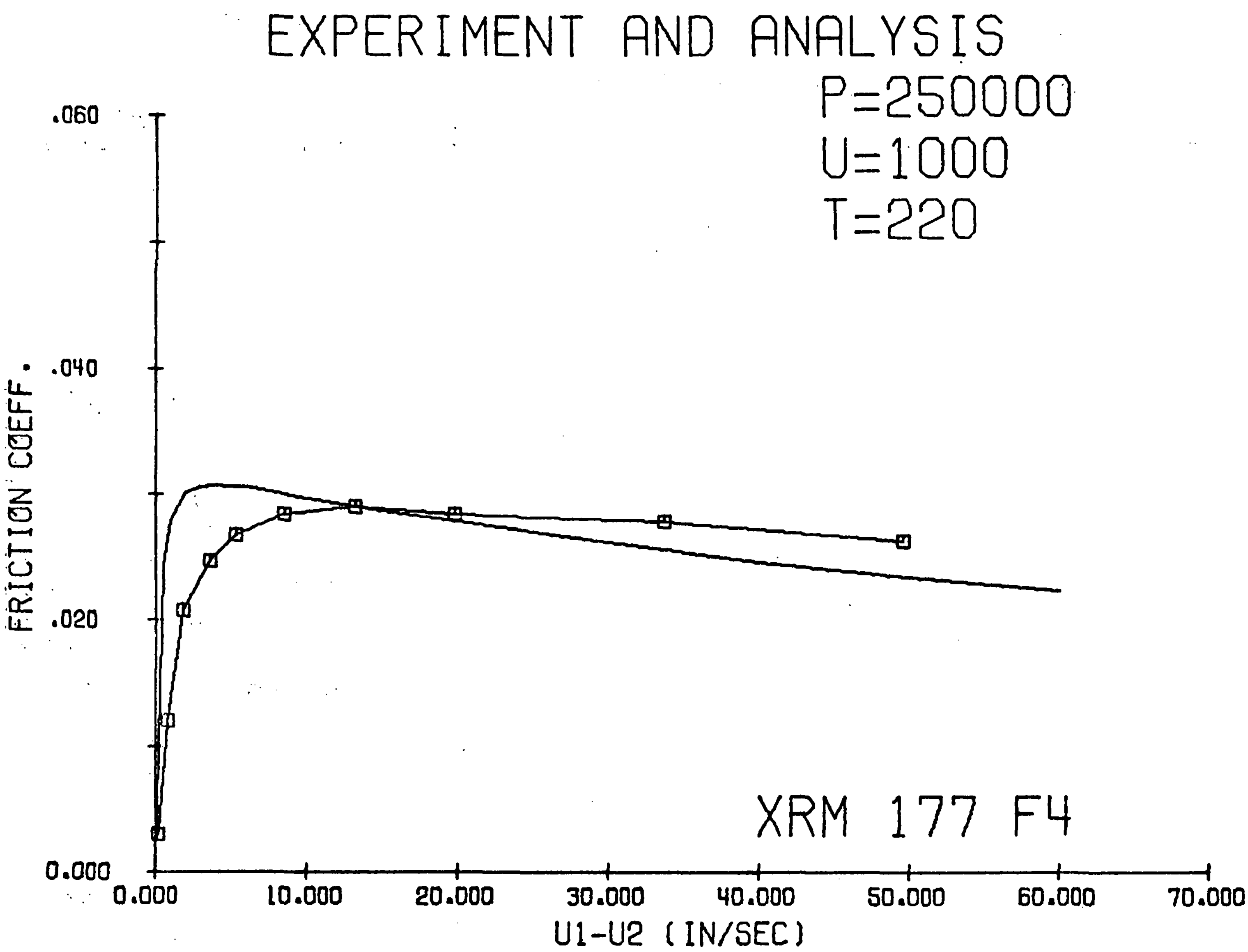

Figure 6.31. Correlation of theoretical friction with experimental data.

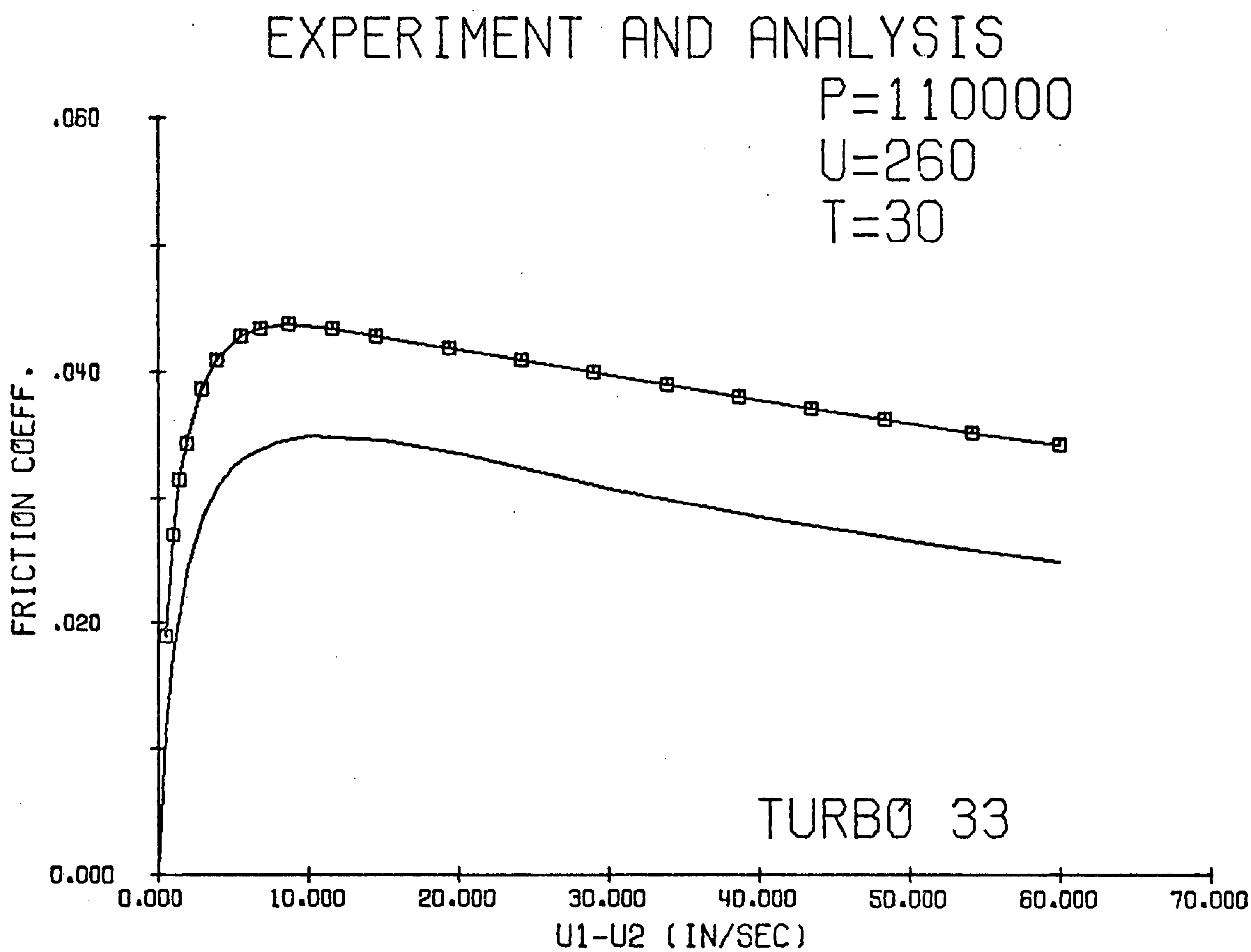

Figure 6.32. Correlation of theoretical friction with experimental data.

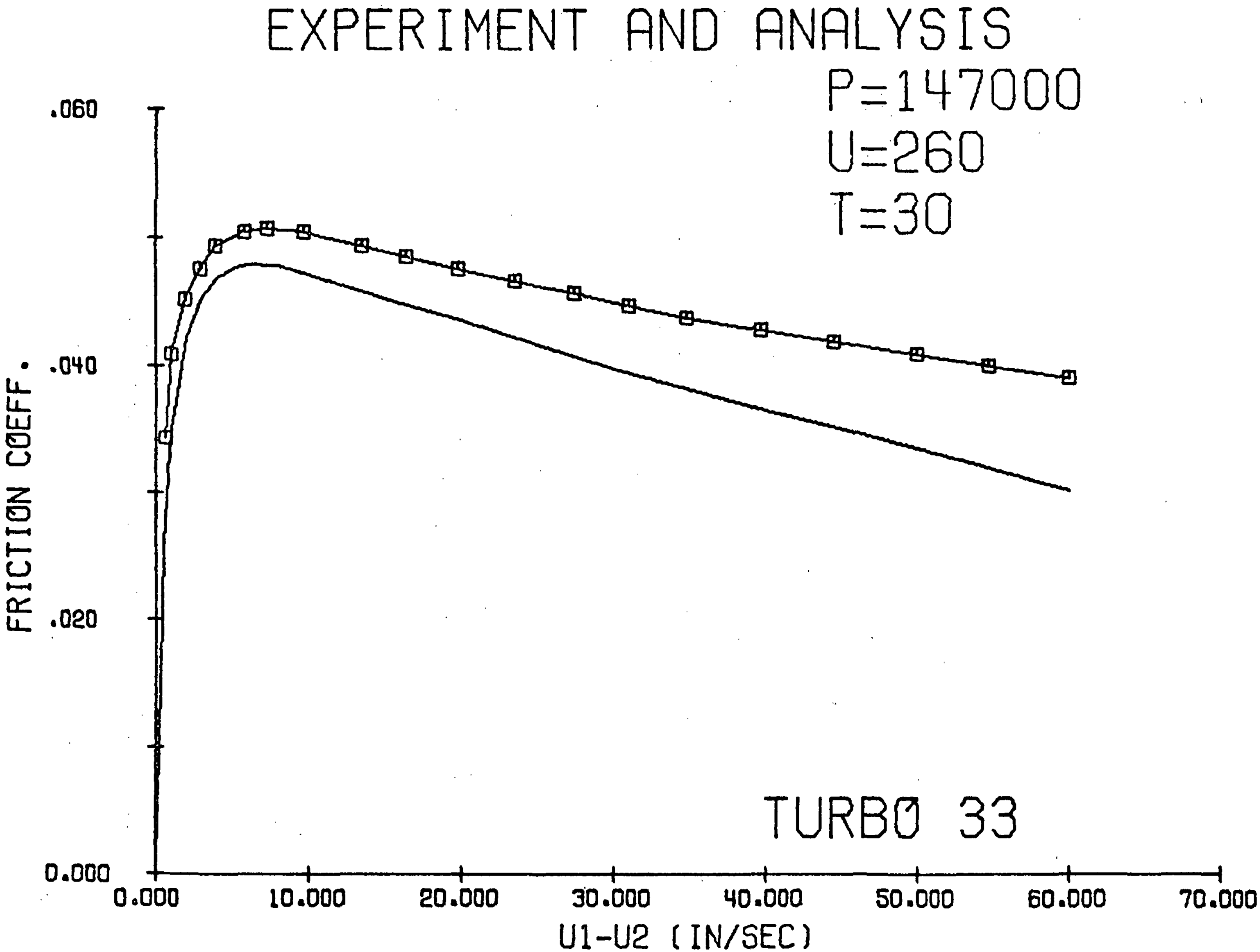

Figure 6.33. Correlation of theoretical friction with experimental data.

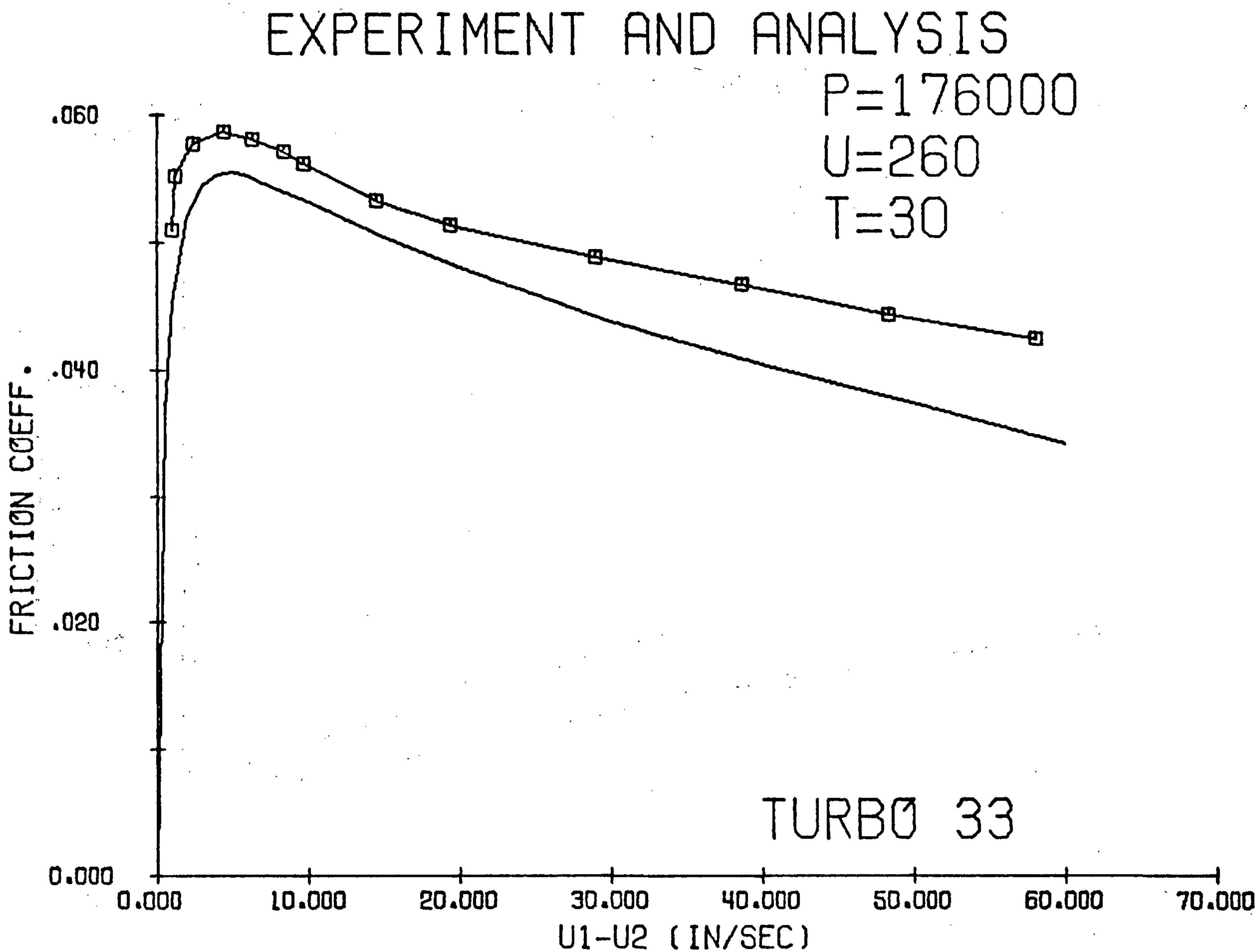

Figure 6.34. Correlation of theoretical friction with experimental data.

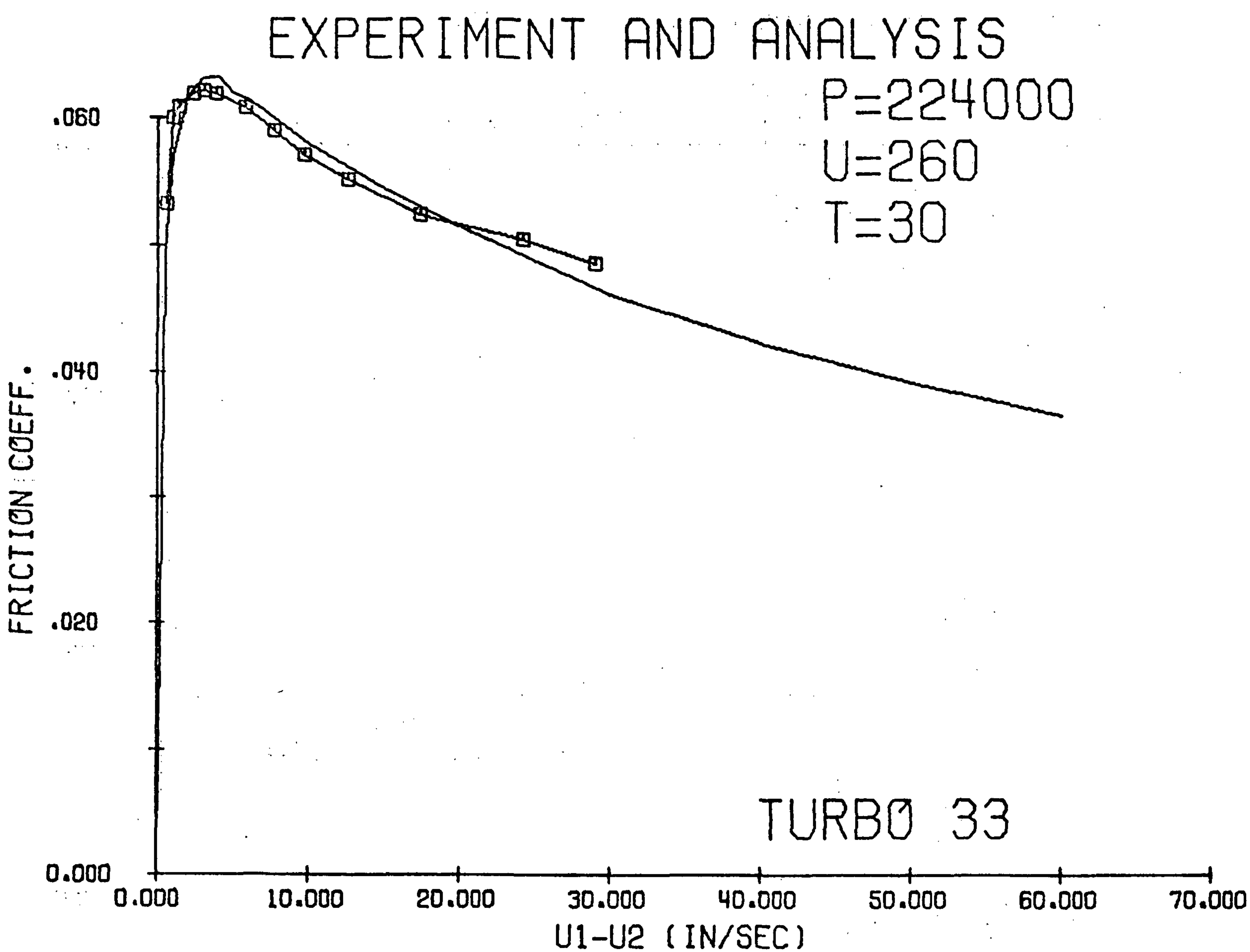

Figure 6.35. Correlation of theoretical friction with experimental data.

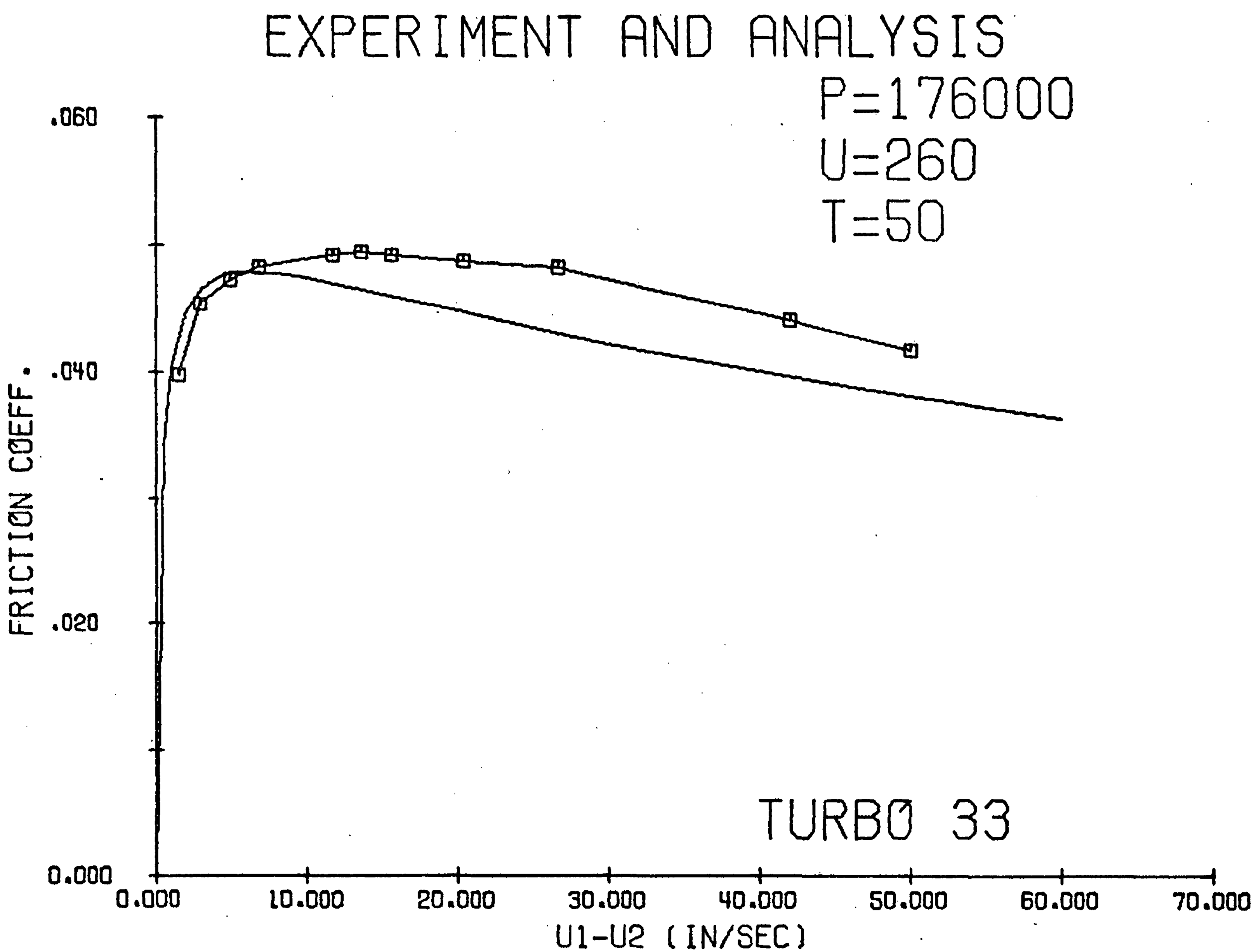

Figure 6.36. Correlation of theoretical friction with experimental data.

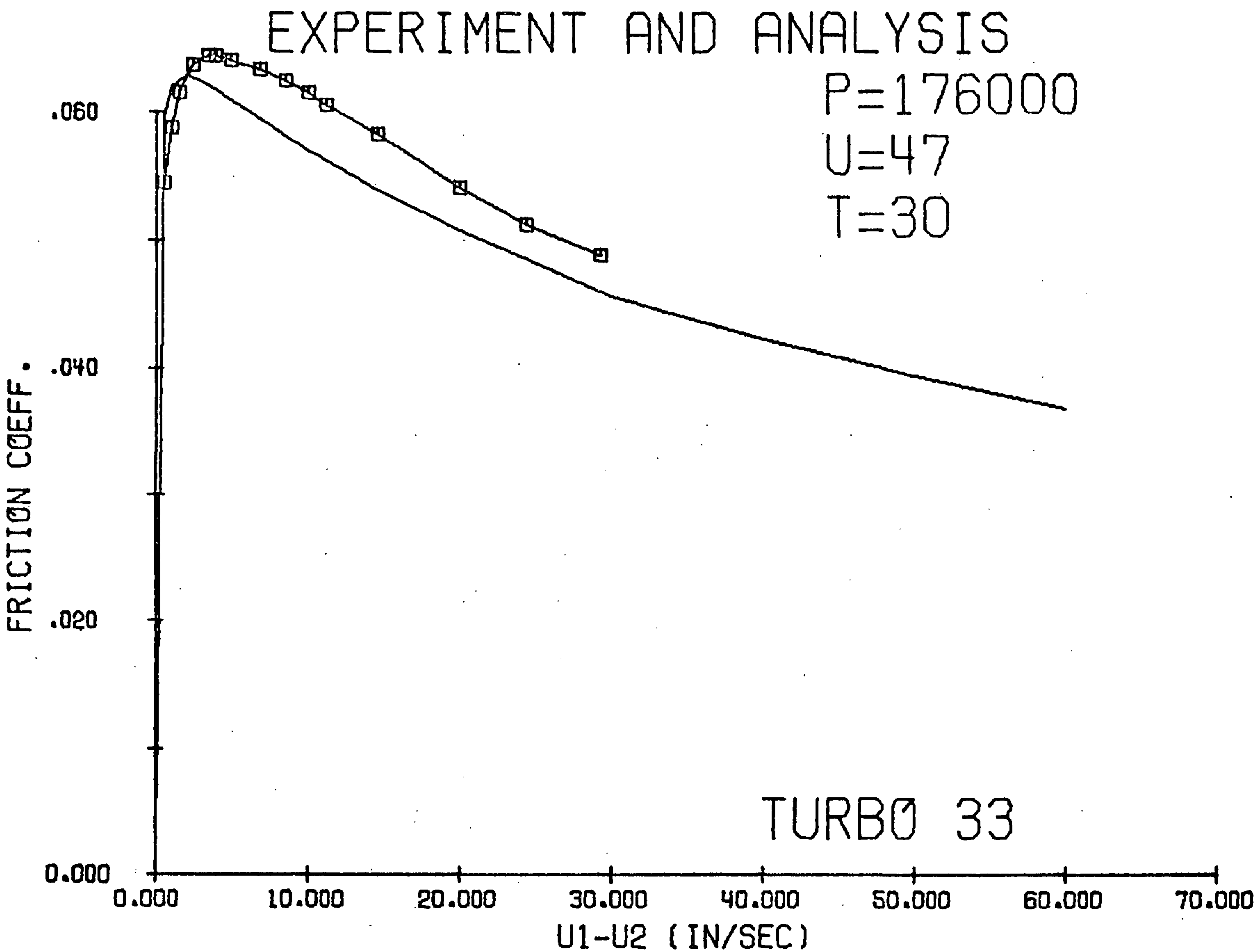

Figure 6.37. Correlation of theoretical friction with experimental data.

lubricant consists of the Mobil 109 F4 as a base with an anti-fatigue polymer additive. This additive may change the limiting shear modulus function which corresponds to a change in the hyperbolic model constant c. A more likely possibility, however, is that the additive increases the film thickness. If this is the case, the shear rates would be lower in the low sliding speed region and the film temperatures would be higher in the high sliding speed region. As previously discussed in section 6.1, this would lower the entire friction coefficient curve. Thus, if the additive does cause an increase in the film thickness, the hyperbolic model with c = .25 might hold true for this lubricant also.

Figure 6.38 shows a comparison of friction versus sliding speed curves analytically determined using the viscosity relationships adopted by Cheng (equation 4.27) and Chu and Cameron (equation 4.26). The curves are extremely close at low sliding speeds but begin to diverge at higher sliding speeds as the temperature rise in the lubricant film becomes larger. The divergence is due to the higher temperature dependence of the Chu and Cameron formulation. It is of little consequence which formulation is used at low sliding speeds since the compressional viscoelastic effects dampen the effects of small changes in equilibrium viscosity. The Cheng formulation gives a slightly better correlation with all experimental data. Unitl extremely high pressure viscosity data is available for lubricants, there will be no other means of choosing among empirical pressure-temperature-viscosity functions.

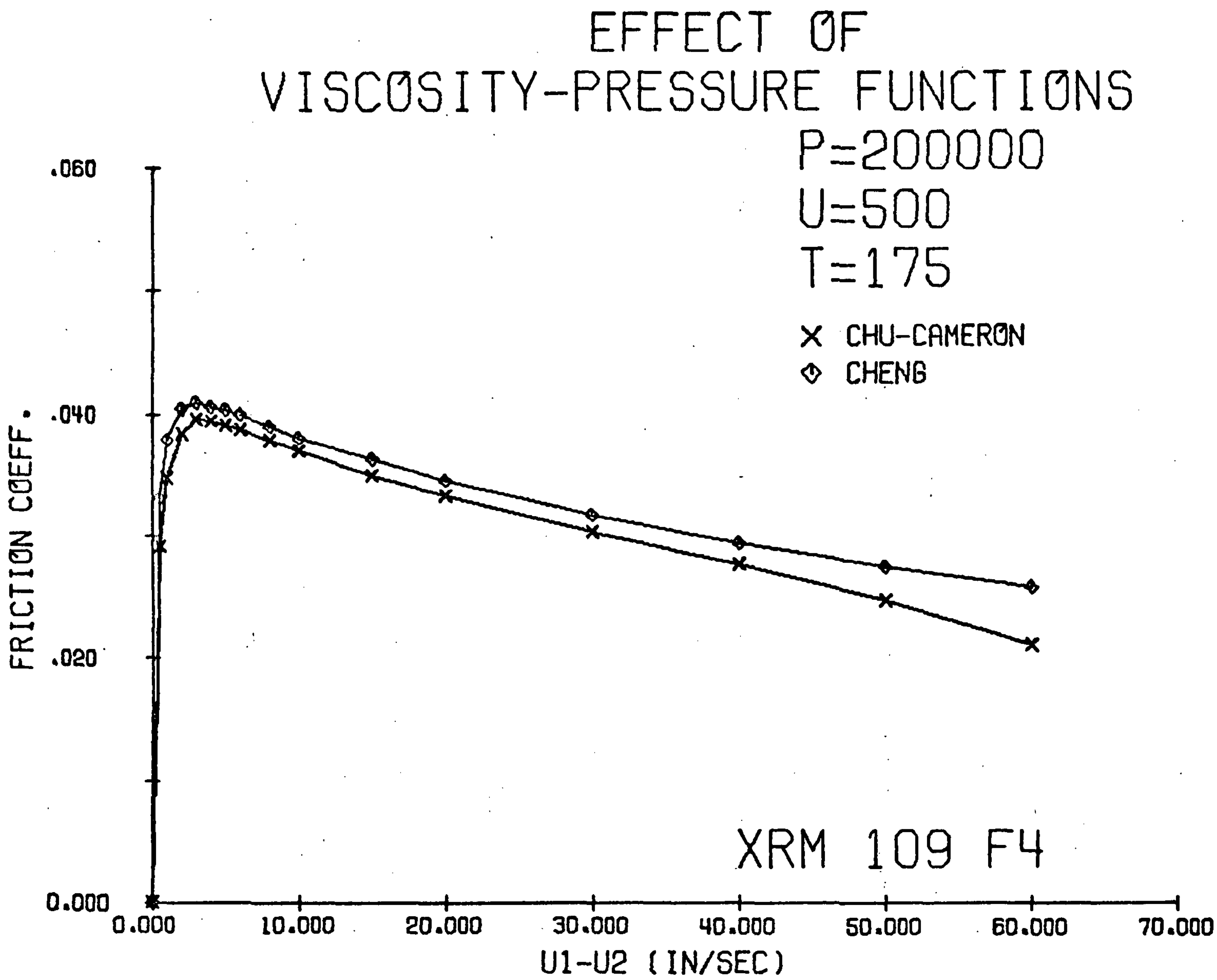

Figure 6.38. Comparison of friction curves based upon different viscosity functions.

6.3 Fluid Property Profiles

In addition to calculating the friction coefficient, the numerical solution of the momentum and energy equations also determines the fluid property profiles in the lubricant film. The profiles confirm the qualitative estimates of Plint [13].

As the lubricant enters the contact zone, the temperature, and therefore the viscosity and the limiting shear modulus are constant across the film. At small sliding speeds and low pressures, the temperature across the film remains constant and equal to the disk surface temperature. The velocity profile is linear and the other property profiles are easily predicted.

Under more severe conditions such as higher sliding speeds and pressures, the thermal effects dominate the profiles. The temperature profile becomes parabolic, and at the most severe conditions, almost triangular. The central plane temperature is 100 ^{o}F to 150 ^{o}F higher than the disk surface temperature. This results in a sharp S-shaped velocity profile with an enormous velocity gradient at the central plane of the lubricant film. The viscosity, and usually more important under these conditions, the limiting shear modulus have minimum values on the central plane. Thus, even though the material properties and the fluid flow are continuous, the conditions are close to those that would occur in a fluid undergoing a discontinuous shear failure on the plane of minimum limiting shear stress.

Two examples of the profiles at the center of the contact zone, those of temperature, velocity, viscosity and limiting shear modulus, are shown in Figures 6.39 and 6.40 for the analysis of Mobil XRM 109 F4 at 200,000 psi maximum Hertzian pressure, 500 in/sec rolling speed and 175 ^{o}F oil inlet temperature. Figure 6.39 is for a 2 in/sec sliding velocity where the velocity profile is no longer linear. Figure 6.40 is for a 50 in/sec sliding velocity where the shear rates at the center plane are extremely high.

6.4 Effect of Convective Heat Transfer

The simplified energy balance given by equation (4.18) was derived by assuming the heat transported by convection was negligible as compared with the heat conducted in the two disks. A ratio of convection to conduction is estimated in equation (4.17) as

$$\frac{\rho c U h^2}{2\ bk}$$

Convection has its largest effect for a maximum value of (Uh^2/b). This corresponds to the condition of maximum rolling speed and minimum load. A program was written to include the effects of convection. Figure 6.41, the friction coefficient-sliding speed curves, include and neglect the convective heat transfer.

As expected, the convection will carry some heat from the contact zone and the lubricant will be slightly cooler. For example, under the conditions for maximum convection, the mid-film temperature at the center of the contact zone is determined by the analysis to be 5 ^{o}F cooler; that is, 210 ^{o}F compared with 215 ^{o}F, at the point of maximum friction coefficient. This only affects the friction coefficient at higher sliding speeds where the temperature gradient in the film becomes significant.

The program including the convective effects takes four times

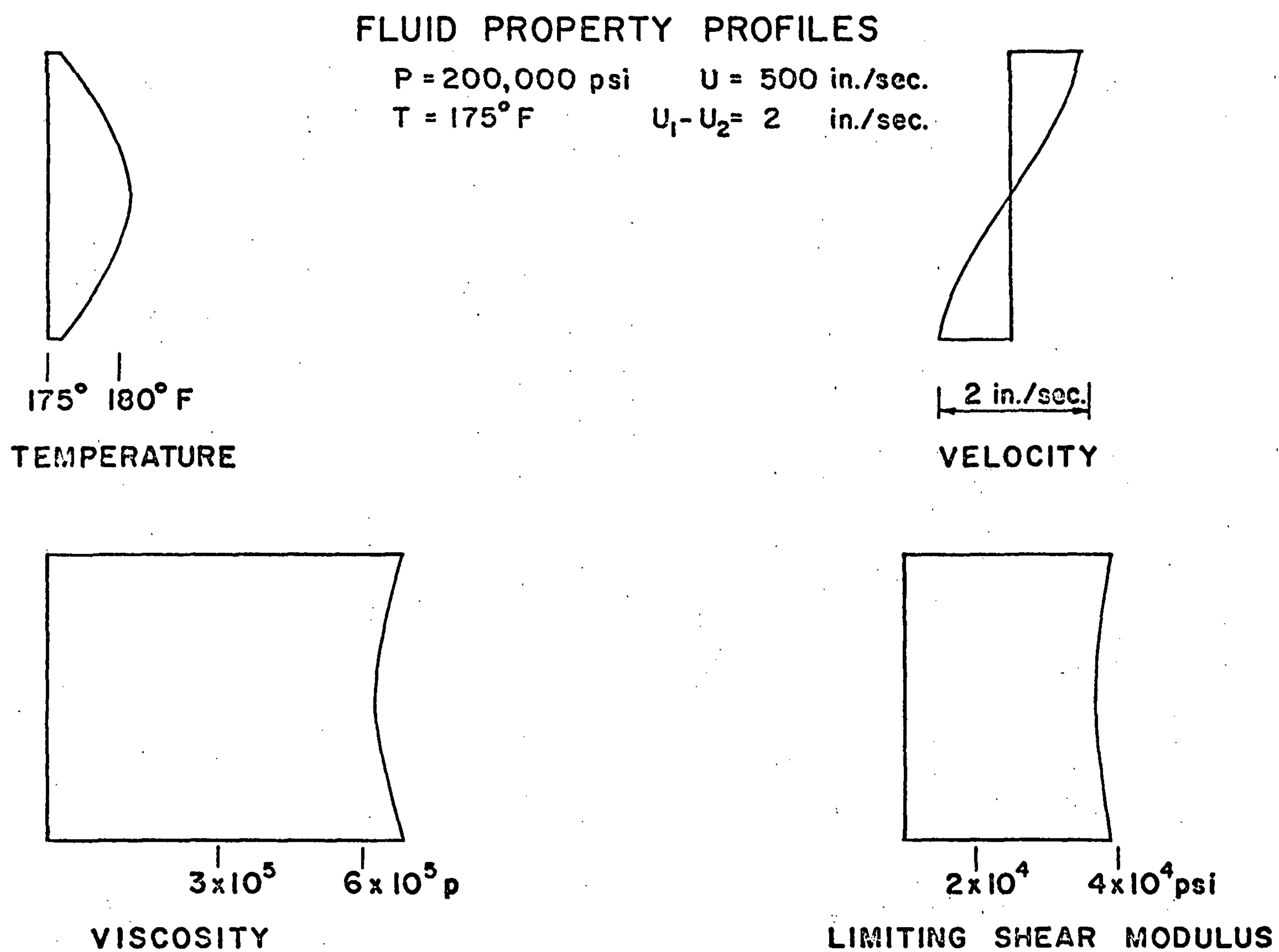

Figure 6.39. Fluid property profiles in the concentrated contact.

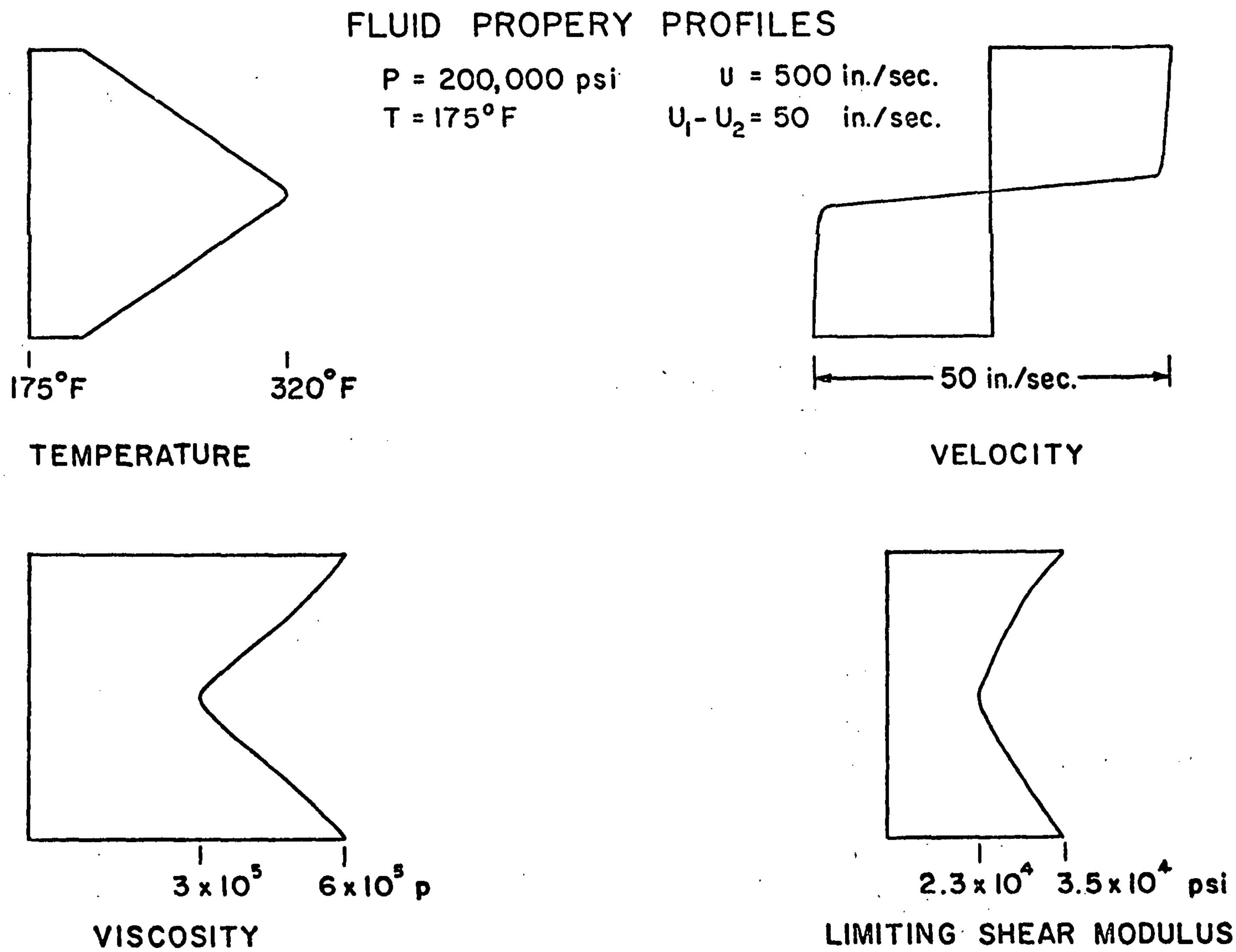

Figure 6.40. Fluid property profiles in the concentrated contact.

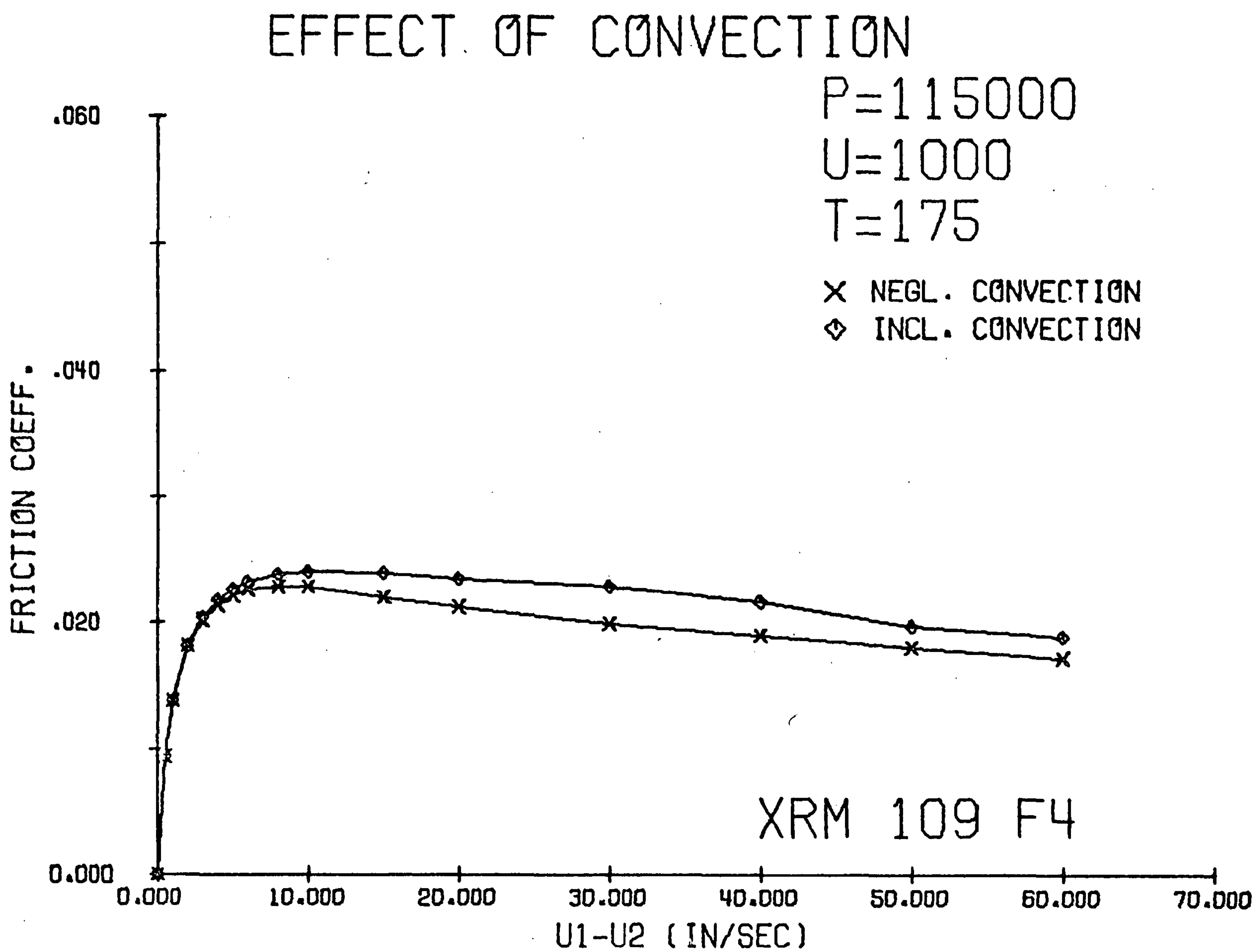

Figure 6.41. The effect of convective heat transfer on the friction coefficient.

the time required by the simpler program which considers conduction only. The results, differing by 5-10% at a maximum, do not warrant this expenditure.

6.5 Effect of Compressional Viscoelasticity

The overall effect of compressional viscoelasticity on the friction coefficient is seen in Figure 6.42. The most prominent feature is the shifting of the maximum value to higher sliding speeds. This is the same effect a longer shear relaxation time would have on the curve. At higher sliding speeds, the flow is dominated by the limiting shear modulus. Therefore, to study the effects of compressional viscoelasticity, attention is focused on the region of low sliding speeds.

The values of traction coefficient for very low sliding speeds have been calculated are are shown in Figures 6.43, 6.44 and 6.45 plotted as a function of the ratio of sliding speed to rolling speed, $\xi = U_1 - U_2/U$, for fixed values of peak pressure and U. To simplify comparisons with experimental data, the calculations have been made for the conditions used by Johnson and Cameron [11] ; that is, hard steel disks of 3 in diameter, a lubricant of viscosity 84 cP at atmospheric pressure and 30 $^{\circ}$C, and maximum Hertzian pressures of 87, 110, 147, 176 and 224 x 10^3 psi.

The variation of traction coefficient with rolling speed may also be presented in terms of an effective viscosity. The effective viscosity $\bar{\eta}$ is defined as that constant viscosity which, for a contact area of width 2b and uniform thickness 2h, would give rise to the measured tractional force. Then the effective viscosity may be

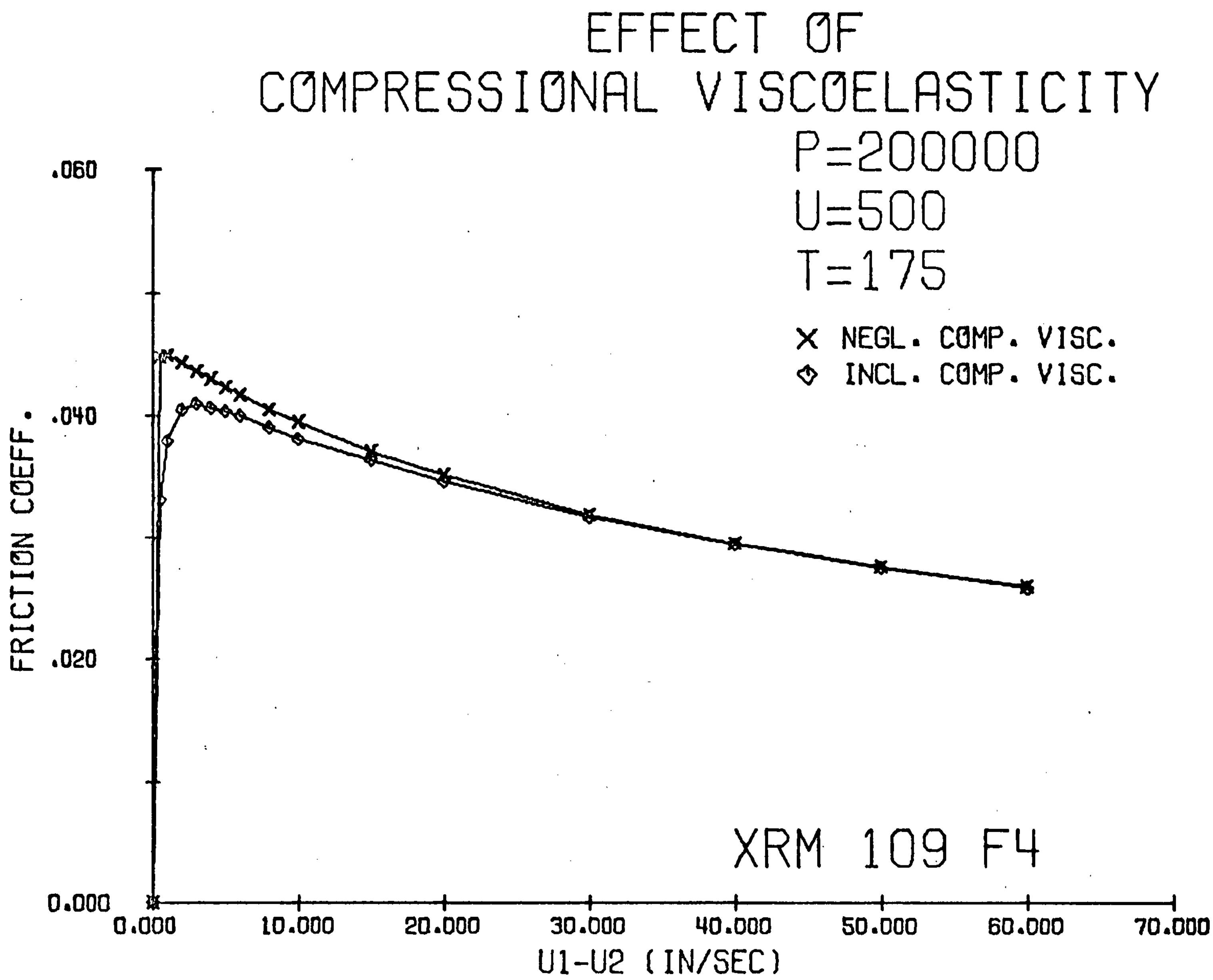

Figure 6.42. The effect of compressional viscoelasticity on the friction coefficient.

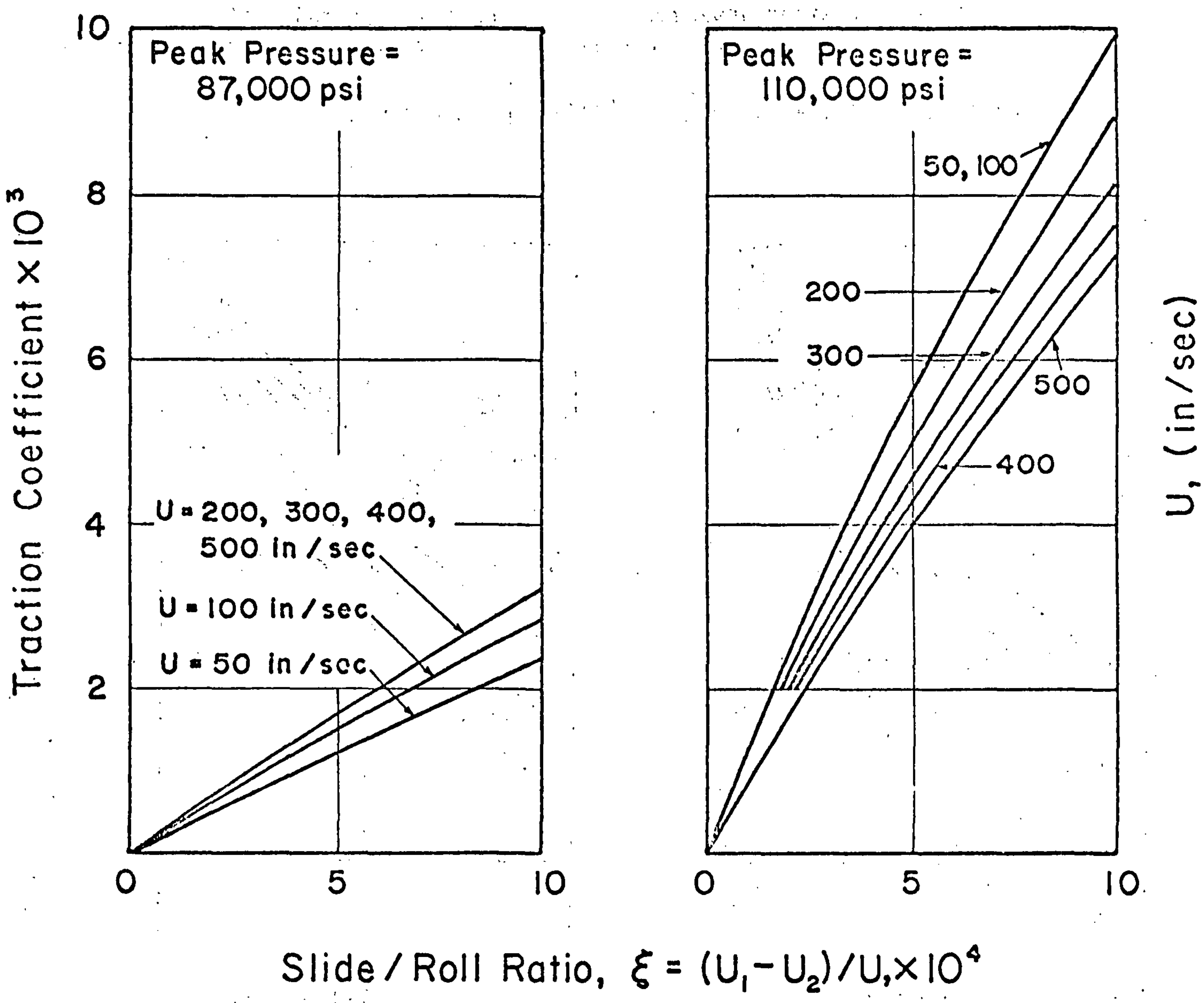

Figure 6.43. Traction coefficient versus slide/roll ratio, at peak Hertzian pressures of 87,000 psi and 110,000 psi, for different rolling speeds.

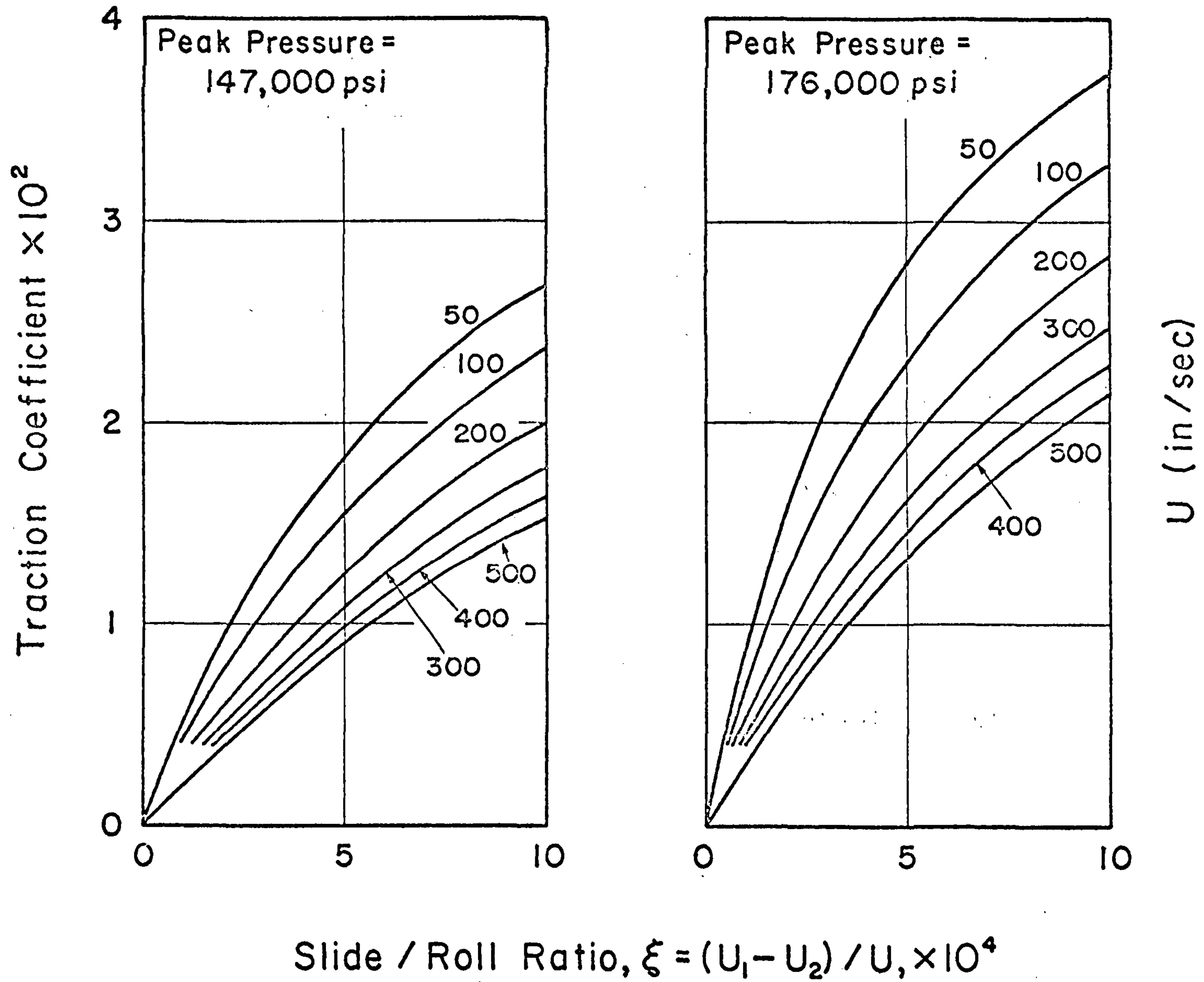

Figure 6.44. Traction coefficient versus slide/roll ratio, at peak Hertzian pressures of 147,000 psi and 176,000 psi, for different rolling speeds.

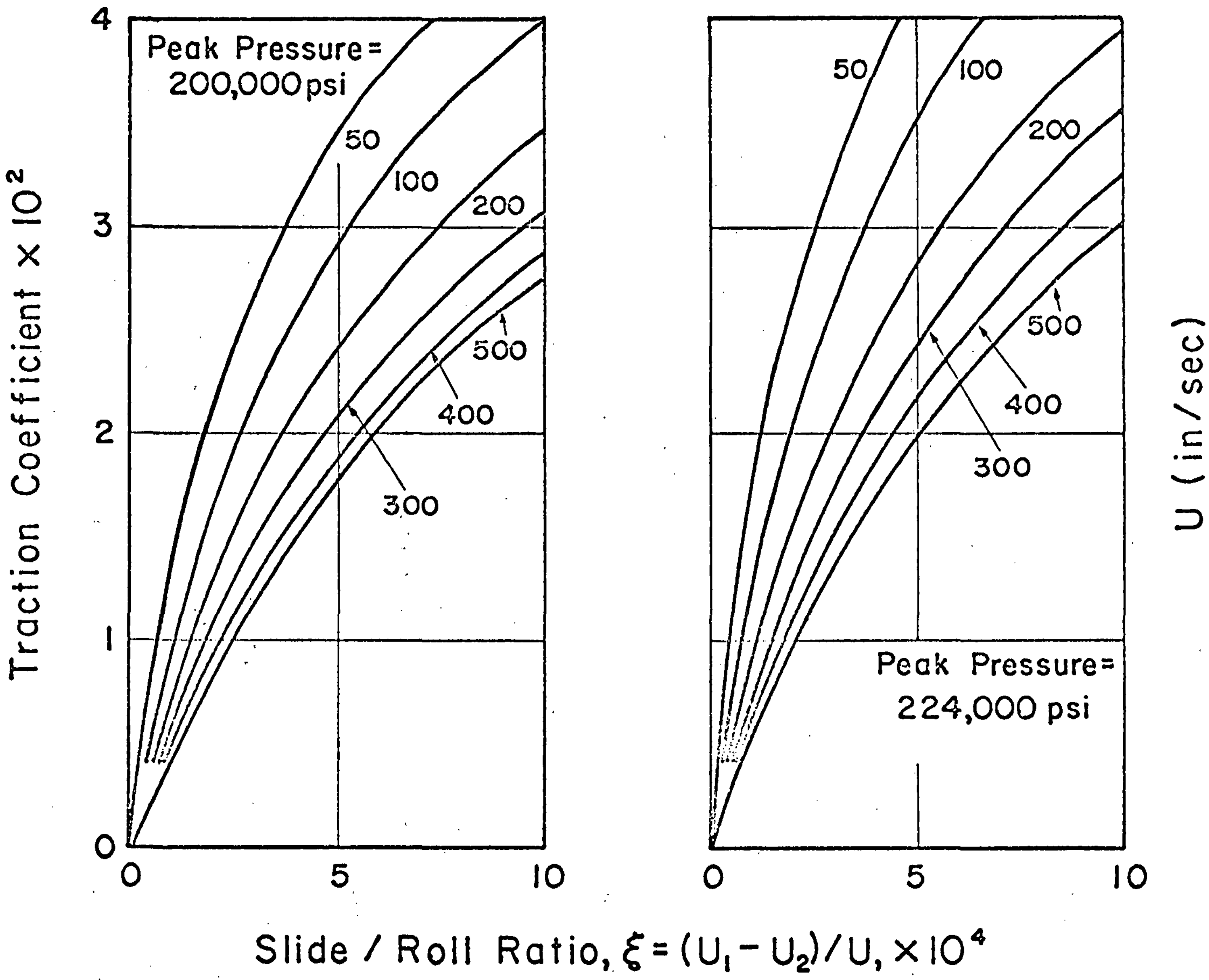

Figure 6.45. Traction coefficient versus slide/roll ratio, at peak Hertzian pressures of 200,000 psi and 224,000 psi, for different rolling speeds.

calculated from the traction coefficient μ by the expression

$$\bar{\eta} = \frac{\mu W h}{(U_1 - U_2) b} \tag{6.4}$$

Alternatively,

$$\bar{\eta} = \left(\frac{\mu}{\xi}\right) \times \frac{Wh}{bU} \tag{6.5}$$

where μ/ξ is the initial slope of the traction curve when plotted as a function of the slide/roll ratio. Values of $\bar{\eta}$ calculated in this way, in the limit of zero sliding speed, are plotted as a function of rolling speed in Figure 6.46.

The calculated values of traction coefficient show a small dependence on rolling speed when plotted as a function of the ratio of sliding speed to rolling speed. Johnson and Cameron [11] report that the traction coefficient was experimentally found to depend only on the slide/roll ratio and to be independent of the rolling speed. In the present analysis, this behavior is found only at the lower pressures, and then only over a limited range of rolling speeds (Figure 6.43), although the values of traction coefficient are similar to those meaured by Johnson and Cameron.

The curvature of the lines in Figures 6.43, 6.44 and 6.45 reflects the departure from Newtonian behavior of the lubricant with increasing shear rate. At low sliding speeds, the heat generated due to shearing in the lubricant is negligible. No temperature gradient exists within the lubricant film, and the temperature throughout the contact zone remains equal to the disk temperature. The decreasing slope of the traction coefficient curves with increasing sliding speed is thus a consequence of the decrease in the apparent viscosity with increasing shear rate. The effect is most marked at the higher pressures and lower

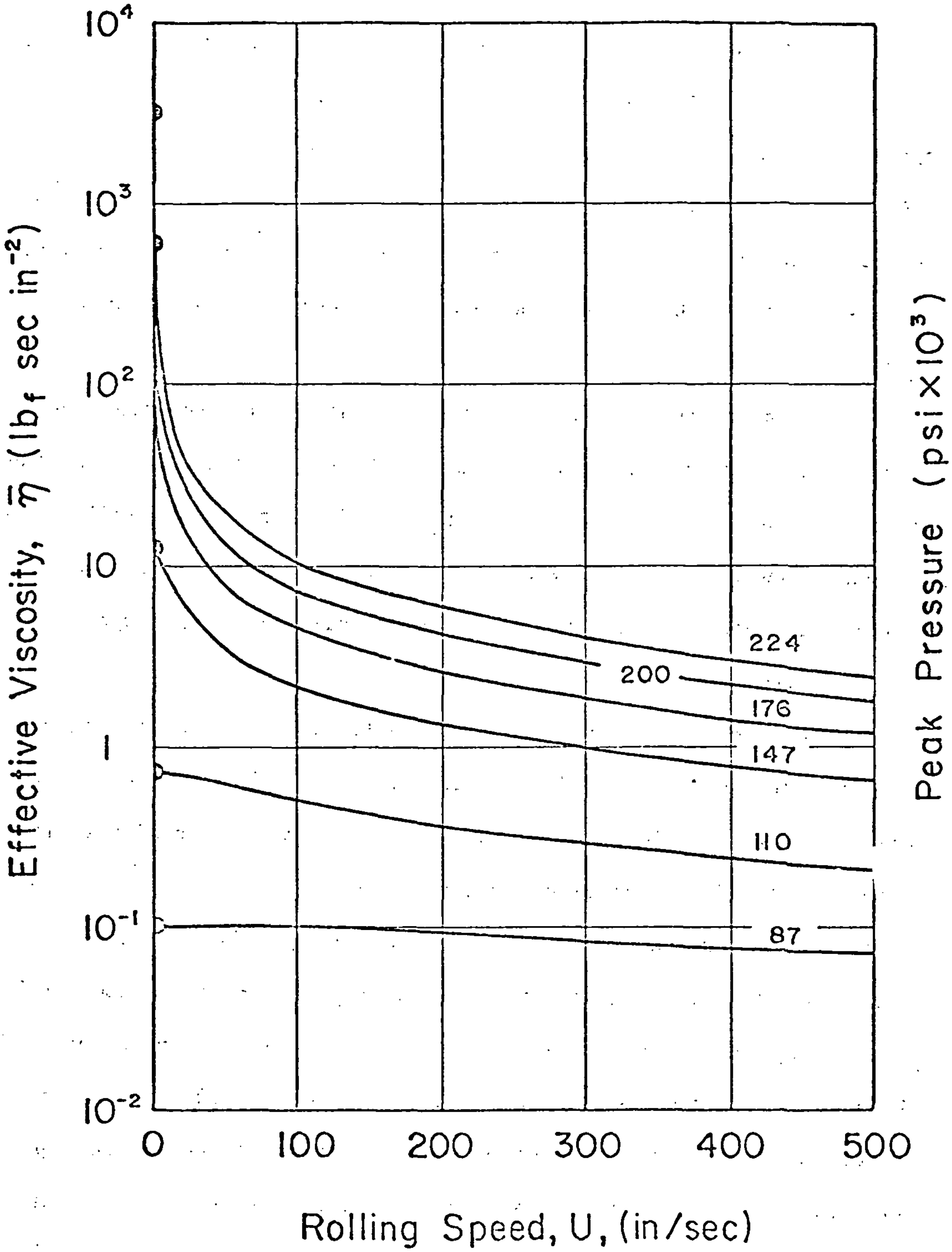

Figure 6.46. Effective viscosity versus rolling speed, in the limit of zero sliding speed, for different values of peak Hertzian pressure.

rolling speeds when the small values of film thickness result in higher values of shear rate. The variation of traction coefficient with sliding speed is shown in more detail in Figure 6.47 for a peak pressure of 176,000 psi. The behavior at the other measures conforms to the same general pattern. In Figure 6.47 Newtonian behavior, a viscosity which is independent of shear rate, is shown by a straight line of unity slope.

It may be calculated from Figure 6.47 that at low rolling speeds it is experimentally impossible to obtain Newtonian conditions, as the low sliding speeds required -- less than 0.01 in/sec -- are well below the experimental range. This fact has important consequences when attempts are made to evaluate the effective viscosity from experimental data at lower rolling speed.

Two features of Figure 6.46, showing the variation of effective viscosity with rolling speed under isothermal and Newtonian conditions, merit special attention. The first of these is the great similarity in the shapes of the curves at rolling speeds above 50 in/sec, at all but the lowest pressure. This type of behavior has been observed experimentally, as seen, for example, in Figure 6.48 taken from Crook [4]. The second feature is the extremely rapid fall in the effective viscosity at low rolling speeds for pressures above 110,000 psi. Reliable measurement of the traction force is difficult at rolling speeds below 10 in/sec and high values of peak pressure, as the small film thickness becomes comparable with the dimensional irregularities of the disk surfaces, and full elastohydrodynamic conditions no longer exist. Extrapolation of results obtained at higher rolling speeds is

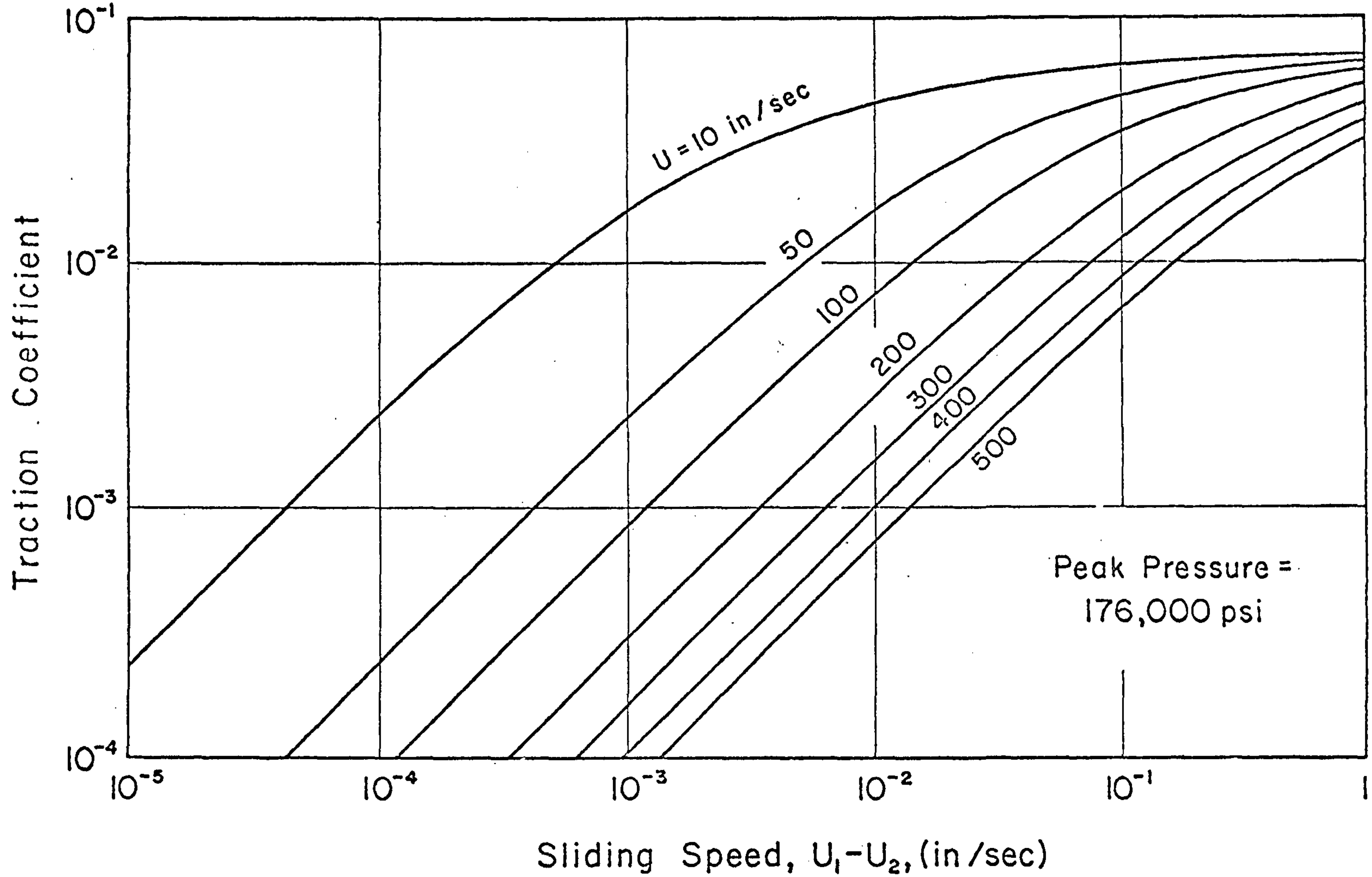

Figure 6.47. Traction coefficient versus sliding speed, at a peak Hertzian pressure of 176,000 psi, for different rolling speeds.

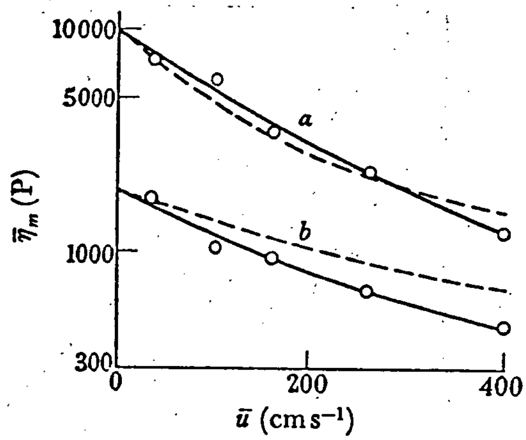

Figure 6.48.

The effective viscosity ($\bar{\eta}_m$) as a function of rolling speed. (*a*) 30 °C; (*b*) 45 °C. —o— deduced from experimental results; ----, calculated from visco-elastic hypothesis. Load = $7{\cdot}4 \times 10^7$ dyn cm^{-1}.

Curve from Crook [4].

therefore necessary if a value of effective viscosity at zero rolling speed is desired. Furthermore, the present analysis predicts that shear rate effects will be significant even at the lowest sliding speeds which can be reached experimentally. The measured values of the traction force will therefore be less than the values which would be obtained under Newtonian conditions. This effect, taken in conjunction with the rapid change in value of the effective viscosity at low rolling speeds, makes the extrapolation of experimental data to zero rolling speed subject to extremely large errors, the magnitude of the error increasing as the peak pressure is increased.

It is suggested therefore, that the observation of Johnson and Cameron, [11 , Figure 15] whereby the same reduction in effective viscosity with rolling speed was observed at all pressures, is a consequence of the errors inherent in such an extrapolation. If this is so, it follows that the sharp change in the rate of increase of viscosity with pressure at pressures above 110,000 psi shown in Figure 6.49, from Johnson and Cameron's paper [11], is also a consequence of the errors in extrapolation, and is not a true property of the lubricant.

To explore this possibility in detail, hypothetical values of effective viscosity at zero rolling speed have been obtained by extrapolation of the curves of Figure 6.46, ignoring the calculated values at rolling speeds below 50 in/sec. The shear rate dependence of the lubricant viscosity is included by using values of effective viscosity calculated at a sliding speed of 0.02 in/sec instead of at the limit of zero sliding speed. The values so obtained are shown in Figure 6.50, plotted as a function of rolling speed over the range 50 to 500 in/sec.

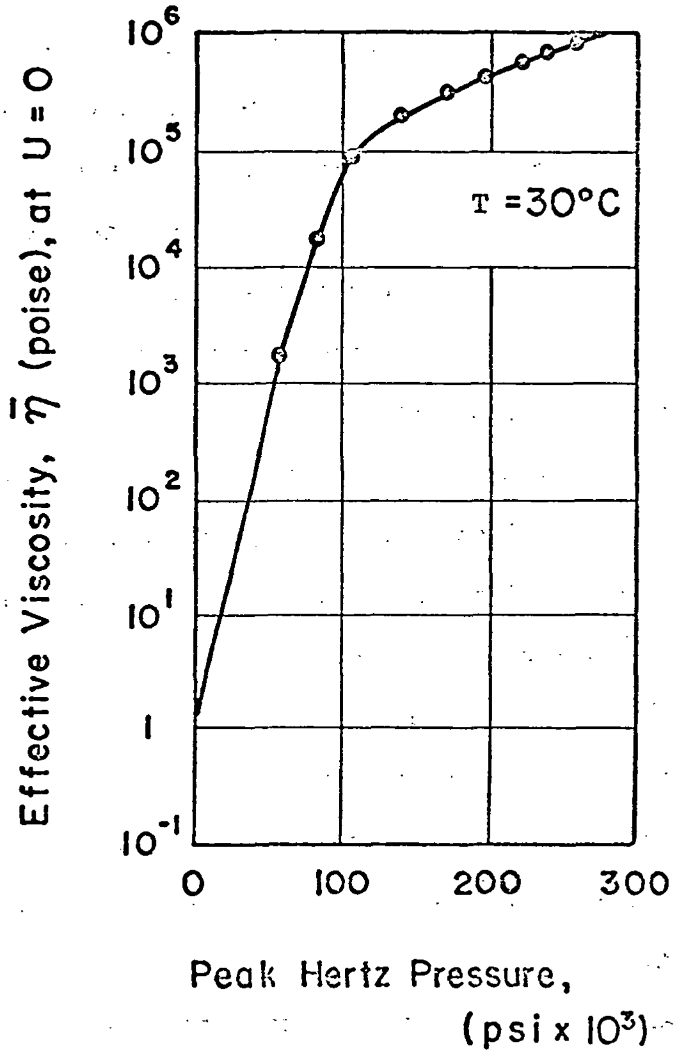

Figure 6.49. Measured variation of effective viscosity versus peak Hertzian pressure, from Johnson and Cameron [11].

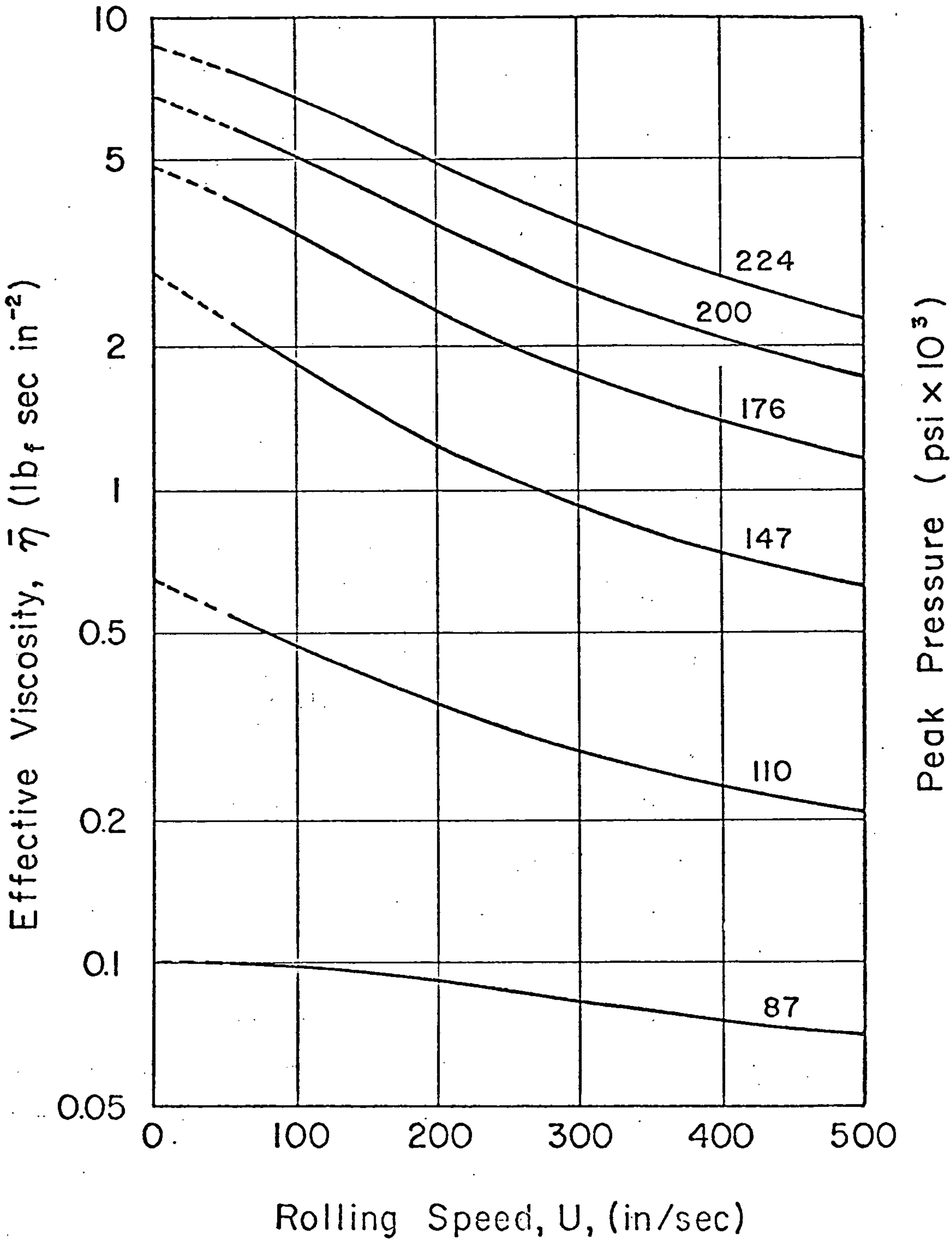

Figure 6.50. Effective viscosity at a sliding speed of 0.02 in/sec versus rolling speed for different values of peak Hertzian pressure. Below 50 in/sec, the curves have been extrapolated to zero rolling speed (dashed line).

The curves are then extrapolated below 50 in/sec to obtain a hypothetical value of effective viscosity at zero rolling speed. These values are plotted in Figure 6.51 to a base of peak pressure (dashed line), and show a large deviation from the true values of effective viscosity (solid line) at pressures above 120,000 psi. The experimentally determined values of effective viscosity shown in Figure 6.49 are also plotted in Figure 6.51. The close agreement between the hypothetical viscosity curve and the experimental values strongly supports the contention that the change in the slope of the viscosity-pressure curve at high pressures is an artifact arising from the difficulties inherent in the extrapolation procedure, and is not a physical property of the lubricant.

It has been found that by plotting the data of Figure 6.46 on a logarithmic, instead of a linear, scale of rolling speed, the separate curves for the different pressures can be combined into a single normalized curve. The effective viscosity values are normalized with respect to the value at the limit of zero rolling speed $\bar{\eta}_{U=0}$, and the rolling speed values are normalized with respect to U^*, the rolling speed at which the effective viscosity is equal to $0.5\bar{\eta}_{U=0}$. The resulting curve of $\log(\bar{\eta}/\bar{\eta}_{U=0})$ versus $\log(U/U^*)$ is shown in Figure 6.52. The variation of U^* with the peak pressure in the contact is shown in Figure 6.53. These two graphs provide a quick and simple method of determining the variation of the effective viscosity with rolling speed for a given value of maximum pressure.

In this study of the role of compressional viscoelasticity in a rolling contact system, it has been necessary to simplify the analysis

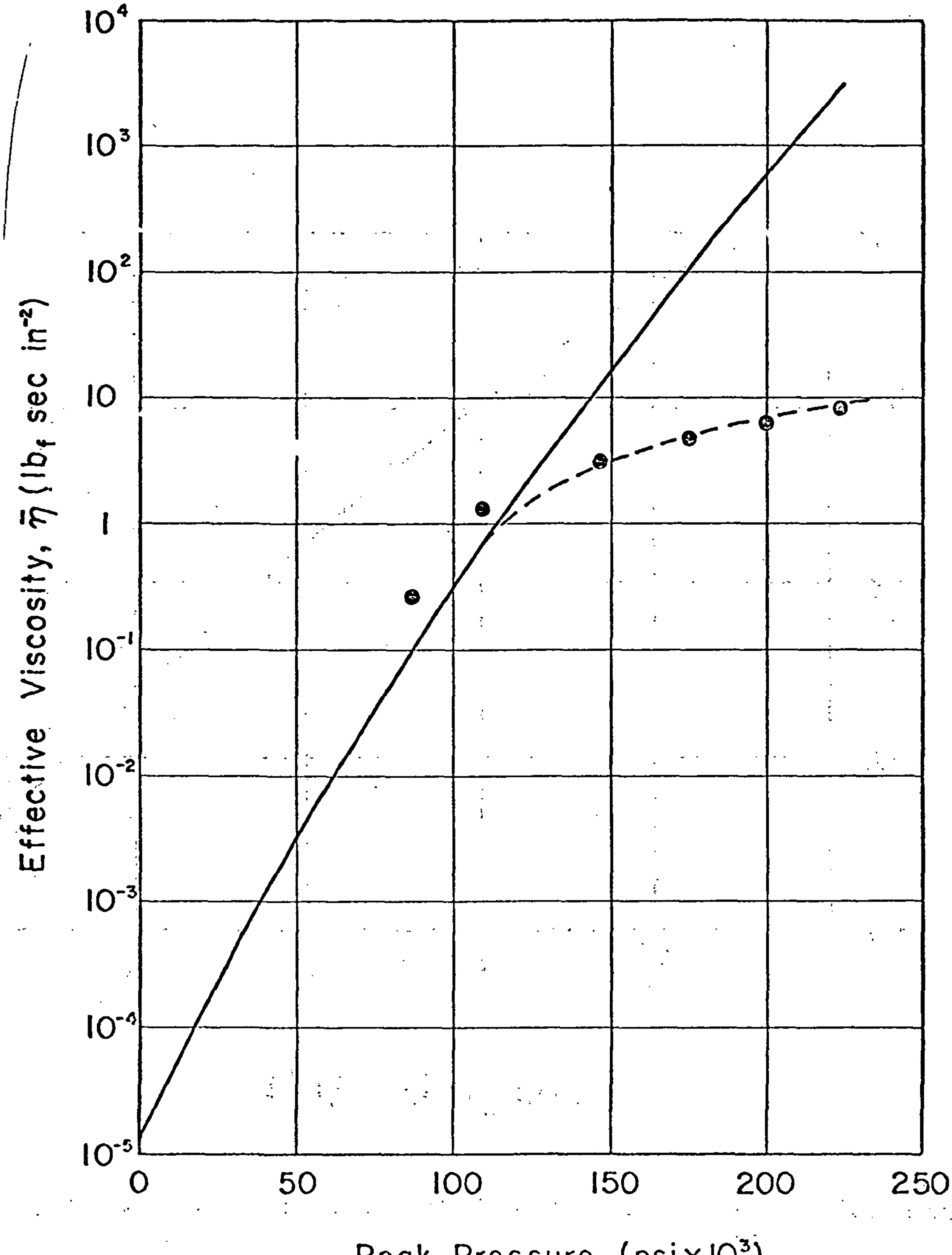

Figure 6.51. Effective viscosity versus peak Hertzian pressure
———; values at zero rolling speed, in the limit of zero sliding speed
---------; values obtained by extrapolation to zero rolling speed, from Figure 6.50
● ; measured values, from Johnson and Cameron [11]

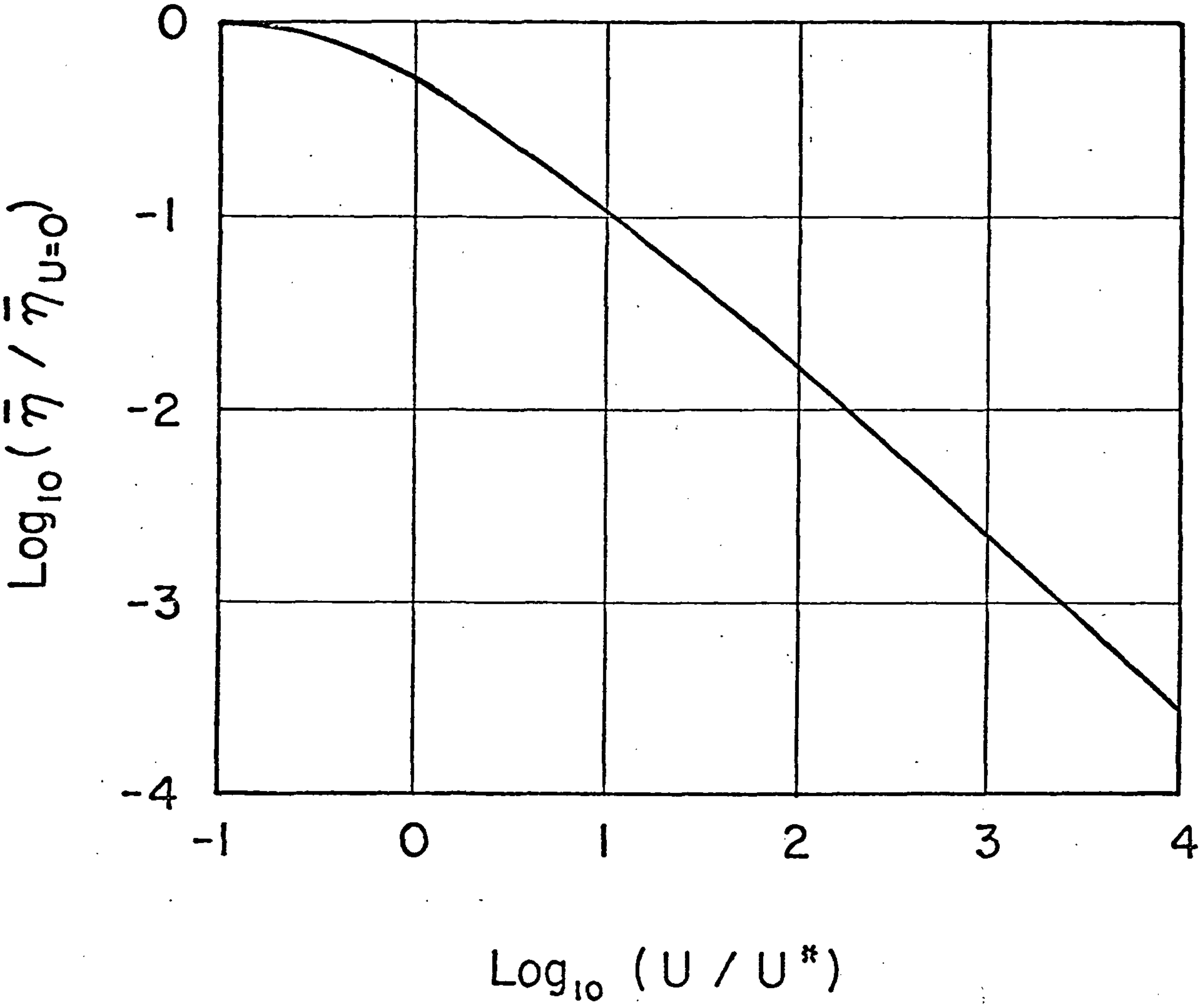

Figure 6.52. Normalized plot of effective viscosity versus rolling speed.

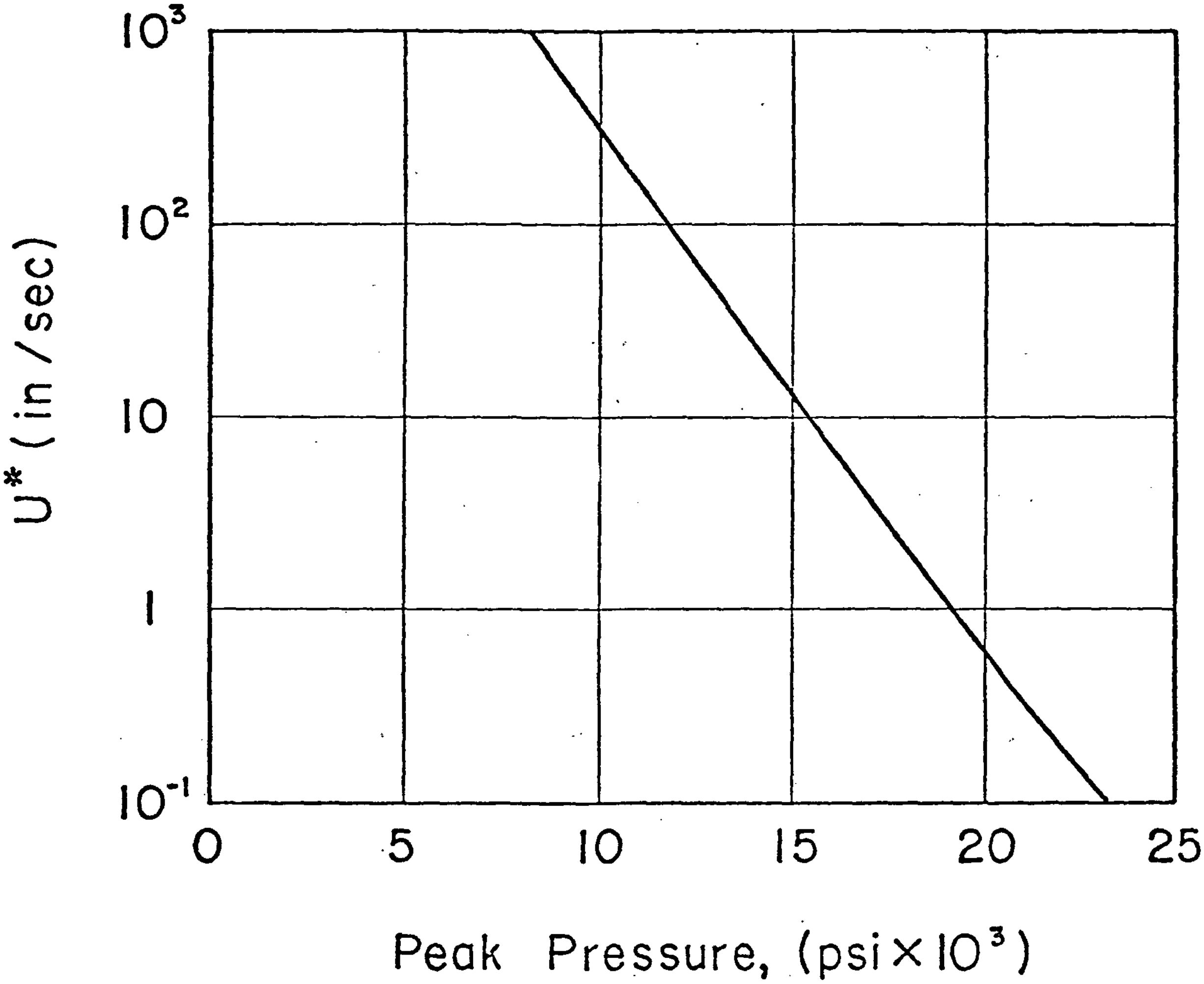

Figure 6.53. Variation of U^*, the rolling speed at which the effective viscosity is reduced by a factor 2, versus peak Hertzian pressure.

as developed in Chapter III. Among these simplifications, the most important are the use of a viscoelastic model with only a single retardation time, and the assumption of a symmetrical viscosity distribution over the contact zone. It has also been necessary to estimate the viscosity η_f and the bulk modulus K_f as discussed in detail in section 3.3. The simplifications could be eliminated in a more detailed analysis. Such improvements are of little value, however, unless they are matched by improved information about the physical properties of the lubricant under the extreme conditions found in bearings and other heavily loaded contacts.

6.6 Comparison of Thermal Theories

A comparison of several thermal analyses is shown in Figure 6.54. These include the Johnson-Crook analysis and the author's numerical analysis for the Maxwell-limiting shear stress model and the hyperbolic liquid model (c = .25) corresponding to the B. E. L.-limiting shear stress model. Friction coefficients were also calculated neglecting the effects of compressional viscoelasticity. It is apparent that these effects must be considered to predict an accurate value of the maximum friction coefficient at the correct value of sliding speed.

6.7 Summary and Conclusions

1. The results of this study demonstrate that values of friction coefficient calculated according to the hyperbolic liquid model (c = .25) have a good correlation with those determined by experiment for the two lubricants, Mobil XRM 109 F4 and Shell Turbo 33. A similar correlation is obtained using c = .20 for Mobil XRM 177 F4.

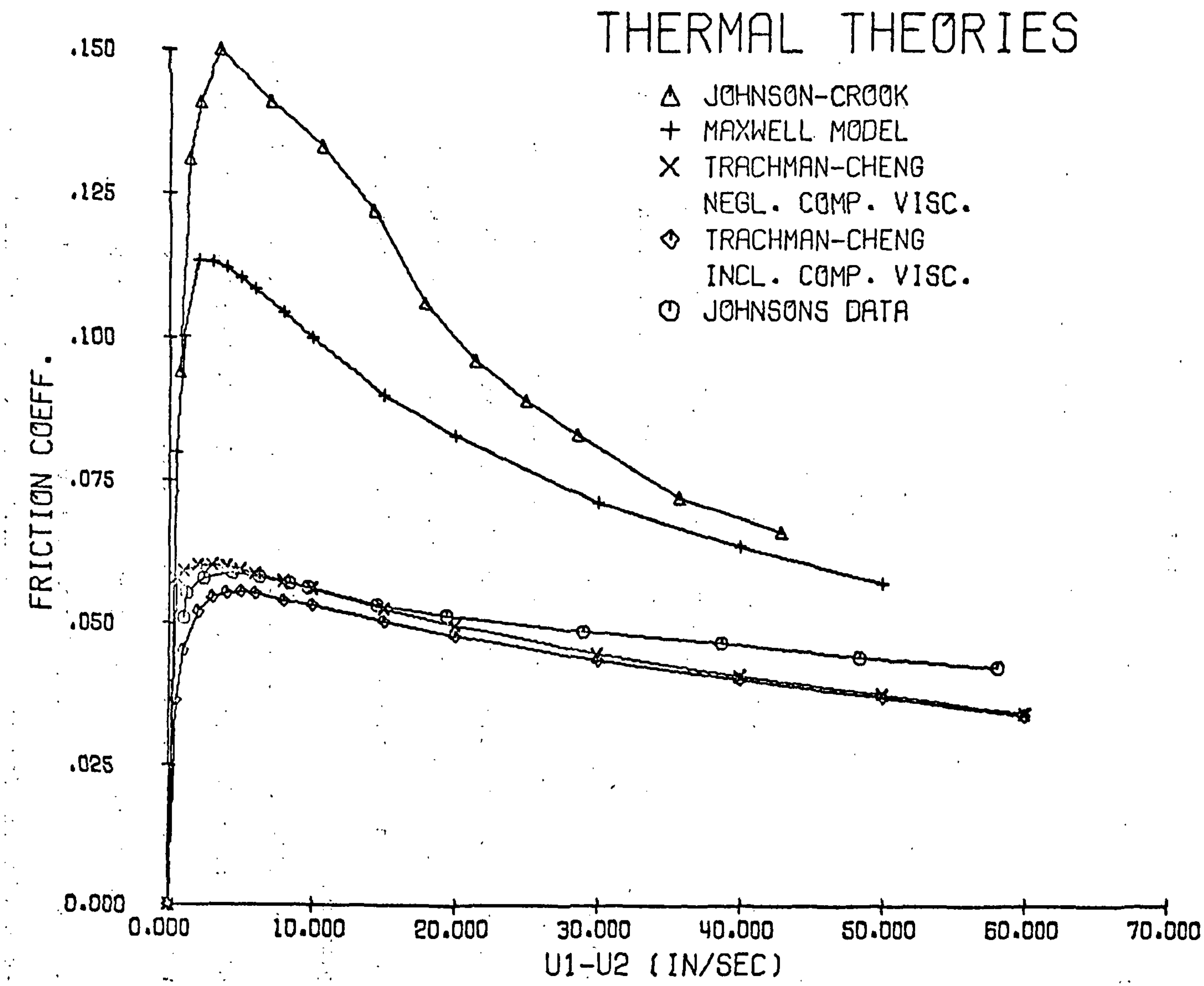

Figure 6.54. Comparison of the experimental friction curve for Shell Turbo 33 at P = 176,000 psi, U = 260 in/sec and T = 30 ^{o}C and those calculated by several theoretical analyses.

This change in the value of c might possibly be explained by an increased film thickness due to the polymer additives in this fluid. This hypothesis is described in section 6.2.

2. The effects of shear rate and time are separated and explained by the two phenomena of shear viscoelasticity and compressional viscoelasticity, respectively.

3. A unified description of the non-Newtonian shear rate dependence of the viscosity is presented as a new hyperbolic liquid model. With this model, the transition from the non-linear region to the shear modulus dominated region is shown to be a smooth one. In the high-slip region, where the friction is dominated by the shear modulus, the variation of friction with load is very sensitive to the pressure dependence of the shear modulus.

4. The friction coefficient rises to a maximum value with increasing sliding speed and then decreases with any further increase in the sliding speed. The coefficient is also found to increase with increasing load and to decrease with increasing rolling speed and temperature.

5. The effects of compressional viscoelasticity are developed in terms of a simple model for the volume creep of a liquid following the application of a pressure step. This model is used to determine the dependence on rolling speed of the friction coefficient between highly loaded rolling contacts. Curves are presented which show the variation with rolling speed of the effective viscosity of the lubricant in the contact zone under isothermal conditions. Both the shape of the curves and the values of effective viscosity are consistent with the results of experimental measurements. The shape of the curves

in this region is found to be nearly independent of the peak pressure in the contact.

6. At very low values of rolling speed, in a region which is experimentally inaccessible, the analysis predicts a very rapid variation of effective viscosity with rolling speed. It is shown that, as a consequence, the extrapolation of experimental data to zero rolling speed can result in extremely large errors in the estimated values of effective viscosity.

The results of this study suggest future work that will increase the understanding of friction in elastohydrodynamic lubrication. The most urgently needed research is in the field of fluid rheology. The viscosity and density of lubricants at high pressures would be extremely helpful, and shear and compressional relaxation experiments must be performed to measure the fluid moduli at high pressures. This work is needed to confirm and expand our understanding of the mechanism of flow under EHD conditions.

APPENDIX A

NUMERICAL INTEGRATION OF A NON-EQUIDISTANTLY TABULATED FUNCTION

A method of overlapping parabolas is employed to yield a second order approximation to the integral of a non-equidistantly tabulated function graphically represented in Figure A.1.

The function f(x) may be represented by a second order Taylor's series expansion about x_n:

$$f(x) = f(x_n) + \frac{(x-x_n)}{1!} f'(x_n) + \frac{(x-x_n)^2}{2!} f''(x_n) + \cdots \tag{A.1}$$

Accordingly,

$$f_{n+1} = f_n + h_n f'_n + \frac{h_n^2}{2} f''_n + \cdots \tag{A.2}$$

and

$$f_{n-1} = f_n - h_{n-1} f'_n + \frac{h_{n-1}^2}{2} f''_n + \cdots \tag{A.3}$$

where
$$f_{n+1} \equiv f(x_{n+1})$$
$$f_{n-1} \equiv f(x_{n-1})$$
$$h_n \equiv (x_{n+1} - x_n)$$
$$h_{n-1} \equiv (x_n - x_{n-1})$$

Equations (A.2) and (A.3) are solved simultaneously to yield

$$f''_n = \frac{2}{h_{n-1}(h_{n-1}+h_n)} f_{n-1} - \frac{2}{h_{n-1}h_n} f_n + \frac{2}{h_n(h_{n-1}+h_n)} f_{n+1} \tag{A.4}$$

and

$$f'_n = \frac{-h_n}{h_{n-1}(h_{n-1}+h_n)} f_{n-1} + \frac{(h_n - h_{n-1})}{h_{n-1}h_n} f_n + \frac{h_{n-1}}{h_n(h_{n-1}+h_n)} f_{n+1} \tag{A.5}$$

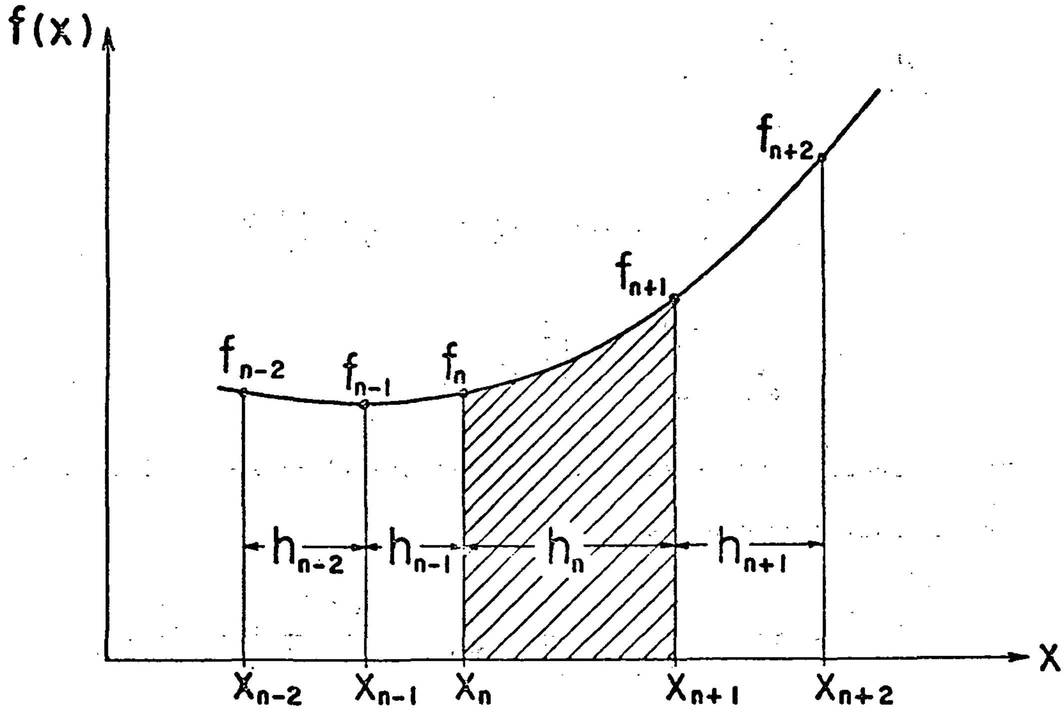

Figure A.1. Graphical representation of the non-equidistantly tabulated function f(x).

The shaded area of Figure A.1 is calculated by integrating f(x) between the limits x_n and x_{n+1}. The function is approximated by a parabolic curve through f_{n-1}, f_n and f_{n+1}. This integral is called ${}_1I_n^{n+1}$:

$$
\begin{aligned}
{}_1I_n^{n+1} &= \int_{x_n}^{x_{n+1}} f(x)\,dx \\
&= \int_{x_n}^{x_{n+1}} \left[f_n + (x-x_n)f'_n + \tfrac{1}{2}(x-x_n)^2 f''_n\right] dx \\
&= h_n f_n + \frac{h_n^2}{2} f'_n + \frac{h_n^3}{6} f''_n \qquad \text{(A.6)}
\end{aligned}
$$

The derivatives are evaluated by equations (A.4) and (A.5), resulting in the following expression:

$$
\begin{aligned}
{}_1I_n^{n+1} &= \frac{-h_n^3}{6h_{n-1}(h_{n-1} + h_n)} f_{n-1} + \frac{h_n(3h_{n-1} + h_n)}{6h_{n-1}} f_n \\
&+ \frac{h_n(3h_{n-1} + 2h_n)}{6(h_{n-1} + h_n)} f_{n+1} \qquad \text{(A.7)}
\end{aligned}
$$

Similarly, the same integral may be calculated using a parabolic approximation for f(x) through the points f_n, f_{n+1}, and f_{n+2}. Equation (A.1) determines

$$
f_{n+2} = f_n + (h_{n+1} + h_n)f'_n + \tfrac{1}{2}(h_{n+1} + h_n)^2 f''_n \qquad \text{(A.8)}
$$

This second integral, ${}_2I_n^{n+1}$, is defined by the Taylor's series expansion about x_{n+1} :

$$
{}_2I_n^{n+1} = \int_{x_n}^{x_{n+1}} \left[f_{n+1} + (x - x_{n+1}) f'_{n+1} + \tfrac{1}{2}(x - x_{n+1})^2 f''_{n+1} \right] dx
$$

$$
= h_n f_{n+1} - \frac{h_n^2}{2} f'_{n+1} + \frac{h_n^3}{6} f'_{n+1} \qquad (A.9)
$$

The derivatives f''_{n+1} and f'_{n+1} are evaluated in exactly the same manner as determined equations (A.4) and (A.5). These results are substituted into equation (A.9) yielding

$$
{}_2I_n^{n+1} = \frac{h_n(2h_n + 3h_{n+1})}{6(h_n + h_{n+1})} f_n + \frac{h_n(h_n + 3h_{n+1})}{6h_{n+1}} f_{n+1}
$$

$$
+ \frac{-h_n^3}{6h_{n+1}(h_n + h_{n+1})} f_{n+2} \qquad (A.10)
$$

The best possible second order approximation of the integral is the average of the two values just calculated; this is the method of overlapping parabolas. Therefore, the average integral, I_n^{n+1}, is defined as

$$
I_n^{n+1} = \tfrac{1}{2} \left[{}_1I_n^{n+1} + {}_2I_n^{n+1} \right] \qquad (A.11)
$$

where ${}_1I_n^{n+1}$ and ${}_2I_n^{n+1}$ are defined by equations (A.7) and (A.10), respectively.

The integral of the function f(x) between the limits x = a and x = b is defined by equation (A.12):

$$
\int_a^b f(x)\, dx \approx {}_1I_a^{a+1} + \sum_{n=a+1}^{b-2} I_n^{n+1} + {}_2I_{b-1}^{b} \qquad (A.12)
$$

In order to keep the integral a function only of values in the range of integration, the method of overlapping parabolas is not used on the two extreme intervals.

APPENDIX B

NUMERICAL ANALYSIS

The FORTRAN IV coding of the friction analysis is listed in this appendix. It is followed by examples of data cards and the optional subroutines.

```
      PROGRAM CONTROL(INPUT,TAPE60=INPUT,OUTPUT,PUNCH)
* * * * * * * * * * * * * * * * * * * * * * * * * * * * * * * * * * * *
*                                                                     *
*     PROGRAM CONTROL                                                 *
*     ------- -------                                                 *
*                                                                     *
*     CALCULATES THE FRICTION AND VELOCITY AND TEMPERATURE PROFILES   *
*     IN AN ELASTOHYDRODYNAMIC LUBRICATED CONTACT.                    *
*                                                                     *
*     REQUIRED SUBPROGRAMS -                                          *
*     SUBROUTINE PRINTS                                               *
*     FUNCTION VISC                                                   *
*     FUNCTION ZERO                                                   *
*     FUNCTION PSI                                                    *
*     SUBROUTINE SECANT                                               *
*     FUNCTION EXPI                                                   *
*     SUBROUTINE INTEG                                                *
*     SUBROUTINE RTMI                                                 *
*                                                                     *
* * * * * * * * * * * * * * * * * * * * * * * * * * * * * * * * * * * *
*                                                                     *
*     PROGRAM SET UP FOR MOBIL DATA      NEGLECTING CONVECTION
      COMMON C,GC,LLLL
      COMMON /CPSI/ GINF,ETA0,T,Y,H,U2U1,NP,DUDY,IC,TG,OMEGA,CH,AH
      COMMON /CPSI0/ XK1,XK0
      COMMON /CQ/ Q
      COMMON /CZERO/ IPTRANS,TRANS(6)
      COMMON /CPR/ ETA2
      DIMENSION GINF(21),ETA0(21),T(21),Y(21),DUDY(21),TG(21),OMEGA(21)
      DIMENSION Q(21)
      DIMENSION C(2,3,21),GC(21,21)
      DIMENSION ETA2(21)
      DIMENSION DTDY(21),NEWT(21),TRACTCF(20),SLIP(20)
      EXTERNAL PSI
      REAL LOGETA,NEWT
      INTEGER COUNT
*
*     PHYSICAL CONSTANTS AND DATA
*
*      IRDP      MAXIMUM HERTZIAN PRESSURE / 1000.
*      IRDU      MEAN ROLLING SPEED
*      IRDT      LUBRICANT INLET TEMPERATURE
*     PHIT       THERMAL REDUCTION FACTOR
*     AH, CH     HYPERBOLIC LIQUID MODEL PARAMETERS
 9000 READ 9001,IRDP,IRDU,IRDT,PHIT,AH,CH
 9001 FORMAT(4XI3,I5,I4,F6.3,10XF3.1,6XF4.2)
      IF(EOF(60))9999,9002
 9002 CONTINUE
      PUNCH 9003
 9003 FORMAT(/)
      PHZ=1000.*FLOAT(IRDP)
      U=FLOAT(IRDU)
      TOIL=FLOAT(IRDT)+460.
*     NP        NUMBER OF GRID POINTS ACROSS THE HALF-FILM THICKNESS
      NP=11
      NH = NP - 1
*     NIP       NUMBER OF PRESSURE STEPS IN HALF CONTACT-LENGTH
      NIP=3
```

```
      TW=TOIL
      TMAX=950.
*     COND        THERMAL CONDUCTIVITY OF THE LUBRICANT
      COND=.1*778./3600.
*     CYLW        CONTACT WIDTH OF THE DISKS
      CYLW=0.25
*     R1, R2      RADII OF THE DISKS
      R1=R2=3.0
*     E1, E2      ELASTIC MODULUS OF THE DISKS
      E1=E2=30.E+6
*     POIS1, POIS2  POISSONS RATIO FOR THE DISKS
      POIS1=POIS2=0.3
*     ALPHA       VISCOSITY PRESSURE COEFFICIENT FOR THE LUBRICANT
      ALPHA=1.04E-4
      BETA=5.1E7*ALPHA
      GAMMA=930.*ALPHA
*     DK          THERMAL CONDUCTIVITY OF THE DISKS
      DK=21.7*778./3600.
*     DRHO        DENSITY OF THE DISKS
      DRHO=.283
*     DC          SPECIFIC HEAT OF THE DISKS
      DC=.109*778.*12.
*     HERSA, HERSB  CONSTANTS FOR THE HERSHEL VISCOSITY EQUATION
      HERSA=8.974
      HERSB=-3.2
*     NGRAPH      REQUIRED NUMBER OF GRAPHS FOR EACH TEMPERATURE PROFILE
      NGRAPH=0
*     MGRAPH      REQUIRED NUMBER OF GRAPHS OF TRACTION COEF. VS SLIP
      MGRAPH=1
*     PRNT=2HON     GIVES ADDITIONAL OUTPUT FOR DEBUGGING PURPOSES
      PRNT=3HOFF
*
*     INITIALIZATION AND BOUNDARY CONDITIONS
*
      COUNT=0
      IC = 1
      DTDY(1)=0.0
      Y(1)=0.0
      TRACT=0.0
      FLASH=0.0
      PI=3.1415927
      DO 10 I=1,NP
      NEWT(I)=10.*(1.-Y(I))+TW
      IF (I.LT.NP) Y(I+1)=Y(I)+1./FLOAT(NH)
   10 CONTINUE
*
      R=R1*R2/(R1+R2)
      E=2./((1.-POIS1*POIS1)/E1+(1.-POIS2*POIS2)/E2)
      B=4.*R/E*PHZ
      FLASHK=0.24/SQRT(PI*PHZ*DK*DRHO*DC*U*R/E)
      TRANS(1)=B/U/6.
      TRANS(2)=B/U/6.
      TRANS(3)=B/U/2.
*
*      CALCULATION OF LOAD
*
      W=PHZ*PHZ*PI*(2./E)*R
      PRINT 2,PHZ,W,R,E
    2 FORMAT(*1CONTROL   PHZ = *E15.8,*  W = *E15.8,*  R     = *E15.8,
```

```
     1*  E     = *E15.8)
*
*     CALCULATION OF HALF-FILM THICKNESS
*
      ETAENT=10.**(HERSA+HERSB*ALOG10(TOIL-460.))*1.45E-7
      H=1.6*ALPHA**0.6*(ETAENT*U)**0.7*E**0.03*R**0.43/W**0.13
      H=1.2*H
      H=PHIT*H
      H=0.5*H
      PRINT 1,H,ALPHA,ETAENT,U,CH,AH
    1 FORMAT(*0H = *E12.5,*  ALPHA = *E12.5,*  ETAENT = *E12.5,
     1* U = *F6.0,* CH = *F5.3,* AH = *F7.3)
*
*     SLIP LOOP
*
      NSLIP=15
      DATA (SLIP(IU),IU=1,20)/.5,1.,2.,3.,4.,5.,6.,8.,10.,15.,20.,30.,40
     1.,50.,60.,5*0.0/
      DO 6000 IU=1,NSLIP
      DATA (TRACTCF(IP),IP=1,20)/20*0.0/
      FLASH=FLASHK*TRACT*SLIP(IU)
      PRINT 6,FLASH
    6 FORMAT(* CONTROL     FLASH = *E15.8)
      U2U1=0.5*SLIP(IU)
      PRINT 8,IU,SLIP(IU)
    8 FORMAT(*1CONTROL            IU = *I3,*     SLIP = *E15.8)
*
*     HERTZIAN PRESSURE LOOP
*
      TRACT=0.0
      DO 5999 IP=1,NIP
      IPTRANS=IP
      XB=(2.*FLOAT(IP)-1.)/2./FLOAT(NIP)
      P=PHZ*SQRT(XB*(2.-XB))
*
*     SOLVE MOMENTUM EQUATION
*
      ITCOUNT=0
    4 IF (PRNT.EQ.2HON) PRINT 44,COUNT
   44 FORMAT(*0COUNT = *I3)
      COUNT=0
      DO 11 I=1,NP
      IF (ITCOUNT.EQ.0.OR.ITCOUNT.GT.10) T(I)=NEWT(I)
      IF (ITCOUNT.GT.0.AND.ITCOUNT.LE.10) T(I)=0.5*(T(I)+NEWT(I))
      IF (ITCOUNT.GT.100) GO TO 6003
      IF (T(I).GT.TMAX) T(I)=TMAX
      TW=TOIL+FLASH
      GINF(I)=1.2*P/(2.52+.01333*(T(I)-492.))-1.45E4
      IF (GINF(I).LT.1.) GINF(I)=1.
*     CALCULATION OF STEADY-STATE VISCOSITY
      ETEXP=ALPHA*P+(BETA+GAMMA*P)*(680.-T(I))/680./T(I)
      ETA2(I)=.62*EXP(ETEXP)*1.45E-5
*     CALCULATION OF TIME-DEPENDENT VISCOSITY
      ETA0(I)=VISC(P,ETA2(I),IVCODE)
   11 CONTINUE
      DUMMY=PSI0(0.0)
      CALL SECANT(XK0,XK1,TAU,PSI,XK,.001,500,ITERR)
      IF (ITERR.EQ.1) STOP
```

```
      IF (PRNT.EQ.2HON) PRINT 41,TAU
   41 FORMAT(*0TAU   = *E15.8)
*
*     SOLVE ENERGY EQUATION
*
      DO 5000 I=1,NP
      Q(I)=-TAU*DUDY(I)/COND*H
 5000 CONTINUE
      IF (PRNT.EQ.2HON) CALL PR1
      DO 5010 I=2,NP
      CALL INTEG1(0.,Y(I),Y,Q,NP,DTDY(I),C,GC,LLLL,IERR)
 5010 IF(IERR.NE.0) PRINT 5012,IERR
 5012 FORMAT(* INTEGRATING Q, IERR = *I3)
      DO 5020 I=2,NP
      CALL INTEG1(0.,Y(I),Y,DTDY,NP,NEWT(I),C,GC,LLLL,IERR)
 5020 IF(IERR.NE.0) PRINT 5022,IERR
 5022 FORMAT(* INTEGRATING DTDY, IERR = *I3)
      XK7=TW-NEWT(NP)
      ITCOUNT=ITCOUNT+1
      NEWT(1)=0.0
      DO 5030 I=1,NP
      NEWT(I)=NEWT(I)+XK7
 5030 IF(ABS(1.-(T(I)/NEWT(I))).LT.0.001) COUNT=COUNT+1
      IF(COUNT.NE.NP) GO TO 4
      IF (IVCODE.NE.0) PRINT 5034
 5034 FORMAT(*0       MINIMUM VISCOSITY REDUCTION*)
      CALL PR1
      PRINT 99
      PRINT 5040,((NEWT(I),I),I=1,NP)
 5040 FORMAT(* NEW TEMP = *F7.2,* I = *I4)
*
*     CALCULATION OF TRACTION
*
      TRACT=TRACT+2.*B/NIP*TAU
 5999 CONTINUE
      TRACTCF(IU)=TRACT/W
      PRINT 6002,TRACTCF(IU)
 6002 FORMAT(*0CONTROL    TRACTCF(IU) = *E15.8)
*
*     PLOT TEMPERATURE PROFILE
*
      IF(NGRAPH.EQ.0) GO TO 6000
      DO 5052 NGR=1,NGRAPH
      PRINT 5050,SLIP(IU)
 5050 FORMAT(*1(U2 - U1) = *E15.8)
      PRINT 99
      CALL STPLT1(1,NEWT,Y,NP,1H*,1,1HY)
      PRINT 5051
 5051 FORMAT(1H0,92X,11HTEMPERATURE)
 5052 CONTINUE
 6000 CONTINUE
 6003 PRINT 98
      PRINT 6001,((TRACTCF(IU),SLIP(IU)),IU=1,NSLIP)
 6001 FORMAT(* CONTROL      TRACT = *E15.8,*  U2-U1 = *E15.8)
      PUNCH 6005,((SLIP(IU),TRACTCF(IU)),IU=1,NSLIP)
 6005 FORMAT(2F10.5)
*
*     PLOT TRACTION COEFFICIENT
*
```

```
      IF(MGRAPH.EQ.0) GO TO 6013
      DO 6012 MGR=1,MGRAPH
      PRINT 98
      CALL STPLT1(1,SLIP,TRACTCF,NSLIP,1H*,14,14HTRACTION COEF.)
      PRINT 6011
 6011 FORMAT(1H0,100X,7HU2 - U1)
 6012 CONTINUE
 6013 CONTINUE
   98 FORMAT(*1*)
   99 FORMAT(*0*)
      GO TO 9000
 9999 CONTINUE
      STOP
      END
```

```
      SUBROUTINE PRINTS                                                 PRINT
      COMMON /CPSI/ GINF,ETA0,T,Y,H,U2U1,NP,DUDY,IC,TG,OMEGA,CH,AH      PRINT
      COMMON /CQ/ Q                                                     PRINT
      COMMON /CPR/ ETA2                                                 PRINT
      DIMENSION GINF(21),ETA0(21),T(21),Y(21),DUDY(21),TG(21),OMEGA(21) PRINT
      DIMENSION Q(21)                                                   PRINT
      DIMENSION ETA2(21)                                                PRINT
      ENTRY PR1                                                         PRINT
      PRINT 1                                                           PRINT
    1 FORMAT(*0 I    Y(I)     T(I)        GINF(I)         TG(I)       ETA0(I) PRINT
     1       ETA2(I)      OMEGA(I)        DUDY(I)         Q(I)*)        PRINT
      PRINT 99                                                          PRINT
      PRINT 3,((I,Y(I),T(I),GINF(I),TG(I),ETA0(I),ETA2(I),OMEGA(I),DUDY(PRINT
     1I),Q(I)),I=1,NP)                                                  PRINT
    3 FORMAT(* *I2,F7.2,F9.2,7(2XE11.4))                                PRINT
   99 FORMAT(*0*)                                                       PRINT
      RETURN                                                            PRINT
      END                                                               PRINT
```

```
      FUNCTION VISC(P,ETA2,CODE)
* * * * * * * * * * * * * * * * * * * * * * * * * * * * * * * * * * *
      *                                                               *
*     FUNCTION VISC                                                   *
*     -------- ----                                                   *
      *                                                               *
*     CALCULATES THE TRANSIENT VALUE OF THE LUBRICANT VISCOSITY.      *
      *                                                               *
*     ARGUMENTS -                                                     *
*     P          PRESSURE                                             *
*     ETA2       EQUILIBRIUM VALUE OF VISCOSITY                       *
*     CODE       ERROR PARAMETER                                      *
*                                                                     *
*     REQUIRED SUBPROGRAMS -                                          *
*     FUNCTION ZERO                                                   *
*     FUNCTION EXPI                                                   *
*                                                                     *
*     COMMON STORAGE -                                                *
*     THE VARIABLE TAUP MUST BE IN LABELED COMMON CVISC.              *
*                                                                     *
*     ERROR INDICATIONS -                                             *
*     CODE = 0   INDICATES NO ERROR.                                  *
*     CODE = 1   INDICATES THE TRUE TRANSIENT VISCOSITY IS OUT OF THE *
*                RANGE OF THE PROGRAM AND THE MAXIMUM POSSIBLE        *
*                VISCOSITY REDUCTION WAS ASSUMED.                     *
*                                                                     *
* * * * * * * * * * * * * * * * * * * * * * * * * * * * * * * * * * *
      *                                                               *
      COMMON /CVISC/ TAUP
      EXTERNAL ZERO
      REAL KF
      INTEGER RTMIERR,CODE
      PRNT=3HOFF
      CODE=0
      KF=3.5E5+9.*P
      TAUP=50.*ETA2/KF
      IF (PRNT.EQ.2HON) PRINT 81,KF,TAUP,P,ETA2
   81 FORMAT(* VISC      KF = *E13.6,*      TAUP = *E13.6,*   P = *E13.6,
     1*   ETA2 = *E13.6)
*
*     TEST OF RANGE
*
      IF (ZERO(-.01)*ZERO(-20.).GT.0.) GO TO 60
*
*     ROUGH BOUNDING OF ZERO
*
      IF (ZERO(-5.)*ZERO(-20.).GT.0.) GO TO 30
*     ROOT IS BETWEEN -20. AND -5.
      XLI=-20.
      XRI=-5.
      GO TO 50
*     ROOT IS BETWEEN -5. AND -.01
   30 ICOUNT=0
      XLI=-5.
      XRI=-3.
      ZEROXRI=ZERO(XRI)
      ZEROXLI=ZERO(XLI)
   40 IF (ZEROXRI*ZEROXLI.LE.0.) GO TO 50
```

```
      IF (XRI.GT.-.01) GO TO 60
      XLI=XRI
      XRI=XRI/3.
      ZEROXLI=ZEROXRI
      ZEROXRI=ZERO(XRI)
      ICOUNT=ICOUNT+1
      IF (ICOUNT.GT.100) GO TO 92
      GO TO 40
*
*     PRECISE DETERMINATION OF ZERO
*
   50 CALL RTMI(SI,ZEROSI,ZERO,XLI,XRI,.05,100,RTMIERR)
      IF (RTMIERR.NE.0) GO TO 90
      VISC=ETA2*EXP(SI)
      RETURN
*
*     OUT OF RANGE
*
   60 IF (ZERO(-20.).LT.0.) GO TO 70
*
*     NEGLECT VISCOSITY REDUCTION OF LESS THAN 1. PER CENT
*
      VISC=ETA2
      RETURN
*
*     MAXIMUM VISCOSITY REDUCTION
*
   70 VISC=ETA2*EXP(-20.)
      CODE=1
      RETURN
*
*     ERROR MESSAGES
*
   90 PRINT 91,RTMIERR
   91 FORMAT(* VISC      ERROR IN RTMI      ERR = *I2)
      STOP
   92 PRINT 93
   93 FORMAT(* VISC      MAX NO. OF ITERIONS EXCEEDED IN PRERTMI PROC.*)
      STOP
      END
```

```
      FUNCTION ZERO(SI)
* * * * * * * * * * * * * * * * * * * * * * * * * * * * * * * * * * * * * *
*                                                                        *
*     FUNCTION ZERO                                                      *
*     -------- ----                                                      *
*                                                                        *
*     THIS EXTERNALLY SUPPLIED FUNCTION IS NEEDED BY SUBROUTINE RTMI     *
*     CALLED FOR IN FUNCTION VISC.  IT MYST BE PRESENT WHEN A TIME-      *
*     DEPENDENT VISCOSITY FUNCTION IS USED.                              *
*                                                                        *
* * * * * * * * * * * * * * * * * * * * * * * * * * * * * * * * * * * * * *
      COMMON /CZERO/ IPTRANS,TRANS(6)
      COMMON /CVISC/ TAUP
      INTEGER EXPIERR
      PRNT=3HOFF
      IF (SI.GE.-20.) GO TO 10
      SI=-20.
      PRINT 20
   20 FORMAT(*ZERO      SI HAS BEEN READJUSTED TO -20.*)
   10 CONTINUE
      CALL EXPI(EISI,SI,EXPIERR)
      IF (EXPIERR.NE.0) GO TO 90
      ZERO=TRANS(IPTRANS)+TAUP*(EISI-0.05*EXP(SI))
      IF (PRNT.EQ.2HON) PRINT 81,SI,EISI,TRANS(IPTRANS),ZERO
   81 FORMAT(* ZERO      SI =*E13.6,*   EISI = *E13.6,*   TRANS = *E13.6,
     1*   ZERO = *E13.6)
      RETURN
*
*     ERROR MESSAGE
*
   90 PRINT 91,EXPIERR
   91 FORMAT(* ZERO      ERROR IN EXPI      ERR = *I3)
      STOP
      END
```

```
      FUNCTION PSI(TAU)
* * * * * * * * * * * * * * * * * * * * * * * * * * * * * * * * * * * * *
*                                                                       *
*     FUNCTION PSI                                                      *
*     -------- ---                                                      *
*                                                                       *
*     THIS FUNCTION SUBROUTINE SUPPLIES THE RHEOLOGICAL MODEL           *
*     FOR THE LUBRICANT.  IN THIS CASE, WE ARE USING THE                *
*     HYPERBOLIC MODEL.                                                 *
*                                                                       *
* * * * * * * * * * * * * * * * * * * * * * * * * * * * * * * * * * * * *
      COMMON C,GC,LLLL
      COMMON /CPSI/ GINF,ETA0,T,Y,H,U2U1,NP,DUDY,IC,TG,OMEGA,CH,AH
      COMMON /CPSI0/ XK1,XK0
      DIMENSION GINF(21),ETA0(21),T(21),Y(21),DUDY(21),TG(21),OMEGA(21)
      DIMENSION C(2,3,21),GC(21,21)
      REAL INTG
      PRNT=3HOFF
  100 CONTINUE
      IF (PRNT.EQ.2HON) PRINT 200,TAU
  200 FORMAT(*0TAU = *E15.8)
      DO 210 I=1,NP
      TG(I)=TAU/GINF(I)
      IF(TG(I).LT.CH) GO TO 205
      TAU=0.99999999*CH*GINF(I)
      GO TO 100
  205 OMEGA(I)=CH*TG(I)*(AH*CH*TG(I)+(TG(I)-CH)*(TG(I)-CH))/(CH-TG(I))**
     13
      DUDY(I)=GINF(I)/ETA0(I)*OMEGA(I)*H
  210 CONTINUE
      GO TO (220,230),IC
  220 CALL INTEG (0.,1.,Y,DUDY,NP,INTG,C,GC,LLLL,IERR)
      IC = 2
      GO TO 240
  230 CALL INTEG2(0.,1.,Y,DUDY,NP,INTG,C,GC,LLLL,IERR)
  240 IF (IERR.NE.0) PRINT 241,IERR,TAU
  241 FORMAT(* IERR = *I4,* AT TAU = *E15.8)
      PSI=ALOG10(INTG/U2U1)
      IF (PRNT.EQ.2HON) PRINT 250,INTG,PSI
  250 FORMAT(* INTG = *E15.8,*   PSI = *E15.8)
      TDUDY=0.0
      DO 310 I=1,NP
  310 TDUDY=TDUDY+DUDY(I)
      ADJ=U2U1*FLOAT(NP)/TDUDY
      IF (ADJ.GT.0.99) GO TO 390
      DO 320 I=1,NP
  320 DUDY(I)=ADJ*DUDY(I)
  390 CONTINUE
      RETURN
      ENTRY PSI0
      XK1=0.20*CH*GINF(1)
      XK0=0.5*XK1
      PSI=0.0
      RETURN
      END
```

```
      SUBROUTINE SECANT(X0,X1,XFINAL,FUNC,X,CONV,MAXIT,IERR)             SECNT   1
* * * * * * * * * * * * * * * * * * * * * * * * * * * * * * * * * * * * SECNT   2
*                                                                      *SECNT   3
*     SUBROUTINE SECANT                                                *SECNT   4
*     ---------- ------                                                *SECNT   5
*                                                                      *SECNT   6
*     SECANT METHOD SOLUTION OF FUNC(X) = 0.                           *SECNT   7
* *** ALLOWS POSITIVE X ONLY                                           *SECNT   8
*                                                                      *SECNT   9
*     ARGUMENTS -                                                      *SECNT  10
*     X0, X1      TWO INITIAL GUESSES OF ROOT                          *SECNT  11
*     XFINAL      FINAL ESTIMATE OF ROOT                               *SECNT  12
*     FUNC        EXTERNALLY SUPPLIED FUNCTION FUNC                    *SECNT  13
*     X           PARAMETER OF FUNCTION FUNC                           *SECNT  14
*     CONV        TEST FOR CONVERGENCE                                 *SECNT  15
*     MAXIT       MAXIMUM NUMBER OF ITERATIONS TO FIND SOLUTION        *SECNT  16
*     IERR        ERROR PARAMETER                                      *SECNT  17
*                                                                      *SECNT  18
*     REQUIRED SUBPROGRAMS -                                           *SECNT  19
*     FUNCTION FUNC(X)                                                 *SECNT  20
*                                                                      *SECNT  21
*     COMMON STORAGE - NONE                                            *SECNT  22
*                                                                      *SECNT  23
*     ERROR INDICATIONS -                                              *SECNT  24
*     IERR = 0   INDICATES NO ERROR.                                   *SECNT  25
*     IERR = 1   INDICATES THE MAX. NO. OF ITERATIONS WERE EXCEEDED    *SECNT  26
*                                                                      *SECNT  27
*     EDWARD G. TRACHMAN                         M.E. DEPT.   492-5640 *SECNT  28
*                                                                      *SECNT  29
* * * * * * * * * * * * * * * * * * * * * * * * * * * * * * * * * * * * SECNT  30
      PRNT=3HOFF                                                         SECNT  31
      IT = 0                                                             SECNT  32
      IERR=0                                                             SECNT  33
      XMIN=-1.E99                                                        SECNT  34
      XMAX= 1.E99                                                        SECNT  35
      FXMIN=-2.E99                                                       SECNT  36
      FXMAX= 2.E99                                                       SECNT  37
      F0=FUNC(X0)                                                        SECNT  38
      IF (F0.LT.0.) XMIN=X0                                              SECNT  39
      IF (F0.LT.0.) FXMIN=F0                                             SECNT  40
      IF (F0.GT.0.) XMAX=X0                                              SECNT  41
      IF (F0.GT.0.) FXMAX=F0                                             SECNT  42
      F1=FUNC(X1)                                                        SECNT  43
    1 IF (F1.LT.0..AND.X1.GT.XMIN) GO TO 50                              SECNT  44
   51 IF (F1.GT.0..AND.X1.LT.XMAX) GO TO 52                              SECNT  45
   53 IF (PRNT.EQ.2HON) PRINT 2,X0,X1                                    SECNT  46
    2 FORMAT(* SECANT    X0 = *E15.8,*    X1 = *E15.8)                   SECNT  47
      IF (ABS(F1).LT.CONV) GO TO 10                                      SECNT  48
      IT = IT + 1                                                        SECNT  49
      IF (IT.GT.MAXIT) GO TO 99                                          SECNT  50
      SLOPE=(F1-F0)/(X1-X0)                                              SECNT  51
      CLOSE=DIM(ABS(F0),ABS(F1))                                         SECNT  52
      IF (PRNT.EQ.2HON) PRINT 80,X0,X1,F0,F1,SLOPE                       SECNT  53
   80 FORMAT(*0SECANT    X0 = *E15.8,*  X1 = *E15.8,*  F0 = *E15.8,*  F1 SECNT  54
     1= *E15.8,*  SLOPE = *E15.8)                                        SECNT  55
      IF (CLOSE.GT..0001) 5,6                                            SECNT  56
*     USE X1                                                             SECNT  57
    5 DELX=-F1/SLOPE                                                     SECNT  58
```

```
      X0=X1
      F0=F1
      GO TO 7
*     USE X0
    6 DELX=-F0/SLOPE
    7 X1=X0+DELX
***   ALLOWS POSITIVE X ONLY
      IF (X1.LE.0.) X1=1.E-8
      IF (X1.GT.XMIN) GO TO 8
      X1=XMIN
      F1=FXMIN
      GO TO 1
    8 IF (X1.LT.XMAX) GO TO 9
      X1=XMAX
      F1=FXMAX
      GO TO 1
    9 F1=FUNC(X1)
      GO TO 1
   10 XFINAL=X1
      IF (PRNT.EQ.2HON) PRINT 11,XFINAL,F1,IT
   11 FORMAT(*0SECANT   XFINAL = *E15.8,*   F(XFINAL) = *E15.8,*   IT =
     1*I4)
      RETURN
   50 XMIN=X1
      FXMIN=F1
      GO TO 51
   52 XMAX=X1
      FXMAX=F1
      GO TO 53
   99 PRINT 100
  100 FORMAT(* SECANT     MAXIMUM NUMBER OF ITERATIONS EXCEEDED*)
      IERR=1
      RETURN
      END
```

```
      SUBROUTINE EXPI(RES,X,IERR)
* * * * * * * * * * * * * * * * * * * * * * * * * * * * * * * * * * * * *
*                                                                     *
*     SUBROUTINE EXPI                                                 *
*     ---------- ----                                                 *
*                                                                     *
*     COMPUTES THE EXPONENTIAL INTEGRAL FOR NEGATIVE ARGUMENTS        *
*     IN THE RANGE -20 TO ZERO.                                       *
*                                                                     *
*     FOR X EQUAL TO 0 THE RESULT VALUE IS SET TO 1.E75.              *
*     FOR X LESS THAN -20 OR GREATER THAN ZERO THE CALCULATION IS     *
*     BYPASSED AND THE ARGUMENT REMAINS UNCHANGED.                    *
*                                                                     *
*     THE EXPONENTIAL INTEGRAL IS DEFINED AS THE                      *
*     RES INTEGRAL (EXP(-T)/T,SUMMED OVER T FROM X TO INFINITY).      *
*                                                                     *
*     A POLYNOMIAL APPROXIMATION IS USED FOR ARGUMENTS IN THE         *
*     RANGE -5 TO ZERO.                                               *
*     REF.   LUKE AND WIMP,-JACOBI POLYNOMIAL EXPANSIONS OF A         *
*     GENERALIZED HYPERGEOMETRIC FUNCTION OVER A SEMI-INFINITE RANGE-, *
*     MATHEMATICAL TABLES AND OTHER AIDS TO COMPUTATION,              *
*     VOL. 17, 1963, ISSUE 84, PP. 395-404.                           *
*                                                                     *
*     AN EXPONENTIAL APPROXIMATION IS USED FOR ARGUMENTS IN THE       *
*     RANGE -20 TO -5.                                                *
*                                                                     *
*     ARGUMENTS -                                                     *
*     RES        RESULT VALUE.                                        *
*     X          ARGUMENT OF EXPONENTIAL INTEGRAL.                    *
*     IERR       RESULTANT ERROR PARAMETER.                           *
*                                                                     *
*     REQUIRED SUBPROGRAMS - NONE                                     *
*                                                                     *
*     COMMON STORAGE - NONE                                           *
*                                                                     *
*     ERROR INDICATIONS -                                             *
*     IERR = 0  INDICATES NO ERROR.                                   *
*     IERR = 1  INDICATES X IS LESS THAN -20.                         *
*     IERR = 2  INDICATES X IS POSITIVE.                              *
*                                                                     *
*     EDWARD G. TRACHMAN                    M.E. DEPT.  492-5640      *
* * * * * * * * * * * * * * * * * * * * * * * * * * * * * * * * * * * * *
*
*     TEST OF RANGE
*
      IERR=0
      IF (X.GT.0.) GO TO 60
      IF (X.GT.-5.) GO TO 35
      IF (X.LT.-20.) GO TO 55
*
*     ARGUMENT IS BETWEEN -20 AND -5.
*
*     C=-1.09414E-3/3.**-5
      C=-2.65876020E-01
      RES=C*3.**X
      RETURN
*
*     ARGUMENT IS BETWEEN -5 AND ZERO.
```

```
*
   35 X=-X
      IF(X) 40,50,40
   40 RES=-ALOG(ABS(X))-(((((((((((((.10317602E-11*X-.15798675E-10)*X+
     1.16826592E-9)*X-.21915699E-8)*X+.27635830E-7)*X-.30726221E-6)*X+
     2.30996040E-5)*X-.28337590E-4)*X+.23148392E-3)*X-.0016666906)*X+
     3.010416662)*X-.055555520)*X+.25)*X-1.0)*X-.57721566
      RES=-RES
      X=-X
      RETURN
*
*     ARGUMENT IS EQUAL TO ZERO.
*
   50 RES=1.E75
      RES=-RES
      X=-X
      RETURN
*
*     ARGUMENT IS LESS THAN -20.
*
   55 IERR=1
      RETURN
*
*     ARGUMENT IS POSITIVE.
*
   60 IERR=2
      RETURN
      END
```

```
      SUBROUTINE INTEG(A,B,X,F,NP,VALUE,C,GC,L,IERR)
* * * * * * * * * * * * * * * * * * * * * * * * * * * * * * * * * * * * * * *
*                                                                             *
*     SUBROUTINE INTEG                                                        *
*     ---------- -----                                                        *
*                                                                             *
*     INTEGRATES THE NON EQUIDISTANTLY TABULATED FUNCTION F(X(I))             *
*     BETWEEN THE LIMITS A AND B, WHERE A OR B MUST EQUAL F(X(1)).            *
*                                                                             *
*     A MODIFIED METHOD OF OVERLAPPING PARABOLAS IS EMPLOYED.                 *
*                                                                             *
*     ENTRY POINTS -                                                          *
*     INTEG      FIRST TIME SUBROUTINE IS CALLED AND                          *
*                WHEN NEW ABSCISSAS ARE USED.                                 *
*     INTEG1     WHEN NEW LIMITS OF INTEGRATION ARE USED.                     *
*     INTEG2     WHEN USING THE SAME ABSCISSAS AND                            *
*                LIMITS OF INTEGRATION AS THE LAST CALL.                      *
*                                                                             *
*     ARGUMENTS -                                                             *
*     A          LOWER LIMIT OF INTEGRATION.                                  *
*     B          UPPER LIMIT OF INTEGRATION.                                  *
*     X          ARRAY OF ARGUMENT VALUES.  MUST BE MONOTONICALLY             *
*                INCREASING AND MUST BE DIMENSIONED NP.                       *
*     F          ARRAY OF FUNCTION VALUES. MUST BE DIMENSIONED NP.            *
*     NP         NUMBER OF POINTS.  NP MUST BE GREATER THAN 3.                *
*     VALUE      RESULTANT VALUE OF THE INTEGRATION.                          *
*     C, GC      WEIGHTING FUNCTIONS PASSED TO THE MAIN PROGRAM               *
*                FOR STORAGE.                                                 *
*     L          LIMITS OF INTEGRATION PASSED TO THE MAIN PROGRAM             *
*                FOR STORAGE.                                                 *
*     IERR       RESULTANT ERROR PARAMETER.                                   *
*                                                                             *
*     REQUIRED SUBPROGRAMS - NONE                                             *
*                                                                             *
*     COMMON STORAGE -                                                        *
*     THE WEIGHTING FUNCTIONS C AND GC ARE STORED IN THE MAIN PROGRAM         *
*     AND REQUIRE THE FOLLOWING DIMENSION STATEMENT WHERE D.GE.NP.            *
*                DIMENSION C(2,3,D),GC(D,D)                                   *
*                                                                             *
*     ERROR INDICATIONS -                                                     *
*     IERR = 0   INDICATES NO ERROR.                                          *
*     IERR = 1   INDICATES NP IS LESS THAN 4.                                 *
*     IERR = 2   INDICATES THE LIMITS OF INTEGRATION ARE NOT AT NODES         *
*                OR ARE OUT OF THE RANGE OF THE TABLE.                        *
*                                                                             *
*     EDWARD G. TRACHMAN                          M.E. DEPT.   492-5640       *
*                                                                             *
* * * * * * * * * * * * * * * * * * * * * * * * * * * * * * * * * * * * * * *
      DIMENSION X(NP),F(NP),C(2,3,NP),GC(NP,NP)
      DIMENSION H(100)
*
*     NP MUST BE GREATER THAN 3
*
      IF (NP.LE.3) GO TO 96
*
*     CALCULATION OF INTERVALS OF X
*
      NH=NP-1
```

```
      DO 10 I=1,NH
   10 H(I)=X(I+1)-X(I)
      DO 20 I=1,NH
      IF (I.EQ.1) GO TO 15
*
*     DEFINE COEFFICIENTS OF FIRST PARABOLA
*
      C(1,1,I)=-(H(I))**3/(6.*H(I-1)*(H(I-1)+H(I)))
      C(1,2,I)=H(I)*(3.*H(I-1)+H(I))/(6.*H(I-1))
      C(1,3,I)=H(I)*(3.*H(I-1)+2.*H(I))/(6.*(H(I-1)+H(I)))
   15 CONTINUE
      IF (I.EQ.NH) GO TO 20
*
*     DEFINE COEFFICIENTS OF SECOND PARABOLA
*
      C(2,1,I)=H(I)*(2.*H(I)+3.*H(I+1))/(6.*(H(I)+H(I+1)))
      C(2,2,I)=H(I)*(H(I)+3.*H(I+1))/(6.*H(I+1))
      C(2,3,I)=-(H(I))**3/(6.*H(I+1)*(H(I)+H(I+1)))
   20 CONTINUE
*
*     DEFINE GROUPED COEFFICIENTS
*
      DO 61 L=1,NP
      DO 61 I=1,NP
   61 GC(I,L)=0.0
      GC(1,1)=C(2,1,1)
      GC(2,1)=C(2,2,1)
      GC(3,1)=C(2,3,1)
      NPM2=NP-2
      DO 65 L=2,NPM2
      LP2=L+2
      DO 65 I=1,LP2
      CA=0.0
      CB=0.0
      IF(I-L+2.GT.0.AND.I-L+2.LT.4) CA=C(1,I-L+2,L)
      IF(I-L+1.GT.0.AND.I-L+1.LT.4) CB=C(2,I-L+1,L)
   65 GC(I,L)=GC(I,L-1)+0.5*(CA+CB)
      NPM3=NP-3
      DO 66 I=1,NPM3
   66 GC(I,NP-1)=GC(I,NP-2)
      GC(NP-2,NP-1)=GC(NP-2,NP-2)+C(1,1,NP-1)
      GC(NP-1,NP-1)=GC(NP-1,NP-2)+C(1,2,NP-1)
      GC(NP,NP-1)=GC(NP,NP-2)+C(1,3,NP-1)
*
      ENTRY INTEG1
*
*     SETTING LIMITS OF INTFGRATION
*
      IF (B-A) 40,92,30
*
*     B IS GREATER THAN A
*
   30 ALIM = A
      BLIM = B
      SIGN = 1.0
      GO TO 50
*
*     A IS GREATER THAN B
*
```

```
   40 ALIM = B
      BLIM = A
      SIGN =-1.0
   50 NH=NP-1
      II = 0
      DO 59 I=1,NP
      IF (II-2) 55,57,599
   55 XXXX=ALIM-X(I)
      IF (ABS(XXXX).LT..0000000001) GO TO 56
      IF (XXXX.GT.0.0) 57,97
   56 IALIM = I
      II = II + 2
   57 IF (II.EQ.1) GO TO 59
      XXXX=BLIM-X(NP+1-I)
      IF (ABS(XXXX).LT..0000000001) GO TO 58
      IF (XXXX.GT.0.0) 97,59
   58 IBLIM = NP+1-I
      II = II + 1
   59 CONTINUE
  599 IF (II.NE.3) GO TO 97
      IF (IALIM.NE.1) GO TO 97
      L=IBLIM-1
*
      ENTRY INTEG2
*
*     CALCULATION OF INTEGRAL OVER SUBINTERVAL
*
      VALUE = 0.0
      LP2=L+2
      IF (LP2.GT.NP) LP2=NP
      DO 80 I=1,LP2
   80 VALUE=VALUE+GC(I,L)*F(I)
*
*     CALCULATE THE FINAL VALUE OF THE INTEGRAL
*
      VALUE=SIGN*VALUE
*
*     SET ERROR PARAMETER FOR NORMAL RETURN
*
   92 IERR = 0
      RETURN
*
*     SET ERROR PARAMETER FOR TOO FEW POINTS
*
   96 IERR = 1
      RETURN
*
*     SET ERROR PARAMETER FOR A AND/OR B NOT AT NODES
*     OR OUT OF RANGE OF THE TABLE
*
   97 IERR = 2
      RETURN
      END
```

TYPICAL DATA CARDS

```
00000000011111111112222222222333333333344444444445555555555666666666677777777778
12345678901234567890123456789012345678901234567890123456789012345678901234567890

 16 115   500 175   .81       AH=0.0   CH=0.25    PROG(MOBIL)     VISC    23J71
 16 154   500 175   .81       AH=0.0   CH=0.25    PROG(MOBIL)     VISC    23J71
 16 200   500 175   .81       AH=0.0   CH=0.25    PROG(MOBIL)     VISC    23J71
 16 250   500 220   .89       AH=0.0   CH=0.25    PROG(MOBIL)     VISC    23J71
 16 115  1000 175   .58       AH=0.0   CH=0.25    PROG(MOBIL)     VISC    23J71
 16 154  1000 175   .58       AH=0.0   CH=0.25    PROG(MOBIL)     VISC    23J71
 16 200  1000 175   .58       AH=0.0   CH=0.25    PROG(MOBIL)     VISC    23J71
 16 200  1000 220   .72       AH=0.0   CH=0.25    PROG(MOBIL)     VISC    23J71
 16 115   500 175   .81       AH=0.0   CH=0.20    PROG(MOBIL)     VISC    23J71
 16 154   500 175   .81       AH=0.0   CH=0.20    PROG(MOBIL)     VISC    23J71
 16 200   500 175   .81       AH=0.0   CH=0.20    PROG(MOBIL)     VISC    23J71
 16 250   500 175   .81       AH=0.0   CH=0.20    PROG(MOBIL)     VISC    23J71
 16 250   500 220   .89       AH=0.0   CH=0.20    PROG(MOBIL)     VISC    23J71
 16 115  1000 175   .58       AH=0.0   CH=0.20    PROG(MOBIL)     VISC    23J71
 16 154  1000 175   .58       AH=0.0   CH=0.20    PROG(MOBIL)     VISC    23J71
 16 250  1000 220   .72       AH=0.0   CH=0.20    PROG(MOBIL)     VISC    23J71
```

```
      PROGRAM CONTROL(INPUT,TAPE60=INPUT,OUTPUT,PUNCH)
* * * * * * * * * * * * * * * * * * * * * * * * * * * * * * * * * * * * *
*                                                                       *
*     PROGRAM CONTROL                                                   *
*     ------- -------                                                   *
*                                                                       *
*     CALCULATES THE FRICTION AND VELOCITY AND TEMPERATURE PROFILES     *
*     IN AN ELASTOHYDRODYNAMIC LUBRICATED CONTACT.  THIS VERSION OF     *
*     THE PROGRAM INCLUDES THE EFFECTS OF CONVECTIVE HEAT TRANSFER.     *
*                                                                       *
*     REQUIRED SUBPROGRAMS -                                            *
*     SUBROUTINE PRINTS                                                 *
*     FUNCTION VISC                                                     *
*     FUNCTION ZERO                                                     *
*     FUNCTION PSI                                                      *
*     SUBROUTINE SECANT                                                 *
*     FUNCTION EXPI                                                     *
*     SUBROUTINE INTEG                                                  *
*     SUBROUTINE RTMI                                                   *
*                                                                       *
* * * * * * * * * * * * * * * * * * * * * * * * * * * * * * * * * * * * *
*                                                                       *
*     PROGRAM SET UP FOR MOBIL XRM OIL   WITH CONVECTION
      COMMON C,GC,LLLL
      COMMON /CPSI/ GINF,ETAO,T,Y,H,U2U1,NP,DUDY,IC,TG,OMEGA,CH,AH
      COMMON /CPSIO/ XK1,XKO
      COMMON /CQ/ Q
      COMMON /CZERO/ IPTRANS,TRANS(6)
      COMMON /CPR/ ETA2
      DIMENSION GINF(21),ETAO(21),T(21),Y(21),DUDY(21),TG(21),OMEGA(21)
      DIMENSION Q(21)
      DIMENSION C(2,3,21),GC(21,21)
      DIMENSION ETA2(21)
      DIMENSION DTDY(21),NEWT(21),TRACTCF(20),SLIP(20)
      DIMENSION TJM1(21)
      EXTERNAL PSI
      REAL LOGETA,NEWT
*
*     PHYSICAL CONSTANTS AND DATA
*
 9000 READ 9001,IRDP,IRDU,IRDT,PHIT,AH,CH
 9001 FORMAT(4XI3,I5,I4,F6.3,10XF3.1,6XF4.2)
      IF(EOF(60))9999,9002
 9002 CONTINUE
      PUNCH 9003
 9003 FORMAT(/)
      PHZ=1000.*FLOAT(IRDP)
      U=FLOAT(IRDU)
      TOIL=FLOAT(IRDT)+460.
*     NP         NUMBER OF GRID POINTS ACROSS THE HALF-FILM THICKNESS
      NP=11
      NH = NP - 1
*     NIP        NUMBER OF PRESSURE STEPS IN HALF CONTACT-LENGTH
      NIP=3
      NIP2=2*NIP
      TW=TOIL
*     COND       THERMAL CONDUCTIVITY OF THE LUBRICANT
      COND=.1*778./3600.
*     OILRHO     DENSITY OF THE LUBRICANT
```

```
      OILRHO=.0325
*     OILC        SPECIFIC HEAT OF THE LUBRICANT
      OILC=.4*778.*12.
      CYLW=0.25
*     CYLW        CONTACT WIDTH OF THE DISKS
*     R1, R2      RADII OF THE DISKS
      R1=R2=3.0
*     E1, E2      ELASTIC MODULUS OF THE DISKS
      E1=E2=30.E+6
*     POIS1, POIS2  POISSONS RATIO FOR THE DISKS
      POIS1=POIS2=0.3
*     ALPHA       VISCOSITY PRESSURE COEFFICIENT FOR THE LUBRICANT
      ALPHA=1.04E-4
      BETA=5.1E7*ALPHA
      GAMMA=930.*ALPHA
*     DK          THERMAL CONDUCTIVITY OF THE DISKS
      DK=21.7*778./3600.
*     DRHO        DENSITY OF THE DISKS
      DRHO=.283
*     DC          SPECIFIC HEAT OF THE DISKS
      DC=.109*778.*12.
*     HERSA, HERSB  CONSTANTS FOR THE HERSHEL VISCOSITY EQUATION
      HERSA=8.974
      HERSB=-3.2
*     NGRAPH      REQUIRED NUMBER OF GRAPHS FOR EACH TEMPERATURE PROFILE
      NGRAPH=0
*     MGRAPH      REQUIRED NUMBER OF GRAPHS OF TRACTION COEF. VS SLIP
      MGRAPH=1
*     PRNT=2HON    GIVES ADDITIONAL OUTPUT FOR DEBUGGING PURPOSES
      PRNT=3HOFF
*
*     INITIALIZATION AND BOUNDARY CONDITIONS
*
      IC = 1
      DTDY(1)=0.0
      Y(1)=0.0
      TRACT=0.0
      FLASH=0.0
      PI=3.1415927
      DO 10 I=1,NP
      NEWT(I)=1.*(1.-Y(I))+TW
      IF (I.LT.NP) Y(I+1)=Y(I)+1./FLOAT(NH)
   10 CONTINUE
*
      R=R1*R2/(R1+R2)
      E=2./((1.-POIS1*POIS1)/E1+(1.-POIS2*POIS2)/E2)
      B=4.*R/E*PHZ
      FLASHK=0.24/SQRT(PI*PHZ*DK*DRHO*DC*U*R/E)
      TRANS(1)=B/U/6.
      TRANS(2)=B/U/6.
      TRANS(3)=B/U/2.
      TRANS(4)=TRANS(3)
      TRANS(5)=TRANS(2)
      TRANS(6)=TRANS(1)
      DELXB=B/FLOAT(NIP)
*
*      CALCULATION OF LOAD
*
```

```
      W=PHZ*PHZ*PI*(2./E)*R
      PRINT 2,PHZ,W,R,E
    2 FORMAT(*1CONTROL    PHZ = *E15.8,*  W = *E15.8,*  R     = *E15.8,
     1*  E     = *E15.8)
*
*     CALCULATION OF HALF-FILM THICKNESS
*
      ETAENT=10.**(HERSA+HERSB*ALOG10(TOIL-460.))*1.45E-7
      H=1.6*ALPHA**0.6*(ETAENT*U)**0.7*E**0.03*R**0.43/W**0.13
      H=1.2*H
      H=PHIT*H
      H=0.5*H
      PRINT 1,H,ALPHA,ETAENT,U,CH,AH
    1 FORMAT(*0H = *E12.5,*  ALPHA = *E12.5,*  ETAENT = *E12.5,
     1* U = *F6.0,* CH = *F5.3,* AH = *F7.3)
*
*     SLIP LOOP
*
      NSLIP=15
      DATA (SLIP(IU),IU=1,20)/.5,1.,2.,3.,4.,5.,6.,8.,10.,15.,20.,30.,40
     1.,50.,60.,5*0.0/
      DO 6000 IU=1,NSLIP
      DATA (TRACTCF(IP),IP=1,20)/20*0.0/
      FLASH=FLASHK*TRACT*SLIP(IU)
      IF (FLASH.LT.0.5) FLASH=0.0
      TW=TOIL+FLASH
      PRINT 6,FLASH
    6 FORMAT(* CONTROL      FLASH = *E15.8)
      U2U1=0.5*SLIP(IU)
      PRINT 8,IU,SLIP(IU)
    8 FORMAT(*1CONTROL               IU = *I3,*     SLIP = *E15.8)
*
*     HERTZIAN PRESSURE LOOP
*
      TRACT=0.0
      DO 5999 IP=1,NIP2
      IPTRANS=IP
      XB=(2.*FLOAT(IP)-1.)/2./FLOAT(NIP)
      P=PHZ*SQRT(XB*(2.-XB))
      DO 3 I=1,NP
      IF (IP.EQ.1) TJM1(I)=TOIL
      IF (IP.GT.1) TJM1(I)=NEWT(I)
    3 CONTINUE
*
*     SOLVE MOMENTUM EQUATION
*
      ITCOUNT=0
      IT=0
      ITC=1
      TMAX=950.
      T(1)=951.
    4 IF (PRNT.EQ.2HON) PRINT 44,IT
   44 FORMAT(*0IT = *I3)
      IF (ITC.EQ.0) GO TO 4970
      IT=IT+1
      IF (IT.GT.1) TMAX=T(IT-1)
      TMIN=TOIL
      ITC=0
 4970 DO 11 I=IT,NP
```

```
      IF (ITCOUNT.EQ.0) TEMT=NEWT(I)
      IF (ITCOUNT.GT.0) TEMT=0.5*(T(I)+NEWT(I))
      IF (ITCOUNT.GT.200) GO TO 6003
      IF (IP.LE.NIP.AND.TEMT.LT.TJM1(I)) 4980,4979
 4979 IF (IP.GT.NIP.AND.TEMT.LT.TJM1(I)) 4982,4985
 4980 TEMT=0.5*(TJM1(I)+T(I))
      GO TO 4985
 4982 TEMT=0.5*(TOIL+Y(I)*FLASH+T(I))
 4985 IF (I.GT.IT) GO TO 4987
*     UPDATE TMAX AND TMIN
      IF (TEMT.LT.T(IT).AND.T(IT).LT.TMAX.AND.T(IT).GT.TMIN) TMAX=T(IT)
      IF (TEMT.GT.T(IT).AND.T(IT).GT.TMIN.AND.T(IT).LT.TMAX) TMIN=T(IT)
      IF (PRNT.EQ.2HON) PRINT 4988,TMAX,TMIN,TEMT
 4988 FORMAT(*0TMAX = *F9.4,*   TMIN = *F9.4,*   TEMT = *F9.4)
*     BOUND TEMPERATURE
      IF (TEMT.GT.TMAX.OR.TEMT.LT.TMIN) TEMT=0.5*(TMAX+TMIN)
      IF (PRNT.EQ.2HON) PRINT 4989,TEMT,T(IT)
 4989 FORMAT(* TEMT = *F9.4,*   T(IT) = *F9.4)
*     TEST FOR CONVERGENCE
      IF (ABS(TEMT-T(IT)).LT..3) 4986,4987
 4986 ITC=1
      IF (IT.EQ.NP) 5032,11
 4987 T(I)=TEMT
      GINF(I)=1.2*P/(2.52+.01333*(T(I)-492.))-1.45E4
      IF (GINF(I).LT.1.) GINF(I)=1.
*     CALCULATION OF STEADY-STATE VISCOSITY
      ETEXP=ALPHA*P+(BETA+GAMMA*P)*(680.-T(I))/680./T(I)
      ETA2(I)=.62*EXP(ETEXP)*1.45E-5
*     CALCULATION OF TIME-DEPENDENT VISCOSITY
      ETA0(I)=VISC(P,ETA2(I),IVCODE)
   11 CONTINUE
      DUMMY=PSI0(0.0)
      CALL SECANT(XK0,XK1,TAU,PSI,XK,.001,500,ITERR)
      IF (ITERR.EQ.1) STOP
      IF (PRNT.EQ.2HON) PRINT 41,TAU
   41 FORMAT(*0TAU  = *E15.8)
*
*     SOLVE ENERGY EQUATION
*
      DO 5000 I=1,NP
      Q(I)=-TAU*DUDY(I)/COND*H
      QC=+OILRHO*OILC/COND*H*H*U*(T(I)-TJM1(I))/DELXB
      Q(I)=Q(I)+QC
 5000 CONTINUE
      IF (PRNT.EQ.2HON) CALL PR1
      DO 5010 I=2,NP
      CALL INTEG1(0.,Y(I),Y,Q,NP,DTDY(I),C,GC,LLLL,IERR)
 5010 IF(IERR.NE.0) PRINT 5012,IERR
 5012 FORMAT(* INTEGRATING Q, IERR = *I3)
      DO 5020 I=2,NP
      CALL INTEG1(0.,Y(I),Y,DTDY,NP,NEWT(I),C,GC,LLLL,IERR)
 5020 IF(IERR.NE.0) PRINT 5022,IERR
 5022 FORMAT(* INTEGRATING DTDY, IERR = *I3)
      XK7=TW-NEWT(NP)
      ITCOUNT=ITCOUNT+1
      NEWT(1)=0.0
      DO 5030 I=1,NP
 5030 NEWT(I)=NEWT(I)+XK7
```

```
      GO TO 4
 5032 DO 5033 I=1,NP
 5033 NEWT(I)=T(I)
      IF (IVCODE.NE.0) PRINT 5034
 5034 FORMAT(*0      MINIMUM VISCOSITY REDUCTION*)
      CALL PRI
      PRINT 99
      PRINT 5040,((NEWT(I),I),I=1,NP)
 5040 FORMAT(* NEW TEMP = *F7.2,* I = *I4)
*
*     CALCULATION OF TRACTION
*
      TRACT=TRACT+B/FLOAT(NIP)*TAU
 5999 CONTINUE
      TRACTCF(IU)=TRACT/W
      PRINT 6002,TRACTCF(IU)
 6002 FORMAT(*0CONTROL    TRACTCF(IU) = *E15.8)
*
*     PLOT TEMPERATURE PROFILE
*
      IF(NGRAPH.EQ.0) GO TO 6000
      DO 5052 NGR=1,NGRAPH
      PRINT 5050,SLIP(IU)
 5050 FORMAT(*1(U2 - U1) = *E15.8)
      PRINT 99
      CALL STPLT1(1,NEWT,Y,NP,1H*,1,1HY)
      PRINT 5051
 5051 FORMAT(1H0,92X,11HTEMPERATURE)
 5052 CONTINUE
 6000 CONTINUE
 6003 PRINT 98
      PRINT 6001,((TRACTCF(IU),SLIP(IU)),IU=1,NSLIP)
 6001 FORMAT(* CONTROL      TRACT = *E15.8,*  U2-U1 = *E15.8)
      PUNCH 6005,((SLIP(IU),TRACTCF(IU)),IU=1,NSLIP)
 6005 FORMAT(2F10.5)
*
*     PLOT TRACTION COEFFICIENT
*
      IF(MGRAPH.EQ.0) GO TO 6013
      DO 6012 MGR=1,MGRAPH
      PRINT 98
      CALL STPLT1(1,SLIP,TRACTCF,NSLIP,1H*,14,14HTRACTION COEF.)
      PRINT 6011
 6011 FORMAT(1H0,100X,7HU2 - U1)
 6012 CONTINUE
 6013 CONTINUE
   98 FORMAT(*1*)
   99 FORMAT(*0*)
      GO TO 9000
 9999 CONTINUE
      STOP
      END
```

```
      FUNCTION PSI(TAU)
* * * * * * * * * * * * * * * * * * * * * * * * * * * * * * * * * * * *
*                                                                      *
*     FUNCTION PSI                                                     *
*     -------- ---                                                     *
*                                                                      *
*     THIS FUNCTION SUBROUTINE SUPPLIES THE RHEOLOGICAL MODEL          *
*     FOR THE LUBRICANT.  IN THIS CASE, WE ARE USING THE               *
*     BARLOW AND LAMB VISCOELASTIC MODEL WITH A LIMITING SHEAR STRESS. *
*                                                                      *
* * * * * * * * * * * * * * * * * * * * * * * * * * * * * * * * * * * *
      COMMON C,GC,LLLL
      COMMON /CPSI/ GINF,ETAO,T,Y,H,U2U1,NP,DUDY,IC,TG,OMEGA,CH,AH
      COMMON /CPSIO/ XK1,XKO
      DIMENSION GINF(21),ETAO(21),T(21),Y(21),DUDY(21),TG(21),OMEGA(21)
      DIMENSION C(2,3,21),GC(21,21)
      REAL INTG
      PRNT=3HOFF
  100 CONTINUE
      IF (PRNT.EQ.2HON) PRINT 200,TAU
  200 FORMAT(*OTAU = *E15.8)
      DO 210 I=1,NP
      TG(I)=TAU/GINF(I)
      IF(TG(I).LT.0.25) GO TO 205
*     SLIP REGION
      OMEGA(I)=(TG(I)-.2499963)*1.E6
      GO TO 208
*     VISCOELASTIC REGION
  205 OMEGA(I)=55.2*TG(I)*TG(I)+TG(I)
  208 DUDY(I)=GINF(I)/ETAO(I)*OMEGA(I)*H
  210 CONTINUE
      GO TO (220,230),IC
  220 CALL INTEG (0.,1.,Y,DUDY,NP,INTG,C,GC,LLLL,IERR)
      IC = 2
      GO TO 240
  230 CALL INTEG2(0.,1.,Y,DUDY,NP,INTG,C,GC,LLLL,IERR)
  240 IF (IERR.NE.0) PRINT 241,IERR,TAU
  241 FORMAT(* IERR = *I4,* AT TAU = *E15.8)
      PSI=ALOG10(INTG/U2U1)
      IF (PRNT.EQ.2HON) PRINT 250,INTG,PSI
  250 FORMAT(* INTG = *E15.8,*   PSI = *E15.8)
      TDUDY=0.0
      DO 310 I=1,NP
  310 TDUDY=TDUDY+DUDY(I)
      ADJ=U2U1*FLOAT(NP)/TDUDY
      IF (ADJ.GT.0.99) GO TO 390
      DO 320 I=1,NP
  320 DUDY(I)=ADJ*DUDY(I)
  390 CONTINUE
      RETURN
      ENTRY PSIO
*     CHECK OMEGA = 3.7
      XK1=TAU=0.25*GINF(1)
      DO 410 I=1,NP
      TG(I)=TAU/GINF(I)
      OMEGA(I)=55.2*TG(I)*TG(I)+TG(I)
  410 DUDY(I)=GINF(I)/ETAO(I)*OMEGA(I)*H
      CALL INTEG (0.,1.,Y,DUDY,NP,INTG,C,GC,LLLL,IERR)
```

```
      IF (IERR.NE.0) PRINT 241,IERR,TAU                                  PSIBL 59
      IF (ALOG10(INTG/U2U1)) 20,20,30                                    PSIBL 60
*     SLIP MODEL                                                         PSIBL 61
   20 XKO=10.*XK1                                                        PSIBL 62
      PSI=0.0                                                            PSIBL 63
      RETURN                                                             PSIBL 64
*     VISCOELASTIC MODEL                                                 PSIBL 65
   30 XKO=0.1*XK1                                                        PSIBL 66
      PSI=0.0                                                            PSIBL 67
      RETURN                                                             PSIBL 68
      END                                                                PSIBL 69
```

```
      FUNCTION PSI(TAU)
* * * * * * * * * * * * * * * * * * * * * * * * * * * * * * * * * * * * *
*                                                                       *
*     FUNCTION PSI                                                      *
*     -------- ---                                                      *
*                                                                       *
*     THIS FUNCTION SUBROUTINE SUPPLIES THE RHEOLOGICAL MODEL           *
*     FOR THE LUBRICANT.  IN THIS CASE, WE ARE USING THE                *
*     MAXWELL VISCOELASTIC MODEL WITH A LIMITING SHEAR STRESS.          *
*                                                                       *
* * * * * * * * * * * * * * * * * * * * * * * * * * * * * * * * * * * * *
      COMMON C,GC,LLLL
      COMMON /CPSI/ GINF,ETA0,T,Y,H,U2U1,NP,DUDY,IC,TG,OMEGA,CH,AH
      COMMON /CPSI0/ XK1,XK0
      DIMENSION GINF(21),ETA0(21),T(21),Y(21),DUDY(21),TG(21),OMEGA(21)
      DIMENSION C(2,3,21),GC(21,21)
      REAL INTG
      PRNT=3HOFF
  100 CONTINUE
      IF (PRNT.EQ.2HON) PRINT 200,TAU
  200 FORMAT(*0TAU = *E15.8)
      DO 210 I=1,NP
      TG(I)=TAU/GINF(I)
      IF(TG(I).LT.0.50) GO TO 205
*     SLIP REGION
      OMEGA(I)=(TG(I)-0.4999990)*1.E6
      GO TO 208
*     VISCOELASTIC REGION
  205 GINFK=0.5/TG(I)
      OMEGA(I)=1./(GINFK+SQRT(GINFK*GINFK-1.))
  208 DUDY(I)=GINF(I)/ETA0(I)*OMEGA(I)*H
  210 CONTINUE
      GO TO (220,230),IC
  220 CALL INTEG (0.,1.,Y,DUDY,NP,INTG,C,GC,LLLL,IERR)
      IC = 2
      GO TO 240
  230 CALL INTEG2(0.,1.,Y,DUDY,NP,INTG,C,GC,LLLL,IERR)
  240 IF (IERR.NE.0) PRINT 241,IERR,TAU
  241 FORMAT(* IERR = *I4,* AT TAU = *E15.8)
      PSI=ALOG10(INTG/U2U1)
      IF (PRNT.EQ.2HON) PRINT 250,INTG,PSI
  250 FORMAT(* INTG = *E15.8,*   PSI = *E15.8)
      TDUDY=0.0
      DO 310 I=1,NP
  310 TDUDY=TDUDY+DUDY(I)
      ADJ=U2U1*FLOAT(NP)/TDUDY
      IF (ADJ.GT.0.99) GO TO 390
      DO 320 I=1,NP
  320 DUDY(I)=ADJ*DUDY(I)
  390 CONTINUE
      RETURN
      ENTRY PSI0
*     CHECK OMEGA =1
      XK1=TAU=0.50*GINF(1)
      DO 410 I=1,NP
      TG(I)=TAU/GINF(I)
      GINFK=0.5/TG(I)
      OMEGA(I)=1./(GINFK+SQRT(GINFK*GINFK-1.))
```

```
  410 DUDY(I)=GINF(I)/ETA0(I)*OMEGA(I)*H
      CALL INTEG (0.,1.,Y,DUDY,NP,INTG,C,GC,LLLL,IERR)
      IF (IERR.NE.0) PRINT 241,IERR,TAU
      IF (ALOG10(INTG/U2U1)) 20,20,30
*     SLIP MODEL
   20 XK0=10.*XK1
      PSI=0.0
      RETURN
*     VISCOELASTIC MODEL
   30 XK0=0.1*XK1
      PSI=0.0
      RETURN
      END
```

```
      SUBROUTINE RTMI(X• F• FCT• XLI• XRI• EPS• IEND• IER)
C
C     ..................................................................
C
C        SUBROUTINE RTMI
C
C        PURPOSE
C           TO SOLVE GENERAL NONLINEAR EQUATIONS OF THE FORM FCT(X)=0
C           BY MEANS OF MULLER-S ITERATION METHOD.
C
C        USAGE
C           CALL RTMI (X•F•FCT•XLI•XRI•EPS•IEND•IER)
C           PARAMETER FCT REQUIRES AN EXTERNAL STATEMENT.
C
C        DESCRIPTION OF PARAMETERS
C           X      - RESULTANT ROOT OF EQUATION FCT(X)=0.
C           F      - RESULTANT FUNCTION VALUE AT ROOT X.
C           FCT    - NAME OF THE EXTERNAL FUNCTION SUBPROGRAM USED.
C           XLI    - INPUT VALUE WHICH SPECIFIES THE INITIAL LEFT BOUND
C                    OF THE ROOT X.
C           XRI    - INPUT VALUE WHICH SPECIFIES THE INITIAL RIGHT BOUND
C                    OF THE ROOT X.
C           EPS    - INPUT VALUE WHICH SPECIFIES THE UPPER BOUND OF THE
C                    ERROR OF RESULT X.
C           IEND   - MAXIMUM NUMBER OF ITERATION STEPS SPECIFIED.
C           IER    - RESULTANT ERROR PARAMETER CODED AS FOLLOWS
C                     IER=0 - NO ERROR.
C                     IER=1 - NO CONVERGENCE AFTER IEND ITERATION STEPS
C                             FOLLOWED BY IEND SUCCESSIVE STEPS OF
C                             BISECTION.
C                     IER=2 - BASIC ASSUMPTION FCT(XLI)*FCT(XRI) LESS
C                             THAN OR EQUAL TO ZERO IS NOT SATISFIED.
C
C        REMARKS
C           THE PROCEDURE ASSUMES THAT FUNCTION VALUES AT INITIAL
C           BOUNDS XLI AND XRI HAVE NOT THE SAME SIGN. IF THIS BASIC
C           ASSUMPTION IS NOT SATISFIED BY INPUT VALUES XLI AND XRI. THE
C           PROCEDURE IS BYPASSED AND GIVES THE ERROR MESSAGE IER=2.
C
C        SUBROUTINES AND FUNCTION SUBPROGRAMS REQUIRED
C           THE EXTERNAL FUNCTION SUBPROGRAM FCT(X) MUST BE FURNISHED
C           BY THE USER.
C
C        METHOD
C           SOLUTION OF EQUATION FCT(X)=0 IS DONE BY MEANS OF MULLER-S
C           ITERATION METHOD OF SUCCESSIVE BISECTIONS AND INVERSE
C           PARABOLIC INTERPOLATION, WHICH STARTS AT THE INITIAL BOUNDS
C           XLI AND XRI. CONVERGENCE IS QUADRATIC IF THE DERIVATIVE OF
C           FCT(X) AT ROOT X IS NOT EQUAL TO ZERO. ONE ITERATION STEP
C           REQUIRES TWO EVALUATIONS OF FCT(X). FOR TEST ON SATISFACTORY
C           ACCURACY SEE FORMULAE (3,4) OF MATHEMATICAL DESCRIPTION.
C           FOR REFERENCE, SEE G. K. KRISTIANSEN, ZERO OF ARBITRARY
C           FUNCTION, BIT, VOL. 3 (1963), PP.205-206.
C
C     ..................................................................
C
C
C
```

```
C
C
C
C     PREPARE ITERATION
      IER=0
      XL=XLI
      XR=XRI
      X=XL
      TOL=X
      F=FCT(TOL)
      IF(F)1,16,1
    1 FL=F
      X=XR
      TOL=X
      F=FCT(TOL)
      IF(F)2,16,2
    2 FR=F
      IF(SIGN(1.,FL)+SIGN(1.,FR))25,3,25
C
C     BASIC ASSUMPTION FL*FR LESS THAN 0 IS SATISFIED.
C     GENERATE TOLERANCE FOR FUNCTION VALUES.
    3 I=0
      TOLF=100.*EPS
C
C
C     START ITERATION LOOP
    4 I=I+1
C
C     START BISECTION LOOP
      DO 13 K=1,IEND
      X=.5*(XL+XR)
      TOL=X
      F=FCT(TOL)
      IF(F)5,16,5
    5 IF(SIGN(1.,F)+SIGN(1.,FR))7,6,7
C
C     INTERCHANGE XL AND XR IN ORDER TO GET THE SAME SIGN IN F AND FR
    6 TOL=XL
      XL=XR
      XR=TOL
      TOL=FL
      FL=FR
      FR=TOL
    7 TOL=F-FL
      A=F*TOL
      A=A+A
      IF(A-FR*(FR-FL))8,9,9
    8 IF(I-IEND)17,17,9
    9 XR=X
      FR=F
C
C     TEST ON SATISFACTORY ACCURACY IN BISECTION LOOP
      TOL=EPS
      A=ABS(XR)
      IF(A-1.)11,11,10
   10 TOL=TOL*A
   11 IF(ABS(XR-XL)-TOL)12,12,13
   12 IF(ABS(FR-FL)-TOLF)14,14,13
   13 CONTINUE
```

```
C      END OF BISECTION LOOP
C
C      NO CONVERGENCE AFTER IEND ITERATION STEPS FOLLOWED BY IEND
C      SUCCESSIVE STEPS OF BISECTION OR STEADILY INCREASING FUNCTION
C      VALUES AT RIGHT BOUNDS. ERROR RETURN.
       IER=1
    14 IF(ABS(FR)-ABS(FL))16,16,15
    15 X=XL
       F=FL
    16 RETURN
C
C      COMPUTATION OF ITERATED X-VALUE BY INVERSE PARABOLIC INTERPOLATION
    17 A=FR-F
       DX=(X-XL)*FL*(1.+F*(A-TOL)/(A*(FR-FL)))/TOL
       XM=X
       FM=F
       X=XL-DX
       TOL=X
       F=FCT(TOL)
       IF(F)18,16,18
C
C      TEST ON SATISFACTORY ACCURACY IN ITERATION LOOP
    18 TOL=EPS
       A=ABS(X)
       IF(A-1.)20,20,19
    19 TOL=TOL*A
    20 IF(ABS(DX)-TOL)21,21,22
    21 IF(ABS(F)-TOLF)16,16,22
C
C      PREPARATION OF NEXT BISECTION LOOP
    22 IF(SIGN(1.,F)+SIGN(1.,FL))24,23,24
    23 XR=X
       FR=F
       GO TO 4
    24 XL=X
       FL=F
       XR=XM
       FR=FM
       GO TO 4
C      END OF ITERATION LOOP
C
C
C      ERROR RETURN IN CASE OF WRONG INPUT DATA
    25 IER=2
       RETURN
       END
```

APPENDIX C

NOMENCLATURE

a	rise parameter of the hyperbolic model
b	$= 4p_{Hz}R/E$, half-width of Hertzian contact
c	limiting shear stress/limiting shear modulus ratio
c	specific heat of the lubricant
c_m	specific heat of the disk
D	shear rate
E	$= \frac{1}{2}[(1-\nu_1^2/E_1) + (1-\nu_2^2/E_2)]$, effective modulus of elasticity of the disks
E_1, E_2	elastic moduli of the two disks
$Ei(x)$	exponential integral
f	fractional free volume
f_2	equilibrium free volume
G^*	complex shear modulus
G_∞	high frequency limiting shear modulus
$\overline{G}_\infty$	$= G_\infty/K$
h	half-parallel lubricant film thickness
h_o	minimum lubricant film thickness
k	thermal conductivity of the lubricant
k_m	thermal conductivity of the disk
K	Oldroyd-Dyson parameter
K	bulk modulus
K_o	low frequency bulk modulus
K_∞	high frequency bulk modulus
K_f	bulk modulus associated with molecular rearrangements in free volume
K_r	complex relaxational modulus

K_2 high frequency value of K_r

K_t torsional spring constant

J inertia

J^* complex compliance

p pressure

p_{Hz} maximum Hertzian pressure

P maximum Hertzian pressure (on graphs)

P pressure step

P_{--} normal stress

R $= R_1R_2/(R_1 + R_2)$, effective radius of the disk pair

R_1, R_2 radii of the disks

s $= \ln(\eta_2/\eta)$

s_1 $= \ln(\eta_2/\eta_1)$

t time

T temperature

T lubricant inlet temperature (on graphs)

T_b bulk temperature of the disk

T_{ent} lubricant entrance temperature

T_s mean surface temperature of the disk in the contact zone, "flash temperature"

T_o reference temperature at which there is no free volume

u,v velocity components in the fluid film

U mean rolling speed

U_1, U_2 surface speeds of the disks

U^* reference rolling speed at which $\bar{\eta} = \frac{1}{2}\,\bar{\eta}_{U=0}$

v specific volume

v_f free volume

v_i	specific volume after elastic deformation only
v_o	occupied volume
v_1	initial specific volume
v_2	equilibrium specific volume
w	load per unit length of cylinder
x,y,z	Cartesian coordinates
Z^*	complex shear mechanical impedance
α	viscosity-pressure coefficient
γ	shear strain
$\dot{\gamma}$	shear rate
η	shear viscosity
η_{ent}	viscosity of the lubricant at entrance conditions
η_f	free volume viscosity
η_v	volume viscosity
η_1	initial viscosity
η_2	equilibrium viscosity
$\bar{\eta}$	effective viscosity
λ	Maxwell relaxation time
λ_f	retardation time
λ_v	volume relaxation time
μ	coefficient of friction
μ^*	complex fluidity
ν_1, ν_2	Poisson's ratio for the two disks
ξ	slide/roll ratio
ρ	density of the lubricant
ρ_m	density of the disk
τ	shear stress

Φ_T film thickness thermal reduction factor

ω angular frequency

Ω non-dimensional shear rate

REFERENCES

1. Cameron, A., and Newman, A. D., Proceedings of the Conference on Steam Turbine Research and Development, London: The Institution of Mechanical Engineers, 1953.

2. Misharin, J. A., "Influence of the Friction Conditions on the Magnitude of the Friction Coefficient in the Case of Rolling with Sliding," Proceedings of the International Conference on Gearing, London: The Institution of Mechanical Engineers, pp. 159-164, 1958.

3. Benedict, G. H., and Kelley, B. W., "Instantaneous Coefficients of Gear and Tooth Friction," ASLE Transactions, Vol. 4, pp. 59-70, 1959.

4. Crook, A. W., "The Lubrication of Rollers. IV. Measurements of Friction and Effective Viscosity," Philosophical Transactions of The Royal Society of London, Series A, Vol. 255, pp. 281-312, 1963.

5. Cheng, H. S., "A Refined Solution to the Thermal-Elastohydrodynamic Lubrication of Rolling and Sliding Cylinders," Transaction of ASLE, Vol. 8, No. 4, Oct. 1965, p. 397.

6. Bell, J. C., Kennel, J. W., and Allen, C. M., "The Rheological Behavior of the Lubricant in the Contact Zone of a Rolling Contact System," Journal of Basic Engineering, Trans. ASME, Series D, Vol. 86, pp. 423-432, 1964.

7. Ree, T., and Eyring, H., "Theory of Non-Newtonian Flow. I. Solid Plastic System, and Theory of Non-Newtonian Flow. II. Solution System of High Polymers," Journal of Applied Physics, Vol. 26, pp. 793-800 (Part I) and 800-809 (Part II), 1955.

8. Smith, F. W., "Rolling Contact Lubrication. The Application of Elastohydrodynamic Theory," Journal of Basic Engineering, Trans. ASME, Series D, Vol. 87, pp. 170-176, 1965.

9. McGrew, J. M., Gu, A., Cheng, H. S., and Murray, S. F., "Elastohydrodynamic Lubrication. Preliminary Design Manual," Technical Report AFAPL-TR-70-27, 1970.

10. Smith, F. W., "Lubricant Behavior in Concentrated Contact Systems -- The Caster Oil-Steel System," Wear, Vol. 2, pp. 250-263, 1959.

11. Johnson, K. L., and Cameron, R., "Shear Behavior of Elastohydrodynamic Oil Films at High Rolling Contact Pressure," Proceedings of the Institution of Mechanical Engineers, Vol. 182, Part 1, pp. 307-319, 1968.

12. Jefferis, J. A., and Johnson, K. L., "Sliding Friction Between Lubricated Rollers," Proceedings of the Institution of Mechanical Engineers, Vol. 182, Part 1, pp. 281-291, 1968.

13. Plint, M. A., "Traction in Elastohydrodynamic Contacts," Proceedings of the Institution of Mechanical Engineers, Vol. 182, Part 1, pp. 300-306, 1968.

14. Dowson, D., and Holmes, T. L., "Effect of Surface Quality Upon the Traction Characteristics of Lubricated Cylindrical Contacts," Proceedings of the Institution of Mechanical Engineers, Vol. 182, Part 1, pp. 292-299, 1968.

15. Dyson, A., "Frictional Traction and Lubricant Rheology in Elastohydrodynamic Lubrication," Philosophical Transactions of the Royal Society of London, Series A, Vol. 266, pp. 1-33, 1970.

16. Kovacs, A. J., "Bulk Creep and Recovery in Systems with Viscosity Dependent Upon Free Volume," Transactions of the Society of Rheology, Vol. 5, pp. 285-296, 1961.

17. Gross, B., Mathematical Structure of the Theories of Viscoelasticity, Paris: Herman et Cie, 1953.

18. Alfrey, T. Jr., Mechanical Behavior of High Polymers, New York: Interscience, 1948.

19. Barlow, A. J., and Lamb, J., "The Visco-Elastic Behavior of Lubricating Oils Under Cyclic Shearing Stress," Proceedings of the Royal Society of London, Series A, Vol. 253, pp. 52-69, 1959.

20. Maxwell, J. C., "On The Dynamical Theory of Gases," The London, Edinburgh, and Dublin Philosophical Magazine and Journal of Science, Series 4, Vol. 35, pp. 129-145 and 185-217, 1868.

21. Gruber, G. J., and Litovitz, T. A., "Shear and Structural Relaxation in Molten Zinc Chloride," Journal of Chemical Physics, Vol. 40, pp. 13-26, 1964.

22. Barlow, A. J., Lamb, J., and Matheson, A. J., "Viscous Behavior of Supercooled Liquids," Proceedings of the Royal Society of London, Series A, Vol. 292, pp. 322-342, 1966.

23. Barlow, A. J., Erginsav, A., and Lamb, J., "Viscoelastic Relaxation of Supercooled Liquids. II," Proceedings of the Royal Society of London, Series A, Vol. 298, pp. 481-494, 1967.

24. Doolittle, A. K., "Studies in Newtonian Flow. II. The Dependence of the Viscosity of Liquids on Free Space," Journal of Applied Physics, Vol. 22, pp. 1471-1475, 1951.

25. Barlow, A. J., Lamb, J., Matheson, A. J., Padminim P. R. K. L., and Richter, J., "Viscoelastic Relaxation of Supercooled Liquids. I," Proceedings of the Roual Society of London, Series A, Vol. 298, pp. 467-480, 1967.

26. Lamb, J., "Physical Properties of Fluid Lubricants: Rheological and Viscoelastic Behavior," Proceedings of the Institution of Mechanical Engineers, Vol. 182, Part 3A, pp. 293-310, 1968.

27. Dyson, A., "Flow Properties of Mineral Oils in Elastohydrodynamic Lubrication," Philosophical Transactions of the Royal Society of London, Series A, Vol. 258, pp. 529-564, 1965.

28. Russel, R. J., "The Determination of the Basic Rheological Constants Governing the Flow of Pseudo-Plastic Substances," Ph.D. Thesis, University of London, 1946.

29. Smith, F. W., "Lubricant Behavior in Concentrated Contact -- Some Rheological Problems," ASLE Transactions, Vol. 3, pp. 18-25, 1960.

30. Fein, R. S., "Possible Role of Compressional Viscoelasticity in Concentrated Contact Lubrication," Journal of Lubrication Technology, Trans. ASME, Series F, Vol. 89, pp. 127-131.

31. Litovitz, T. A., and Davis, C. M., "Structural and Shear Relaxation in Liquids," Physical Acoustics, ed. W. P. Mason, New York: Academic Press, Vol. IIA, Chap. 5, 1965.

32. Barlow, A. J., Lamb, J., and Taskŏprülü, "Ultrasonic and Viscoelastic Relaxation in bis[m-(m-phenoxyphenoxy)phenyl]ether," Journal of the Acoustical Society of America, Vol. 46, pp. 569-573, 1969.

33. Hutton, J. F., "Viscoelastic Relaxation Spectra of Lubricating Oils and Their Component Fractions," Proceedings of the Royal Society of London, Series A, Vol. 304, pp. 65-80, 1968.

34. Pressure-Viscosity Report, New York: ASME, Vols. I and II, 1953.

35. Dowson, D., and Higginson, G. R., "New Roller-Bearing Lubrication Formula," Engineering, Vol. 192, pp. 158-159, 1961.

36. Dowson, D., and Higginson, G. R., Elastohydrodynamic Lubrication, New York: Pergamon Press, 1966.

37. Cheng, H. S., "Calculation of Elastohydrodynamic Film Thickness in High Speed Rolling and Sliding Contacts," Mechanical Technology Report 67TR24, 1967.

38. Blok, H., "Les Temperatures de Surface dans des Conditions de Graissage sous Pression Extrême," Second World Petroleum Congress, Paris, Section 4, pp. 471-486, 1937.

39. Oldroyd, J. G., "Non-Newtonian Effects in Steady Motion of Some Idealised Elastico-Viscous Liquids," Proceedings of the Royal Society of London, Series A, Vol. 245, pp. 278-297, 1958.

40. Appeldoorn, J. K., "A Simplified Viscosity-Pressure-Temperature Equation," SAE Journal, Vol. 71, p. 108, June 1963.

41. Chu, P. S. Y., and Cameron, A., "Pressure-Viscosity Characteristics of Lubricating Oils," Journal of the Institute of Petroleum, Vol. 48, pp. 147-155, 1962.

42. Luke, Y. L., and Wimp, J., "Jacobi Polynominal Expansions of a Generalized Hypergeometric Functions over a Semi-Infinite Ray," Mathematics of Computation, Vol. 17, pp. 395-404, 1963.

43. Kloeffler, S. M., Kerchner, M. S., and Brenneman, E. E., Direct-Current Machinery, New York: The Macmillian Company, Chap. 13, 1949.

44. Crook, A. W., "The Lubrication of Rollers. II. Film Thickness with Relation to Viscosity and Speed. III. Theoretical Discussion of Friction and the Temperature in the Oil Film," Philosophical Transactions of the Royal Society of London, Series A, Vol. 254, pp. 223-258,1961.

45. Tasköprülü, N. S., Barlow, A. J., and Lamb, J., "Ultrasonic and Viscoelastic Relaxation in a Lubrication Oil," Journal of the Acoustical Society of America, Vol. 33, pp. 278-285, 1961.

46. Herschel, W. H., "The Change in Viscosity of Oils with Temperature," Industrial and Engineering Chemistry, Vol. 14, pp. 715-723, 1922.

☆ U.S. GOVERNMENT PRINTING OFFICE: 1973 - 736-454, REGION NO. 3-II

NATIONAL AERONAUTICS AND SPACE ADMINISTRATION
WASHINGTON, D.C. 20546

OFFICIAL BUSINESS
PENALTY FOR PRIVATE USE $300

SPECIAL FOURTH-CLASS RATE
BOOK

POSTAGE AND FEES PAID
NATIONAL AERONAUTICS AND
SPACE ADMINISTRATION
451

U.S.MAIL

POSTMASTER: If Undeliverable (Section 158 Postal Manual) Do Not Return

---

"The aeronautical and space activities of the United States shall be conducted so as to contribute . . . to the expansion of human knowledge of phenomena in the atmosphere and space. The Administration shall provide for the widest practicable and appropriate dissemination of information concerning its activities and the results thereof."

—NATIONAL AERONAUTICS AND SPACE ACT OF 1958

NASA SCIENTIFIC AND TECHNICAL PUBLICATIONS

TECHNICAL REPORTS: Scientific and technical information considered important, complete, and a lasting contribution to existing knowledge.

TECHNICAL NOTES: Information less broad in scope but nevertheless of importance as a contribution to existing knowledge.

TECHNICAL MEMORANDUMS: Information receiving limited distribution because of preliminary data, security classification, or other reasons. Also includes conference proceedings with either limited or unlimited distribution.

CONTRACTOR REPORTS: Scientific and technical information generated under a NASA contract or grant and considered an important contribution to existing knowledge.

TECHNICAL TRANSLATIONS: Information published in a foreign language considered to merit NASA distribution in English.

SPECIAL PUBLICATIONS: Information derived from or of value to NASA activities. Publications include final reports of major projects, monographs, data compilations, handbooks, sourcebooks, and special bibliographies.

TECHNOLOGY UTILIZATION PUBLICATIONS: Information on technology used by NASA that may be of particular interest in commercial and other non-aerospace applications. Publications include Tech Briefs, Technology Utilization Reports and Technology Surveys.

Details on the availability of these publications may be obtained from:

SCIENTIFIC AND TECHNICAL INFORMATION OFFICE

NATIONAL AERONAUTICS AND SPACE ADMINISTRATION

Washington, D.C. 20546